SANDIA REPORT
SAND2006-3784
Unlimited Release
Printed June 2006

Joint Sandia/NIOSH Exercise on Aerosol Contamination Using the BROOM Tool

Richard O. Griffith, James L. Ramsey, Patrick D. Finley, Brad J. Melton, John E. Brockmann, Dan A. Lucero, Sean A. McKenna, Chad E. Peyton, Robert G. Knowlton, Wayne Einfeld, Pauline Ho, Gary S. Brown, and Mark D. Tucker

Prepared by
Sandia National Laboratories
Albuquerque, New Mexico 87185 and Livermore, California 94550

Sandia is a multiprogram laboratory operated by Sandia Corporation,
a Lockheed Martin Company, for the United States Department of Energy's
National Nuclear Security Administration under Contract DE-AC04-94AL85000.

Sandia National Laboratories

Issued by Sandia National Laboratories, operated for the United States Department of Energy by Sandia Corporation.

Printed in the United States of America. This report has been reproduced directly from the best available copy.

Available to DOE and DOE contractors from
U.S. Department of Energy
Office of Scientific and Technical Information
P.O. Box 62
Oak Ridge, TN 37831

Telephone: (865) 576-8401
Facsimile: (865) 576-5728
E-Mail: reports@adonis.osti.gov
Online ordering: http://www.osti.gov/bridge

Available to the public from
U.S. Department of Commerce
National Technical Information Service
5285 Port Royal Rd.
Springfield, VA 22161

Telephone: (800) 553-6847
Facsimile: (703) 605-6900
E-Mail: orders@ntis.fedworld.gov
Online order: http://www.ntis.gov/help/ordermethods.asp?loc=7-4-0#online

SAND2006-3784
Unlimited Release
Printed June 2006

Joint Sandia/NIOSH Exercise on Aerosol Contamination Using the BROOM Tool

Richard O. Griffith, James L. Ramsey, Patrick D. Finley, Brad J. Melton, John E. Brockmann, Dan A. Lucero,

Plasma/Aerosol/Non-Continuum Processes Department

Sean A. McKenna, Chad E. Peyton

Geohydrology Department

Robert G. Knowlton, Wayne Einfeld, Pauline Ho, Gary S. Brown, Mark D. Tucker,

Chemical and Biological Systems Department

Sandia National Laboratories

P.O. Box 5800

Albuquerque, NM 87185

Abstract

In February of 2005, a joint exercise involving Sandia National Laboratories (SNL) and the National Institute for Occupational Safety and Health (NIOSH) was conducted in Albuquerque, NM. The SNL participants included the team developing the Building Restoration Operations and Optimization Model (BROOM), a software product developed to expedite sampling and data management activities applicable to facility restoration following a biological contamination event. Integrated data-collection, data-management, and visualization software improve the efficiency of cleanup, minimize facility downtime, and provide a transparent basis for reopening. The exercise was held at an SNL facility, the Coronado Club, a now-closed social club for Sandia employees located on Kirtland Air Force Base. Both NIOSH and SNL had specific objectives for the exercise, and all objectives were met.

Acknowledgments

The authors thank the Office of Research and Development at the U.S. Department of Homeland Security for funding this work. We especially thank Ken Martinez, Rob McCleery, Greg Burr, Brad King, Chad Dowell, Donnie Boomer, Kevin Dunn and James Bennett at NIOSH for their enthusiastic participation in this exercise and feedback. We thank Duane Lindner and J. Bruce Kelley for their management support and Veronica Lopez for her administrative support of the project.

This work was performed at Sandia National Laboratories under a WFO agreement for the U.S. Department of Homeland Security. Sandia is a multiprogram laboratory operated by Sandia Corporation, a Lockheed Martin Company, for the United States Department of Energy under contract DE-AC04-94AL85000.

Contents

Figures

Tables

Joint Sandia/NIOSH Exercise on Aerosol Contamination Using the BROOM Tool

1 Introduction

The events of Fall 2001 demonstrated that the U.S. is not prepared to deal with the consequences of biological terrorism. Despite the increasing awareness of the threat and the potential impact of a release of biological agent, significant gaps exist in response and decision-making capabilities. These deficiencies were particularly evident with respect to the contamination of public and private facilities from letters containing *Bacillus anthracis* spores. The remediation of the Hart Senate Office Building, for example, took several months at a considerable cost before it was considered safe enough for reentry. Fumigations at the seven sites involved in these incidents took months or years to complete, and each remediation effort involved thousands of characterization and clearance samples.

In February of 2005, a joint exercise involving Sandia National Laboratories (SNL) and the National Institute for Occupational Safety and Health (NIOSH) was conducted in Albuquerque, NM. The SNL participants included the team developing the Building Restoration Operations and Optimization Model (BROOM), a software product developed to expedite sampling and data management activities applicable to facility restoration following a biological contamination event. Integrated data-collection, data-management, and visualization software improve the efficiency of cleanup, minimize facility downtime, and provide a transparent basis for reopening. The exercise was held at an SNL facility, the Coronado Club, a now-closed social club for Sandia employees located on Kirtland Air Force Base.

Both NIOSH and SNL had specific objectives for the exercise.

BROOM team objectives included:

- demonstration of the BROOM sample management tool under "real life" conditions by experienced sample collection teams,
- demonstration of the BROOM contamination mapping module,
- demonstration of the BROOM sampling strategy planning tool, and
- development of an actual surface contamination database following a tracer aerosol release for evaluation of statistical algorithms.

NIOSH team objectives included:

- demonstration of mobile sampling deployment capabilities,
- demonstration of semi-automated sample logging hardware (ruggedized PC-tablet), and
- evaluation of onsite decontamination procedures for removal of a tracer aerosol contamination.

The NIOSH team met all their objectives, Figure 1-1. This report documents how the objectives of the SNL team were met. Table 1-1 lists the participants in the exercise and their roles.

DEPARTMENT OF HEALTH AND HUMAN SERVICES

Public Health Service

National Institute for Occupational
Safety and Health
Robert A. Taft Laboratories
4676 Columbia Parkway
Cincinnati OH 45226-1998

March 3, 2005

Gary Brown
Sandia National Laboratories
P.O. Box 5800, Mail Stop 0734
Albuquerque, New Mexico 87185-0734

Dear Mr. Brown:

On behalf of the NIOSH Environmental Sampling Team, I wanted to thank you, the entire Sandia National Lab (SNL) BROOM Team, and Mr. Argo (Fire Protection Engineering, SNL) for the hospitality and assistance provided to us to ensure the environmental sampling effort and the SNL/NIOSH goals were met. Without everyone's planning, training, and professionalism, we would not have been able to complete our efforts as quickly and efficiently as was accomplished during February 21-25, 2005. Please forward this letter and/or its message to the individuals involved in this exercise as appropriate.

Again, thank you for your assistance.

Sincerely yours,

Robert E. McCleery, MSPH, CIH
Industrial Hygienist
Hazard Evaluations and Technical
Assistance Branch
Division of Surveillance, Hazard
Evaluations and Field Studies

cc:
James Ramsey
Bernard "Pete" Argo

Figure 1-1. Letter from NIOSH about joint exercise.

Table 1-1. Participants in Sandia/NIOSH Exercise

Institution	Name	Role
DHS	Dawn Myscofski	Program Sponsor
	Teresa Lustig	Program Sponsor
NIOSH	Ken Martinez	NIOSH Project Manager
	Rob McCleery	Team Lead and Sampling using Traditional Methods
	Greg Burr	Sampling using Traditional Methods
	Brad King	Sampling using BROOM Tool
	Chad Dowell	Sampling using BROOM Tool
	Donnie Boomer	Equipment Setup and Support for Samplers
	Kevin Dunn	Equipment Setup and Support for Samplers
	James Bennett	CFD Modeling of Gas/Particle Transport
Sandia	Duane Lindner	SNLChem Bio National Security Program Manager
	Richard Griffith	Deputy SNL CBNS Program Manager
	Jim Ramsey	BROOM Team Lead
	Patrick Finley	BROOM Developer
	Brad Melton	BROOM Developer
	John Brockmann	Aerosol Release and Transport PI
	Dan Lucero	Aerosol Measurement Technology
	Todd Rudolph	Aerosol Measurement Technology
	Veronica Lopez	Financial and Administrative Project Support
	Taunya Crilly	Administrative Support
	Sean McKenna	Geostatistical Analysis Methodologies
	Mark Tucker	Project Manager and Technical Team Lead
	Bob Knowlton	Geostatistical Analysis Methodologies
	Wayne Einfeld	Project Planning and Support
	Pauline Ho	Project Planning and Support
	Gary Brown	Sampling Efficiency and Sample Analysis PI
	Mollye Wilson	Sample analysis and initial sample collection
	Kit Walsh	Sample analysis and initial sample collection
	Jonathan Leonard	Sample analysis and initial sample collection
	Matt Tezak	Sample analysis and initial sample collection
	Brian Patterson	Sample analysis and initial sample collection
	Ray Boucher	Sample analysis and initial sample collection

2 Exercise Plan

In this exercise, a fluorescent-tagged tracer aerosol (Visolite) was used as a bioaerosol stimulant. The median particle diameter of the tracer aerosol was on the order of a micrometer which is roughly comparable to a bacterial spore. Two variations of the aerosol tracer were used during the exercise. As part of the preparation for the visit of the NIOSH team, yellow fluorescent variant of the tracer aerosol was released, extensively sampled, and quantitatively analyzed. The analytical results were used to not only generate a detailed contamination distribution map for the facility but are also being used for the further development of statistical sampling algorithms.

For the NIOSH visit, a pink fluorescent variant of the tracer aerosol was released from the same location as the mapping release the day before the sample collection teams entered the facility. Two NIOSH teams collected samples from facility surfaces while in level C Personal Protective Equipment (PPE). All samples collected were analyzed for both pink and yellow aerosol tracer.

Table 2-1 gives a detailed schedule for the NIOSH visit. On the first day, one team collected surface samples in the morning and the other collected samples in the afternoon. On this initial entry, both teams selected sample locations based on expert judgment. All samples were analyzed overnight and concentration data supplied to both teams prior to a second day entry. The NIOSH team performed and evaluated personnel decontamination procedures for each sample collection team as they exited the facility following a sample collection effort (Figure 2-1). Decontamination effectiveness was evaluated following treatment using visual inspection with a UV light that caused any residual bioaerosol simulant to fluoresce.

Table 2-1. Schedule for Sandia/NIOSH exercise: February 20-25, 2005

When	What	Who
Sunday	NIOSH people arrive, and start setting up their equipment	Gary meets them. Keys from Jim.
Monday morning	NIOSH people badged	Mollye or Janet.
Monday morning, early	Release of tracer	John and Dan.
Monday morning	Go over plans with Ken Martinez.	Jim, Gary, and Sean.
Monday morning /afternoon	Train NIOSH team on BROOM and hand-held devices	BROOM Team
Monday afternoon	Brief NIOSH team on scenarios and building	Gary
Tuesday morning	NIOSH enters building for first set of samples	NIOSH team
Tuesday afternoon	NIOSH enters building for second set of samples	NIOSH team
Wednesday morning, early	Results of Tuesday's sampling given to NIOSH	Sean and Gary
Wednesday morning	NIOSH does first round of more extensive sampling using their methods and expert judgment	NIOSH team
Wednesday afternoon	BROOM refresher and distribution of equipment, followed by first round of sampling using BROOM guidance.	NIOSH team / BROOM team
Thursday morning, early	Results of Wednesday's sampling given to NIOSH	Sean and Gary

When	What	Who
Thursday morning	NIOSH does second round of more extensive sampling using their methods and expert judgment	NIOSH team
Thursday afternoon	NIOSH does second round of more extensive sampling using BROOM guidance	NIOSH team
Friday morning	Debrief, comparison of results.	All
Friday afternoon	Cleanup, shut down.	All

Figure 2-1. NIOSH team member in PPE undergoing decontamination with a newly developed apparatus.

On the second day, a NIOSH team entered the facility in the morning and collected additional samples based on information and guidance provided by the BROOM tool. The second team generated contamination maps and additional sample locations by hand based on analytical data and expert judgment, and then entered the facility for an afternoon sample collection effort. All samples were analyzed overnight and concentration data supplied to both teams prior to a third day entry.

The third day mapping and sample collection activities were conducted as on day 2. However, by the end of the day, the NIOSH expert judgment sample collection team had identified the source location of the release.

3 Aerosol Release

D.A. Lucero, J. Brockmann and T. Rudolph

This section provides technical details about the release of the aerosol used as a simulant for a biological weapon agent. The purpose of this work was to determine how to perform the aerosol release in a manner that would provide detectable levels of contamination in many parts of the building for the actual test. This preparatory work would also exercise the sample collection methods and develop the initial contamination map using the BROOM tool.

The first section below describes the experimental apparatus used. Subsequent sections describe specific aerosol tests and present results that characterize the transport of aerosols in the building.

3.1 Experimental Apparatus

3.1.1 Aerosol Test Chamber

A make shift aerosol chamber was setup in the walk-in freezer at the Coronado Club Kitchen. Figure 3-1 shows a photographs of the chamber used to characterize release of the Yellow Visolite powder. Figure 3-2 shows a photograph of the inside. The overall dimensions of this aerosol chamber (Freezer) are 2.0 m wide by 2.7 m high by 3.3 m long (6 ft x 8 ft x 10 ft) with an interior volume of 18.0 m^3 (480 ft^3). One AC powered fan provide convective airflow and circulation for aerosol dispersion and mixing, this fan is rated at 35 cfm.

Figure 3-1. Photograph of Aerosol Chamber used to characterize release of yellow Visolite powder.

Figure 3-2. Photograph of inside of Aerosol Chamber used to characterize release of yellow Visolite powder.

3.1.2 DustTrak Aerosol Monitor

The DustTrak Aerosol Monitor, shown in Figure 3-3, is a portable, battery-operated, laser-photometer that measures and records airborne aerosol concentrations.

The DustTrak measures in real-time, concentrations in milligrams per cubic meter (mg/m^3) while data is simultaneously logged into memory. The measurement range is .001 to 100 mg/m^3. The operational flowrate is nominally 1.7 lpm. The DustTrak was programmed to take data for 24 hours at 2 seconds per data point.

Figure 3-3. Photograph of TSI. MODEL 8520

3.1.3 Visolite Powder and Dispersers

Visolite is a fluorescent inorganic carbonate powder used for leak-checking commercial powder-handling systems. It comes in four colors and has particle sizes in the 2-14 micrometer range. Visolite is available from BHA Group, Inc. Corporate Offices, 8800 East 63rd Street, Kansas City, Missouri USA 64133.

The initial releases were carried out using dry powder dispersers (puffers) intended for dispersing powdered insecticides. These “Crusader” bug sprayers are available from U-SPRAY, INC. 4653 Highway 78, Lilburn, Georgia 30047, Tel: (770) 985-9388. The “Crusader” sprayers and Visolite are shown in Figure 3-4.

Subsequent powder releases were done using a BGI powder disperser. This device fed powder from a hopper into a toothed wheel. The wheel conveyed powder in measured amounts to the inlet of an air eductor that drew the powder into a turbulent gas flow and dispersed it. This device was able to disperse powder more efficiently than the puffer. These devices are available from BGI incorporated, 58 Guinan Street, Waltham, MA 02451, Tel: (701)891-9380, www.bgiusa.com.

Figure 3-4. Photograph of Crusader Bug Sprayer with Visolite Powder

3.1.4 Aerodynamic Particle Sizer (APS)

The APS measures aerodynamic particle size and relative light scattering intensity. It will detect and size particles in the range of 0.5 to 20 micrometers in size. Aerodynamic diameter is defined as the physical diameter of a unit density sphere that settles through the air with a velocity equal to that of the particle in question. It is the most significant aerosol parameter because it describes the particles behavior while airborne; particles exhibiting the same airborne behavior have the same aerodynamic diameter, regardless of their physical size, shape, density or composition. Figure 3-5 is a photograph of the APS, co-located with a DustTrak and a Laptop computer.

Figure 3-5. Photograph of Aerodynamic Particle Sizer

3.2 Monday February 14th – Chamber Test with Yellow Visolite

The make shift aerosol chamber in the walk-in freezer at the Coronado Club Kitchen was used. Sample surfaces were provided and setup by personnel from the Chemical and Biological Systems Department. Two TSI DustTraks and three 25mm filter holders loaded with glass fiber filters were setup in the chamber. The filter flowrates were maintained at 5 lpm with personnel sampling pumps manufactured by SKC. At approximately 5:03pm, 1.25 grams of Yellow Visolite was dispersed into the aerosol chamber using a bug sprayer (puffer). The DustTraks measured and logged the airborne mass concentration at 2 second intervals.

The mass decay rate from the DustTrak measurements in Figure 3-6 gives an estimate of the particle settling rate of 1.7 cm/sec. This is consistent with an aerodynamic particle size of 23 micrometers. This is somewhat higher than the stated native particle size distribution for Visolite, indicating the presence of some agglomerated particles. The initial airborne particle concentration based in the DustTrak measurements is ~7mg/m^3 giving an initial dispersion of 136 mg of powder into the chamber. This is much smaller than the total mass of 1250 mg of Visolite that was dispersed, so the particle concentration measurements indicate that most of the powder was too large to remain suspended and fell out immediately. The observed dispersion efficiency of roughly 10% suggested that the puffers were not an effective method for dispersing the Visolite powder. The filter results in Table 3-1 correspond to an average integral concentration of 150 mg-min/m^3. This is consistent with the observed DustTrak data.

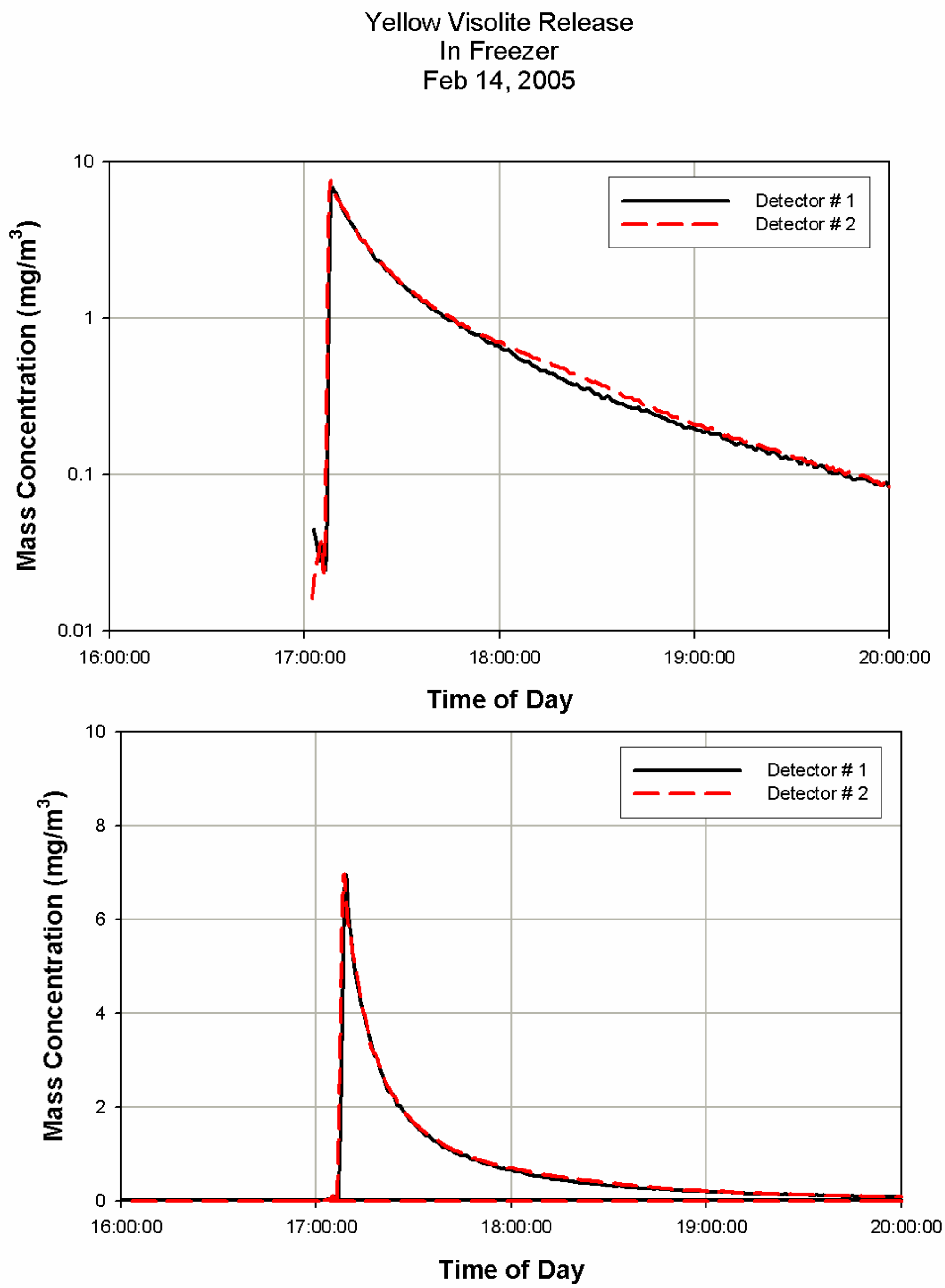

Figure 3-6. Feb. 14, 2005 test. DustTrak plot from yellow Visolite.

Table 3-1. Feb. 14, 2005 test. Filter Data from yellow Visolite release.

SKC pump sample weights - 25 mm filter			
	Pre	Post	Difference (mg)
1	26.05	26.7	0.65
3	25.95	26.62	0.67
4	26.92	27.89	0.97

3.3 Tuesday February 15th – Flow Test with Theatrical Smoke

Two (propylene glycol) smoke tests were conducted to visualize HVAC flow patterns; one release at approximately 12:30pm and the other at approximately 3:30pm. The purpose of this test was to get a qualitative understanding of the air flow in the building, which in turn would assist in selecting the release location for the real test.

The smoke was released on the lower level of the Coronado Club, just to the left of the bottom of the stairs. Figure 3-7 shows the smoke generator in operation at the top of the stairs. Ten TSI DustTraks were deployed at locations, given in Table 3-2, throughout the Coronado club. An Aerodynamic Particle Sizer was also deployed to measure the airborne particle size and concentration.

Figure 3-7. Photograph of Feb. 15, 2005 smoke test of air flows.

Table 3-2. Locations of DustTraks samplers for Feb. 15, 2005 smoke test.

Sampler Number	Location
#1 (22158)	Desk near entrance of ball room, NE side of room
#2 (22247)	Co-Located with APS on table, center of carpet area.
#3 (22242)	Lower Level conference room, on table at Visolite release location.
#4 (22244)	In Bar on post
#5 (22240)	Reception counter near restrooms
#6 (22241)	Desk at North end of dance floor in center
#8 (22239)	Lower Level on water fountain
#9 (22246)	Table East side of Ball room, near windows
#10 (22243)	Top of Stairs
# 11 (22238)	Room at bottom of stairs, Lower Level NE side on table in center of room

The DustTrak results in Figure 3-8 show the arrival of the smoke cloud and the duration of the aerosol concentrations. at different locations. The APS results in Figure 3-9, the size distribution shown in Figure 3-10, and the numerical analysis shown in Table 3-3 indicate that the smoke had a fairly narrow particle size distribution with the number-weighted size close to 1 micrometer. This small size means the aerosol cloud had very low losses and its concentration decline is almost exclusively convection driven. The smoke test should thus give a very good indication of how gas flows through the building.

The final aerosol release location in the basement of the building was selected based on these smoke-tests. The results indicated that an aerosol cloud originating at that location should spread through the building.

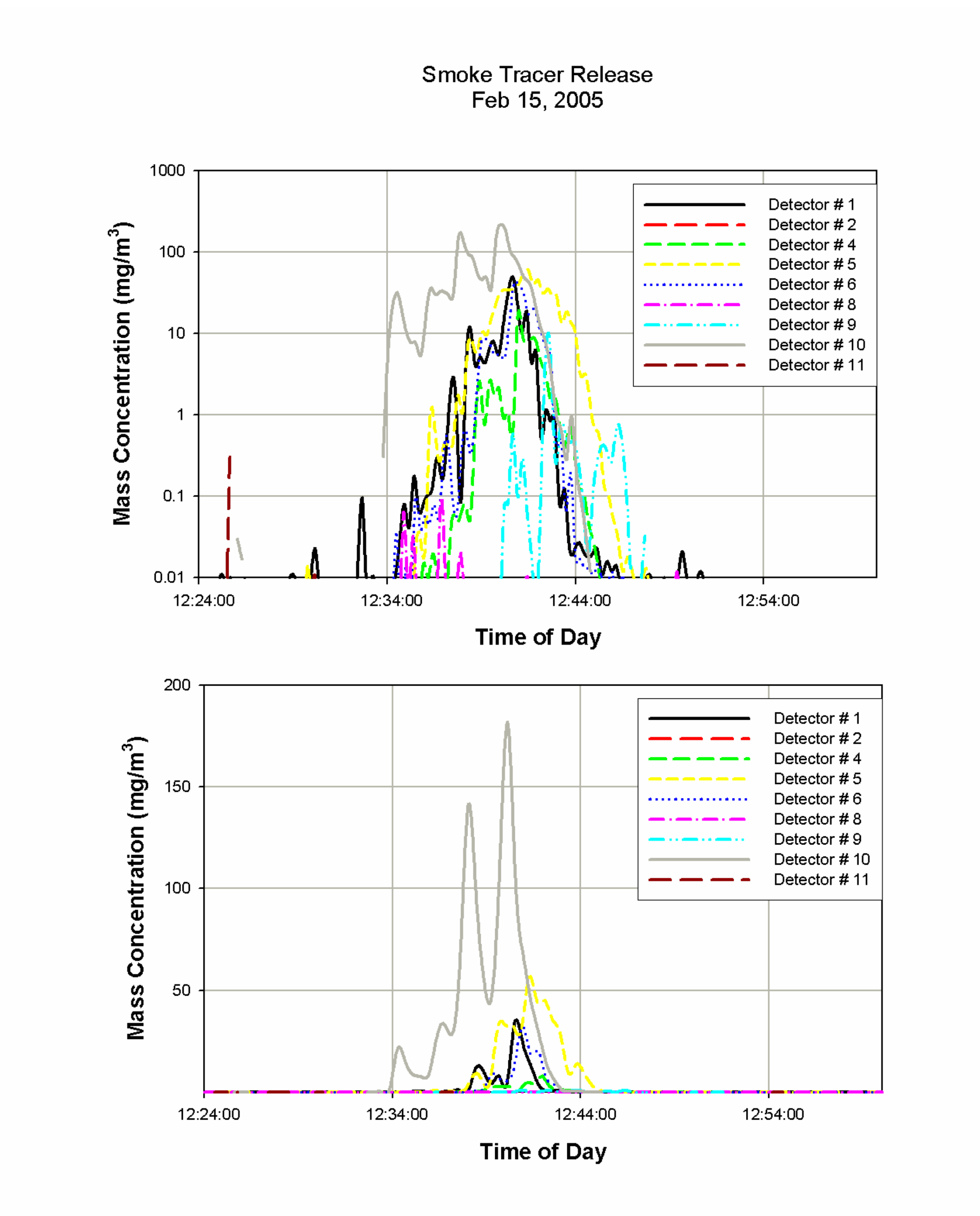

Figure 3-8. Feb. 15, 2005 test. DustTrak Plots from Smoke Release

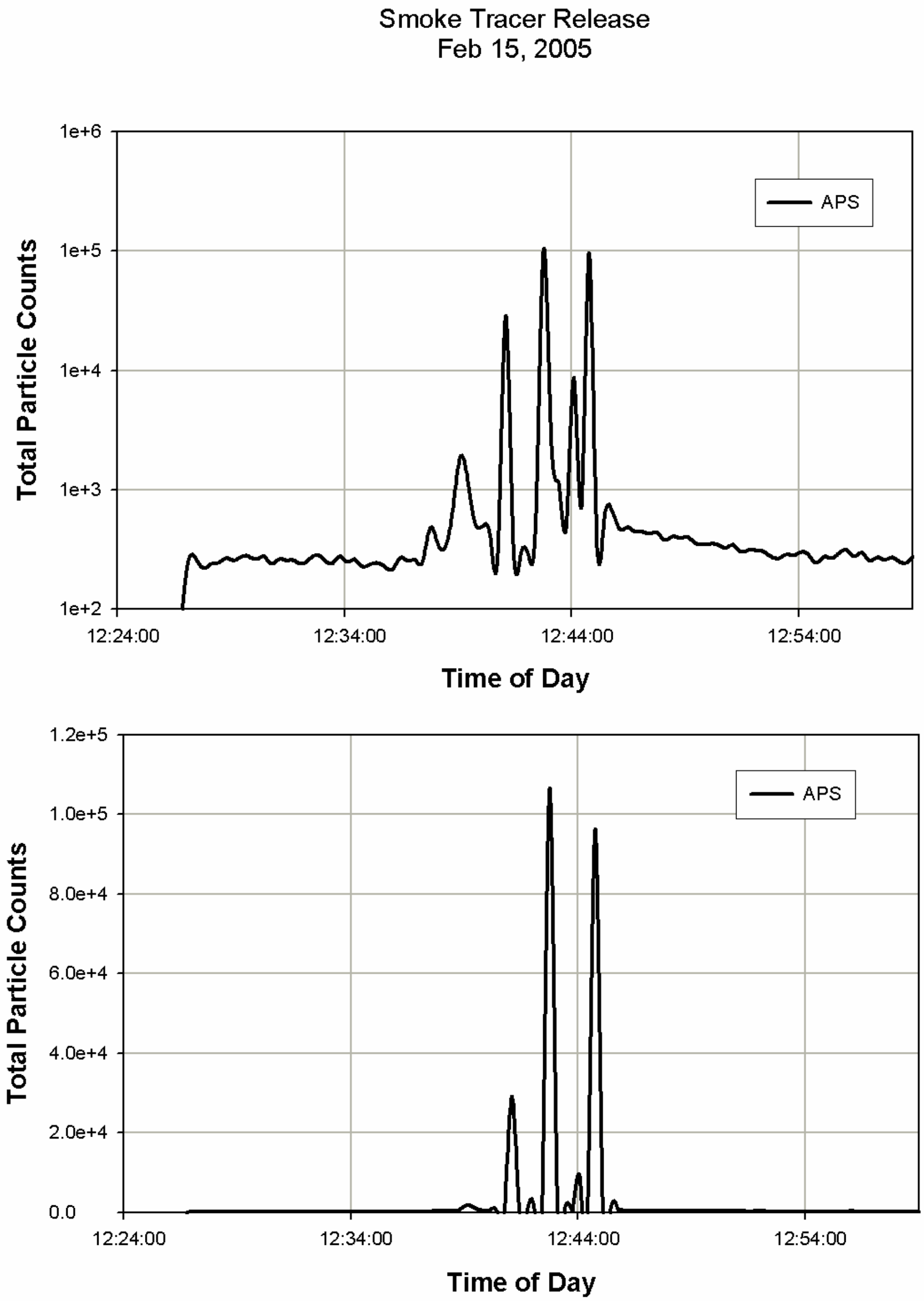

Figure 3-9. Feb. 15, 2005 test. APS plots from Smoke Release.

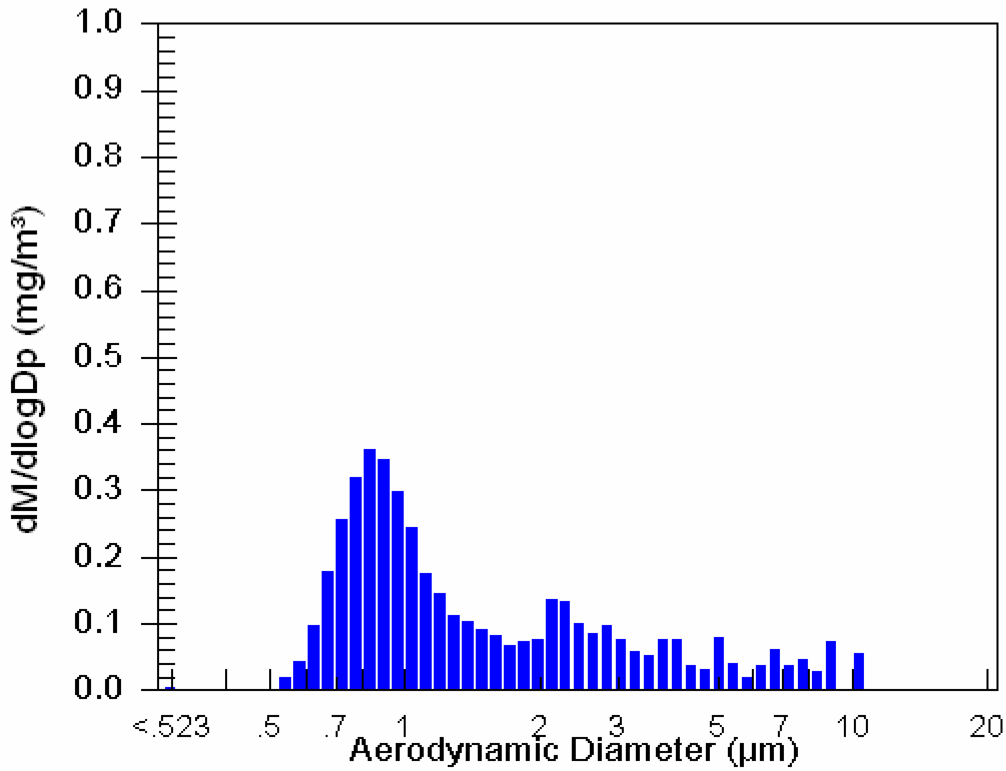

Figure 3-10. Feb. 15, 2005 test. APS size distribution plot.

Table 3-3. Feb. 15, 2005 test. Numerical analysis of APS data.

	Number Weighted Particle Size	**Surface Weighted Particle Size**	**Mass Weighted Particle Size**
Median (µm)	0.782	0.890	1.12
Mean (µm)	0.837	1.21	2.09
Geo. Mean (µm)	0.807	1.03	1.50
Mode (µm)	0.723	0.835	0.835
Geo. St. Dev.	1.28	1.63	2.11
Total Conc.	367(#/cm³)	724(µm²/cm³)	0.142(mg/m³)
Total Counts	96534		

3.4 Wednesday February 16th – Yellow Visolite Tracer Release

Yellow Visolite was used as a Bio-simulant for these tests. At 4:10 pm, approximately 207 grams of yellow Visolite was dispersed into the building using the Puffers (see Figure 3-11). The release location was the conference room on the lower level of the Coronado Club. Ten DustTraks, were deployed at same locations as used the previous day for the smoke test. An APS, two TSI Velocity Meters and three 25mm filter holders loaded with glass fiber filters were also used. The APS was located on a table ~15 feet from the door entrance to the main ballroom, one of the filter holders was co-located there with the APS and a DustTrak. TSI Velocity Meter # 1 was located at the entrance to the Ball Room and Velocity Meter # 2 was located at the top of the stairs. The filter holders were co-located with these. Approximately 240 12”x12” black vinyl tiles were laid down through out the Coronado Club, upper and lower levels. All locations were logged by BROOM PDAs (personal digital assistants).

This Bio-Simulant tracer test was conducted for several reasons:

- To determine Minimum Detection Limits for Sampling Methods and appropriate release amounts.
- To determine transport characteristics of Visolite
- To determine size distributions of Visolite
- To conduct a dry-run test for upcoming NEPA test

Figure 3-11. Feb. 16, 2005 test. Photograph showing release of yellow Visolite with Puffer.

The DustTrak results shown in Figure 3-12, and the APS results in Figure 3-13 show that the aerosol cloud moved up the stairs quite promptly. The concentration remained high for about a half an hour before declining by a combination of mixing of clean air and deposition of the particles on surfaces.

The size distribution shown in Figure 3-14, along with the numerical analysis shown in Table 3-4 indicate that the mean particle size in on the order of a few micrometers. The filter data shown in Table 3-5 indicate that integral concentration seen in the building range from roughly 2 to 20 mg-min/m^3. This is consistent with concentrations observed by the DustTraks.

This release of yellow Visolite powder was the subject of extensive sampling and analysis. This extensive data set, presented in Section 7, provides a baseline case for testing statistical sampling methods, as well as fully characterizing powder release patterns before the joint exercise.

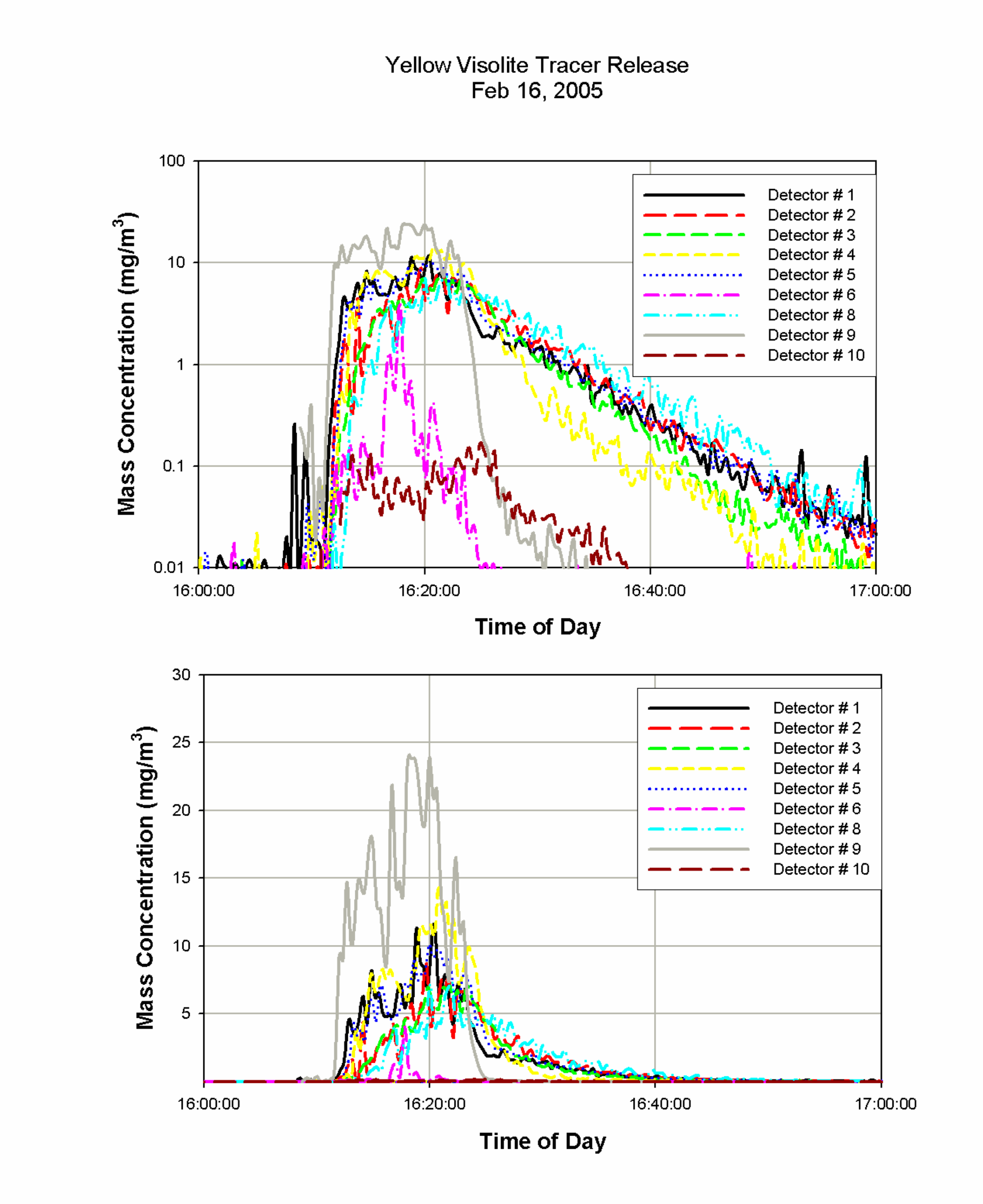

Figure 3-12. Feb. 16, 2005 test. DustTrak plot from yellow Visolite release.

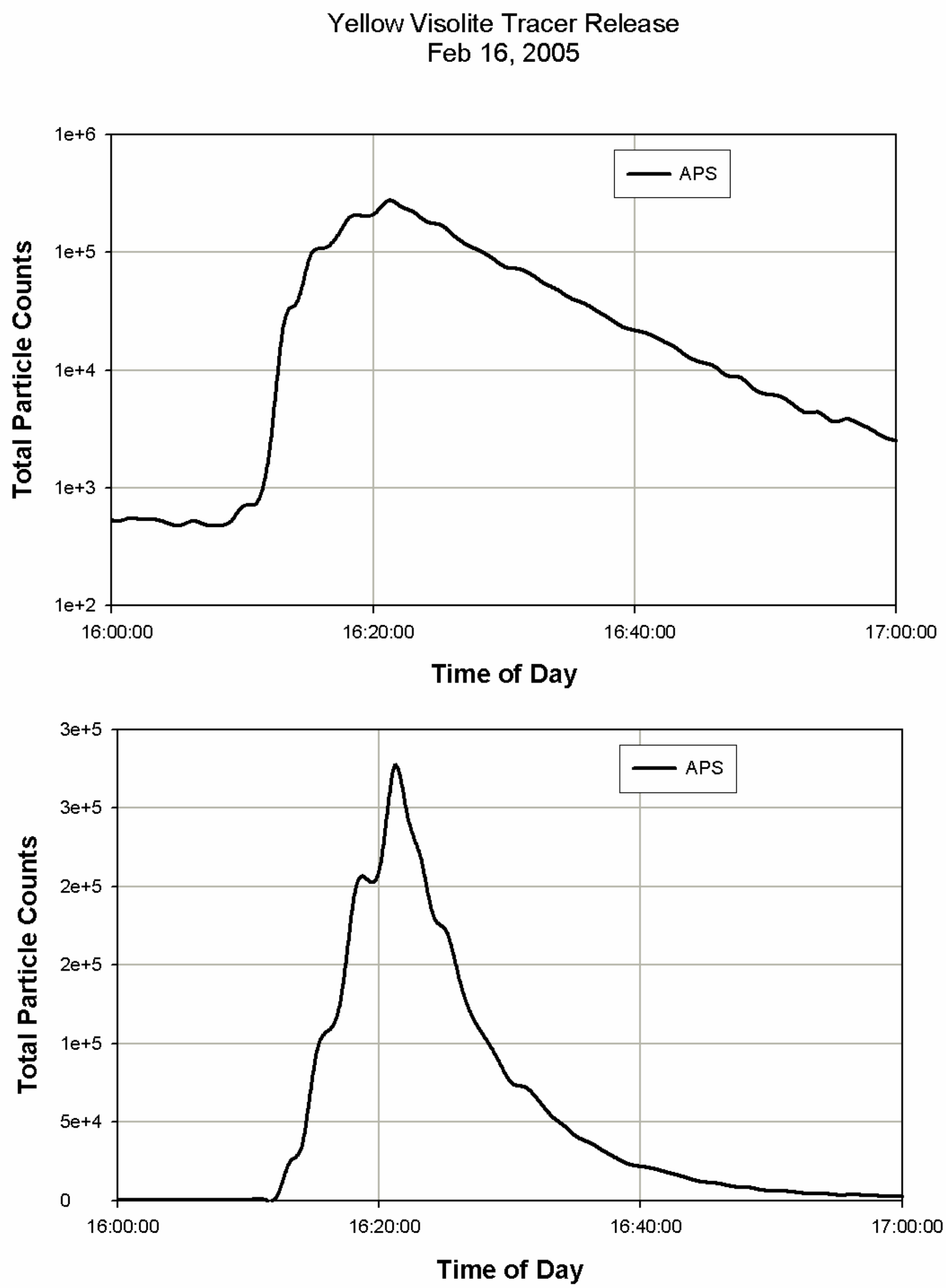

Figure 3-13. Feb. 16, 2005 test. APS plots from yellow Visolite release.

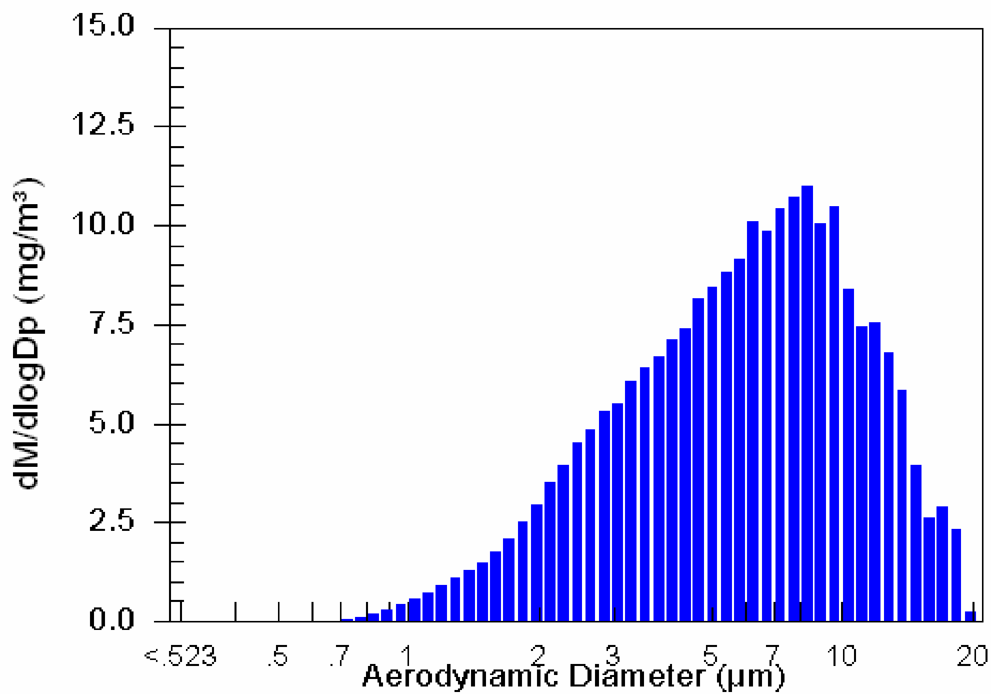

Figure 3-14. Feb. 16, 2005 test. APS size distribution plot of yellow Visolite release.

Table 3-4. Feb. 16, 2005 test. Numerical analysis of APS data of yellow Visolite release..

	Number Weighted Particle Size	**Surface Weighted Particle Size**	**Mass Weighted Particle Size**
Median (µm)	1.49	3.62	6.23
Mean (µm)	1.91	4.61	6.89
Geo. Mean (µm)	1.61	3.65	5.74
Mode (µm)	1.11	2.84	8.35
Geo. St. Dev.	1.72	2.00	1.89
Total Conc.	623(#/cm³)	9.51e+03(µm²/cm³)	7.28(mg/m³)
Total Counts	277036		

Table 3-5. Feb. 16, 2005 test. Filter Data from yellow Visolite release.

2/16/2005 - FACILITY TEST, YELLOW			
FILTER #	PRE	POST	AVERAGE (mg)
1	26.11	26.2	0.09
2	26.83	26.84	0.01
3	26.55	26.58	0.03

3.5 Friday February 18th – Chamber Test with Pink Visolite

Tests were done to experimentally characterize release of the pink Visolite powder. Roughly 3 grams of pink Visolite powder was released into the make shift aerosol chamber in the walk-in freezer using a puffer dispersion device. Powder dispersion in the chamber was measured using the same equipment as for the Feb. 14, 2005 experiments with yellow Visolite.

The DustTrak results shown in Figure 3-15 show a higher initial concentration of ~20 mg/m^3 than the corresponding yellow Visolite test done on Monday February 14th. The concentration decay rate is consistent with a particle size of 33 micrometers, which is comparable with, or slightly larger, than the yellow powder. This is again somewhat higher than the Visolite stated native particle size distribution, indicating the presence of agglomerated particles. The airborne particle concentration based in the DustTrak measurements is initially 20 mg/m^3 giving an initial dispersion of 390 mg into the chamber. 3000 mg of Visolite was dispersed, so the particle concentration measurements indicate that most of the powder was too large to remain suspended and fell out immediately. The observed dispersion efficiency of ~12% suggested that the puffers were not an effective method for dispersing the Visolite powder. The filter results in Table 3-6 correspond to an average integral concentration of 350 $mg\text{-}min/m^3$, which is higher than observed with the yellow Visolite. These measurements are generally consistent with the observed DustTrak data.

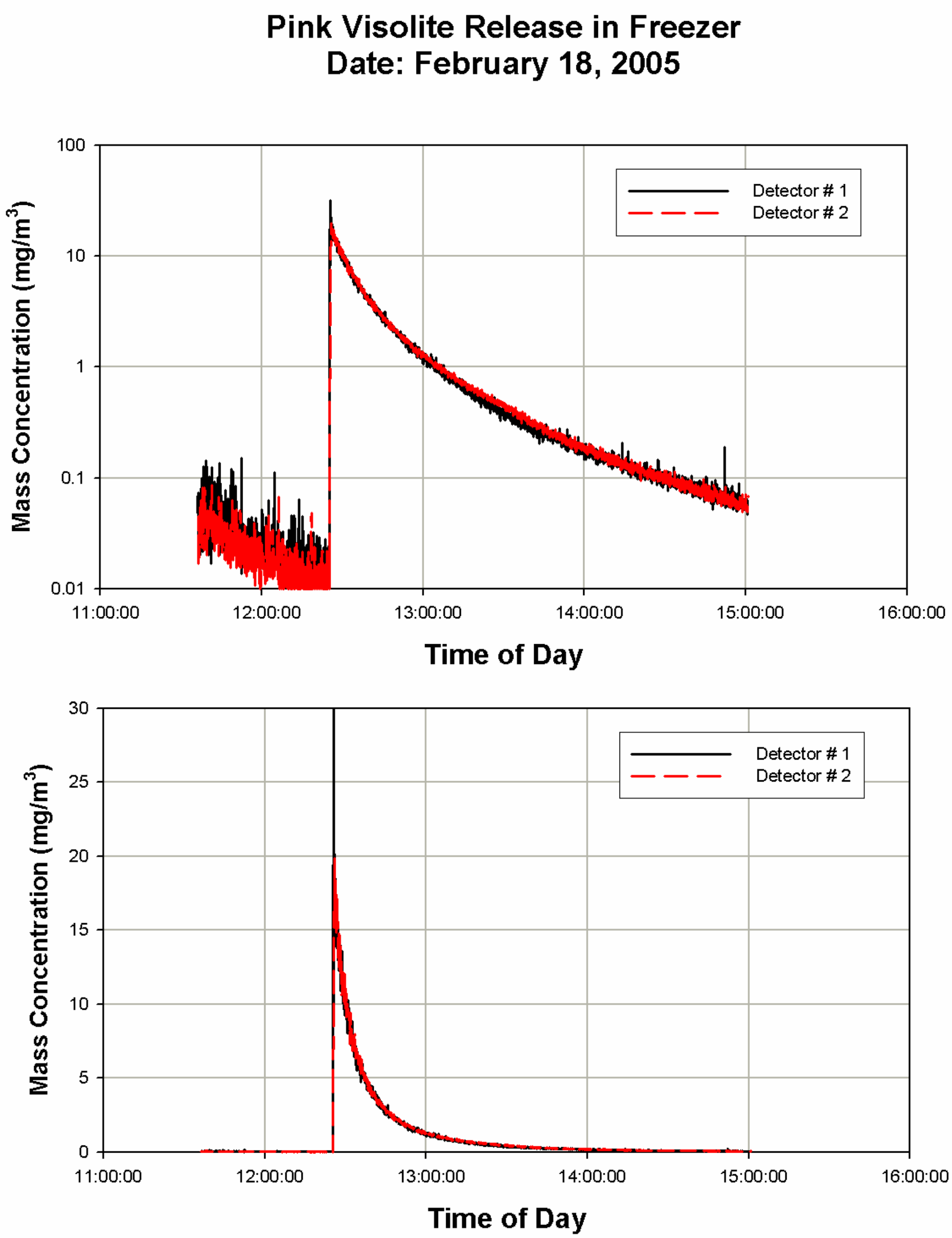

Figure 3-15. Feb. 18, 2005 test. DustTrak plot from pink Visolite.

Table 3-6. Feb. 18, 2005 test. Filter Data from pink Visolite.

2/18/2005 - CHAMBER TEST, PINK			
FILTER #	PRE	POST	AVERAGE
1	52.59	54.32	1.73
2	26.44	28.23	1.79
3	26.45	26.48	0.03 (pump failed)

3.6 Monday February 21th – Pink Visolite Tracer Release, NIOSH Test

Pink Visolite was used as a Bio-simulant for the actual NIOSH joint exercise. At 11:30am, approximately 37 grams of Pink Visolite was dispersed using the BGI powder disperser. The release location is the conference room on the lower level of the Coronado Club. Ten DustTraks, were deployed at same locations as smoke test (Table 3-2). The APS, two TSI Velocity Meters and three 25mm filter holders loaded with glass fiber filters were also used. Velocity Meter # 2 was located at the top of the stairs and Velocity Meter # 1 was located at the entrance to the Ball Room. Approximately 240 plus 12"x12" black vinyl tiles were laid down through out the Coronado Club, upper and lower levels. All locations were logged by BROOM PDA's.

The DustTrak results shown in Figure 3-16 shows how the airborne particle concentrations varied with time at the various locations in the building. Note that the use of the BGI powder disperser allowed comparable aerosol concentrations to be achieved with roughly 6 times less powder.

The APS results in Figure 3-17 shows the same qualitative temporal behavior as DustTrak 2. The size distribution shown in Figure 3-18, the numerical analysis shown in Table 3-7, and the filter data shown in Table 3-8 are consistent with the results obtained for the yellow Visolite. The velocity data in Figure 3-19 indicate that there was consistently airflow through the building, but the HVAC system was cycling on a roughly 20 minute timescale.

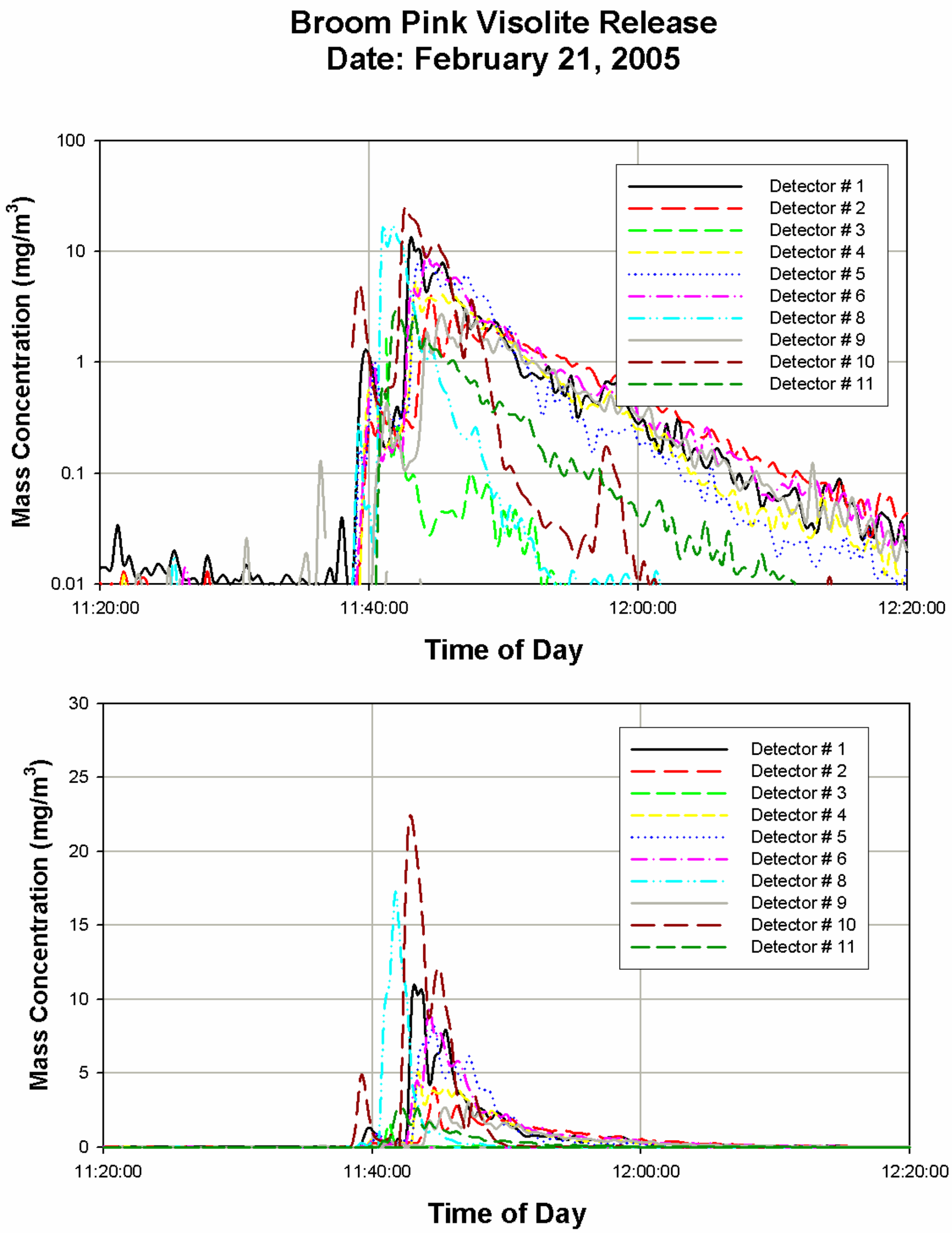

Figure 3-16. Feb. 21, 2005 test. DustTrak plot for Pink Visolite release.

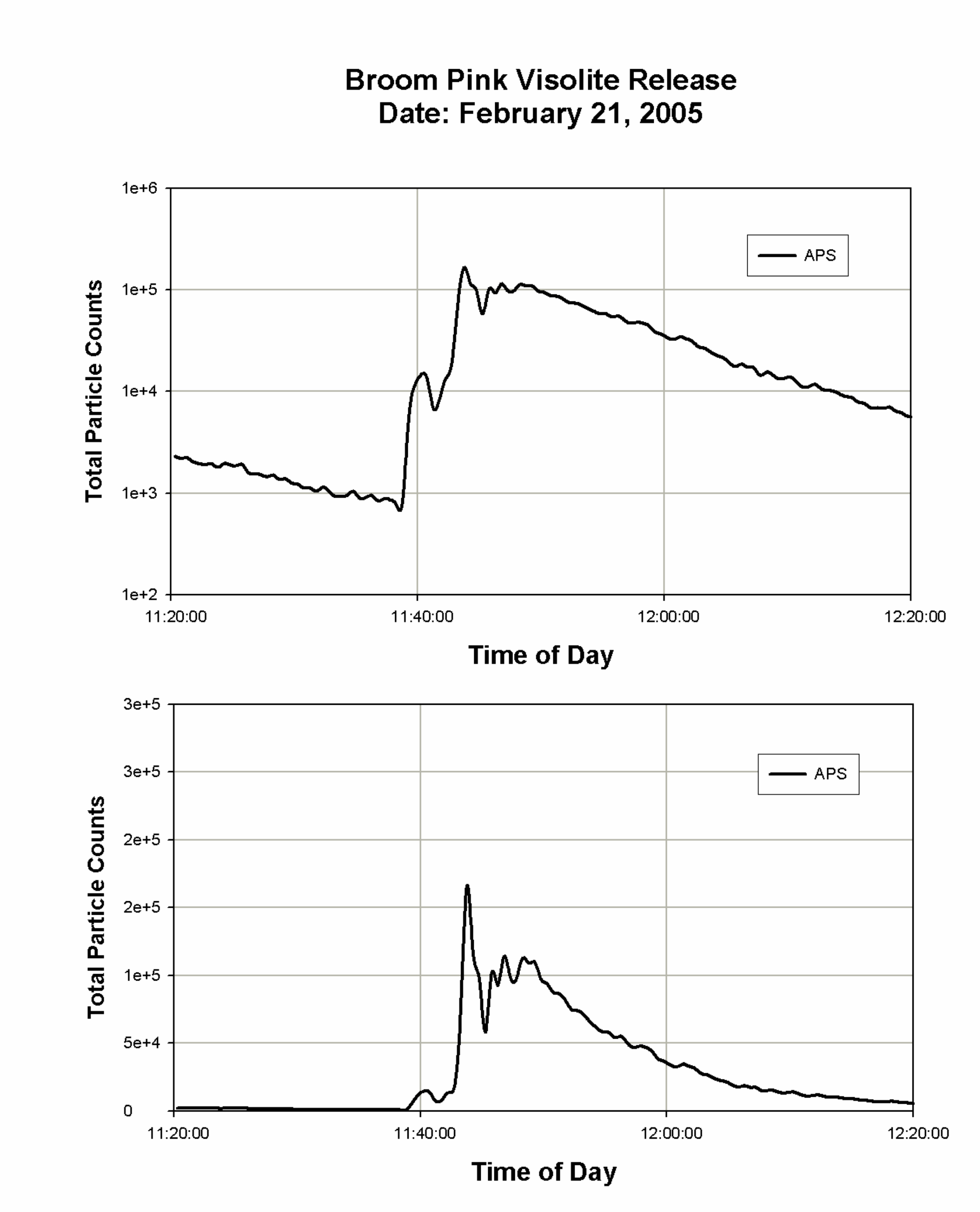

Figure 3-17. Feb. 21, 2005 test. APS plot of pink Visolite release.

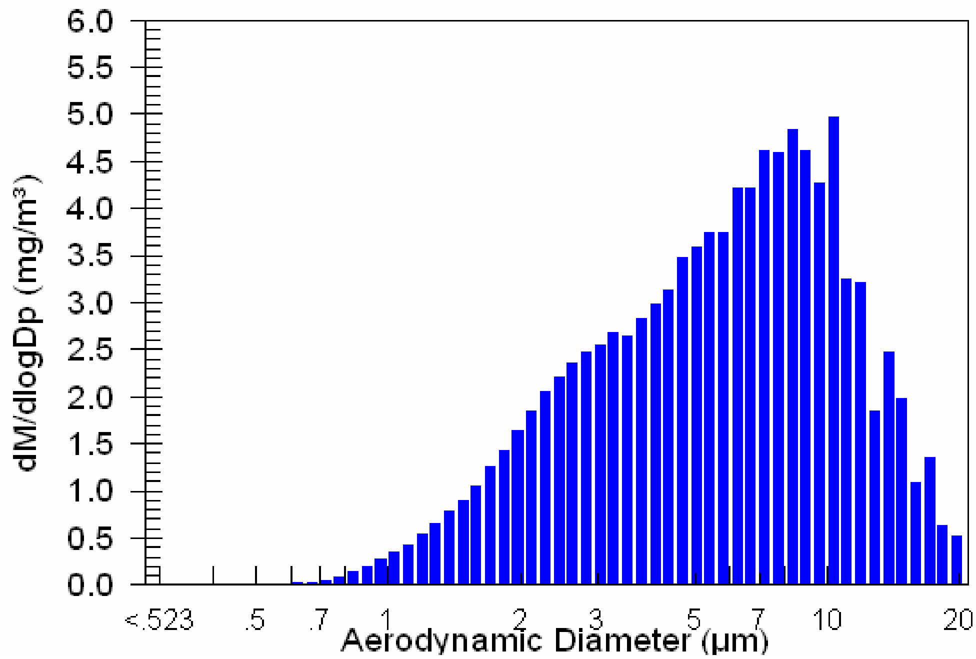

Figure 3-18. Feb. 21, 2005 test. APS size distribution plot of pink Visolite release.

Table 3-7. Feb. 21, 2005 test. Numerical analysis of APS data for pink Visolite release.

	Number Weighted Particle Size	**Surface Weighted Particle Size**	**Mass Weighted Particle Size**
Median (µm)	1.36	3.20	6.08
Mean (µm)	1.71	4.30	6.72
Geo. Mean (µm)	1.46	3.33	5.49
Mode (µm)	1.20	2.46	10.4
Geo. St. Dev.	1.70	2.06	1.96
Total Conc.	378(#/cm³)	4.59e+03(µm²/cm³)	3.28(mg/m³)
Total Counts	166511		

Table 3-8. Feb. 21, 2005 test. Filter Data from pink Visolite release.

2/21/2005 - FACILITY TEST, PINK			
FILTER #	PRE	POST	AVERAGE
1	26.42	26.92	0.5
2	26.51	26.91	0.4
3	26.8	26.86	0.06

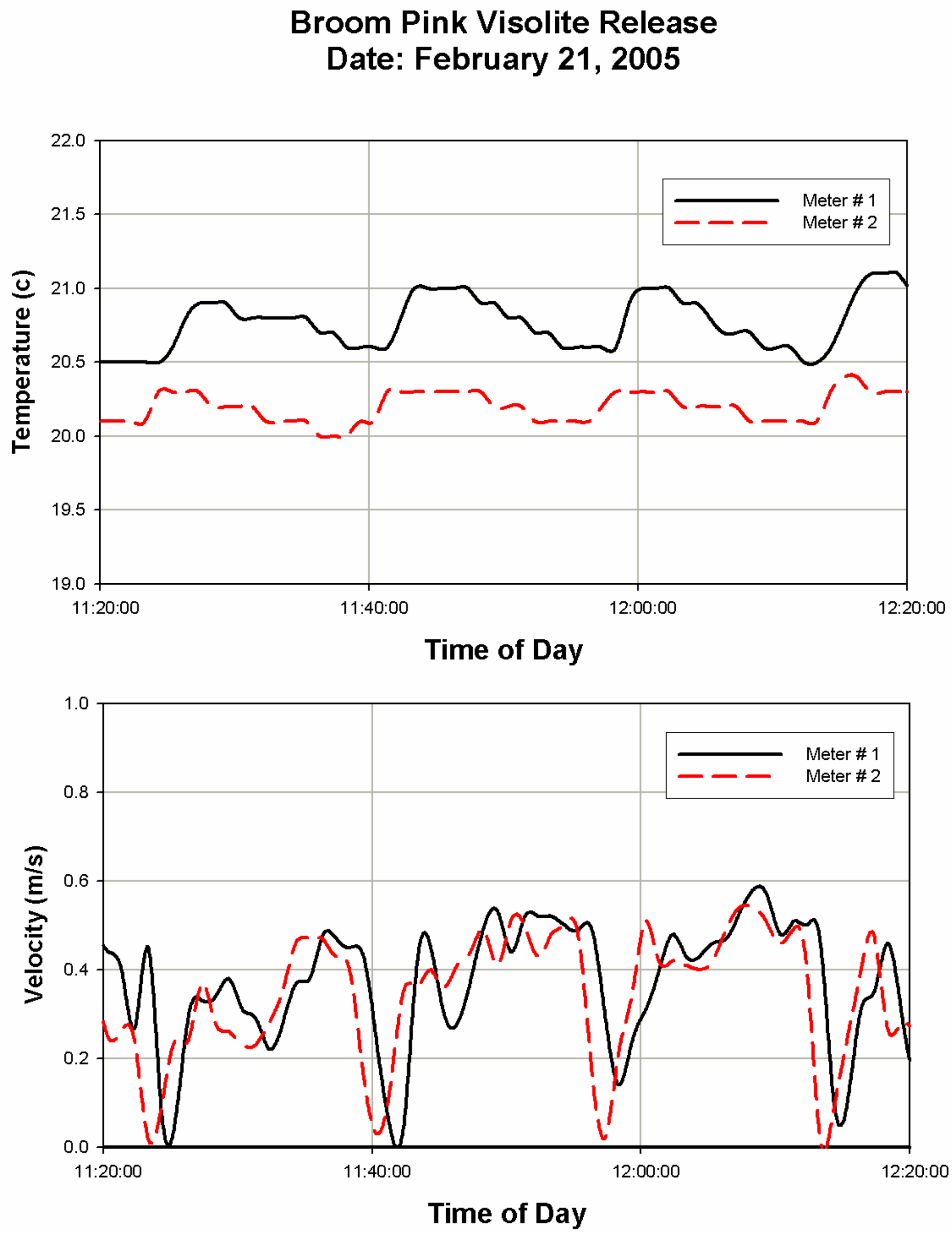

Figure 3-19. Feb. 21, 2005 test. Plot from Velocity Meters.

3.7 Monday February 28th – Chamber Test with Pink Visolite

The make shift aerosol chamber in the walk-in freezer at the Coronado Club Kitchen was used for this test. Sample surfaces were provided and setup by personnel from the Chemical and Biological Systems Department. Two TSI DustTraks and three 25mm filter holders loaded with glass fiber filters were setup in the chamber. The filter flowrates were maintained at 5 lpm with personnel sampling pumps manufactured by SKC. At approximately 2:03 pm, 5.25 grams of pink Visolite was dispersed into the aerosol chamber using a BGI powder disperser. The DustTraks measured and logged the airborne mass concentration at 2 second intervals. The APS was also setup to log data for this test.

The DustTrak results in Figure 3-20 show a higher initial particle concentration than the pink Visolite test done on February 18. This observation is consistent with the BGI powder disperser being more efficient than the puffers. The initial decay rate in the DustTrak curves are consistent with a 33 micrometer particle size. Using this particle size, we conclude that the BGI powder disperser was 17% effective at dispersing the pink Visolite.

The APS size distribution shown in Figure 3-21 shows a smaller peak particle size than obtained by analyzing the DustTrak measurements, but the sensitivity of the APS instrument starts falling off in the 10-20 micrometer size range. The numerical analysis shown in Table 3-9 gives a total mass concentration consistent with the DustTrak results.

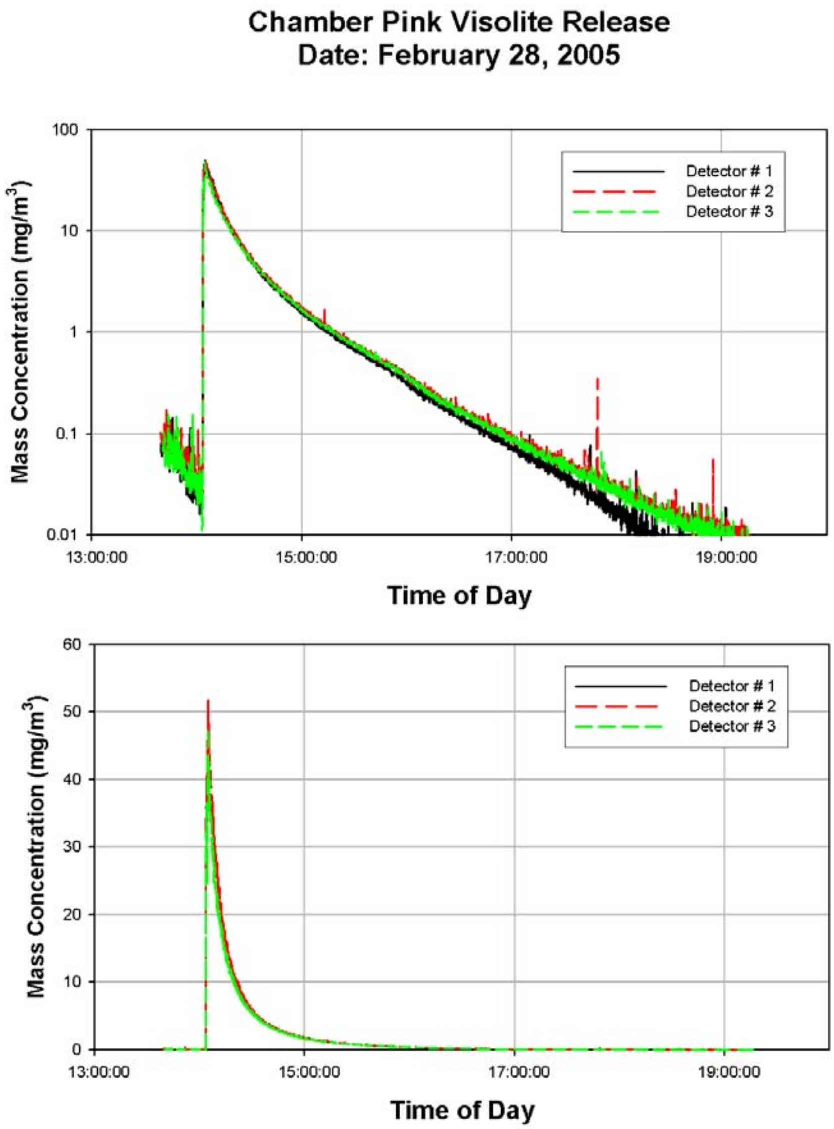

Figure 3-20. Feb. 28, 2005 test. DustTrak plot for Pink Visolite.

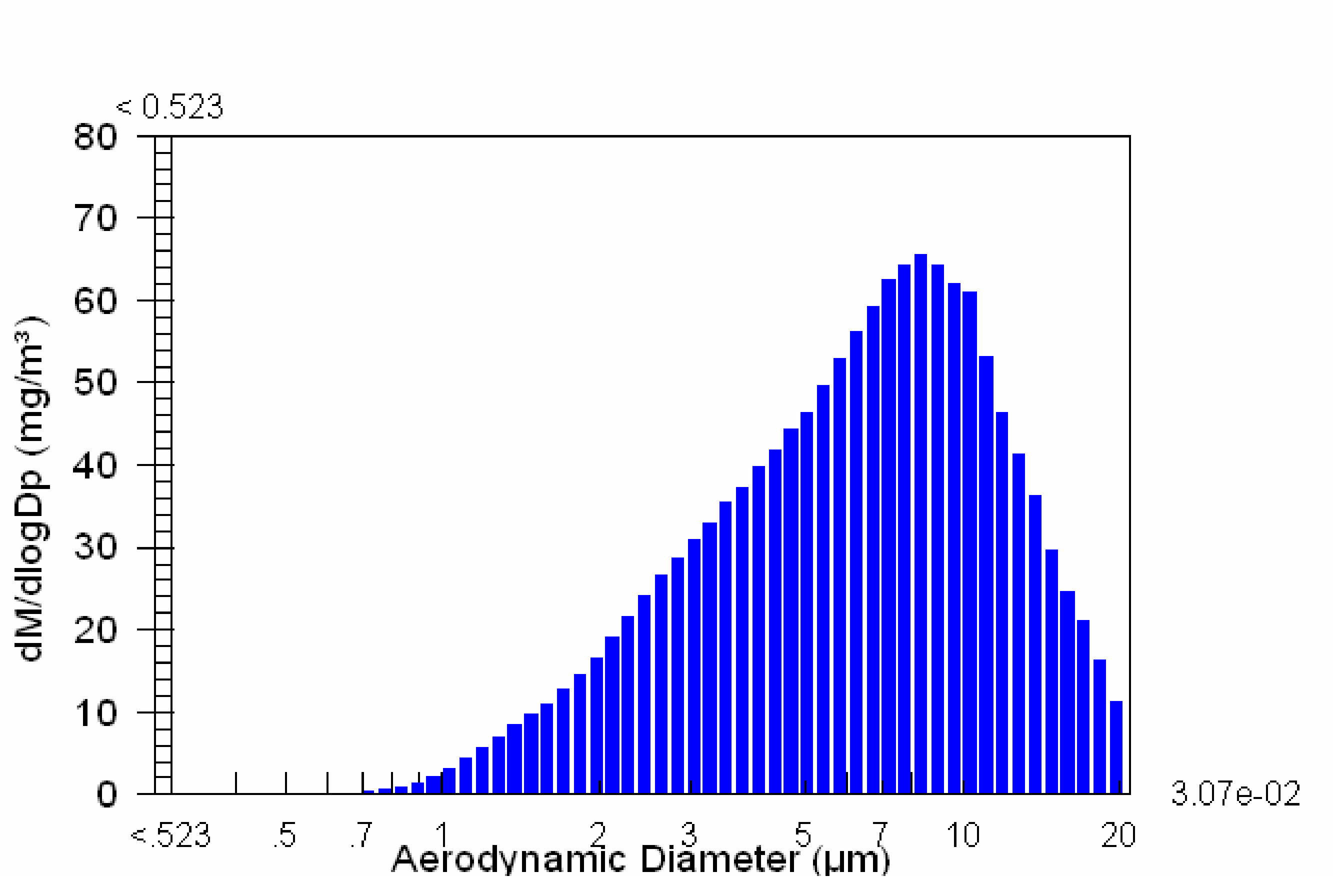

Figure 3-21. Feb. 28, 2005 test. APS size distribution plot of pink Visolite.

Table 3-9. Feb. 28, 2005 test. Numerical analysis of APS data for pink Visolite.

	Number Weighted Particle Size	**Surface Weighted Particle Size**	**Mass Weighted Particle Size**
Median (µm)	1.49	3.70	6.63
Mean (µm)	1.91	4.78	7.29
Geo. Mean (µm)	1.62	3.73	6.03
Mode (µm)	1.20	2.64	8.35
Geo. St. Dev.	1.71	2.04	1.92
Total Conc.	3.69e+03(#/cm³)	5.52e+04(µm²/cm³)	43.9(mg/m³)
Total Counts	1588894		

3.8 Impactor Measurement of Pink Visolite

This measurement was done to provide an independent measurement of the mass-weighted aerosol size distribution. This instrument provides data over a wider size range than the APS.

The Marple 298 impactor is an eight stage, multi-jet cascade impactor, designed to operate at a nominal flowrate of 2 liter per minute. The impactor is designed to measure aerodynamic particle size distributions from 0.4 to 21 microns with a final filter which collects all aerosol analyte. The impactor is constructed of aluminum with glass fiber substrate collection media. Sampled air enters the inlet adapter and accelerates through six radial slots in the first impactor stage. Figure 3-22 is a photograph of the Marple Impactor with the inlet adapter and an exploded view of one of the filter stages. The inlet adapter eliminates ashes and debris from the sampler. Particles larger than the cut-point of the first stage impact on the pre-cut collection substrate. Airstream flows through the narrower slots in the second impactor stage, smaller particles impact on the second collection substrate, and so on. The width of the radial slots is constant for each stage but are smaller for each succeeding stage. Thus, the jet velocity is higher for each succeeding stage, and smaller particles eventually acquire sufficient momentum to impact on one of the collection substrates. After the last impactor stage, remaining fine particles are collected by the built-in 34mm filter.

Figure 3-22. Photograph of Maple Cascade Impactor and collection Substrate

Prior to sampling, collection substrates and back-up filters are weighed, recorded and placed in the impactor. The sampling flow rate is controlled with a critical orifice which is connected to the outlet of the impactor. The sampler flow rate is measured with a Gilibrator Primary Flow Calibrator, Model # D-800268. The sampling flowrate is nominally set at 2 lpm. The impactors are attached to 3/8” Inner diameter tube and sampled from a small aerosol chamber. After sampling, the substrates and filter are weighed. Weight increase on each substrate is the mass of particles in the size range of that impactor stage. The total weight of particles on all stages and filter is added and the percent particle mass in each size range is calculated. Respirable particle mass fraction is determined from the particle size distribution.

Figure 3-23 shows the size distribution measured by the impactor. The particle size distribution measured by the impactor below 10 micrometers is consistent with the APS volume-weighted distribution. The impactor data indicate that material was present with a much larger particle size than the APS could measure. This larger material, however, would fall out rapidly near the dispersion point, and not contribute significantly to deposition at greater distances throughout the building.

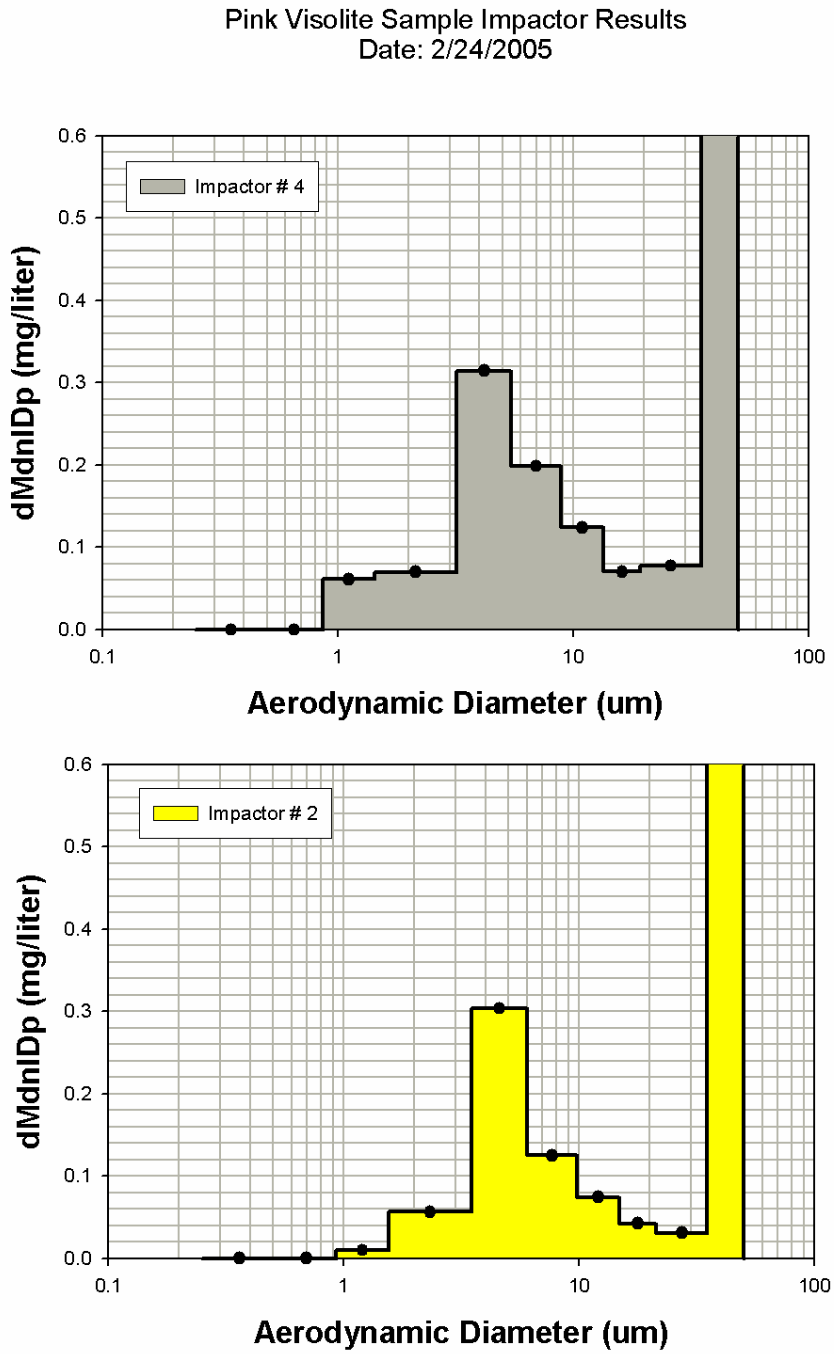

Figure 3-23. Size Distribution plot from Impactor

4 Visolite sampling and analysis methods

Gary S. Brown, Raymond M. Boucher, Jonathan Leonard, Mathew S. Tezak, Kathryn S. Walsh, and Mollye C. Wilson

4.1 Sampling Methods

Environmental surface sampling is used to determine the extent and degree of contamination on indoor surfaces. Environmental samples were collected for the Sandia/NIOSH exercise using Centers for Disease Control and Prevention recommended swab, wipe, and micro-cassette vacuum methods (CDC 2002). The swab sample collection method was used on small area (25 cm^2) non-porous surfaces, such as paint, tile, glass and metal. The wipe sample collection method was used on moderate area (1,000 cm^2) non-porous vinyl tile surfaces. The micro-cassette vacuum sample collection method was used on large area (10,000 cm^2) porous carpet surfaces.

Figure 4-1. Swabs, wipes and micro-cassette vacuum filter used for sampling.

Swab Sample Collection: Visolite swab samples were collected from 25 cm^2 (identified by 2.5 cm x 10 cm cardboard template) non-porous surfaces using clean swabs moistened with 0.05 mL (50 µL) de-ionized water by moving the swab back and forth across the surface with several horizontal strokes, then several vertical strokes. The swab was also rotated during sampling to ensure that the entire surface of the swab was exposed. After sample collection, the swab was placed in a pre-labeled, 15 mL Blue Falcon screw-top tube (Becton Dickinson Labware, Franklin Lakes, NJ) and sealed with a cap.

Wipe Sample Collection: Visolite wipe samples were collected from pre-located 930 cm^2 non-porous vinyl tile surfaces by moistening a clean wipe with 1.0 ml sterile deionized water and thoroughly wiping using several horizontal strokes, folding the exposed side of the pad, and making several vertical strokes over the sample surface area. After sample collection, the wipe was placed in a pre-labeled, 50 mL Blue Falcon screw-top tube (Becton Dickinson Labware, Franklin Lakes, NJ) and sealed with a cap.

Micro-cassette Vacuum Sample Collection: Visolite vacuum samples were collected onto a 37 mm, 0.2 micrometer, PTFE (polytetrafluoroethylene) filter contained in a polycarbonate cassette at a 20 L/min flow rate. Samples were collected from 10,000 cm^2 (identified by 100 cm x 100 cm template) carpet surfaces by slowly moving the 6 mm ID vacuum nozzle back and forth touching the sample surface.

4.2 Visolite Analysis Methods

This section provides experimental details on the processing and analysis of the Visolite samples. The amount of Visolite powder on a sample was determined by extracting the dye from the carbonate powder into isopropanol, then determining the amount of dye in the solution by fluorimetry. The calibration process involved preparing and measuring the fluorescence from standard samples. These consisted of 150 mg of Visolite powder added to 10 ml of isopropanol, which were then diluted to cover a range of concentrations.

For the yellow Visolite powder, the 460-520 nm wavelength range was examined. For the pink Visolite powder, the 540 – 600 nm wavelength range was examined. No background correction was needed. The pink Visolite samples also contained yellow Visolite powder, as the building was not cleaned between releases. Thus, fluorimetry analysis was done twice on those samples using different gain settings in order to allow both the pink and yellow dyes to be quantified.

Swab Analysis: A 10 ml aliquot of isopropanol was added to the 15 ml sample tube containing the swab. The tube was sonicated for 15 minutes at sweeping frequencies between 38.5 and 40.5 kHz and an average power of 180 W to remove Visolite powder from the swab and extract the fluorescent dye into the isopropanol solvent. The tube was then centrifuged to clarify the extraction solution. A 4 ml aliquot of the extraction solution was then pipetted into a 1 cm cuvette and analyzed for fluorescence intensity at the specified wavelength. The resulting integrated fluorescence intensity value was compared to the calibration curve and mass of Visolite powder determined.

Wipe Analysis: A 30 ml aliquot of isopropanol was added to the 50 ml sample tube containing the wipe. The tube was sonicated for 15 minutes at sweeping frequencies between 38.5 and 40.5 kHz and an average power of 180 W to remove Visolite powder from the swab and extract the fluorescent dye into the isopropanol solvent. The tube was then centrifuged to clarify the extraction solution. A 4 ml aliquot of the extraction solution was then pipetted into a 1 cm cuvette and analyzed for fluorescence intensity at the specified wavelength. The resulting integrated fluorescence intensity value was compared to the calibration curve and mass of Visolite powder determined.

Vacuum Filter Analysis: A 30 ml aliquot of isopropanol was added to the 50 ml sample tube containing the vacuum filter. The tube was sonicated for 15 minutes at sweeping frequencies between 38.5 and 40.5 kHz and an average power of 180 W to remove Visolite powder from the swab and extract the fluorescent dye into the isopropanol solvent. The tube was then centrifuged to clarify the extraction solution. A 4 ml aliquot of the extraction solution was then pipetted into a 1 cm cuvette and analyzed for fluorescence intensity at the specified wavelength. The resulting integrated fluorescence intensity value was compared to the calibration curve and mass of Visolite powder determined.

4.3 References

CDC, Centers for Disease Control and Prevention. Procedures for collecting surface environmental samples for culturing *B. anthracis*. 2002. Available from: URL: http://www.bt.cdc.gov/Agent/Anthrax/environmental-sampling-apr2002.asp. Accessed February 6, 2006.

5 BROOM Tool

James Ramsey, Patrick Finley, Brad Melton

5.1 Introduction

The Building Restoration Operations Optimization Model (BROOM) is a software product developed to assist in the restoration of major transport facilities in the event of an attack involving chemical or biological materials. This multifaceted tool is intended to aid the collection of environmental and clearance samples, guide characterization efforts, manage collected data, and provide users with a visual interface to access such data. In this section, we discuss the general structure and capabilities of the tool. The statistical analysis aspects are described in more detail in Section 8.2 of this report.

The BROOM software consists of two independent but interfacing applications. The first application runs on a handheld PDA (personal digital assistant) and is designed to collect and record surface sampling data during the characterization and verification phases of decontamination. The device may also be used to record the position of biological indicators prior to fumigation in the decontamination phase. The second application runs on a Windows desktop platform and serves to manage, analyze, and visualize sampling results. Data is exchanged between the two applications through wireless networking protocols.

The handheld device, shown in Figure 5-1, is optionally equipped with a commercially available barcode scanner and wireless laser range finder. The barcode scanner provides a means of uniquely identifying and tracking samples from the point of origination through the laboratory analysis process. The laser range finder is used to precisely define the location of the sampled surface with respect to interior structures of the building. Additional data, such as the properties of the sampling surface, sample type, date, and time, are also recorded effortlessly. The handheld device can be assembled for about $1800 at the time of this writing.

Figure 5-1. Handheld device part of BROOM tool.

The desktop application, shown in Figure 5-2, works in conjunction with a SQL Server database to store, retrieve, visualize, and analyze the laboratory results of sampling activities. The database design is significant in that it allows simultaneous multiple user access to sample data. Building floor plans and other pertinent drawings of interest are organized by floor and also stored in the database. Database storage is also a key component of the modular software design. Analysis tools can be added relatively quickly to BROOM using generic procedures that retrieve inputs and write outputs to the database. Furthermore, the outputs from one tool are then readily available as inputs to one more other tools.

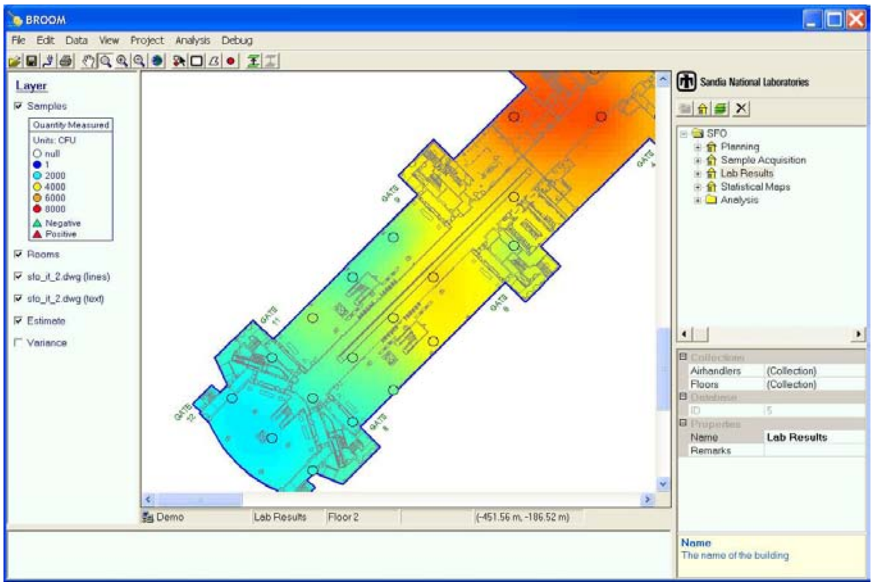

Figure 5-2. Desktop application part of BROOM tool.

5.2 Software Architecture

An overview of the BROOM data flow process is presented in Figure 5-3. Building floor plans and proposed sampling locations can be downloaded from a BROOM equipped computer located either in a clean area inside the building or at a safe distance outside the building to the handheld device over a wireless network. The data collected during sample acquisition are temporarily stored in the handheld device and upon completion, transmitted back to the computer over the same wireless network. The now contaminated handheld device may be left in the building to be fumigated with the rest of the building or inserted in a cradle to charge the batteries for future sampling efforts.

Immediately following the receipt of data from the PDA, the BROOM computer forwards this information on to a SQL Server database where it is permanently stored and maintained. At this point, the data may be accessed by authorized laboratories by querying the database directly or exported to xml using the BROOM desktop software. Similarly, results from laboratory analysis may be imported to BROOM by accessing the database directly or by formatting such data in xml and then reading that data with the desktop application. Other interested parties (i.e. analyst, command center), with appropriate authorization, may display and analyze sampling results concurrent with the data acquisition and laboratory analysis activities through the BROOM desktop application.

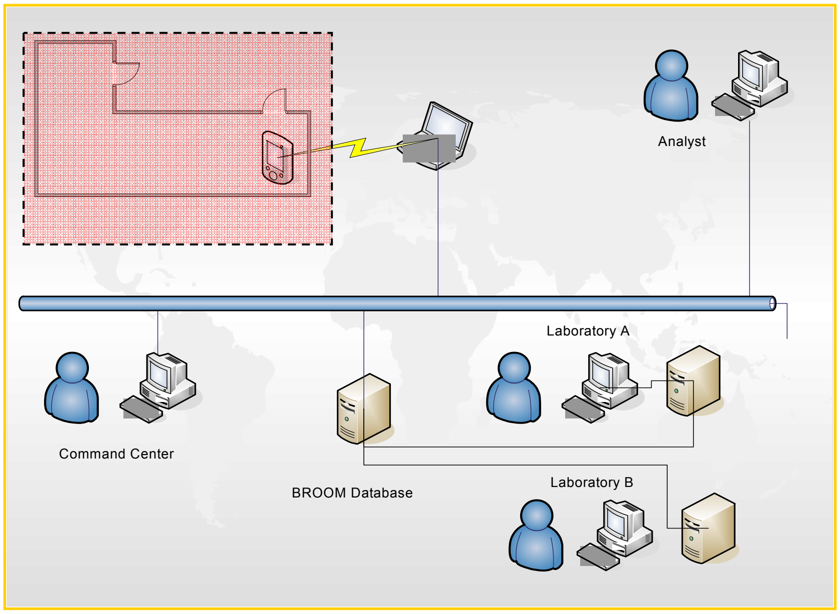

Figure 5-3. Data flow in BROOM tool.

The data in BROOM are organized into projects, as shown Figure 5-4. Each project may contain one or more buildings. Each building is made up of a collection of floors, a sample dataset, and an analysis folder. Selecting a floor displays the samples that have been collected on that floor as well as any drawings of the floor. Analysis results are accessed by opening the analysis folder. These data are subdivided into user defined scenarios (i.e. Characterization), and workspaces (i.e. Contamination Maps). Within a given workspace, the tools used to arrive at a particular objective are displayed and the specific inputs and outputs of each individual tool (i.e. KT3D) may be accessed and viewed.

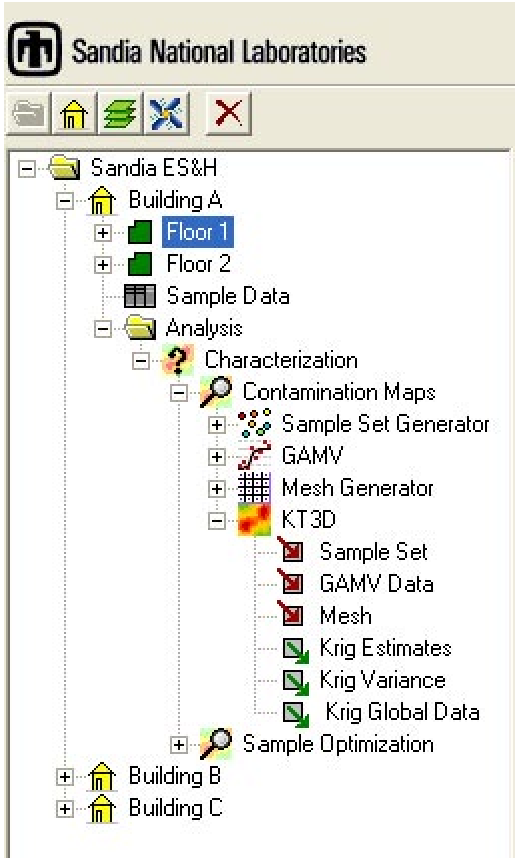

Figure 5-4. Example of data organized into projects within BROOM tool.

5.3 Data Visualization

Sampling results are displayed in a two-dimensional geographical information system (GIS), Figure 5-5, or three-dimensional activeX viewer, Figure 5-6. The complete record of a particular sample is retrieved by simply clicking on the sample point in either the 2D or 3D viewer. This record includes information regarding the location, surface sampled, chain of custody, and laboratory results.

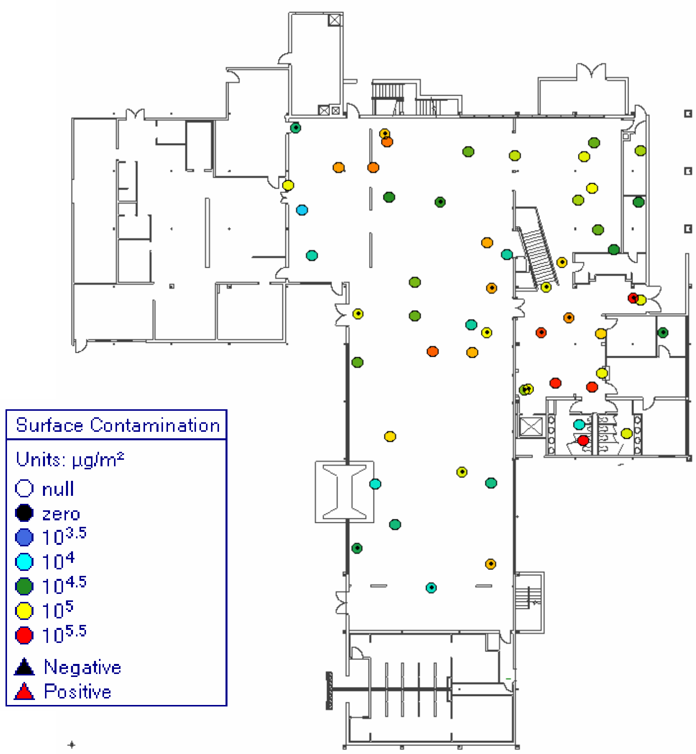

Figure 5-5. Two-dimensional visualization of surface samples in BROOM Tool.

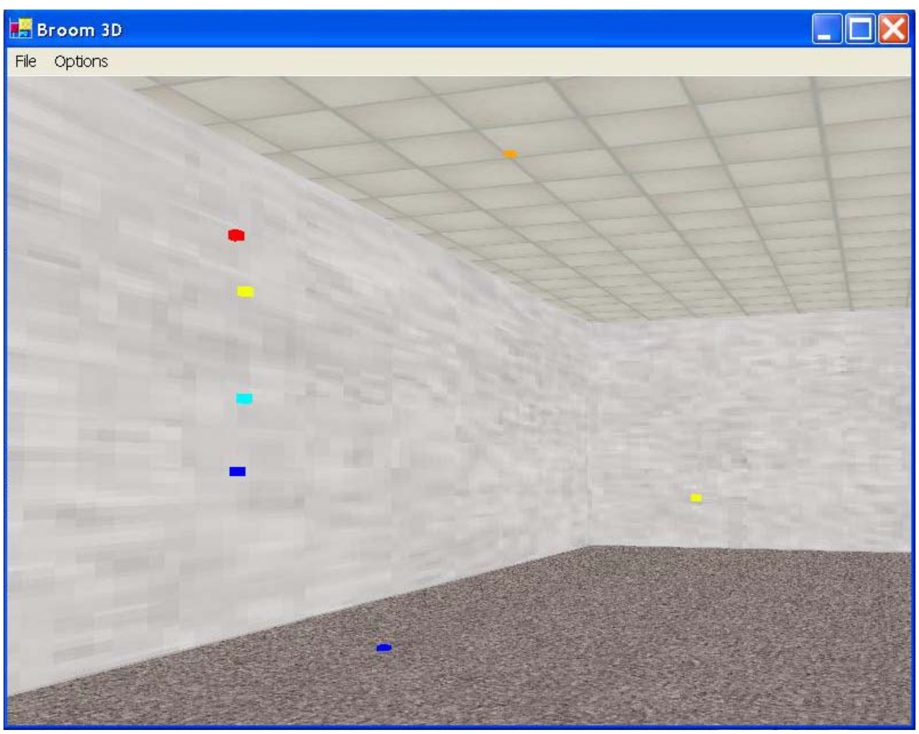

Figure 5-6. Three-dimensional visualization of surface samples in BROOM Tool.

5.4 Analysis

The statistical analysis features of the BROOM tool are briefly presented here and are described in detail in Section 8.2 of this report. Surface sampling measurements may be analyzed for spatial correlation and then interpolated using a stochastic kriging algorithm implemented in BROOM, as shown in the left side of Figure 5-7. Kriging has been shown to provide the best linear unbiased estimate and is widely used in the environmental and natural resource industries (Isaaks and R.M Srivastava, 1989), and is described in detail in Section 8.2. The kriging algorithm also provides an estimate of prediction uncertainty via the kriging variance, as shown in the right side of Figure 5-7. Combining the information from the two maps can provide a strong basis to specify the probability of exceeding specific threshold contaminant level, as well as guiding subsequent sampling efforts.

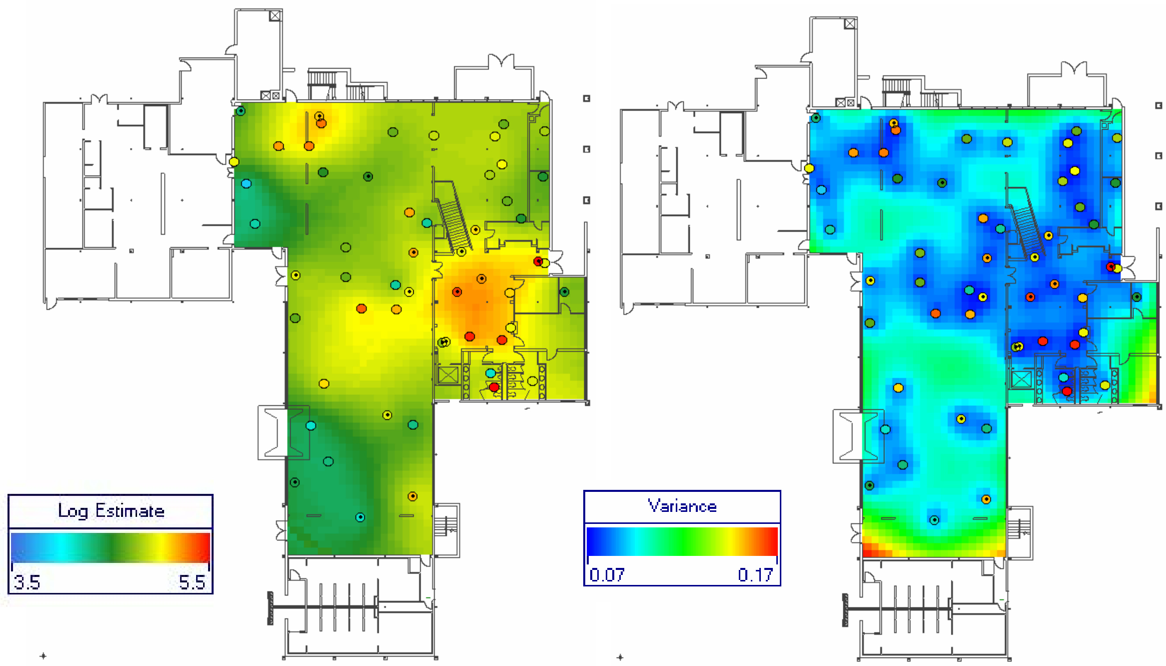

Figure 5-7. Example of statistical analysis in BROOM tool. Kriging estimate (left), Kriging Variance (right).

5.5 Conclusions

BROOM is a powerful sample acquisition, data management, visualization, and analysis tool, designed to speedup and improve the overall efficiency of the restoration process for an indoor facility contaminated by a biological agent. The PDA application utilizes readily available commercial hardware and has unique indoor positioning capabilities. The desktop application works in conjunction with a SQL Server database to store, retrieve, visualize, and analyze the laboratory results of sampling activities. Kriging is used to produce maps of the contamination and also provides an estimate of the uncertainty in that map. Finally, the tool is capable of recommending optimal sampling locations to characterize hotspots or define the extent of contamination.

5.6 References

E.H. Isaaks and R.M Srivastava, An Introduction to Applied Geostatistics, Oxford University Press, Oxford, 1989, p. 278.

6 Building Data

James Ramsey

6.1 Facility Description

The Coronado Club (C-Club), shown in Figure 6-1, is a one-story recreational facility with a large underground basement. The main floor covers approximately 15,000 ft^2 and includes a large open area running north to south that is similar in many regards to a short segment of an airport concourse or subway station, Figure 6-2. In contrast, the basement is made up of several divided meeting rooms and smaller office spaces spanning 9000 ft^2, Figure 6-3. These rooms are comparable in many aspects to common office space and/or shopping areas. Together, the two floors cover approximately 24,000 ft^2 and include a variety of room shapes and sizes similar to what one might find at a public transportation facility.

Figure 6-1. Air Photo of Coronado Club showing Facility Layout. North is to right edge of photo.

The ceiling height is nominally 10 ft on the main floor. There are two regions in the ballroom and dining area that reach as high as 13 ft. In the basement, a false ceiling has been installed at 7 ft 9 inches. The plenum space above the false ceiling is 1 ft 9 inches high. The total distance from the basement floor to the main floor is approximately 20 ft.

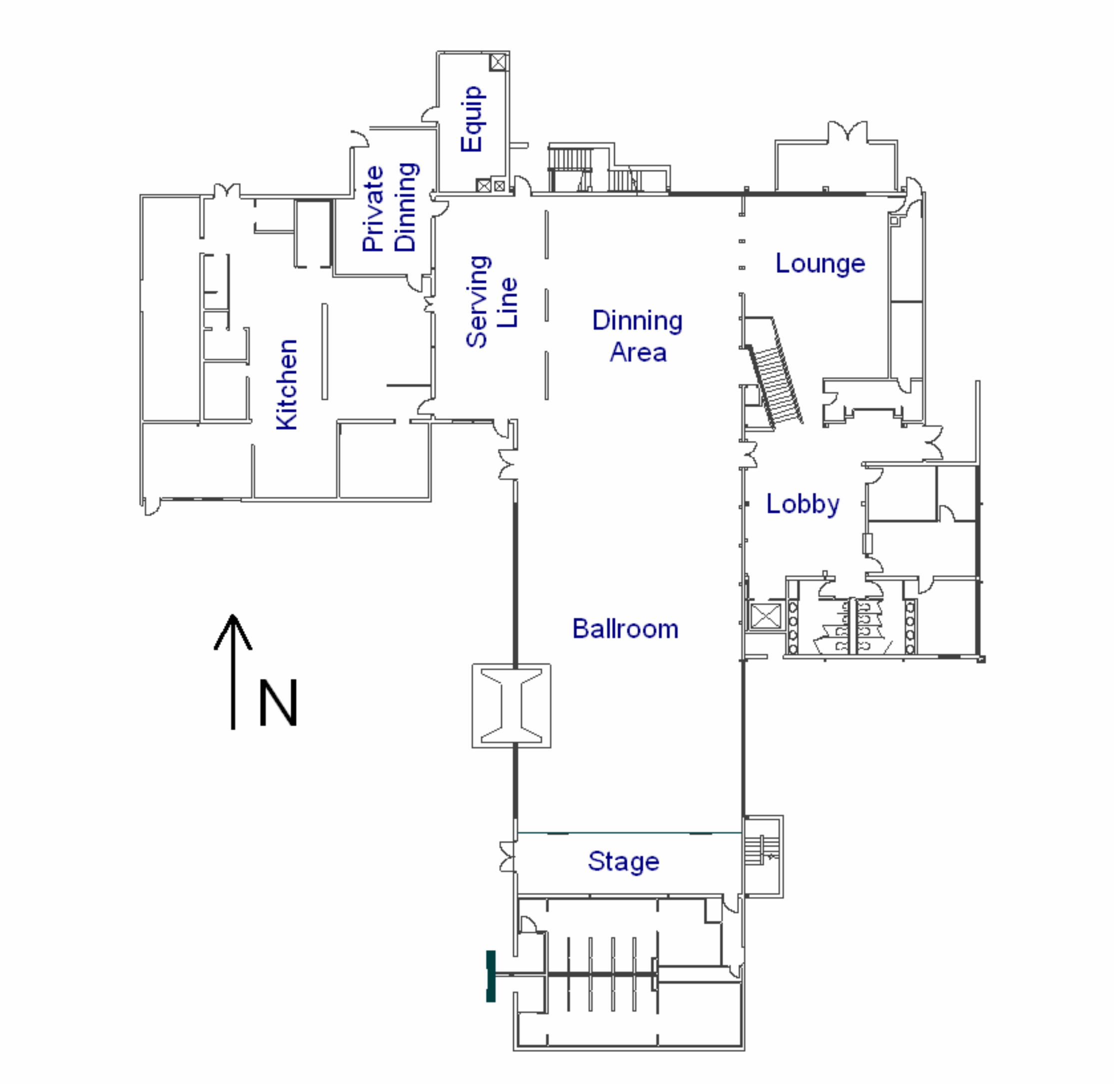

Figure 6-2. Coronado Club Main Level Floor Plan

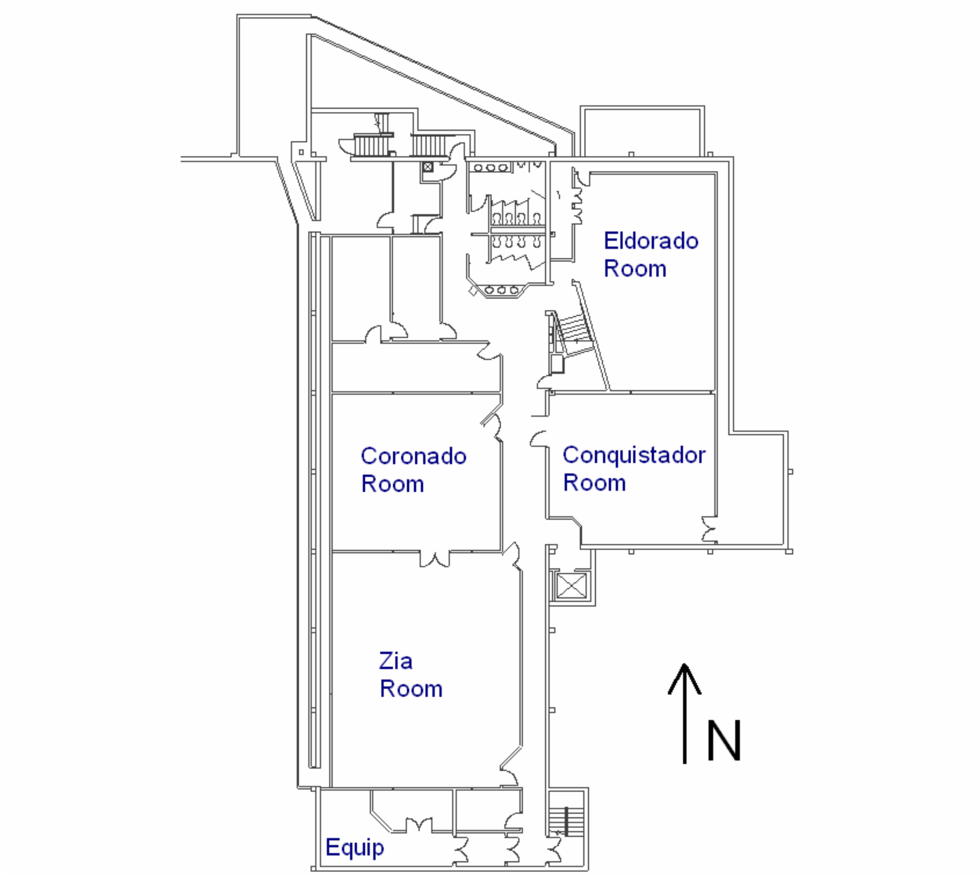

Figure 6-3. Coronado Club Basement Level Floor Plan

6.2 HVAC Systems

The building is heated principally by forced air generated at four separate air handling systems. A small area on the main floor consisting of the lobby and adjacent offices are heated by convective hot water running along the baseboard and the kitchen is not heated.

The main floor is conveniently divided into four principal HVAC zones (Figure 6-4). The *Convective* zone is heated by baseboard heat and was thus not directly served by a forced-air system during the period of this test. The *AH4* zone covers the northern portion of the main floor, enclosing the private dining room, the serving line, the dining room, the lounge and approximately half of the lobby. This zone is served by a large airhandler unit located in the large mechanical equipment room off of the north wall of the structure. The *AH5* zone covers the ballroom and is served by a roof-mounted air handler. The kitchen and locker rooms are not served by a central forced air system and are grouped into the *Not Served* HVAC zone.

Two HVAC zones divide the basement along the central corridor (Figure 6-5). The larger *AH1* zone includes the corridor and all rooms west of it. It is served by an air handler located in the mechanical room in the northwest corner of the basement. The *AH2* covers only the Eldorado and Conquistador rooms. It is served by an air handling unit located in the mechanical room due north of the Eldorado room.

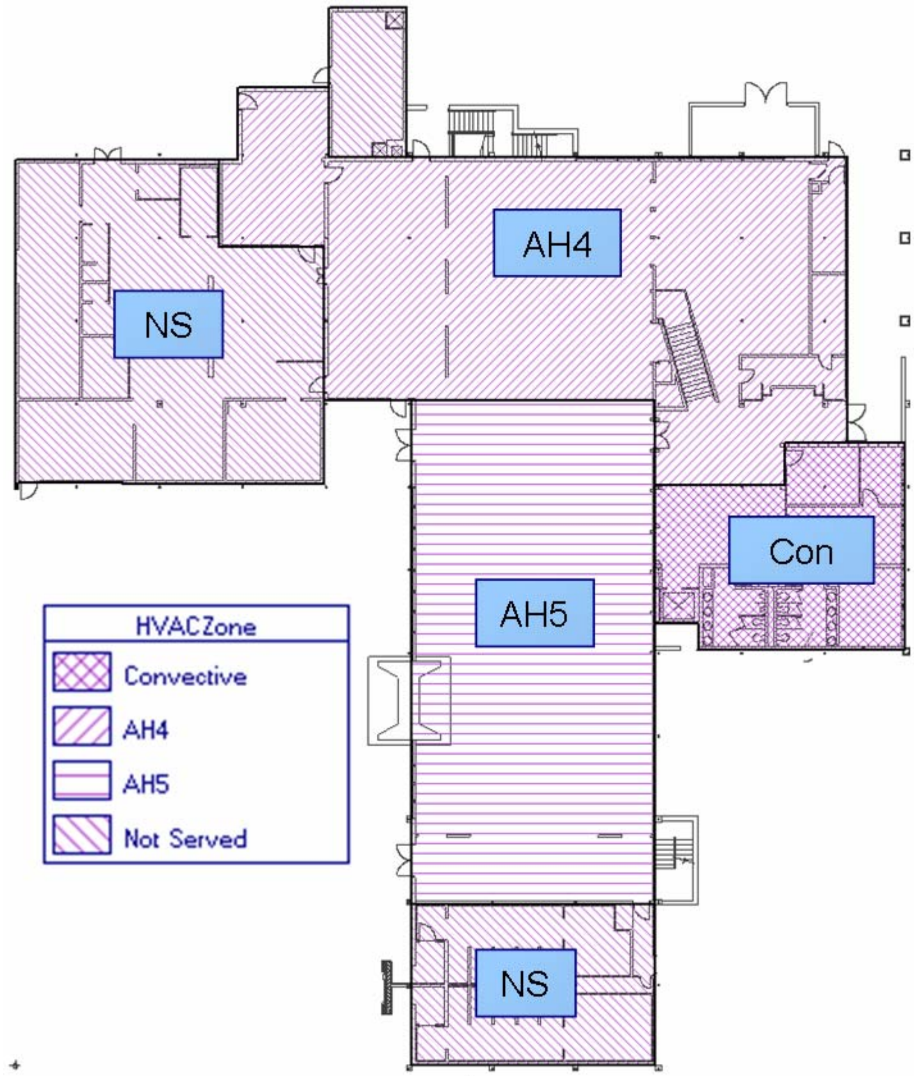

Figure 6-4. Coronado Club Main Level HVAC Zones

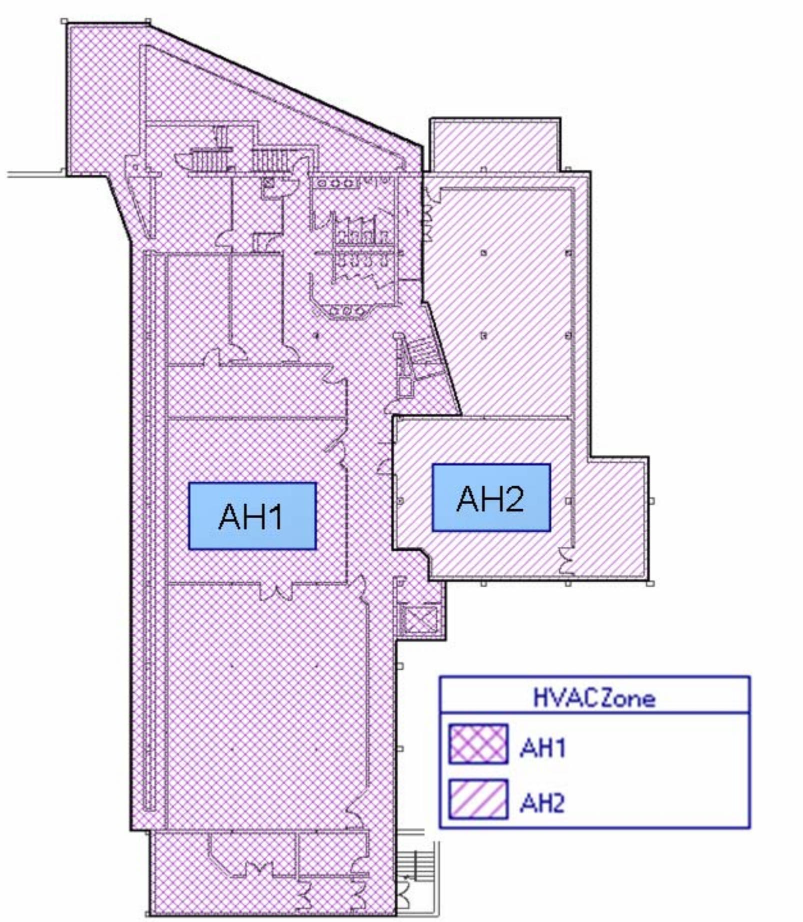

Figure 6-5. Coronado Club Basement Level HVAC Zones

Detailed mechanical drawings of the HVAC systems are provided in Section 6.4, below.

6.3 Air Flow Patterns

Prior to release of the simulant, air flow velocities were measured at various doorways on the main floor and basement. Figure 6-6 summarizes the location and maximum flow velocities found at those locations on the main floor, while Figure 6-7 gives the results for the basement. Air flow on the main floor appears to be dominated by air blowing up from the basement through the staircase. From the top of the staircase the air flow splits, with most turning west into the ballroom, and the balance turning north and going into the lounge. Measurements on the basement level tend to support these observations with air flowing from the meeting rooms west of the corridor into the corridor. Air then flows from the basement corridor into the stairwell.

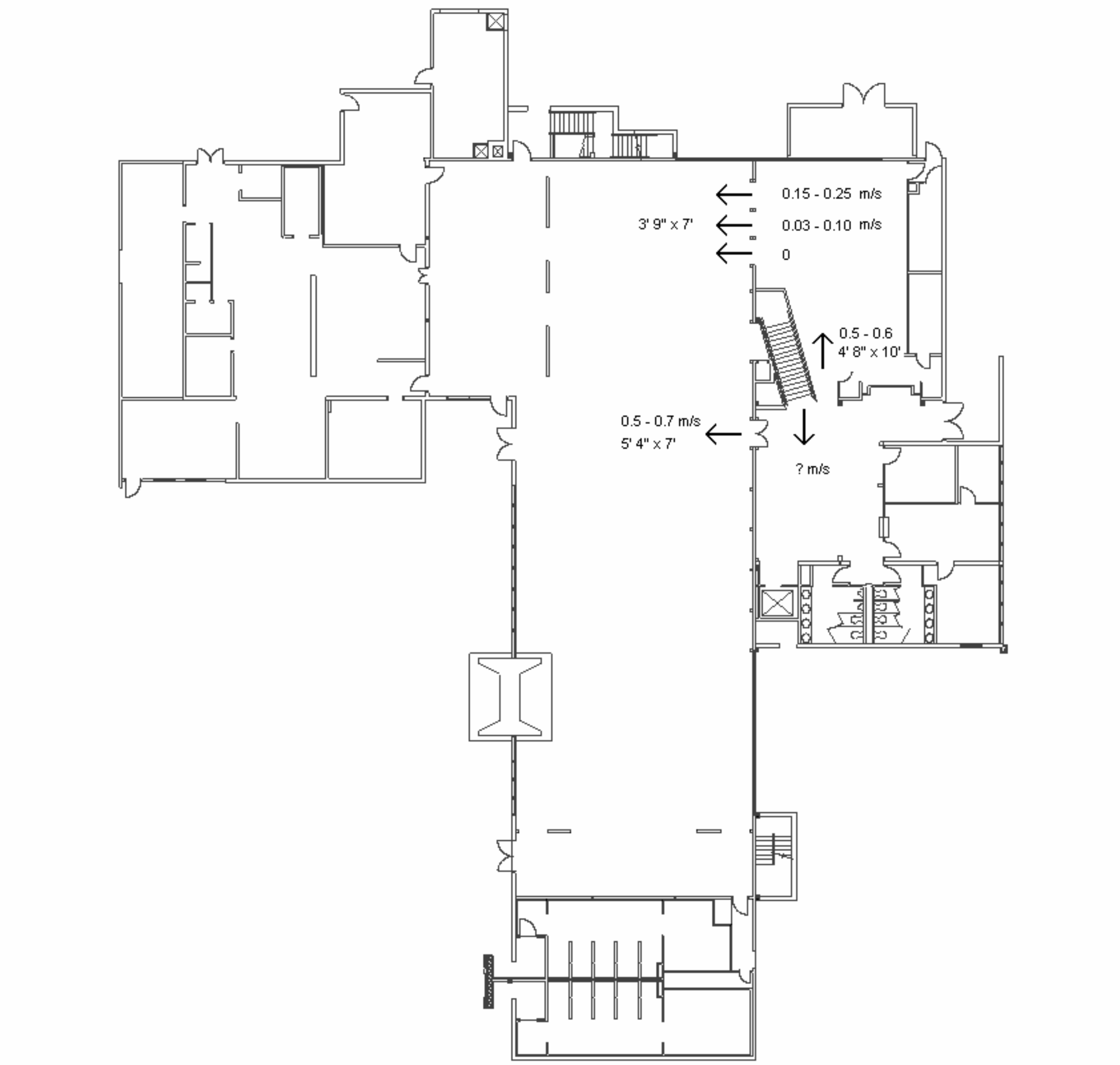

Figure 6-6. Coronado Club Main Level Air Flow Measurements. Dimensions refer to door or passageway opening size.

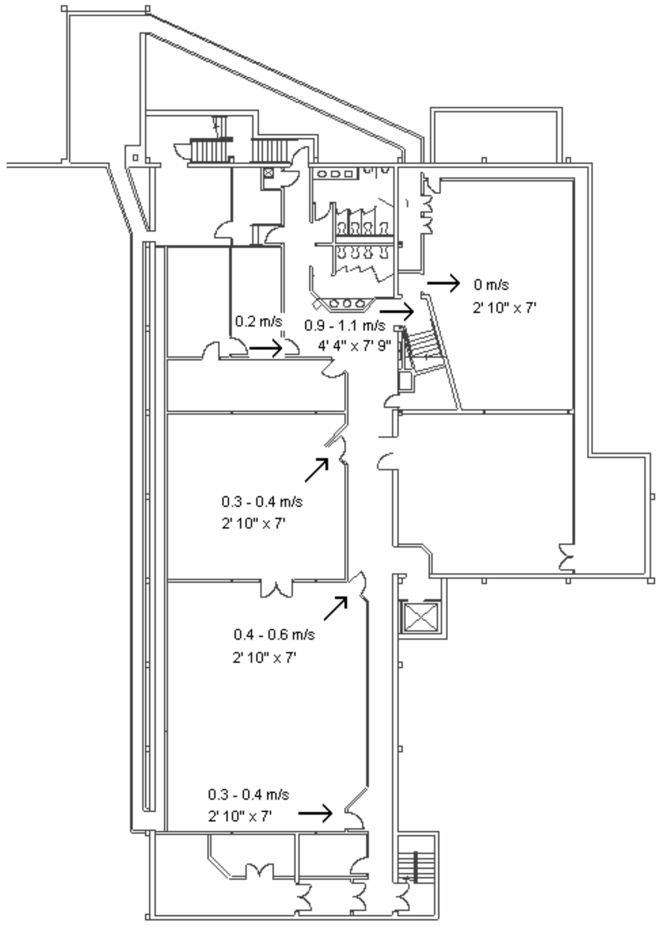

Figure 6-7. Coronado Club Basement Level Air Flow Measurements. Dimensions refer to door or passageway opening size.

6.4 Detailed HVAC Drawings

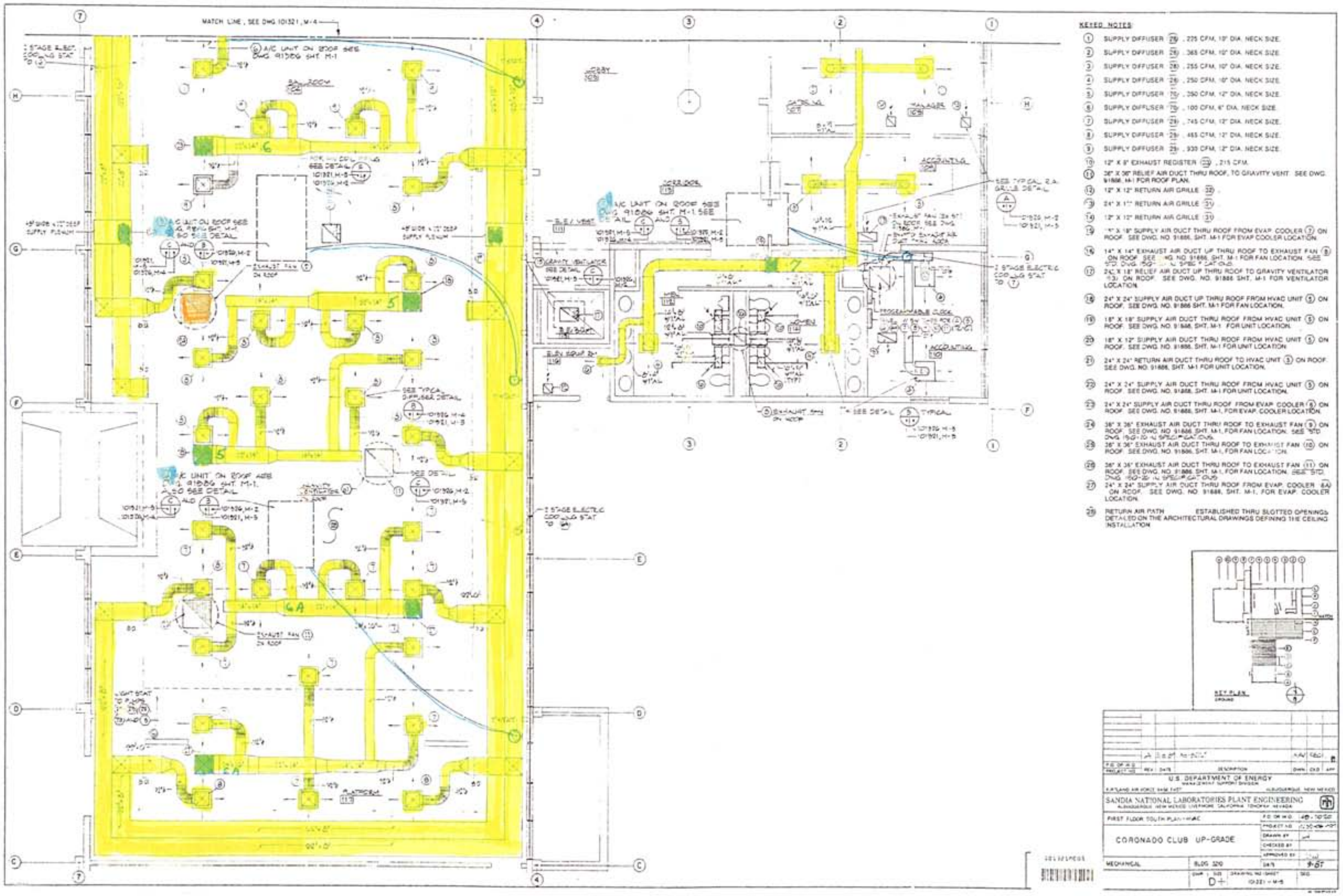

Figure 6-8. HVAC Drawing of Main floor, South

HVAC PLAN - 1ST FLOOR - EAST [MH10063210.dgn]

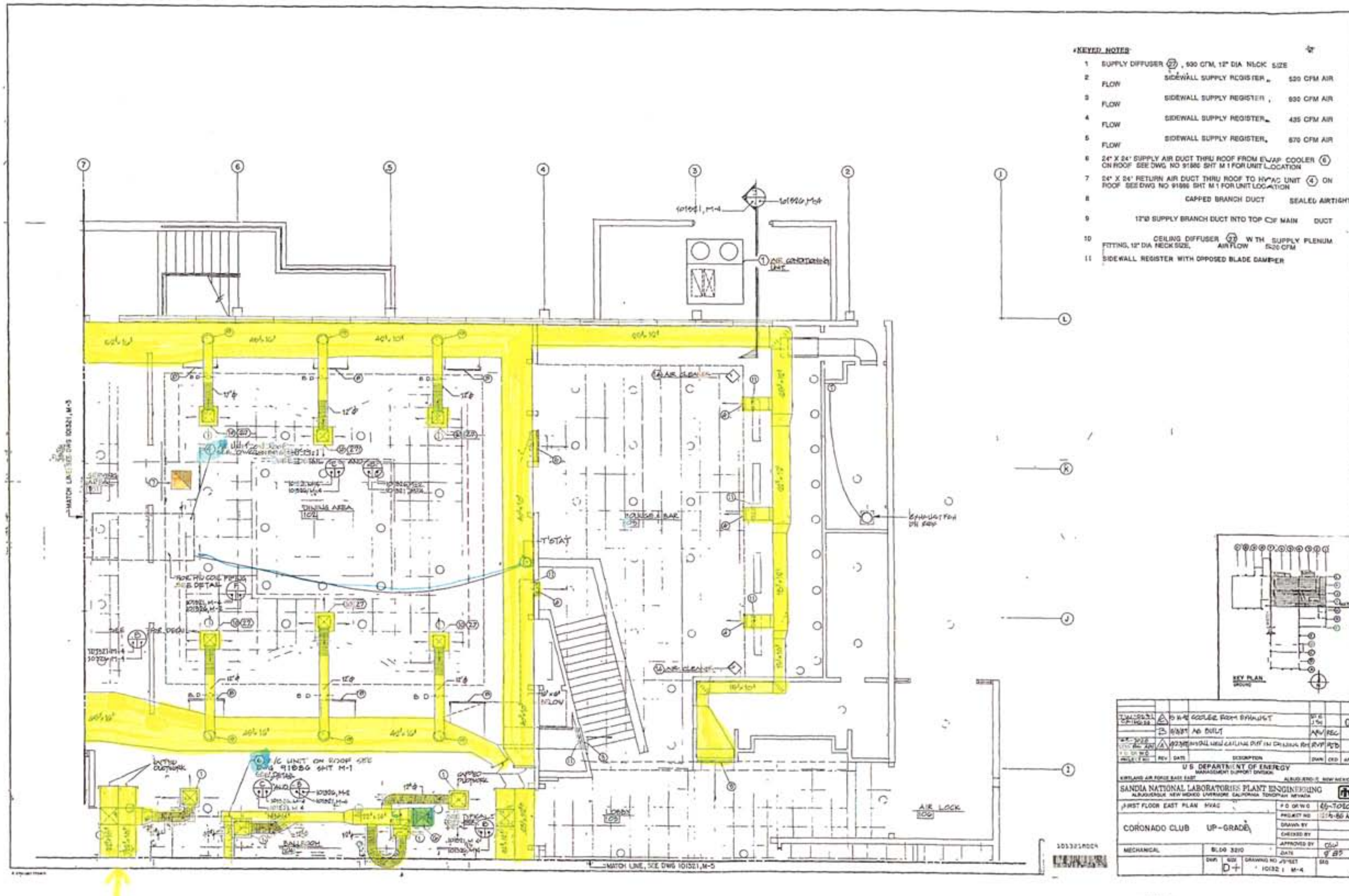

Figure 6-9. HVAC Drawing of Main floor, East

HVAC PLAN - 1ST FLOOR - WEST [MH10053210.dgn]

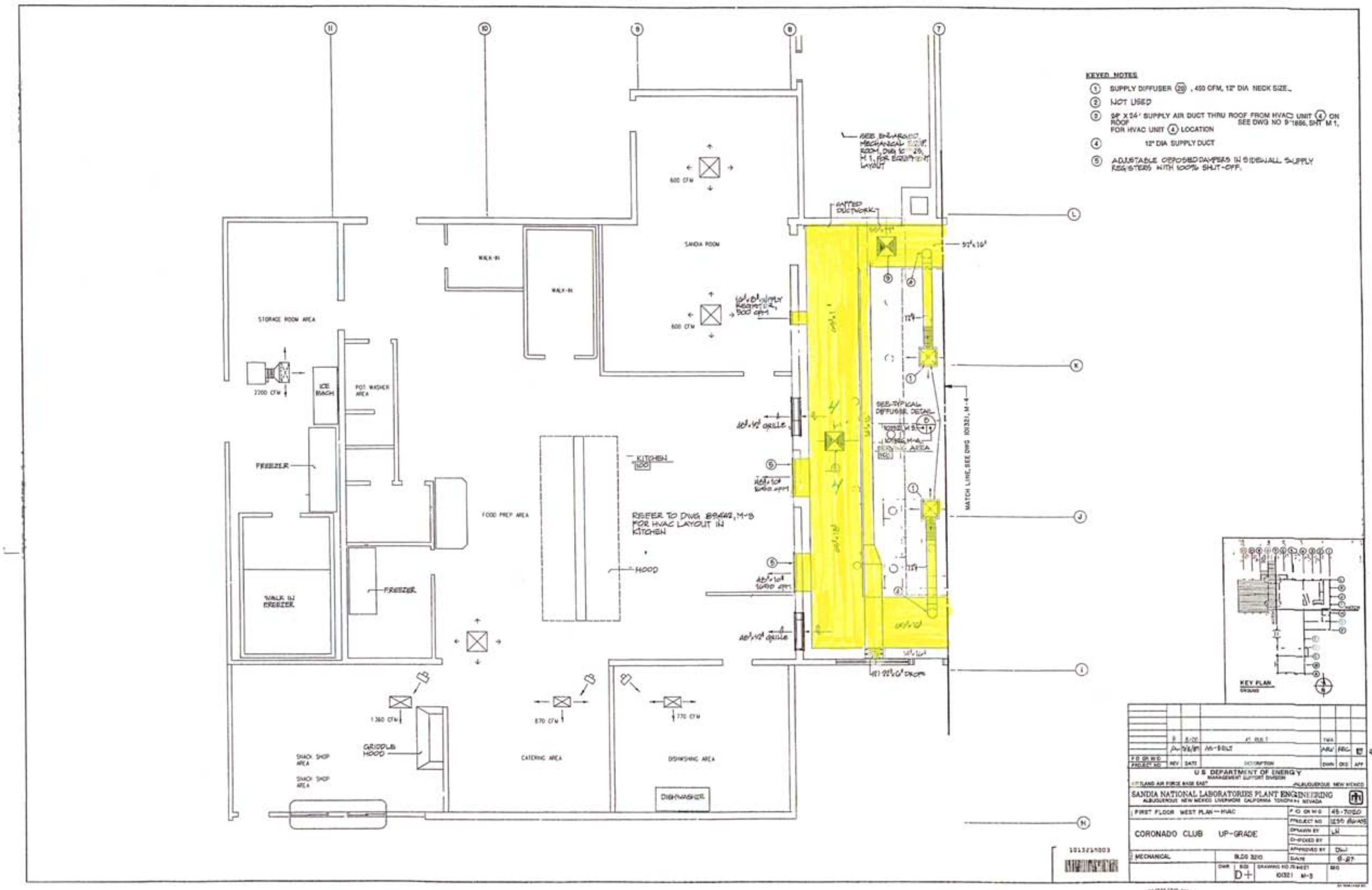

Figure 6-10. HVAC Drawing of Main floor, West

3210

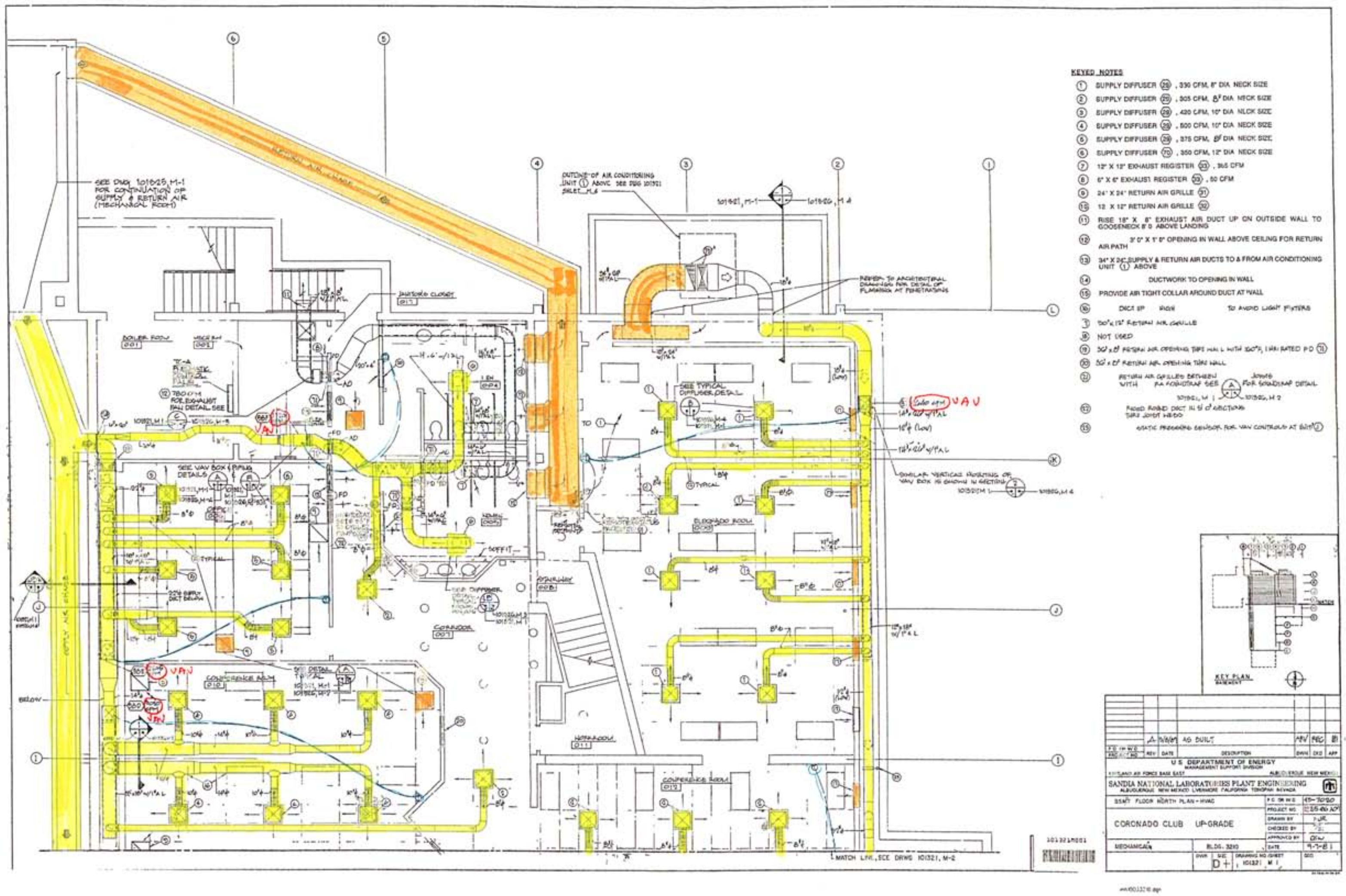

Figure 6-11. HVAC Drawing of Basement, North

HVAC PLAN - BASEMENT - SOUTH [MH10043210.dgn]

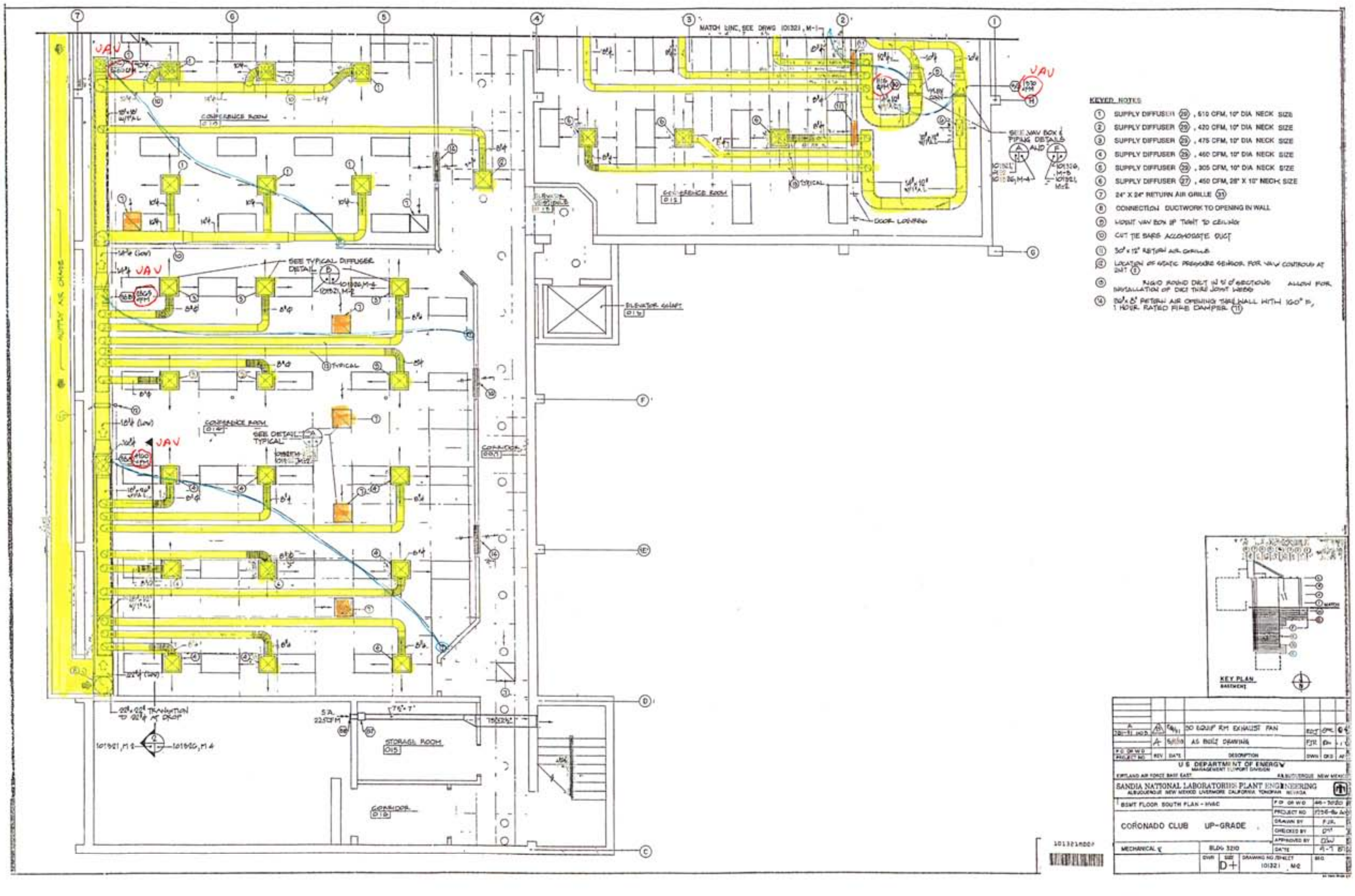

Figure 6-12. HVAC Drawing of Basement, South

7 Experimental Results

7.1 Sampling Data

The raw sampling data from the Visolite releases, as output from the BROOM tool, are given in Table 7-1 for the yellow powder release on Feb. 16, 2005 and in Table 7-2 for the pink powder release on Feb. 25, 2005. For the pink release, the Nxxxx barcodes indicate data taken using the PDA and the long numeric barcodes indicate data taken in the traditional style and hand entered into BROOM from the paper data sheets.

In these tables, all X, Y, and Z locations are given in meters relative to the origin of the building maps loaded into BROOM. All Z locations are absolute (rather than relative to the floor on which the sample was taken). A FloorID of 1 corresponds to the basement, whereas a Floor ID of 2 corresponds to the main floor of the Coronado Club. The Extraction Efficiency and Detection Efficiency numbers are estimated values included in the BROOM tool. At the time of this exercise, the sampling efficiency studies done by Brown and coworkers (see SAND2006-3560) were in an early stage, so the numbers in these tables do not reflect the sampling efficiency results.

In the yellow Visolite dataset, some air monitoring devices were entered as samples via the PDA merely as a convenience for marking their locations. There are also some background samples. These entries in the table have n/a for "Analysis Method" and "Amount Measured". The yellow Visolite dataset also contains some samples that were collected with mini-vacuums and some that were collected with HEPA sock vacuums. At the time of the exercise, BROOM merely had a single "vacuum" type of collection method. Since then, "vacuum" was changed to "minivac" and a new "HEPA vac" collection method was added to the software. Because this distinction was made long after the exercise, all vacuum samples are marked with the "minivac" collection method, despite some being minivacs and some being HEPA vacs.

Table 7-1. Data from Feb. 16, 2005 release of Yellow Visolite powder.

barcode ID	floor ID	X loc. (m)	Y loc. (m)	Z loc. (m)	Surf. Type	Surf. Orient.	Surf. Area (m^2)	Collect. Method	notes	analysis Method	Amt. Meas. (mg)	Extr. Eff.	Detn. Eff.
10	2	40.894	39.547	4.15	smooth	horiz. up	0.1	air pump	air pump	n/a	n/a	1	1
4	2	42.439	48.379	4.1	smooth	horiz. up	0.1	air pump	air pump	n/a	n/a	1	1
6	2	28.75	31.083	3	smooth	horiz. up	0.1	air pump	air pump	n/a	n/a	1	1
8	1	33.018	45.141	0.88	smooth	horiz. up	0.1	air pump	air pump	n/a	n/a	1	1
BG!	2	34.638	46.392	3	smooth	horiz. up	0.01	minivac		n/a	n/a	1	1
BG2	2	25.511	19.234	3	smooth	horiz. up	0.01	minivac	background	n/a	n/a	1	1
BG3	1	40.746	50.514	0	smooth	horiz. up	0.01	minivac		n/a	n/a	1	1
BG4	1	35.153	38.517	0	smooth	horiz. up	0.01	air pump		n/a	n/a	1	1
DET1	2	34.564	33.954	3.74	smooth	horiz. up	0.1	air pump	airpump	n/a	n/a	1	1
DET11	1	43.396	46.687	0.75	smooth	horiz. up	0.1	air pump	airpumo	n/a	n/a	1	1
DET2	2	32.798	40.725	3.74	smooth	horiz. up	0.1	air pump	airpump	n/a	n/a	1	1
DET3	1	27.793	34.616	0.74	smooth	horiz. up	0.1	air pump	airpump	n/a	n/a	1	1
det5	2	45.015	31.01	4.35	smooth	horiz. up	0.1	air pump	airpump	n/a	n/a	1	1
DET9	2	35.668	23.797	3.74	smooth	horiz. up	0.1	air pump	airpump	n/a	n/a	1	1
mv1	2	41.041	33.954	3	smooth	horiz. up	0.01	minivac	minivac	fluorometric	9.28	0.85	1
MV10	1	29.633	32.261	0	smooth	horiz. up	0.01	minivac		fluorometric	2.16	0.85	1
MV11	1	33.754	43.522	0	smooth	horiz. up	0.01	minivac		fluorometric	4.71	0.85	1
MV12	1	37.434	43.154	0	smooth	horiz. up	0.01	minivac		fluorometric	21.92	0.85	1
MV13	1	38.465	42.197	0.9	smooth	horiz. up	0.01	minivac		fluorometric	9.07	0.85	1
MV14	1	37.361	39.695	0	smooth	horiz. up	0.01	minivac		fluorometric	27.61	0.85	1
MV15	1	33.166	37.781	0	smooth	horiz. up	0.01	minivac		fluorometric	69.21	0.85	1
MV16	1	35.006	44.184	0	smooth	horiz. up	0.01	minivac		fluorometric	1.37	0.85	1
MV17	1	34.785	38.738	0	smooth	horiz. up	0.01	minivac		fluorometric	174.64	0.85	1
mv2	2	39.716	34.763	3	smooth	horiz. up	0.01	minivac	minivac	fluorometric	20.59	0.85	1
MV3	2	31.031	21.957	3	smooth	horiz. up	0.01	minivac		fluorometric	0.68	0.85	1
MV4	2	30.442	23.135	3	smooth	horiz. up	0.01	minivac	microvac	fluorometric	1.22	0.85	1
MV5	2	41.114	47.717	3	smooth	horiz. up	0.01	minivac		fluorometric	4.71	0.85	1
MV6	2	40.526	49.042	3	smooth	horiz. up	0.01	minivac		fluorometric	6.89	0.85	1
MV7	1	28.382	31.525	0	smooth	horiz. up	0.01	minivac		fluorometric	1.25	0.85	1
MV8	1	28.75	32.408	0	smooth	horiz. up	0.01	minivac		fluorometric	0.60	0.85	1

barcode ID	floor ID	X loc. (m)	Y loc. (m)	Z loc. (m)	Surf. Type	Surf. Orient.	Surf. Area (m^2)	Collect. Method	notes	analysis Method	Amt. Meas. (mg)	Extr. Eff.	Detn. Eff.
MV9	1	29.338	31.231	0	smooth	horiz. up	0.01	minivac		fluorometric	5.87	0.85	1
W2002	1	33.828	32.555	0	smooth	horiz. up	0.1	wipe		fluorometric	8.96	0.85	1
W2004	1	30.516	34.763	0.78	smooth	horiz. up	0.1	wipe	tabletop	fluorometric	11.77	0.85	1
W2005	1	34.638	44.184	0	carpet	horiz. up	0.25	minivac		fluorometric	144.87	0.85	1
W2006	1	29.854	34.395	0.78	smooth	horiz. up	0.1	wipe		fluorometric	6.05	0.85	1
W2007	1	34.564	43.669	0	carpet	horiz. up	0.25	minivac		fluorometric	162.38	0.85	1
W2008	1	33.754	30.127	0	smooth	horiz. up	0.1	wipe		fluorometric	6.56	0.85	1
W2010	1	30.958	32.187	0	smooth	horiz. up	0.1	wipe		fluorometric	8.73	0.85	1
W2012	1	30.222	33.88	0	smooth	horiz. up	0.1	wipe		fluorometric	7.01	0.85	1
W2013	1	34.122	43.669	0	carpet	horiz. up	0.25	minivac		fluorometric	190.44	0.85	1
W2014	1	30.295	34.395	0.78	smooth	horiz. up	0.1	wipe		fluorometric	7.04	0.85	1
W2016	1	30.295	34.763	0.78	smooth	horiz. up	0.1	wipe		fluorometric	5.36	0.85	1
W2018	1	32.356	31.157	0	smooth	horiz. up	0.1	wipe		fluorometric	7.79	0.85	1
W2020	1	29.854	34.837	0.78	smooth	horiz. up	0.1	wipe		fluorometric	6.01	0.85	1
W2021	1	36.919	27.256	0	smooth	horiz. up	0.1	wipe		fluorometric	5.22	0.85	1
W2022	1	36.919	51.765	0	smooth	horiz. up	0.1	wipe		fluorometric	2.70	0.85	1
W2023	2	31.399	43.301	3	smooth	horiz. up	0.1	wipe		fluorometric	32.79	0.85	1
W2024	1	32.945	45.215	0.93	smooth	horiz. up	0.001	swab		fluorometric	2.95	0.85	1
W2025	2	31.841	45.583	12.74	smooth	horiz. up	0.1	wipe		fluorometric	18.39	0.85	1
W2026	1	33.902	34.616	0	smooth	horiz. up	0.1	wipe		fluorometric	302.57	0.85	1
W2027	2	31.841	44.92	3.74	smooth	horiz. up	0.1	wipe		fluorometric	18.63	0.85	1
W2028	1	33.239	36.015	0	smooth	horiz. up	0.1	wipe		fluorometric	2257.54	0.85	1
W2029	2	28.308	19.528	3	smooth	horiz. up	0.1	wipe		fluorometric	24.81	0.85	1
W2030	1	34.785	45.288	0.9	smooth	horiz. up	0.1	wipe		fluorometric	3.90	0.85	1
W2031	2	23.45	17.762	3	smooth	horiz. up	0.001	swab		fluorometric	1.11	0.85	1
W2032	1	34.417	35.941	1.4	porous	horiz. up	0.1	wipe		fluorometric	47.03	0.85	1
W2033	2	31.326	19.528	3	smooth	horiz. up	0.1	wipe		fluorometric	-999.00	0.85	1
W2034	1	32.503	33.365	0	smooth	horiz. up	0.1	wipe		fluorometric	11.47	0.85	1
W2035	2	28.382	16.584	3	smooth	horiz. up	0.1	wipe		fluorometric	25.91	0.85	1
W2036	1	30.81	34.763	0.78	smooth	horiz. up	0.1	wipe		fluorometric	5.54	0.85	1
W2037	2	31.473	16.584	3	smooth	horiz. up	0.1	wipe		fluorometric	22.26	0.85	1
W2038	1	31.841	35.426	0	smooth	horiz. up	0.1	wipe		fluorometric	21.30	0.85	1
W2039	2	25.364	13.787	3	smooth	horiz. up	0.1	wipe		fluorometric	20.01	0.85	1

barcode ID	floor ID	X loc. (m)	Y loc. (m)	Z loc. (m)	Surf. Type	Surf. Orient.	Surf. Area (m²)	Collect. Method	notes	analysis Method	Amt. Meas. (mg)	Extr. Eff.	Detn. Eff.
W2040	1	32.871	45.141	0.93	smooth	horiz. up	0.001	swab		fluorometric	2.96	0.85	1
W2041	2	34.49	52.354	3	smooth	horiz. up	0.1	wipe		fluorometric	33.26	0.85	1
W2042	1	29.706	31.819	0	smooth	horiz. up	0.0929	wipe		fluorometric	5.06	0.85	1
W2043	2	31.399	49.483	3	smooth	horiz. up	0.1	wipe		fluorometric	22.72	0.85	1
W2044	1	30.516	34.469	0.78	smooth	horiz. up	0.1	wipe	tabletop	fluorometric	23.66	0.85	1
W2045	2	36.33	51.176	3	smooth	horiz. up	0.1	wipe		fluorometric	35.48	0.85	1
W2046	1	27.13	30.053	0	smooth	horiz. up	0.1	wipe		fluorometric	4.98	0.85	1
W2047	1	26.983	26.299	0	smooth	horiz. up	0.1	wipe		fluorometric	3.88	0.85	1
W2048	1	30.222	30.053	0	smooth	horiz. up	0.1	wipe		fluorometric	5.92	0.85	1
W2049	2	36.257	43.743	3	smooth	horiz. up	0.1	wipe		fluorometric	22.68	0.85	1
W2050	1	36.846	15.48	0	smooth	horiz. up	0.1	wipe		fluorometric	4.01	0.85	1
W2051	1	30.369	45.435	0	smooth	horiz. up	0.1	wipe		fluorometric	3.55	0.85	1
W2052	1	32.43	48.6	0	smooth	horiz. up	0.1	wipe		fluorometric	4.83	0.85	1
W2053	1	34.196	52.575	0	smooth	horiz. up	0.1	wipe		fluorometric	3.66	0.85	1
W2054	1	34.343	35.941	1.2	smooth	horiz. up	0.001	swab		fluorometric	55.95	0.85	1
W2055	2	34.196	43.301	3	smooth	horiz. up	0.1	wipe		fluorometric	28.07	0.85	1
W2056	1	37.14	45.877	0	smooth	horiz. up	0.1	wipe		fluorometric	4.40	0.85	1
W2057	2	47.959	42.639	3	smooth	horiz. up	0.1	wipe		fluorometric	5.45	0.85	1
W2058	1	32.43	52.133	0	smooth	horiz. up	0.1	wipe		fluorometric	4.15	0.85	1
W2059	2	31.841	45.215	3.74	smooth	horiz. up	0.1	wipe		fluorometric	18.98	0.85	1
W2060	1	32.798	44.994	0.93	smooth	horiz. up	0.1	wipe	fountain	fluorometric	2.59	0.85	1
W2061	2	40.231	33.218	3	smooth	horiz. up	0.1	wipe		fluorometric	100.51	0.85	1
W2062	1	35.006	43.963	0	smooth	horiz. up	0.0929	wipe		fluorometric	48.97	0.85	1
W2063	2	39.716	36.603	3	smooth	horiz. up	0.1	wipe		fluorometric	134.99	0.85	1
W2064	1	35.742	41.461	0	smooth	horiz. up	0.1	wipe		fluorometric	1242.36	0.85	1
W2065	2	38.538	36.824	3	smooth	horiz. up	0.1	wipe		fluorometric	140.56	0.85	1
W2066	2	30.81	22.546	3	smooth	horiz. up	1	minivac	HEPA vac ballroom S	fluorometric	798.88	0.85	1
W2067	2	40.378	34.984	3	smooth	horiz. up	0.1	wipe		fluorometric	114.51	0.85	1
W2068	2	40.746	48.232	3	carpet	horiz. up	0.25	minivac	HEPA quad SW	fluorometric	282.23	0.85	1
W2069	2	41.262	37.045	3	smooth	horiz. up	0.1	wipe		fluorometric	114.90	0.85	1
W2070	1	31.105	46.76	0	smooth	horiz. up	0.1	wipe		fluorometric	4.93	0.85	1
W2071	2	43.322	37.045	3	smooth	horiz. up	0.1	wipe		fluorometric	75.73	0.85	1

barcode ID	floor ID	X loc. (m)	Y loc. (m)	Z loc. (m)	Surf. Type	Surf. Orient.	Surf. Area (m^2)	Collect. Method	notes	analysis Method	Amt. Meas. (mg)	Extr. Eff.	Detn. Eff.
W2072	1	41.703	32.629	0.78	smooth	horiz. up	0.1	wipe		fluorometric	6.13	0.85	1
W2073	2	39.127	31.304	3	smooth	horiz. up	0.1	wipe		fluorometric	119.81	0.85	1
W2074	1	36.919	22.104	0	smooth	horiz. up	0.1	wipe		fluorometric	4.17	0.85	1
W2075	2	41.114	34.395	3	smooth	horiz. up	0.0929	wipe		fluorometric	115.47	0.85	1
W2076	1	36.919	32.114	0	smooth	horiz. up	0.1	wipe		fluorometric	5.65	0.85	1
W2077	2	41.335	31.157	3	smooth	horiz. up	0.1	wipe		fluorometric	96.28	0.85	1
W2078	1	46.487	32.776	0	smooth	horiz. up	0.1	wipe		fluorometric	4.81	0.85	1
W2079	2	40.967	39.032	3	smooth	horiz. up	0.1	wipe		fluorometric	125.95	0.85	1
W2080	1	38.17	39.695	0	smooth	horiz. up	0.1	wipe		fluorometric	25.24	0.85	1
W2081	2	44.574	39.253	3	smooth	horiz. up	0.1	wipe		fluorometric	62.88	0.85	1
W2082	1	36.846	18.645	0	smooth	horiz. up	0.1	wipe		fluorometric	4.59	0.85	1
W2083	2	39.274	38.811	3	smooth	horiz. up	0.1	wipe		fluorometric	183.60	0.85	1
W2084	1	28.382	47.938	0	smooth	horiz. up	0.1	wipe		fluorometric	3.21	0.85	1
W2085	2	40.231	37.855	3	smooth	horiz. up	0.1	wipe		fluorometric	149.82	0.85	1
W2086	1	27.278	45.435	0	smooth	horiz. up	0.1	wipe		fluorometric	3.56	0.85	1
W2087	2	40.378	33.586	3	smooth	horiz. up	0.1	wipe		fluorometric	93.47	0.85	1
W2088	1	32.945	26.226	0	smooth	horiz. up	0.1	wipe		fluorometric	3.79	0.85	1
W2089	2	42.292	35.941	3	smooth	horiz. up	0.1	wipe		fluorometric	107.79	0.85	1
W2090	2	40.894	47.717	3	smooth	horiz. up	0.1	wipe		fluorometric	59.32	0.85	1
W2091	2	37.95	35.72	3	smooth	horiz. up	0.1	wipe		fluorometric	124.79	0.85	1
W2092	2	40.894	49.115	3	smooth	horiz. up	0.1	wipe		fluorometric	54.98	0.85	1
W2093	2	39.716	34.395	3	smooth	horiz. up	0.0929	wipe		fluorometric	127.49	0.85	1
W2094	2	41.482	48.306	3	smooth	horiz. up	0.1	wipe		fluorometric	-999.00	0.85	1
W2095	2	38.98	38.591	3	smooth	horiz. up	0.1	wipe		fluorometric	134.28	0.85	1
W2096	2	41.114	48.232	3	carpet	horiz. up	0.25	minivac	HEPA quad SE	fluorometric	301.96	0.85	1
W2097	2	39.863	28.434	3	smooth	horiz. up	0.1	wipe		fluorometric	88.51	0.85	1
W2098	1	43.396	31.231	0	smooth	horiz. up	0.1	wipe		fluorometric	5.21	0.85	1
W2099	2	40.158	35.794	3	smooth	horiz. up	0.1	wipe		fluorometric	129.88	0.85	1
W2100	2	40.746	48.674	3	carpet	horiz. up	0.25	minivac	HEPA quad NW	fluorometric	323.31	0.85	1
W2101	2	34.196	33.807	3.74	smooth	horiz. up	0.1	wipe		fluorometric	34.71	0.85	1
W2102	1	30.958	36.971	0	smooth	horiz. up	0.1	wipe		fluorometric	11.94	0.85	1
W2103	2	25.438	37.413	3	smooth	horiz. up	0.1	wipe		fluorometric	34.13	0.85	1

barcode ID	floor ID	X loc. (m)	Y loc. (m)	Z loc. (m)	Surf. Type	Surf. Orient.	Surf. Area (m^2)	Collect. Method	notes	analysis Method	Amt. Meas. (mg)	Extr. Eff.	Detn. Eff.
W2104	1	29.044	31.157	0	smooth	horiz. up	0.0929	wipe		fluorometric	5.93	0.85	1
W2105	2	32.871	36.309	3	smooth	horiz. up	0.1	wipe		fluorometric	100.01	0.85	1
W2106	1	29.044	32.555	0	smooth	horiz. up	0.0929	wipe		fluorometric	5.55	0.85	1
W2107	2	36.478	39.842	3	smooth	horiz. up	0.1	wipe		fluorometric	60.89	0.85	1
W2108	1	29.338	36.235	0	smooth	horiz. up	0.1	wipe		fluorometric	7.40	0.85	1
W2109	2	35.3	39.032	3	smooth	horiz. up	0.1	wipe		fluorometric	128.85	0.85	1
W2110	1	30.81	34.469	0.78	smooth	horiz. up	0.1	wipe		fluorometric	5.20	0.85	1
W2111	2	28.529	40.357	3	smooth	horiz. up	0.1	wipe		fluorometric	47.80	0.85	1
W2112	1	27.057	34.101	0	smooth	horiz. up	0.1	wipe		fluorometric	6.26	0.85	1
W2113	2	31.399	37.413	3	smooth	horiz. up	0.1	wipe		fluorometric	88.20	0.85	1
W2114	1	36.33	45.215	0	smooth	horiz. up	0.1	wipe		fluorometric	34.69	0.85	1
W2115	2	25.438	34.469	3	smooth	horiz. up	0.1	wipe		fluorometric	38.48	0.85	1
W2116	1	25.29	42.859	0	smooth	horiz. up	0.1	wipe		fluorometric	3.86	0.85	1
W2117	2	34.196	33.439	3.74	smooth	horiz. up	0.1	wipe		fluorometric	30.91	0.85	1
W2118	1	25.806	45.067	0.8	smooth	horiz. up	0.1	wipe		fluorometric	2.85	0.85	1
W2119	2	33.902	33.439	3.74	smooth	horiz. up	0.1	wipe		fluorometric	31.81	0.85	1
W2120	1	24.702	47.717	0.8	smooth	horiz. up	0.1	wipe		fluorometric	3.37	0.85	1
W2121	2	42.807	27.33	3	smooth	horiz. up	0.1	wipe		fluorometric	7.48	0.85	1
W2122	1	24.702	31.967	0	smooth	horiz. up	0.1	wipe		fluorometric	5.25	0.85	1
W2123	2	51.05	31.083	3	smooth	horiz. up	0.1	wipe		fluorometric	62.79	0.85	1
W2124	1	29.265	31.525	0	smooth	horiz. up	0.25	minivac		fluorometric	135.24	0.85	1
W2125	2	48.18	34.837	3	smooth	horiz. up	0.1	wipe		fluorometric	45.74	0.85	1
W2126	1	27.204	36.162	0	smooth	horiz. up	0.1	wipe		fluorometric	7.19	0.85	1
W2127	2	50.83	35.573	3	smooth	horiz. up	0.1	wipe		fluorometric	43.85	0.85	1
W2128	1	29.412	32.04	0	smooth	horiz. up	0.25	minivac		fluorometric	155.88	0.85	1
W2129	2	48.033	31.746	3	smooth	horiz. up	0.1	wipe		fluorometric	66.41	0.85	1
W2130	1	28.75	32.04	0	smooth	horiz. up	0.25	minivac		fluorometric	164.43	0.85	1
W2131	2	50.167	26.447	3	smooth	horiz. up	0.1	wipe		fluorometric	48.88	0.85	1
W2132	1	29.706	38.296	0	smooth	horiz. up	0.1	wipe		fluorometric	9.36	0.85	1
W2133	2	35.374	35.941	3	smooth	horiz. up	0.1	wipe		fluorometric	140.41	0.85	1
W2134	1	28.234	31.819	0	smooth	horiz. up	0.0929	wipe		fluorometric	5.81	0.85	1
W2135	2	36.919	37.413	3	smooth	horiz. up	0.1	wipe		fluorometric	130.40	0.85	1
W2136	1	24.775	36.088	0	smooth	horiz. up	0.1	wipe		fluorometric	6.45	0.85	1

barcode ID	floor ID	X loc. (m)	Y loc. (m)	Z loc. (m)	Surf. Type	Surf. Orient.	Surf. Area (m^2)	Collect. Method	notes	analysis Method	Amt. Meas. (mg)	Extr. Eff.	Detn. Eff.
W2137	2	34.417	37.339	3	smooth	horiz. up	0.1	wipe		fluorometric	136.62	0.85	1
W2138	1	33.166	38.37	0	smooth	horiz. up	0.0929	wipe		fluorometric	122.35	0.85	1
W2139	2	46.119	33.733	3	smooth	horiz. up	0.1	wipe		fluorometric	36.04	0.85	1
W2140	1	28.676	31.525	0	smooth	horiz. up	0.25	minivac		fluorometric	143.48	0.85	1
W2141	2	37.361	21.515	4.65	porous	horiz. up	0.1	wipe		fluorometric	9.07	0.85	1
W2142	2	42.218	39.4	3	smooth	horiz. up	0.1	wipe		fluorometric	64.26	0.85	1
W2144	2	47.002	38.296	3	smooth	horiz. up	0.1	wipe		fluorometric	66.05	0.85	1
W2145	2	25.364	19.675	3	smooth	horiz. up	0.1	wipe		fluorometric	26.41	0.85	1
W2146	2	37.655	29.832	3	smooth	horiz. up	0.1	wipe		fluorometric	119.22	0.85	1
W2147	2	25.364	16.584	3	smooth	horiz. up	0.1	wipe		fluorometric	20.59	0.85	1
W2148	2	37.95	32.703	3	smooth	horiz. up	0.1	wipe		fluorometric	118.81	0.85	1
W2149	2	25.511	22.546	3	smooth	horiz. up	0.1	wipe		fluorometric	30.59	0.85	1
W2150	2	42.366	32.85	3	smooth	horiz. up	0.1	wipe		fluorometric	79.00	0.85	1
W2151	2	28.308	13.787	3	smooth	horiz. up	0.1	wipe		fluorometric	18.00	0.85	1
W2152	1	27.425	38.37	0	smooth	horiz. up	0.1	wipe		fluorometric	6.95	0.85	1
W2153	2	32.577	10.843	3	smooth	horiz. up	0.1	wipe		fluorometric	14.93	0.85	1
W2154	1	24.628	34.175	0	smooth	horiz. up	0.1	wipe		fluorometric	5.01	0.85	1
W2155	2	29.927	10.843	3	smooth	horiz. up	0.1	wipe		fluorometric	13.42	0.85	1
W2156	1	24.849	38.149	0	smooth	horiz. up	0.1	air pump		fluorometric	7.63	0.85	1
W2157	2	31.326	13.861	3	smooth	horiz. up	0.1	wipe		fluorometric	21.88	0.85	1
W2158	1	24.849	29.979	0	smooth	horiz. up	0.1	wipe		fluorometric	5.53	0.85	1
W2159	2	35.006	13.64	4.16	textured	horiz. up	0.1	wipe		fluorometric	6.77	0.85	1
W2160	1	27.057	31.967	0	smooth	horiz. up	0.1	wipe		fluorometric	5.15	0.85	1
W2161	1	32.209	19.896	0	smooth	horiz. up	0.1	wipe		fluorometric	3.16	0.85	1
W2162	1	35.962	40.283	0	smooth	horiz. up	0.1	wipe		fluorometric	1628.39	0.85	1
W2163	1	36.772	36.824	0	smooth	horiz. up	0.1	wipe		fluorometric	25.30	0.85	1
W2164	1	34.638	43.301	0	smooth	horiz. up	0.0929	wipe		fluorometric	30.56	0.85	1
W2165	1	37.14	39.915	0	smooth	horiz. up	0.1	wipe		fluorometric	379.63	0.85	1
W2166	2	41.114	48.674	3	carpet	horiz. up	0.25	minivac	HEPA quad NE	fluorometric	228.79	0.85	1
W2167	1	35.374	34.322	0	porous	horiz. up	0.1	wipe		fluorometric	6.37	0.85	1
W2168	2	43.249	43.669	3	smooth	horiz. up	0.1	wipe		fluorometric	68.20	0.85	1
W2169	1	30.001	42.491	0	smooth	horiz. up	0.1	wipe		fluorometric	3.37	0.85	1
W2170	1	34.711	36.383	0	smooth	horiz. up	0.1	wipe		fluorometric	44.55	0.85	1

barcode ID	floor ID	X loc. (m)	Y loc. (m)	Z loc. (m)	Surf. Type	Surf. Orient.	Surf. Area (m^2)	Collect. Method	notes	analysis Method	Amt. Meas. (mg)	Extr. Eff.	Detn. Eff.
W2171	1	36.404	24.533	0	smooth	horiz. up	0.1	wipe		fluorometric	4.15	0.85	1
W2172	1	37.655	42.344	0	smooth	horiz. up	0.001	swab		fluorometric	20.14	0.85	1
W2173	1	34.49	36.162	1.15	porous	horiz. up	0.1	wipe		fluorometric	8.42	0.85	1
W2174	2	43.175	47.275	3	smooth	horiz. up	0.1	wipe		fluorometric	47.11	0.85	1
W2175	1	36.478	38.517	0	smooth	horiz. up	0.1	wipe		fluorometric	856.98	0.85	1
W2176	2	40.967	41.461	3	smooth	horiz. up	0.1	wipe		fluorometric	82.78	0.85	1
W2177	1	30.222	28.36	0	smooth	horiz. up	0.1	wipe		fluorometric	3.62	0.85	1
W2178	2	44.206	41.167	4	smooth	horiz. up	0.1	wipe		fluorometric	25.88	0.85	1
W2179	1	30.59	40.431	0	smooth	horiz. up	0.1	wipe		fluorometric	6.76	0.85	1
W2180	2	40.378	45.656	3	smooth	horiz. up	0.1	wipe		fluorometric	65.56	0.85	1
W2181	1	34.196	43.963	0	smooth	horiz. up	0.0929	wipe		fluorometric	9.21	0.85	1
W2182	2	42.292	46.245	3	smooth	horiz. up	0.1	wipe		fluorometric	56.76	0.85	1
W2183	1	37.729	42.344	0	smooth	horiz. up	0.001	swab		fluorometric	26.83	0.85	1
W2184	2	40.158	48.306	3	smooth	horiz. up	0.1	wipe		fluorometric	63.17	0.85	1
W2185	1	35.962	39.327	0	smooth	horiz. up	0.1	wipe		fluorometric	2395.07	0.85	1
W2186	2	42.513	29.906	3	smooth	horiz. up	0.1	wipe		fluorometric	90.26	0.85	1
W2187	1	29.854	22.914	0	smooth	horiz. up	0.1	wipe		fluorometric	3.94	0.85	1
W2188	2	44.353	51.691	4.1	smooth	horiz. up	0.1	wipe	bar	fluorometric	28.18	0.85	1
W2189	1	38.833	32.335	0	smooth	horiz. up	0.1	wipe		fluorometric	5.83	0.85	1
W2190	2	38.17	46.171	3	smooth	horiz. up	0.1	wipe		fluorometric	25.42	0.85	1
W2191	1	33.681	39.547	0	smooth	horiz. up	0.1	wipe		fluorometric	4.26	0.85	1
W2192	2	44.426	44.111	4.1	smooth	horiz. up	0.1	wipe	bar	fluorometric	14.60	0.85	1
W2193	1	47.297	40.136	0	smooth	horiz. up	0.1	wipe		fluorometric	7.54	0.85	1
W2194	1	38.612	30.053	0	smooth	horiz. up	0.1	wipe		fluorometric	-999.00	0.85	1
W2195	1	35.962	39.915	0	smooth	horiz. up	0.1	wipe		fluorometric	1988.78	0.85	1
W2196	1	29.706	46.539	0.79	smooth	horiz. up	0.1	wipe		fluorometric	3.98	0.85	1
W2197	2	39.348	51.839	3	smooth	horiz. up	0.1	wipe		fluorometric	53.70	0.85	1
W2198	1	39.79	39.989	0	smooth	horiz. up	0.1	wipe		fluorometric	30.19	0.85	1
W2199	2	40.526	34.322	3	carpet	horiz. up	1	minivac	HEPA vac lobby	fluorometric	1579.34	0.85	1
W2200	1	28.75	43.595	0.79	smooth	horiz. up	0.1	wipe		fluorometric	2.77	0.85	1
W2201	1	31.326	43.448	0	smooth	horiz. up	0.1	wipe		fluorometric	4.40	0.85	1
W2203	1	36.919	41.24	0	smooth	horiz. up	0.1	wipe		fluorometric	100.03	0.85	1
W2205	1	43.617	35.499	0	smooth	horiz. up	0.1	wipe		fluorometric	5.07	0.85	1

barcode ID	floor ID	X loc. (m)	Y loc. (m)	Z loc. (m)	Surf. Type	Surf. Orient.	Surf. Area (m^2)	Collect. Method	notes	analysis Method	Amt. Meas. (mg)	Extr. Eff.	Detn. Eff.
W2207	1	38.906	36.456	0	smooth	horiz. up	0.1	wipe		fluorometric	5.14	0.85	1
W2209	1	37.508	42.933	0	smooth	horiz. up	0.1	wipe		fluorometric	88.46	0.85	1
W2211	1	47.297	46.098	0	smooth	horiz. up	0.1	wipe		fluorometric	-999.00	0.85	1
W2213	1	26.026	40.21	0	smooth	horiz. up	0.1	wipe		fluorometric	5.92	0.85	1
W2223	1	33.975	40.651	0	smooth	horiz. up	0.1	wipe		fluorometric	6.17	0.85	1
W2225	1	32.43	41.535	0	smooth	horiz. up	0.1	wipe		fluorometric	6.95	0.85	1
W2229	1	44.647	42.639	0	smooth	horiz. up	0.1	wipe		fluorometric	4.37	0.85	1
W2231	1	24.702	21.957	0	smooth	horiz. up	0.1	wipe		fluorometric	3.34	0.85	1
W2233	1	39.569	42.859	0.9	smooth	horiz. up	0.1	wipe	stairs bot	fluorometric	-999.00	0.85	1
W2235	1	38.17	43.595	0	smooth	horiz. up	0.1	wipe		fluorometric	258.96	0.85	1
W2237	1	34.564	44.626	0	smooth	horiz. up	0.0929	wipe		fluorometric	11.14	0.85	1
W2239	1	35.153	41.093	0	smooth	horiz. up	0.1	wipe		fluorometric	1087.40	0.85	1
W2241	1	34.932	36.971	0	smooth	horiz. up	0.1	wipe		fluorometric	1919.45	0.85	1
W2242	2	25.732	43.375	3	smooth	horiz. up	0.1	wipe		fluorometric	35.50	0.85	1
W2243	1	35.962	40.578	0	smooth	horiz. up	0.1	wipe		fluorometric	1615.03	0.85	1
W2244	2	19.991	46.834	3	smooth	horiz. up	0.1	wipe		fluorometric	11.18	0.85	1
W2245	1	27.13	19.896	0	smooth	horiz. up	0.1	wipe		fluorometric	3.94	0.85	1
W2246	2	19.991	50.587	3	smooth	horiz. up	0.1	wipe		fluorometric	12.76	0.85	1
W2247	1	43.69	38.075	0	smooth	horiz. up	0.1	wipe		fluorometric	6.19	0.85	1
W2248	2	34.564	40.283	3	smooth	horiz. up	0.1	wipe		fluorometric	114.07	0.85	1
W2249	1	35.153	38.738	0	smooth	horiz. up	0.0929	wipe		fluorometric	3350.15	0.85	1
W2250	2	31.546	40.283	3	smooth	horiz. up	0.1	wipe		fluorometric	67.33	0.85	1
W2251	1	29.559	15.186	0	smooth	horiz. up	0.1	wipe		fluorometric	3.43	0.85	1
W2252	2	21.316	43.227	3.7	smooth	horiz. up	0.1	wipe		fluorometric	10.27	0.85	1
W2253	1	36.036	29.611	0	smooth	horiz. up	0.1	wipe		fluorometric	4.86	0.85	1
W2254	2	23.377	46.834	3	smooth	horiz. up	0.1	wipe		fluorometric	10.42	0.85	1
W2255	1	33.313	42.712	0	smooth	horiz. up	0.001	swab		fluorometric	3.64	0.85	1
W2256	2	28.308	37.413	3	smooth	horiz. up	0.1	wipe		fluorometric	48.16	0.85	1
W2257	1	35.447	32.114	0	smooth	horiz. up	0.1	wipe		fluorometric	6.92	0.85	1
W2258	2	23.745	40.21	3	smooth	horiz. up	0.1	wipe		fluorometric	15.17	0.85	1
W2260	2	25.658	40.357	3	smooth	horiz. up	0.1	wipe		fluorometric	0.62	0.85	1
W2261	1	39.863	41.682	1.8	smooth	horiz. up	0.1	wipe	stairs mid	fluorometric	23.61	0.85	1
W2262	2	36.478	35.205	3	smooth	horiz. up	0.1	wipe		fluorometric	204.74	0.85	1

barcode ID	floor ID	X loc. (m)	Y loc. (m)	Z loc. (m)	Surf. Type	Surf. Orient.	Surf. Area (m^2)	Collect. Method	notes	analysis Method	Amt. Meas. (mg)	Extr. Eff.	Detn. Eff.
W2263	2	41.262	50.808	3	smooth	horiz. up	0.1	wipe		fluorometric	125.65	0.85	1
W2264	2	34.49	31.304	3	smooth	horiz. up	0.1	wipe		fluorometric	50.74	0.85	1
W2265	1	39.127	39.768	2.7	smooth	horiz. up	0.1	wipe	stairs top	fluorometric	48.98	0.85	1
W2266	2	37.361	32.923	3.1	smooth	horiz. up	0.1	wipe		fluorometric	226.77	0.85	1
W2267	1	38.906	45.067	0	smooth	horiz. up	0.1	wipe		fluorometric	26.01	0.85	1
W2268	2	36.551	32.482	3	smooth	horiz. up	0.1	wipe		fluorometric	106.02	0.85	1
W2269	1	44.206	50.146	0	smooth	horiz. up	0.1	wipe		fluorometric	41.39	0.85	1
W2270	2	34.49	34.322	3	smooth	horiz. up	0.1	wipe		fluorometric	7.85	0.85	1
W2271	1	46.414	37.634	0	smooth	horiz. up	0.1	wipe		fluorometric	81.99	0.85	1
W2272	2	28.529	43.301	3	smooth	horiz. up	0.1	wipe		fluorometric	6.90	0.85	1
W2273	1	38.686	45.951	0	smooth	horiz. up	0.1	wipe		fluorometric	34.03	0.85	1
W2274	2	23.598	50.587	3	smooth	horiz. up	0.1	wipe		fluorometric	57.69	0.85	1
W2275	1	47.297	49.999	0	smooth	horiz. up	0.1	wipe		fluorometric	9.31	0.85	1
W2276	2	25.732	46.392	3	smooth	horiz. up	0.1	wipe		fluorometric	12.13	0.85	1
W2277	1	36.919	34.322	0	porous	horiz. up	0.1	wipe		fluorometric	5.36	0.85	1
W2278	2	25.732	49.263	3	smooth	horiz. up	0.1	wipe		fluorometric	11.11	0.85	1
W2279	1	40.305	46.834	0	smooth	horiz. up	0.1	wipe		fluorometric	8.47	0.85	1
W2280	2	25.438	52.354	3	smooth	horiz. up	0.1	wipe		fluorometric	9.90	0.85	1
W2281	2	47.665	40.651	3	smooth	horiz. up	0.1	wipe		fluorometric	7.34	0.85	1
W2282	2	44.794	35.72	3	smooth	horiz. up	0.1	wipe		fluorometric	86.42	0.85	1
W2283	2	39.716	50.44	3	smooth	horiz. up	0.1	wipe		fluorometric	52.96	0.85	1
W2284	2	45.825	36.677	3	smooth	horiz. up	0.1	wipe		fluorometric	52.31	0.85	1
W2285	2	46.193	45.288	4.1	smooth	horiz. up	0.1	wipe		fluorometric	42.97	0.85	1
W2286	2	44.794	29.832	3	smooth	horiz. up	0.1	wipe		fluorometric	98.84	0.85	1
W2287	2	42.145	42.786	3	smooth	horiz. up	0.1	wipe		fluorometric	74.72	0.85	1
W2288	2	45.162	31.231	4.35	smooth	horiz. up	0.1	wipe		fluorometric	75.77	0.85	1
W2289	2	37.508	49.557	3	smooth	horiz. up	0.1	wipe		fluorometric	14.51	0.85	1
W2290	2	45.236	31.893	4.35	smooth	horiz. up	0.1	wipe	counter	fluorometric	80.68	0.85	1
W2291	2	44.794	40.357	3	smooth	horiz. up	0.1	wipe		fluorometric	9.75	0.85	1
W2292	2	44.353	32.703	3	smooth	horiz. up	0.1	wipe		fluorometric	85.35	0.85	1
W2293	2	42.954	52.722	3	smooth	horiz. up	0.1	wipe		fluorometric	42.95	0.85	1
W2294	2	40.599	25.49	3	smooth	horiz. up	0.1	wipe		fluorometric	7.98	0.85	1
W2295	2	37.655	32.261	3	porous	horiz. up	0.001	swab		fluorometric	1.17	0.85	1

barcode ID	floor ID	X loc. (m)	Y loc. (m)	Z loc. (m)	Surf. Type	Surf. Orient.	Surf. Area (m^2)	Collect. Method	notes	analysis Method	Amt. Meas. (mg)	Extr. Eff.	Detn. Eff.
W2296	2	47.297	27.256	3	smooth	horiz. up	0.1	wipe		fluorometric	15.31	0.85	1
W2297	2	46.193	47.864	4.2	smooth	horiz. up	0.1	wipe		fluorometric	13.08	0.85	1
W2298	2	47.812	25.49	3.9	smooth	horiz. up	0.1	wipe		fluorometric	14.23	0.85	1
W2299	2	37.655	32.629	3	porous	horiz. up	0.1	wipe		fluorometric	38.09	0.85	1
W2300	2	44.132	28.728	3	smooth	horiz. up	0.1	wipe		fluorometric	83.69	0.85	1
W2302	2	33.902	33.807	77	smooth	horiz. up	0.1	wipe		fluorometric	32.06	0.85	1
W2304	2	28.529	31.304	3	smooth	horiz. up	0.1	wipe		fluorometric	46.61	0.85	1
W2306	2	28.455	34.469	3	smooth	horiz. up	0.1	wipe		fluorometric	43.07	0.85	1
W2308	2	33.607	33.439	3.74	smooth	horiz. up	0.1	wipe		fluorometric	35.73	0.85	1
W2310	2	33.607	33.807	3.74	smooth	horiz. up	0.1	wipe		fluorometric	35.40	0.85	1
W2311	1	34.122	44.184	0	carpet	horiz. up	0.25	minivac		fluorometric	137.11	0.85	1
W2321	1	37.582	42.344	0	smooth	horiz. up	0.001	swab		fluorometric	25.31	0.85	1
W2322	2	28.382	25.563	3	smooth	horiz. up	0.1	wipe		fluorometric	35.84	0.85	1
W2323	1	40.746	50.219	0	smooth	horiz. up	0.1	wipe		fluorometric	8.66	0.85	1
W2324	2	30.81	23.135	3	smooth	horiz. up	0.0929	wipe		fluorometric	33.96	0.85	1
W2325	1	44.206	40.725	0	smooth	horiz. up	0.1	wipe		fluorometric	6.27	0.85	1
W2326	2	23.524	30.715	3.3	smooth	horiz. up	0.001	swab		fluorometric	0.82	0.85	1
W2327	1	44.132	46.539	0.78	smooth	horiz. up	0.1	wipe		fluorometric	7.11	0.85	1
W2328	2	31.326	27.992	3	smooth	horiz. up	0.1	wipe		fluorometric	33.82	0.85	1
W2329	2	40.526	41.019	4.16	smooth	horiz. up	0.1	wipe	ledge	fluorometric	82.74	0.85	1
W2330	2	31.399	25.563	3	smooth	horiz. up	0.1	wipe		fluorometric	34.64	0.85	1
W2331	1	28.823	40.21	0	smooth	horiz. up	0.1	wipe		fluorometric	8.04	0.85	1
W2332	2	23.524	30.715	3.2	smooth	horiz. up	0.001	swab		fluorometric	1.60	0.85	1
W2334	2	31.399	31.304	3	smooth	horiz. up	0.1	wipe		fluorometric	45.98	0.85	1
W2336	2	31.473	34.469	3	smooth	horiz. up	0.1	wipe		fluorometric	67.91	0.85	1
W2340	2	23.524	30.642	3.2	textured	horiz. up	0.001	swab		fluorometric	1.63	0.85	1
W2341	1	36.183	42.786	0	smooth	horiz. up	0.1	wipe		fluorometric	320.75	0.85	1
W2342	2	31.105	23.061	3	smooth	horiz. up	0.001	swab		fluorometric	1.45	0.85	1
W2343	1	35.374	22.399	0	smooth	horiz. up	0.1	wipe		fluorometric	3.66	0.85	1
W2344	2	25.364	31.451	3	smooth	horiz. up	0.1	wipe		fluorometric	48.07	0.85	1
W2345	1	35.962	10.181	0	smooth	horiz. up	0.1	wipe		fluorometric	3.92	0.85	1
W2346	2	28.455	28.434	3	smooth	horiz. up	0.1	wipe		fluorometric	38.88	0.85	1
W2347	1	44.426	46.539	0.78	smooth	horiz. up	0.1	wipe		fluorometric	84.63	0.85	1

barcode ID	floor ID	X loc. (m)	Y loc. (m)	Z loc. (m)	Surf. Type	Surf. Orient.	Surf. Area (m²)	Collect. Method	notes	analysis Method	Amt. Meas. (mg)	Extr. Eff.	Detn. Eff.
W2348	2	25.511	28.434	3	smooth	horiz. up	0.1	wipe		fluorometric	36.99	0.85	1
W2349	1	38.906	41.314	1.8	smooth	horiz. up	0.1	wipe	stairs mid	fluorometric	223.31	0.85	1
W2350	2	28.455	22.399	3	smooth	horiz. up	0.1	wipe		fluorometric	31.67	0.85	1
W2351	1	47.297	42.565	0	smooth	horiz. up	0.1	wipe		fluorometric	6.08	0.85	1
W2352	2	30.001	22.399	3	smooth	horiz. up	0.1	wipe		fluorometric	43.99	0.85	1
W2353	2	40.894	39.989	4.16	smooth	horiz. up	0.1	wipe		fluorometric	85.93	0.85	1
W2354	2	30.81	21.81	3	smooth	horiz. up	0.0929	wipe		fluorometric	30.43	0.85	1
W2355	1	40.378	39.915	2.7	smooth	horiz. up	0.1	wipe	stairs top	fluorometric	126.66	0.85	1
W2356	2	30.442	21.957	3	smooth	horiz. up	0.001	swab		fluorometric	1.51	0.85	1
W2357	1	38.759	42.565	0.9	smooth	horiz. up	0.0923	wipe	stairs bot.	fluorometric	238.87	0.85	1
W2358	2	31.473	22.399	3	smooth	horiz. up	0.1	wipe		fluorometric	29.37	0.85	1
W2359	1	41.63	42.344	0	smooth	horiz. up	0.1	wipe		fluorometric	4.79	0.85	1
W2360	2	25.438	25.563	3	smooth	horiz. up	0.1	wipe		fluorometric	38.00	0.85	1
W2362	2	34.49	13.861	3	smooth	horiz. up	0.1	wipe		fluorometric	20.92	0.85	1
W2364	2	34.49	22.546	3	smooth	horiz. up	0.1	wipe		fluorometric	23.02	0.85	1
W2365	2	34.417	49.483	3	smooth	horiz. up	0.1	wipe		fluorometric	31.44	0.85	1
W2366	2	36.551	30.127	3	smooth	horiz. up	0.1	wipe		fluorometric	33.59	0.85	1
W2367	2	34.417	46.392	3	smooth	horiz. up	0.1	wipe		fluorometric	22.93	0.85	1
W2368	2	37.361	21.515	3.8	smooth	horiz. up	0.001	swab		fluorometric	0.96	0.85	1
W2369	2	31.399	46.319	3	smooth	horiz. up	0.1	wipe		fluorometric	27.26	0.85	1
W2370	2	34.343	16.584	3	smooth	horiz. up	0.1	wipe		fluorometric	20.26	0.85	1
W2371	2	35.889	47.57	3	smooth	horiz. up	0.1	wipe		fluorometric	27.30	0.85	1
W2372	2	34.417	19.602	3	smooth	horiz. up	0.1	wipe		fluorometric	21.61	0.85	1
W2373	2	28.234	52.354	3	smooth	horiz. up	0.1	wipe		fluorometric	23.92	0.85	1
W2374	2	37.361	25.784	3.1	smooth	horiz. up	0.1	wipe		fluorometric	35.49	0.85	1
W2375	2	31.473	52.354	3	smooth	horiz. up	0.1	wipe		fluorometric	27.56	0.85	1
W2376	2	34.343	25.563	3	smooth	horiz. up	0.1	wipe		fluorometric	27.47	0.85	1
W2377	2	28.382	49.483	3	smooth	horiz. up	0.1	wipe		fluorometric	17.30	0.85	1
W2378	2	36.625	27.035	3	smooth	horiz. up	0.1	wipe		fluorometric	24.16	0.85	1
W2379	2	28.529	46.392	3	smooth	horiz. up	0.1	wipe		fluorometric	25.09	0.85	1
W2380	2	34.417	28.36	3	smooth	horiz. up	0.1	wipe		fluorometric	33.78	0.85	1

Table 7-2. Data from Feb. 21, 2005 release of Pink Visolite powder.

barcode ID	Floor ID	X loc. (m)	Y loc. (m)	Z loc. (m)	Surf. Type	Surf. Orient.	Surf. Area (m^2)	Collect. Method	Notes	Analysis Method	Amt. Meas. (µg)	Extr. Eff.	Detn. Eff.
20059999-101	2	20.35	41.49	3.90	smooth	horiz. up	0.0025	swab	Food Steam Table	fluorometric	28.80	0.9	1
20059999-102	2	19.54	45.36	3.90	smooth	horiz. up	0.0025	swab	Food Steam Table	fluorometric	12.37	0.9	1
20059999-103	2	22.64	48.95	5.40	smooth	horiz. up	0.0025	swab	Ceiling Supply	fluorometric	292.44	0.9	1
20059999-104	2	18.39	47.42	5.10	smooth	vertical	0.0025	swab	Wall Return	fluorometric	166.01	0.9	1
20059999-105	2	26.93	46.39	3.00	smooth	horiz. up	0.0025	swab	Floor Tile	fluorometric	59.91	0.9	1
20059999-107	2	33.57	50.25	3.70	smooth	horiz. up	0.0025	swab	Desk Top	fluorometric	83.10	0.9	1
20059999-108	2	29.06	39.21	3.00	smooth	horiz. up	0.0025	swab	Floor Tile	fluorometric	93.15	0.9	1
20059999-109	2	44.12	47.21	5.80	smooth	horiz. up	0.0025	swab	Supply Vent Wall above bar	fluorometric	181.51	0.9	1
20059999-110	2	44.23	51.01	4.10	smooth	horiz. up	0.0025	swab	On Bar N. Corner	fluorometric	85.21	0.9	1
20059999-111	2	45.92	41.98	4.10	smooth	horiz. up	0.0025	swab	Counter Behind Bar	fluorometric	53.91	0.9	1
20059999-112	2	37.54	49.93	5.80	smooth	vertical	0.0025	swab	Return Diffuser (Wall)	fluorometric	136.18	0.9	1
20059999-113	2	48.20	37.74	3.00	smooth	horiz. up	0.0025	swab	No Laser Location	fluorometric	164.93	0.9	1
20059999-114	2	44.94	31.54	4.10	smooth	horiz. up	0.0025	swab	No Laser Location	fluorometric	170.81	0.9	1
20059999-115	2	25.70	22.12	3.00	smooth	horiz. up	0.0025	swab	No Laser Location	fluorometric	24.13	0.9	1
20059999-116	2	35.53	22.24	3.70	smooth	horiz. up	0.0025	swab	Table	fluorometric	35.07	0.9	1
20059999-117	2	30.52	13.31	3.00	carpet	horiz. up	0.01	minivac	Mid. Stage	fluorometric	125.17	0.9	1
20059999-118	2	40.26	38.83	3.00	carpet	horiz. up	0.01	minivac	Floor, top of staris No laser loc.	fluorometric	823.67	0.9	1

barcode ID	Floor ID	X loc. (m)	Y loc. (m)	Z loc. (m)	Surf. Type	Surf. Orient.	Surf. Area (m²)	Collect. Method	Notes	Analysis Method	Amt. Meas. (µg)	Extr. Eff.	Detn . Eff.
20059999-119	2	24.27	36.54	3.00	carpet	horiz. up	0.01	minivac	Floor, front of rear double doors (No laser loc)	fluorometric	809.49	0.9	1
20059999-120	2	47.61	37.90	3.00	carpet	horiz. up	0.01	minivac	Floor, by front double door (no Laser loc.)	fluorometric	2767.03	0.9	1
20059999-141	1	46.07	50.89	0.00	smooth	horiz. up	0.0025	swab		fluorometric	164.41	0.9	1
20059999-142	1	44.19	41.01	0.00	smooth	horiz. up	0.0025	swab		fluorometric	4.84	0.9	1
20059999-143	1	47.65	49.62	0.00	smooth	horiz. up	0.0025	swab		fluorometric	425.68	0.9	1
20059999-144	1	46.20	36.12	0.00	smooth	horiz. up	0.0025	swab		fluorometric	0.00	0.9	1
20059999-145	1	47.65	32.03	0.00	smooth	horiz. up	0.0025	swab		fluorometric	107.48	0.9	1
20059999-146	1	38.97	32.20	0.00	smooth	horiz. up	0.0025	swab		fluorometric	0.00	0.9	1
20059999-147	1	36.15	16.30	0.00	smooth	horiz. up	0.0025	swab		fluorometric	42.12	0.9	1
20059999-148	1	32.28	17.67	0.00	smooth	horiz. up	0.0025	swab		fluorometric	0.00	0.9	1
20059999-149	1	25.59	25.17	0.00	smooth	horiz. up	0.0025	swab		fluorometric	0.00	0.9	1
20059999-150	1	29.02	16.77	0.00	smooth	horiz. up	0.0025	swab		fluorometric	53.84	0.9	1
20059999-151	1	26.08	31.04	0.00	smooth	horiz. up	0.0025	swab		fluorometric	0.00	0.9	1
20059999-152	1	29.92	36.26	0.00	smooth	horiz. up	0.0025	swab		fluorometric	0.77	0.9	1
20059999-153	1	27.14	35.77	0.00	smooth	horiz. up	0.0025	swab		fluorometric	131.06	0.9	1
20059999-154	1	30.73	41.15	0.00	smooth	horiz. up	0.0025	swab		fluorometric	3.12	0.9	1
20059999-155	1	29.51	44.66	0.00	smooth	horiz. up	0.0025	swab		fluorometric	5.39	0.9	1
20059999-156	1	25.84	45.07	0.00	smooth	horiz. up	0.0025	swab		fluorometric	5.55	0.9	1
20059999-157	1	31.95	49.47	0.00	smooth	horiz. up	0.0025	swab		fluorometric	791.48	0.9	1
20059999-158	1	38.15	44.66	0.00	carpet	horiz. up	0.01	minivac		fluorometric	2172.29	0.9	1
20059999-159	1	41.33	47.51	0.00	carpet	horiz. up	0.01	minivac		fluorometric	586.54	0.9	1
20059999-160	1	42.07	37.24	0.00	carpet	horiz. up	0.01	minivac		fluorometric	571.67	0.9	1
20059999-161	1	36.68	24.11	0.00	carpet	horiz. up	0.01	minivac		fluorometric	274.46	0.9	1
20059999-162	1	34.32	26.88	0.00	carpet	horiz. up	0.01	minivac		fluorometric	409.60	0.9	1
20059999-163	1	32.85	36.10	0.00	carpet	horiz. up	0.01	minivac		fluorometric	333.22	0.9	1
20059999-164	1	33.42	43.44	0.00	carpet	horiz. up	0.01	minivac		fluorometric	842.41	0.9	1
20059999-167	2	44.57	43.67	3.00	smooth	horiz. up	0.0025	swab		fluorometric	81.40	1	0.9

barcode ID	Floor ID	X loc. (m)	Y loc. (m)	Z loc. (m)	Surf. Type	Surf. Orient.	Surf. Area (m²)	Collect. Method	Notes	Analysis Method	Amt. Meas. (µg)	Extr. Eff.	Detn . Eff.
20059999-168	2	42.91	46.16	3.00	smooth	horiz. up	0.0025	swab		fluorometric	114.18	1	0.9
20059999-169	2	43.41	49.90	3.00	smooth	horiz. up	0.0025	swab		fluorometric	161.08	1	0.9
20059999-170	2	41.00	30.63	3.00	smooth	horiz. up	0.0025	swab		fluorometric	506.16	1	0.9
20059999-171	1	40.86	45.96	0.00	smooth	horiz. up	0.0025	swab		fluorometric	615.36	1	0.9
20059999-172	1	44.99	41.73	0.00	smooth	horiz. up	0.0025	swab		fluorometric	217.36	1	0.9
20059999-173	1	43.73	33.38	0.00	smooth	horiz. up	0.0025	swab		fluorometric	233.86	1	0.9
20059999-174	1	47.14	40.20	0.00	smooth	horiz. up	0.0025	swab		fluorometric	277.17	1	0.9
20059999-175	1	31.97	44.24	0.00	smooth	horiz. up	0.0025	swab		fluorometric	179.12	1	0.9
20059999-176	1	36.10	48.19	0.00	smooth	horiz. up	0.0025	swab		fluorometric	37.22	1	0.9
20059999-177	1	25.86	45.68	0.00	smooth	horiz. up	0.0025	swab		fluorometric	55.11	1	0.9
20059999-178	1	30.26	21.52	0.00	smooth	horiz. up	0.0025	swab		fluorometric	109.92	1	0.9
20059999-179	1	38.70	28.80	0.00	smooth	horiz. up	0.01	minivac		fluorometric	550.56	1	0.9
20059999-180	2	43.37	25.83	3.00	smooth	horiz. up	0.0025	swab		fluorometric	584.64	1	0.9
20059999-181	2	35.20	42.53	3.00	smooth	horiz. up	0.0025	swab		fluorometric	267.53	1	0.9
20059999-182	2	26.76	51.15	3.00	smooth	horiz. up	0.0025	swab		fluorometric	351.59	1	0.9
20059999-183	2	33.94	33.29	3.00	smooth	horiz. up	0.0025	swab		fluorometric	255.63	1	0.9
20059999-184	2	33.14	23.14	3.00	smooth	horiz. up	0.01	minivac		fluorometric	768.16	1	0.9
20059999-185	2	41.58	40.92	3.00	smooth	horiz. up	0.01	minivac		fluorometric	1068.09	1	0.9
20059999-186	2	19.04	52.32	3.00	smooth	horiz. up	0.01	minivac		fluorometric	193.74	1	0.9
20059999-187	2	50.11	34.90	3.00	smooth	horiz. up	0.01	minivac		fluorometric	257.10	1	0.9
20059999-188	2	38.70	30.14	3.00	smooth	horiz. up	0.01	minivac		fluorometric	829.32	1	0.9
20059999-189	2	25.59	48.91	3.00	smooth	horiz. up	0.0025	swab		fluorometric	325.69	1	0.9
20059999-190	2	27.03	26.10	3.00	smooth	horiz. up	0.0025	swab		fluorometric	213.42	1	0.9
20059999-191	2	27.39	18.65	3.00	smooth	horiz. up	0.0025	swab		fluorometric	37.80	1	0.9
20059999-192	2	44.09	30.32	3.00	smooth	horiz. up	0.0025	swab		fluorometric	484.17	1	0.9
20059999-194	1	30.98	40.92	0.00	smooth	horiz. up	0.0025	swab		fluorometric	43.44	1	0.9
20059999-200	2	44.82	34.86	3.00	smooth	horiz. up	0.0025	swab		fluorometric	229.01	1	0.9
20059999-201	2	43.00	27.14	3.00	smooth	horiz. up	0.0025	swab		fluorometric	24.24	1	0.9
20059999-202	2	46.98	26.39	3.00	smooth	horiz. up	0.0025	swab		fluorometric	152.40	1	0.9
20059999-203	2	33.86	35.61	3.00	smooth	horiz. up	0.0025	swab		fluorometric	31.31	1	0.9
20059999-204	2	29.13	36.36	3.00	smooth	horiz. up	0.0025	swab		fluorometric	85.04	1	0.9
20059999-205	2	31.29	45.99	3.00	smooth	horiz. up	0.01	minivac		fluorometric	313.95	1	0.9

barcode ID	Floor ID	X loc. (m)	Y loc. (m)	Z loc. (m)	Surf. Type	Surf. Orient.	Surf. Area (m^2)	Collect. Method	Notes	Analysis Method	Amt. Meas. (µg)	Extr. Eff.	Detn . Eff.
20059999-206	1	37.35	42.42	0.00	smooth	horiz. up	0.0025	swab		fluorometric	1017.02	1	0.9
20059999-207	1	35.27	51.72	0.00	smooth	horiz. up	0.0025	swab		fluorometric	2.02	1	0.9
20059999-208	1	34.77	46.24	0.00	smooth	horiz. up	0.0025	swab		fluorometric	0.00	1	0.9
20059999-209	1	36.77	45.58	0.00	smooth	horiz. up	0.0025	swab		fluorometric	332.75	1	0.9
20059999-210	1	36.77	37.10	0.00	smooth	horiz. up	0.01	minivac		fluorometric	187.48	1	0.9
20059999-211	1	37.43	44.00	0.00	smooth	horiz. up	0.0025	swab		fluorometric	11865.38	1	0.9
20059999-212	1	37.18	43.33	0.00	smooth	horiz. up	0.01	minivac		fluorometric	1841.87	1	0.9
20059999-213	1	39.18	27.64	0.00	smooth	horiz. up	0.0025	swab		fluorometric	0.00	1	0.9
20059999-214	1	33.03	45.08	0.00	smooth	horiz. up	0.0025	swab		fluorometric	347.29	1	0.9
20059999-215	1	40.67	44.50	0.00	smooth	horiz. up	0.0025	swab		fluorometric	33.76	1	0.9
20069999-107	2	36.89	41.60	3.70	smooth	horiz. up	0.0025	swab	Desk Top	fluorometric	30.58	0.9	1
N3001	1	41.70	34.54	0.00	smooth	horiz. up	0.0025	swab		fluorometric	6.11	0.9	1
N3002	1	29.27	32.56	0.00	smooth	horiz. up	0.0025	swab		fluorometric	0.54	0.9	1
N3004	1	38.32	35.50	0.00	smooth	horiz. up	0.0025	swab		fluorometric	0.46	0.9	1
N3005	2	48.03	46.02	3.00	porous	horiz. up	0.0025	swab	at entrance of door	fluorometric	54.78	0.9	1
N3006	2	40.75	25.27	4.00	smooth	horiz. up	0.0025	swab	formica countertop	fluorometric	24.46	0.9	1
N3007	1	28.09	18.28	0.00	smooth	horiz. up	0.0025	swab		fluorometric	4.54	0.9	1
N3009	1	32.65	24.31	0.10	textured	vertical	0.0025	swab		fluorometric	0.00	0.9	1
N3010	2	48.18	50.37	3.00	porous	horiz. up	0.0025	swab		fluorometric	115.01	0.9	1
N3011	1	35.82	48.09	0.00	textured	horiz. up	0.0025	swab	tiles	fluorometric	10.25	0.9	1
N3012	2	48.55	25.12	3.10	smooth	vertical	0.0025	swab		fluorometric	7.47	0.9	1
N3014	1	31.25	49.04	1.00	smooth	vertical	0.0025	swab		fluorometric	41.39	0.9	1
N3031	2	35.23	34.91	3.00	carpet	horiz. up	0.01	minivac		fluorometric	902.58	0.9	1
N3032	2	38.39	30.05	3.00	carpet	horiz. up	0.01	minivac		fluorometric	495.61	0.9	1
N3033	2	26.54	51.77	3.00	carpet	horiz. up	0.01	minivac		fluorometric	1191.97	0.9	1
N3035	2	20.21	52.21	3.00	carpet	horiz. up	0.01	minivac		fluorometric	216.99	0.9	1
N3036	1	42.00	51.10	0.00	carpet	horiz. up	0.01	minivac		fluorometric	283.34	0.9	1
N3037	1	36.92	26.67	0.00	carpet	horiz. up	0.01	minivac		fluorometric	143.30	0.9	1
N3038	2	39.79	34.91	3.00	carpet	horiz. up	0.01	minivac		fluorometric	2241.00	0.9	1

barcode ID	Floor ID	X loc. (m)	Y loc. (m)	Z loc. (m)	Surf. Type	Surf. Orient.	Surf. Area (m²)	Collect. Method	Notes	Analysis Method	Amt. Meas. (µg)	Extr. Eff.	Detn . Eff.
N3039	1	46.49	40.73	0.00	carpet	horiz. up	0.01	minivac		fluorometric	395.92	0.9	1
N3040	1	43.76	38.66	0.00	carpet	horiz. up	0.01	minivac		fluorometric	503.68	0.9	1
N3041	1	37.14	40.80	0.00	carpet	horiz. up	0.01	minivac		fluorometric	2209.74	0.9	1
N3042	1	47.22	45.88	0.00	carpet	horiz. up	0.01	minivac		fluorometric	839.18	0.9	1
N3043	1	45.38	47.79	0.00	carpet	horiz. up	0.01	minivac		fluorometric	323.91	0.9	1
N3044	1	33.68	31.60	0.00	carpet	horiz. up	0.01	minivac		fluorometric	269.56	0.9	1
N3045	1	31.11	34.40	0.00	carpet	horiz. up	0.01	minivac		fluorometric	804.78	0.9	1
N3241	1	47.74	30.64	2.30	textured	vertical	0.0025	swab		fluorometric	116.47	0.9	1
N3242	2	30.59	33.37	3.00	smooth	horiz. up	0.0025	swab		fluorometric	373.60	0.9	1
N3243	1	39.79	50.00	0.00	smooth	horiz. up	0.0025	swab		fluorometric	91.86	0.9	1
N3247	2	24.19	32.41	4.00	carpet	horiz. up	0.0025	swab		fluorometric	80.59	0.9	1
N3248	2	-0.54	17.39	3.00	smooth	horiz. up	0.0025	swab	blank	fluorometric	0.00	0.9	1
N3249	2	0.41	8.05	3.00	smooth	horiz. up	0.0025	swab		fluorometric	0.00	0.9	1
N3252	2	4.31	13.49	3.00	smooth	horiz. up	0.0025	swab		fluorometric	1.44	0.9	1
N3255	1	32.80	26.67	0.00	carpet	horiz. up	0.0025	swab		fluorometric	6.11	0.9	1
N3271	1	36.55	21.59	0.00	carpet	horiz. up	0.01	minivac		fluorometric	249.85	0.9	1
N3272	2	35.59	38.74	3.00	carpet	horiz. up	0.01	minivac		fluorometric	1355.70	0.9	1
N3273	2	42.15	36.16	3.00	carpet	horiz. up	0.01	minivac		fluorometric	1502.23	0.9	1
N3274	2	6.60	19.31	3.00	smooth	horiz. up	0.1	minivac		fluorometric	3.92	0.9	1
N3275	2	4.61	-1.01	3.00	smooth	horiz. up	0.1	minivac		fluorometric	0.61	0.9	1
N3276	2	35.52	15.33	3.00	carpet	horiz. up	0.01	minivac		fluorometric	1222.99	0.9	1
N3277	1	32.87	26.37	0.00	carpet	horiz. up	0.01	minivac		fluorometric	102.92	0.9	1
N3278	2	9.17	5.77	3.00	smooth	horiz. up	0.1	minivac		fluorometric	0.23	0.9	1
N3279	1	31.55	52.28	0.00	carpet	horiz. up	0.01	minivac		fluorometric	212.93	0.9	1
N3280	2	24.26	16.66	3.00	carpet	horiz. up	0.01	minivac		fluorometric	239.21	0.9	1

7.2 Timing Data

In addition to obtaining and analyzing the physical samples, the sampling process itself was of interest in this exercise. The various aspects of the sampling process were timed, including the preparation of the sampling team before going into the contaminated, or “hot” zone, and the cleanup process after they came out.

These were two person teams. Generally one person did the sampling (the "dirty guy"), while the other did the documentation, note taking, labeling, etc. (the "clean guy"). Suiting up to go into the “Hot” zone took 20-35 minutes. Decon and getting out of suits after coming out of the “Hot” zone also took 20-30 minutes. These time periods are significant compared to the ~2 hours that the sampling team can stay in the “Hot” zone in their PPE. The length of time it took to suitup or decon depended on how many people were helping, and whether they were getting photographed/videotaped.

Table 7-3 lists timing results for the various sampling sessions in this exercise, along with the number of samples taken and notes about that session. Although the different sampling methods take different amounts of time, the breakdown for the different collections is not included here. The timing data is imperfect in that one of the sessions using the BROOM tool had equipment failures. Use of the handheld device did not slow down the process of collecting samples once people were comfortable with system. But it appears that there was no large speed up either.

The people participating in this exercise have more and wider experience than the average industrial hygienist. If a major facility gets attacked, the first people who go in would not be experts in sampling, but relatively soon after an event, they would bring in people with more expertise. In the DC responses, the experts wound up supervising many other people with less experience. The job went from a few buildings to ~50 buildings that required assessment in a short period of time. In such a large response, BROOM would be useful as a management tool, combining results from a large numbers of teams. Although originally designed as an analysis tool, BROOM could be more valuable as a data management tool, providing a rapid display of results, as well as a real-time electronic record, which should be much less error-prone than manual data entry.

Table 7-3. Time In “Hot” Zone and Number of Samples Acquired during Various Sampling Sessions.

Session Date	Time In “Hot” Zone	No. of Samples	Notes
Tues. 2/22/05 am	1 hr, 41 minutes	20	Second guy stayed in another 7 minutes taking pictures, while the first one started decon.
Tues. 2/22/05 pm	1 hr, 49 minutes	26	Used their tablet PC tool.
Wed. 2/23/05 am	1 hr, 53 minutes	15	First use of BROOM PDA tool. Had to change batteries in PDA and had a sampling vacuum failure.
Wed. 2/23/05 pm	1 hr, 50 minutes	26	Traditional methods.
Thurs. 2/24/05 am	1 hr, 54 minutes	28, including 6 blanks.	Use BROOM tool. One guy rolled on the floor to get really dirty for decon testing.
Thurs. 2/24/05 pm	1 hr, 46 minutes	20	Put "ground zero" sign in basement.

8 Sample Data Analysis

Sean McKenna, Patrick Finley

Three major analyses were done using the sample data to examine different aspects of the data set and the spatial mapping tools within BROOM. 1) Examination of samples obtained at essentially the same locations using different techniques. This analysis helps to define the very short-scale variation in the Visolite deposition and allows for the calculation of normalization factors that can be used to integrate the different sampling types. 2) Geostatistical estimation techniques are used to map the amount of deposition across both floors of the Coronado Club. This mapping exercise uses traditional estimation techniques that do not account for architectural features within the building. 3) The final analysis examines a new modification to the geostatistical estimation process that accounts for architectural features (walls, doors) in mapping the deposition. This new approach is demonstrated on a sub region of the basement.

8.1 Closely-Spaced Sample Arrays

8.1.1 Introduction

The release of yellow Visolite at the Coronado Club had many different objectives. The release served as a shakedown exercise to prepare for the full field test to be performed the next week with the NIOSH sampling team. Another objective was to generate a large data set for later analysis. Since the yellow Visolite samples were not being collected using full personal protective equipment (PPE), a large number of samples were collected during this exercise. Sampling locations were pre-determined for the yellow Visolite exercise, allowing a full range of sampling methods to be exercised on a variety of surfaces throughout the building.

Seven closely spaced sample arrays were laid out within the Coronado Club. These arrays consisted of groups of six to twelve designated sampling sites in spaced 0.3 to 1m apart. These closely spaced sample arrays were placed throughout the building to provide duplicate samples which would have experienced a similar depositional history. It was hoped that analysis of the data from these arrays could provide more information on reproducibility of sampling and lab procedures. Additionally, sample array data were thought to have the potential to generate values to field-check laboratory based recovery efficiency estimates.

The names assigned to the seven arrays are listed in Table 8-1. The locations of the seven sample arrays are plotted on floor plans of the Coronado Club in Figure 8-1. Of the four arrays on the main floor, only the Entry array is located near the main plume of the release. We assume the main plume of the release followed the prevailing air flow patterns as documented in Section 6.3, which were up the stairwell and into the entryway, then west into the ballroom. Two of the basement arrays were located in the room in which the Visolite release occurred. However, the release was aimed out the door of the room containing the sample arrays so that the arrays were not in the plume of the Visolite release.

Table 8-1. Names and Attributes of Sample Arrays

Name	Floor	Samples	Elevation Above floor
Ballroom Table	Main	6	0.74 m
Ballroom	Main	9	0.0 m
Bar	Main	9	0.0 m
Entry	Main	8	0.0 m
Basement	Basement	12	0.0 m
Basement Table	Basement	8	0.78 m
Hallway	Basement	10	0.0 m

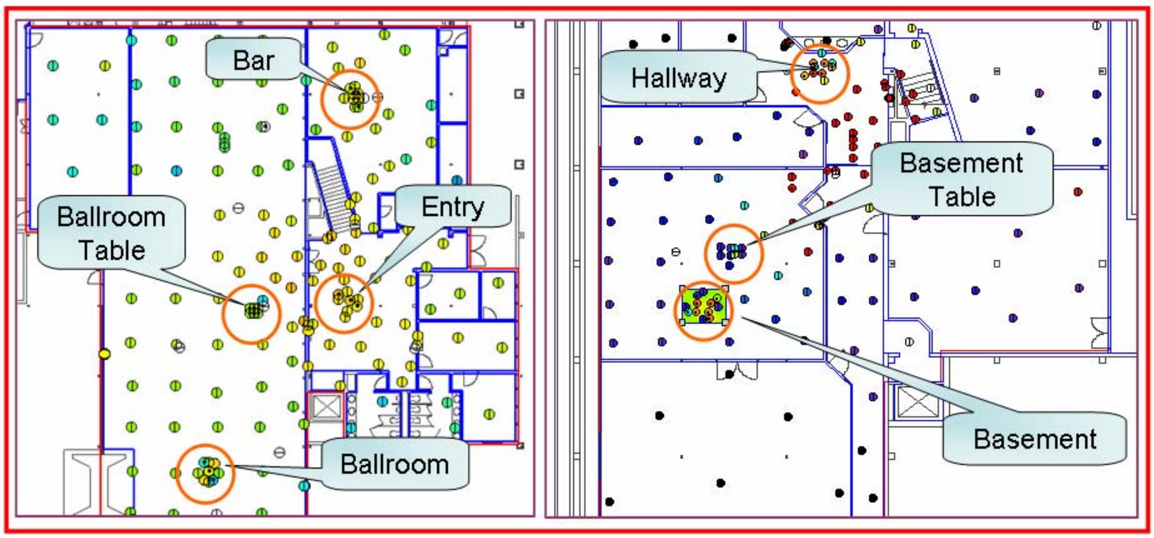

Figure 8-1. Location of Sample Arrays. Main level shown on left, basement shown on right.

8.1.2 Purpose

The purpose of this study was threefold:

1. Establish empirical variance values for yellow Visolite samples for use as nugget input parameters when creating variograms during geostatistical analysis of the dataset.
2. Validate the sample normalization methods used by BROOM to derive Surface Contamination values.
3. Exercise the reporting and data exporting capabilities of broom.

Geostatistical methods use variograms to define the spatial correlation of data sets. A variogram describes how the variability of the data changes with increasing separation between the data points. One important variogram parameter is the nugget value which represents the variability of samples with very little separation between them. The nugget is thus related to the reproducibility of the entire sampling, analysis and reporting sequence. The more precise or reproducible these process are, the smaller the nugget will be. Additionally, the nugget value accounts for variability in the measured values at a spatial scale less than the scale of the sampling, here a nominal 3 m grid. Analysis of these closely spaced sample arrays allows this smaller scale sample variation to be quantified.

BROOM converts sample values reported by the lab to surface contamination values which are corrected for sampling area and possible analyte loss during the sampling and laboratory processes. BROOM relies upon sampling and analytical efficiency estimates generated from laboratory studies of simulants other than Visolite. At the time of this field test, no laboratory values for sampling efficiency for Visolite on different surfaces and with different sampling methods were available for use. Thus, all samples were assigned a constant sampling efficiency of 85% regardless of the surface or method. Examination of the sample arrays with samples collected using different sampling methods can possibly allow us to generate relative recovery efficiency values for Visolite.

BROOM provides a wide range of report and analysis types. However, often an analyst needs to apply a tool which is not available in BROOM. BROOM developers have provided for that need with the *Copy* function which is available on most analysis outputs and map layers. For this study we use the BROOM copy function to transfer sample location, type, and value information to the Windows clipboard and then to various spreadsheet, graphing and statistical packages to demonstrate the advantages of the open architecture approach embraced by the BROOM system.

8.1.3 Methodology

The sample data for each sample array were treated in an identical manner:

1. Sample arrays were located, labeled and mapped
2. Colored contaminant maps were generated of the sample data points within the arrays using BROOM's mapping tools
3. The contaminant maps were analyzed for trends which would indicate lack of depositional uniformity.
4. Sample data from the arrays were copied into the Windows Clipboard
5. Data were pasted into a spreadsheet.
6. Tables were generated from spreadsheet and copied into this document

For some sample arrays with multiple sample collection types, sample data were copied from the spread sheet and pasted to statistical packages to determine relative recovery efficiencies.

8.1.4 Ballroom Table Array

Six wipe samples were located on a table in the ballroom (Figure 8-1). The samples were taken from 1ft^2 (0.093 m^2) floor tiles placed in a rectangular grid on top of an office table (Figure 8-2). Surface contamination values for this array ranged from 363 to 420, with a variance of 600 (Figure 8-3).

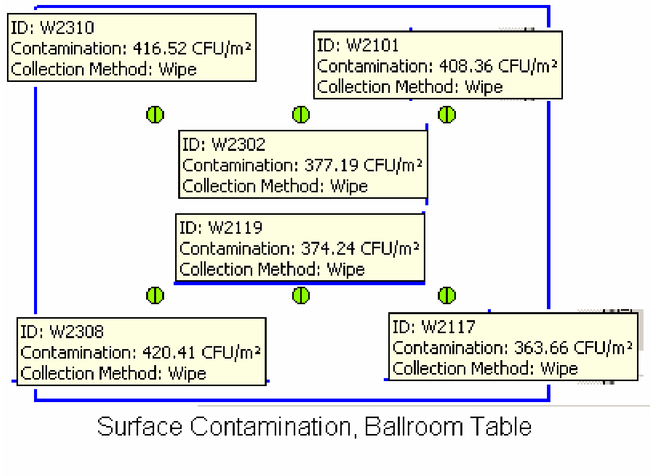

Figure 8-2. Location of Samples within Ballroom Table Sample Array. Blue box is approximately 1.2 m wide.

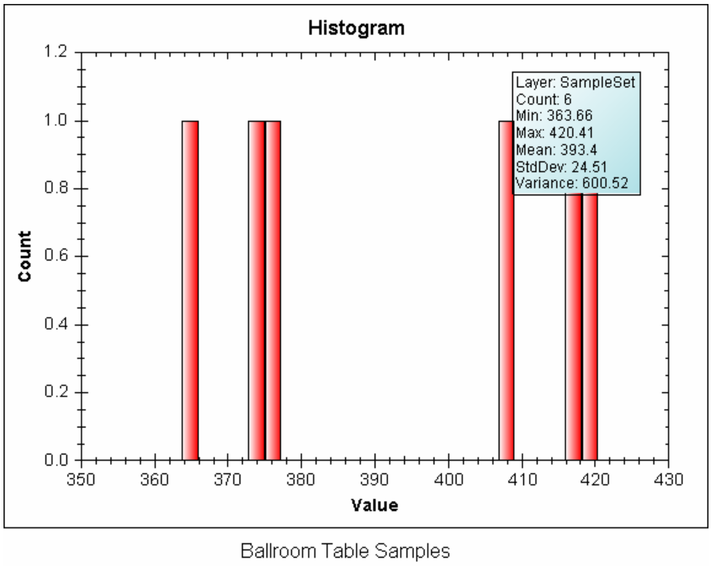

Figure 8-3. Histogram of Surface Contamination Values for Ballroom Table Sample Array.

Mapping of the sample array with colors to show sample values showed no discernable trend of sample values in any preferred direction (Figure 8-4). This indicates that the sample array is in an area of relatively constant deposition and thus was included in this study.

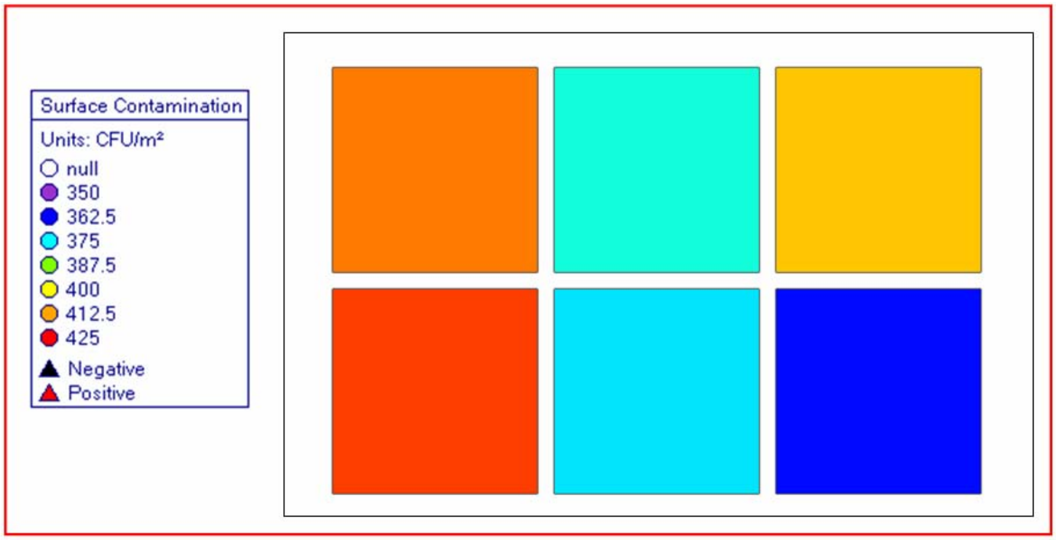

Figure 8-4. Schematic map of Ballroom Table Sample Array. Squares are 1ft (0.305 m) across.

8.1.5 Ballroom Array

The Ballroom sample array consisted of a cross pattern of nine samples. Samples were taken by a variety of collection methods as shown in Figure 8-5.

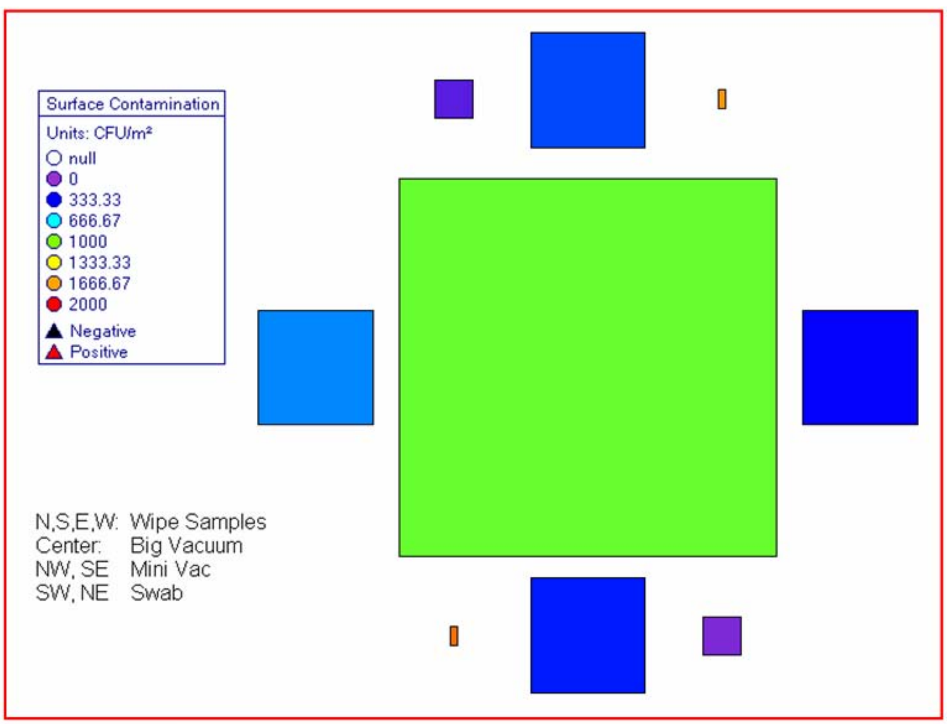

Figure 8-5. Schematic Map of Ballroom Sample Array. Central square is 1m across.

The collection method and measured value for each sample within the array is listed in Table 8-2. The same information is presented in histogram form in Figure 8-6.

Table 8-2. Location and Surface Contamination Values for Ballroom Sample Array

Sampling Method	X	X	Area, m^2	Surface Contam
Wipe	30.001	22.399	0.093	517.5487
Wipe	31.473	22.399	0.093	345.5278
Wipe	30.81	23.135	0.093	430.0265
Wipe	30.81	21.81	0.093	385.3899
Swab	30.442	21.957	0.001	1781.715
Swab	31.105	23.061	0.001	1700.218
MiniVac	31.031	21.957	0.010	79.87796
MiniVac	30.442	23.135	0.010	143.0025
Vacuum	30.81	22.546	1.0	939.86

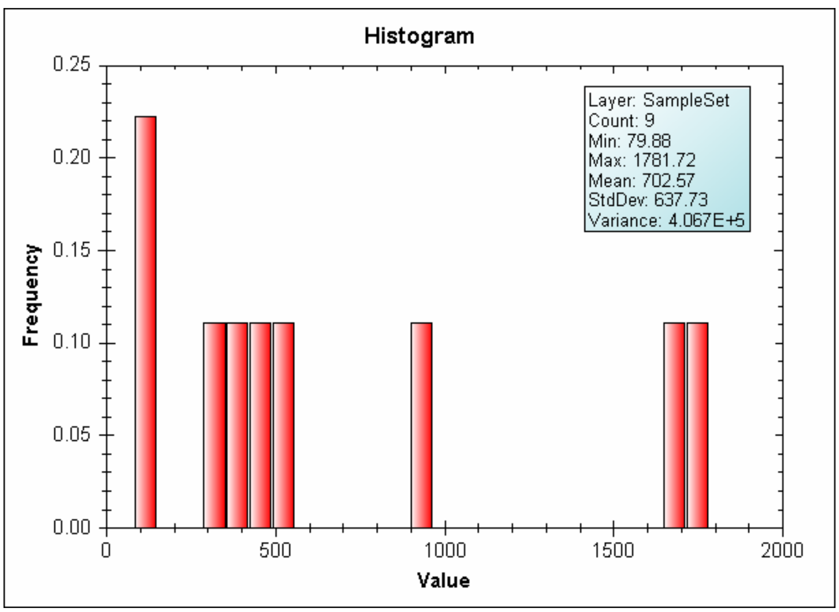

Figure 8-6. Histogram of Surface Contamination Values for Ballroom Sample Array

Table 8-2 and histogram in Figure 8-6 show that different collection methods have markedly different surface contamination values. Since Figure 8-5 shows no discernable trend in concentration, we conclude that the ballroom sample array is an area of consistent deposition. If the sample normalization procedures in BROOM were functioning as designed, we would expect all surface contamination values to be fairly close regardless of the collection method used. Referring back to the Ballroom Table sample array (Figure 8-3) where a single sample collection method was used the standard deviation is about 8% of the mean value. However in ballroom sample array which has 4 different sample collection methods, the standard deviation is about 90% of the mean values. Moreover, comparing Table 8-2 and Figure 8-6 it becomes apparent that values for each sample collection method are tightly clustered, with minivacs having a mean of 111, wipes having a mean of 420, vacuums a value of 940 and swabs with a mean of 1741. This clustering suggests that the recovery efficiencies used to calculate the surface contamination values may not be appropriate for Visolite.

Analysis of Variance (ANOVA) on the sample data shown in Table 8-2 indicates that distinct groups of means exist within the data set at $\alpha = 0.05$. Fisher's least significant difference (LSD) test on the data shows that the mean value of each collection method defines a distinctly resolvable cluster at $\alpha = 0.05$. These statistical results agree with the observations in the previous paragraph that the surface concentration values in the ballroom sample array show systematic differences according to the sample collection method. Since the BROOM sample normalization procedures were designed to eliminate such systematic differences, the procedures or some inputs to the procedures used in the yellow Visolite may need adjustment to function to their maximum potential.

8.1.6 Bar Array

The Bar sample array consists of nine wipe, vacuum and minivac samples taken in a cross pattern (Figure 8-7). The contaminant map shows no obvious trend, suggesting that deposition was consistent across the area.

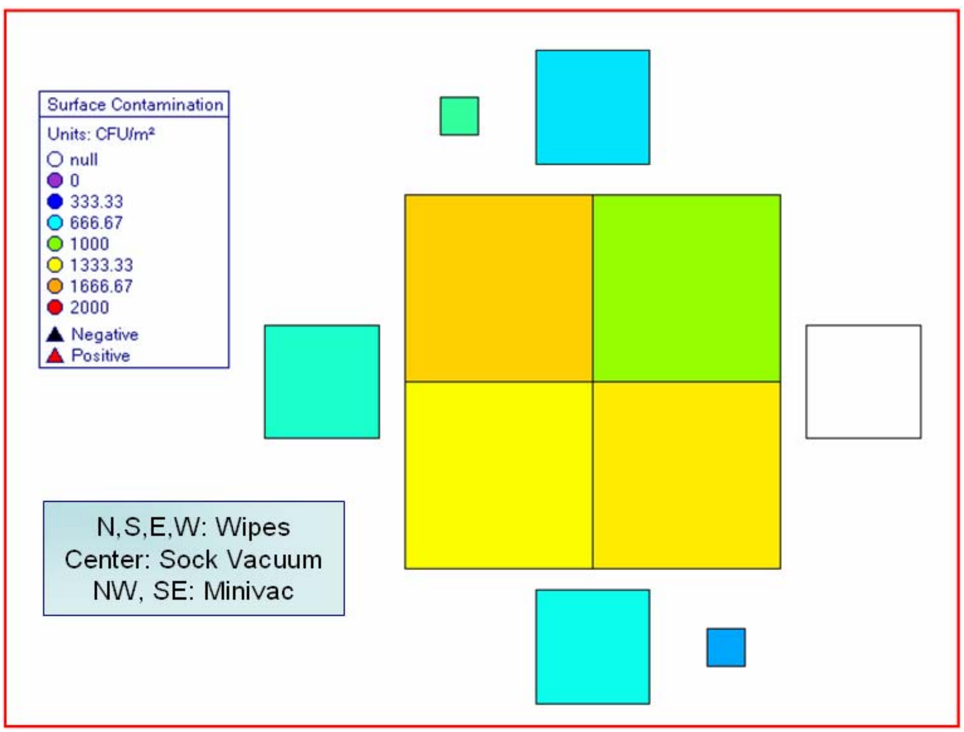

Figure 8-7. Schematic Map of Bar Sample Array. Central 1m square is divided into fourths.

Surface contamination values for this array (Table 8-3, Figure 8-8) show substantially less spread in the Bar array than for the Ballroom array with a standard deviation of about 38% of the mean. Also, the Bar array data do not appear to form clearly separated clusters by sample collection methods, with the wipe and minivac data overlapping (Table 8-4).

Table 8-3. Location and Surface Contamination Values for Bar Sample Array.

Barcode	Method	X	Y	Area, m^2	Surface Contam
W2090	Wipe	40.894	47.717	0.093	697.8877
W2092	Wipe	40.894	49.115	0.093	646.7672
W2184	Wipe	40.158	48.306	0.093	743.1956
W2096	Vacuum	41.114	48.232	0.250	1420.973
W2068	Vacuum	40.746	48.232	0.250	1328.118
W2166	Vacuum	41.114	48.674	0.250	1076.674
W2100	Vacuum	40.746	48.674	0.250	1521.455
MV6	MiniVac	40.526	49.042	0.010	811.083
MV5	MiniVac	41.114	47.717	0.010	554.4202

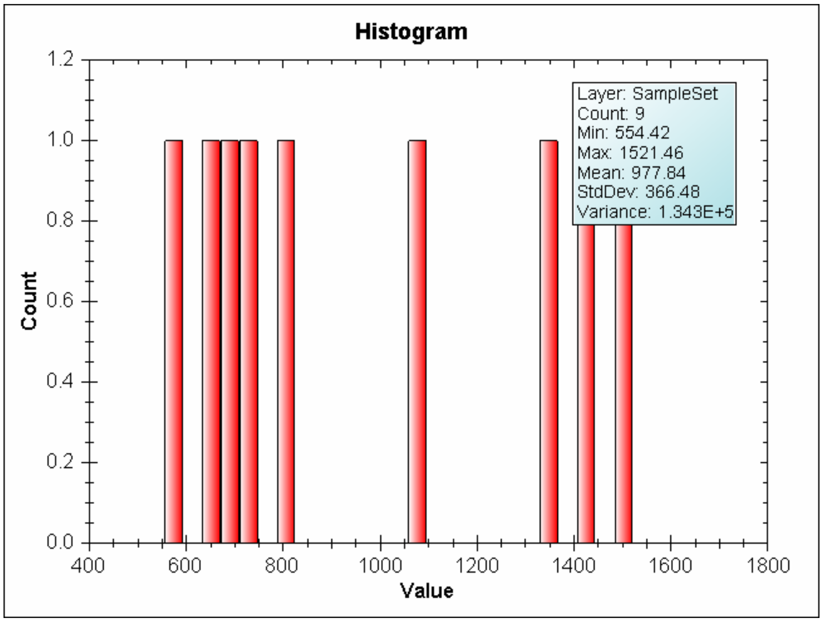

Figure 8-8. Histogram of Surface Contamination Values for Bar Sample Array.

Table 8-4. Summary Statistics by Collection Method for Bar Sample Array.

Collection Method	n	Mean	Standard Deviation	Variance
Wipe	3	696.0	48.2	2,327.2
MiniVac	2	682.7	182.5	32,940
Vacuum	4	1,336.8	190.5	36,310

Statistical analyses support these observations. ANOVA shows that significant groupings of means exist at $\alpha = 0.05$. However, Fisher's LSD test on the data shows that each collection method does not define a distinctly resolvable cluster at $\alpha = 0.05$. Means for vacuums are significantly different from wipes and from minivacs, but means for wipes and minivacs are not significantly different.

The closer agreement of wipe and vacuum data in the Bar array compared to the Ballroom array may reflect the difference in collection surface. The vacuum and minivac samples in the Bar array were all collected from carpet. The vacuum and minivac samples from the Ballroom array were collected from hardwood flooring.

8.1.7 Entry Array

The entry array consists of eight samples in a cross pattern (Figure 8-9). Inspection of the schematic map showed a distinct trend with higher levels in the northwest and lower values in the southeast. The main part of the Visolite plume is located to the northwest of the Entry array. Sample values and summary statistics are listed in Table 8-5 and Table 8-6.

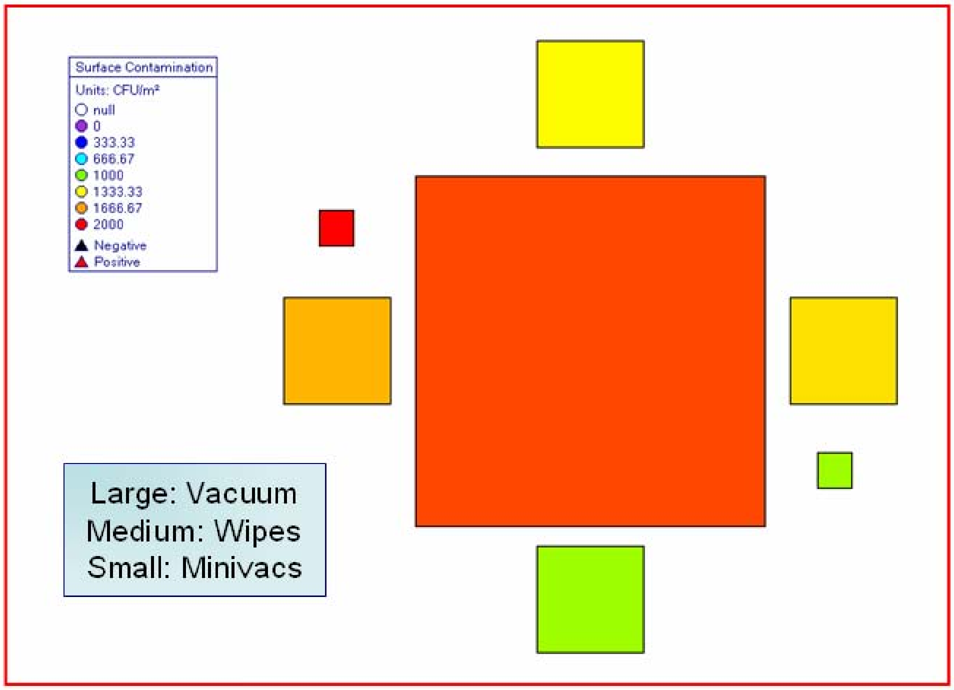

Figure 8-9. Schematic Map of the Entry Sample Array. Large square is 1m wide.

Table 8-5. Surface Contamination Values for the Entry Sample Array.

Barcode	Collection Method	X	Y	Area, m^2	SurfContam
W2087	Wipe	40.378	33.586	0.093	1099.603
W2067	Wipe	40.378	34.984	0.093	1347.124
W2075	Wipe	41.114	34.395	0.093	1462.278
W2093	Wipe	39.716	34.395	0.093	1614.461
mv2	MiniVac	39.716	34.763	0.010	2421.974
mv1	MiniVac	41.041	33.954	0.010	1091.925
W2199	Vacuum	40.526	34.322	1.00	1858.05

Table 8-6. Summary Statistics for the Entry Sample Array.

Collection Method	n	Mean	Standard Deviation	Variance
Wipe	4	1,381	217.1	41,150
Minivac	2	1,756	940	88,450
Vacuum	1	1,858.5	n/a	n/a

This indicated that the array probably does not represent an area of consistent deposition, and its inclusion into the array set used to validate sample normalization procedures might lead to spurious results. Thus, further analysis on the Entry array data was not pursued.

8.1.8 Basement Array

The basement array consists of 12 wipe, minivac and vacuum samples arranged in a cross pattern (Figure 8-10). No consistent trend is noted in the interpolated contaminant map, or in examining the individual sample values (Table 8-7).

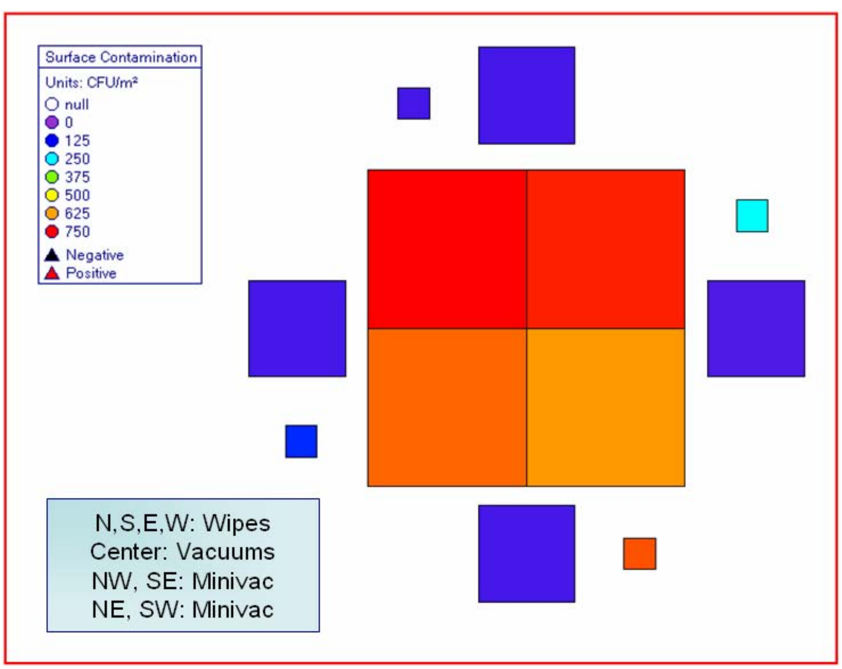

Figure 8-10. Schematic Map of Basement Sample Array. Large central square is 1m across.

Table 8-7. Location and Surface Contamination Values for Basement Sample Array.

Barcode	Method	X	Y	Area, m^2	Surface Contam
W2042	Wipe	29.706	31.819	0.093	64.11601
W2106	Wipe	29.044	32.555	0.093	70.22383
W2104	Wipe	29.044	31.157	0.093	75.07399
W2134	Wipe	28.234	31.819	0.093	73.63583
MV7	MiniVac	28.382	31.525	0.010	147.2756
MV9	MiniVac	29.338	31.231	0.010	691.1087
MV10	MiniVac	29.633	32.261	0.010	253.5648
MV8	MiniVac	28.75	32.408	0.010	70.19563
W2130	Vacuum	28.75	32.04	0.250	773.7699
W2140	Vacuum	28.676	31.525	0.250	675.2006
W2124	Vacuum	29.265	31.525	0.250	636.4085
W2128	Vacuum	29.412	32.04	0.250	733.539

The histogram of the surface contamination values for the basement sample array (Figure 8-11) shows a roughly bimodal distribution with a lower value grouping of the wipe samples and three of the minivac samples, and a higher valued grouping of one minivac sample and all four vacuum samples (Table 8-8).

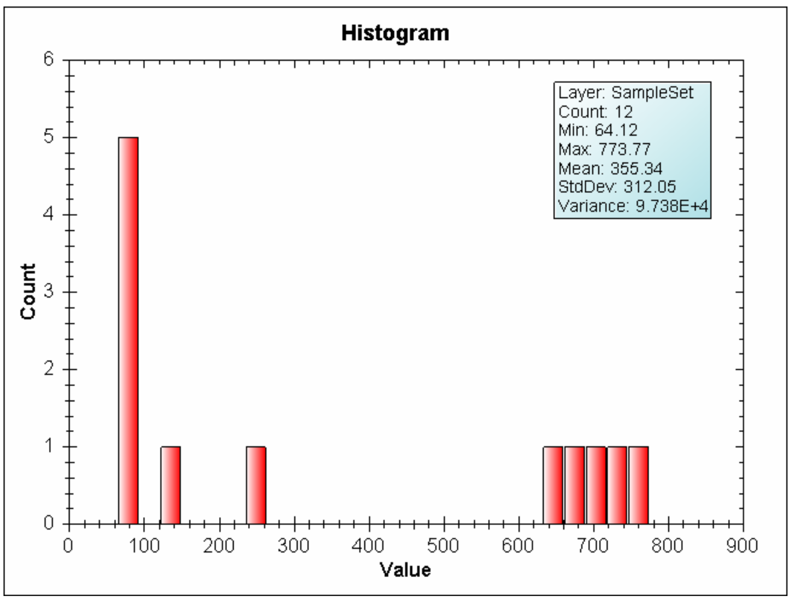

Figure 8-11. Histogram of Surface Contamination Values for Basement Sample Array.

Table 8-8. Summary Statistics of Basment Array Samples by Collection Method.

Collection Method	n	Mean	Standard Deviation	Variance
Wipe	4	70.8	4.9	23.7
MiniVac	4	290.5	277.4	76,900
Vacuum	4	704.7	60.9	3,710

Statistical analyses show that the vacuum values are significantly different from the others. ANOVA shows that significant groupings exist at $\alpha = 0.05$. However, Fisher's LSD test on the data shows that each collection method does not define three distinctly resolvable means at $\alpha = 0.05$. Means for vacuums are significantly different from wipes and from minivacs, but means for wipes and minivacs are not significantly different.

A curious feature of this array dataset is the low values associated with wipe samples. The mean wipe value for the Basement array is 16% of that of the Ballroom array, and 10% of that of the Bar array. However, the vacuum samples are in much closer agreement between the three arrays, with the Basement array vacuum mean being 70% of the Ballroom array vacuum mean, and 53% of the Bar array vacuum mean. The low values for wipes in this area could be interpreted as an indication that the contaminant plume did not flow back into the room. However, similarly low values would be expected in nearby vacuum and minivac samples as well. For now, the unusually low basement wipe values remain unexplained

8.1.9 Basement Table Array

The Basement Table array consists of eight wipe samples in a two-by-four grid pattern (Figure 8-12). No trend of higher values toward the Visolite release source which is located 4 m to the ENE of the map in Figure 8-12.

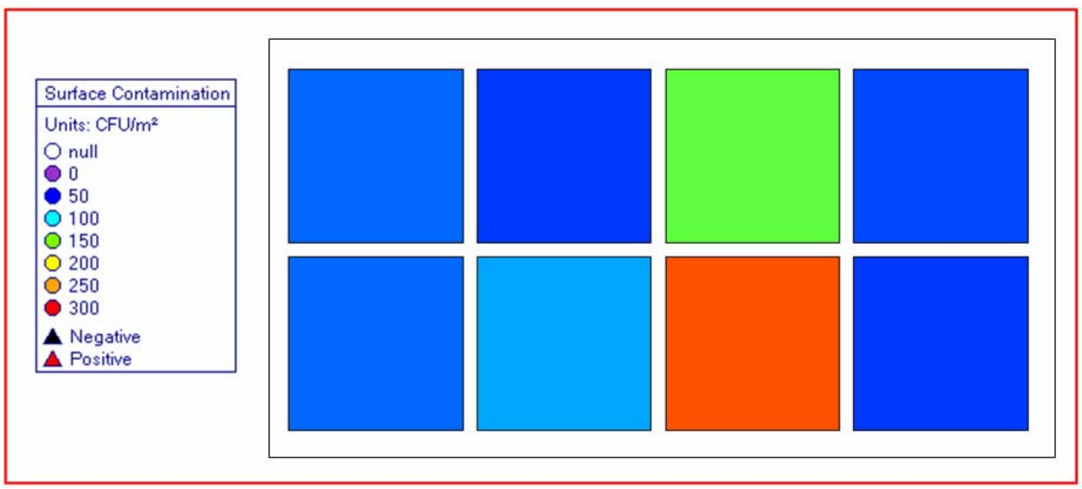

Figure 8-12. Schematic Map of Basement Table Sample Array Squares are 1ft (0.305 m) across.

Surface contamination values for the Basement Table array range from 61.2 to 278.3 (Table 8-9). A mean surface contamination value of 103.9 was calculated, along with a standard deviation of 74.8 and a variance of 5,601.

Table 8-9. Surface Contamination Values for Basement Table Sample Array.

Barcode	Method	X	Y	Area, m^2	Surface Contam
W2020	Wipe	29.854	34.837	0.093	70.75524
W2006	Wipe	29.854	34.395	0.093	71.1447
W2014	Wipe	30.295	34.395	0.093	82.83922
W2016	Wipe	30.295	34.763	0.093	63.11215
W2044	Wipe	30.516	34.469	0.093	278.3195
W2004	Wipe	30.516	34.763	0.093	138.4396
W2110	Wipe	30.81	34.469	0.093	61.23519
W2036	Wipe	30.81	34.763	0.093	65.22171

8.1.10 Hallway Array

The Hallway array consists of 10 wipe, minivac and vacuum samples arranged in a cross pattern in the main corridor of the basement (Figure 8-13). This array is close to the main plume of the Visolite release, which traveled north along the basement corridor, then turned to the southeast and headed up the stairwell.

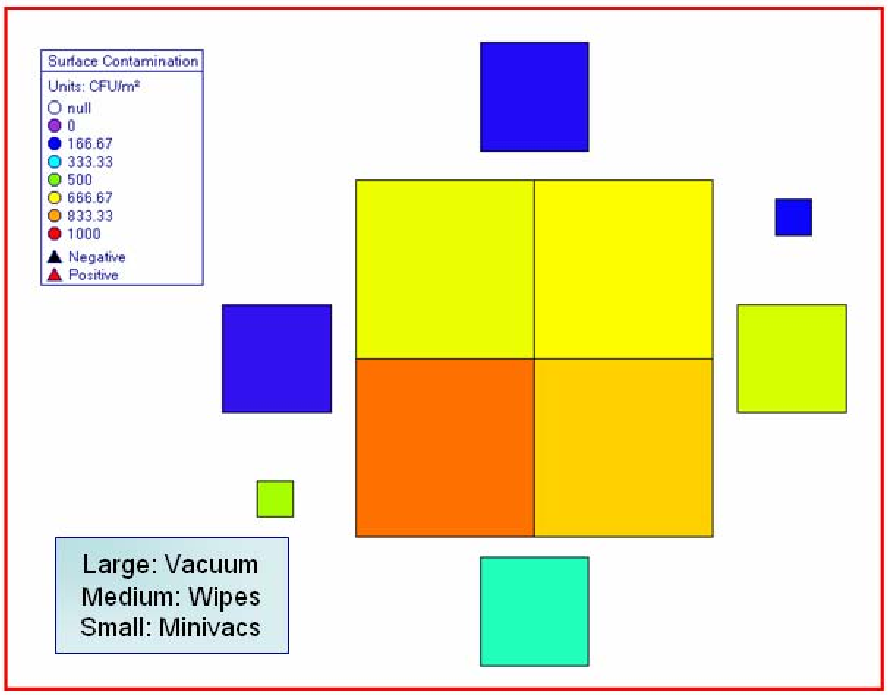

Figure 8-13. Schematic Map of the Basement Sample Array. Large square is 1m wide.

No consistent east-to-west trend is noted in the interpolated contaminant map, or in examining the individual sample values (Table 8-10). However, a north-to-south decrease in the values appears to exist in wipe and vacuum samples. Thus, it appears that depositional conditions were not uniform across the width of this array.

Table 8-10. Surface Contamination Values for the Hallway Sample Array.

Barcode	Method	X	Y	Area, m^2	SurfContam
W2181	Wipe	33.611	43.96417	0.093	116.664
W2237	Wipe	34.564	44.626	0.093	141.054
W2062	Wipe	35.006	43.963	0.093	620.184
W2164	Wipe	34.638	43.301	0.093	387.038
MV11	Minivac	33.754	43.522	0.010	554.203
MV16	Minivac	35.006	44.184	0.010	161.339
W2005	Vacuum	34.638	44.184	0.25	681.745
W2311	Vacuum	34.122	44.184	0.25	645.210
W2013	Vacuum	34.122	43.669	0.25	896.210
W2007	Vacuum	34.564	43.669	0.25	764.146

Summary statistics in Table 8-11 show that vacuum samples average about twice the values that minivac and wipe samples do in this sample array.

Table 8-11. Summary Statistics for the Hallway Sample Array.

Collection Method	n	Mean	Standard Deviation	Variance
Wipe	4	316.24	236.58	55970
Minivac	2	357.77	277.8	77170
Vacuum	4	746.83	111.32	12390

8.1.11 Data Analysis

Data from the individual arrays showed that the sample normalization procedures in BROOM did not always produce consistent results with the default inputs. Samples collected with different methods displayed normalized values with systematic discrepancies. In this section, data from multiple arrays will be compared to attempt to resolve some of the disparities noted.

8.1.11.1 Reproducibility of Wipe Values

Wipe samples were collected in all studied sample arrays. Results from 25 wipe samples are summarized in Table 8-12. The mean, standard deviation and variance values listed in Table 8-12 vary widely since the arrays were located in different parts of the building and thus experienced different depositional environments. The column labeled "CV" lists the coefficient of variation, which is the standard deviation divided by the mean. This scaled value shows that typically, the standard deviation of the wipe samples within an array are less than 10% of the mean value. The mean coefficient of variation for all sample arrays is 22%, but the median is 6.9%

Table 8-12. Summary Statistics for Wipes.

Array	n	Mean	StdDev	CV	Variance
Ballroom Table	6	393.4	24.51	6.2%	600.52
Ballroom	4	419.6	73.85	17.6%	5,454
Bar	3	696.0	48.20	6.9%	2,327
Basement	4	70.8	4.9	6.9%	23.7
Basement Table	8	103.9	74.8	71%	5,601

8.1.11.2 Reproducibility of Minivac Values

Minivac samples were collected in three studied sample arrays. Results from eight minivac samples are summarized in Table 8-13. The mean minivac coefficient of variation value for all sample arrays is 53.9%, higher than the 22% recorded for wipe samples.

Table 8-13. Summary Statistics for Minivacs.

Array	n	Mean	StdDev	CV	Variance
Ballroom	2	111.4	44.6	40%	1,989
Bar	2	682.7	182.5	26.7%	32,940
Basement	4	290.5	277.4	95%	76,900

8.1.11.3 Reproducibility of Vacuum Values

Vacuum samples were collected in three studied sample arrays. Results from nine vacuum samples are summarized in Table 8-14. The mean vacuum coefficient of variation value for all sample arrays is 11.4%, lower than the 22% recorded for wipe samples.

Table 8-14. Summary Statistics for Vacuums.

Array	n	Mean	StdDev	CV	Variance
Ballroom	1	939.8	n/a	n/a	n/a
Bar	4	1336.8	190.5	14%	36,310
Basement	4	704.7	60.9	8.7%	3,710

8.1.11.4 Deriving Sample Normalization Factors

BROOM normalizes sample quantity measured values returned from the laboratory so that they can be displayed in a meaningful way. The system tracks sampling efficiency and sampling area values for each sample taken. Using these values, BROOM calculates a normalized value for surface contamination by the following formula:

Surface Contamination = (Quantity Measured) / (Sampling Efficiency) / (Sampling Area)

The factors used to calculate surface contamination values are summarized in Table 8-15.

Table 8-15. Sample Normalization Parameters

Factor	Description
Surface Contamination (C_s)	Normalized surface contamination = (Q_m) / (E_s) / (A_s)
Quantity Measured (Q_m)	Contaminant value reported by laboratory
Sampling Area (A_s)	Area of surface sampled in meters squared
Sampling Efficiency (E_s)	Net efficiency of sampling process (E_c x E_c x E_c)
Collection Efficiency (E_c)	Fraction of contaminant transferred to sample medium
Extraction Efficiency (E_e)	Fraction of contaminant extracted from sample medium
Detection Efficiency (E_d)	Fraction of contaminant detected by analytical method

In the yellow Visolite test sample dataset these values were used for all samples regardless of sample collection method:

- Collection Efficiency = 1.0
- Extraction Efficiency = 0.85
- Detection Efficiency = 1.0

For the geostatistical analysis presented in Section 8.2, only wipe samples taken from vinyl were used to avoid any complications of variations in these efficiencies across sample types.

Table 8-16 displays the mean values for each collection type in three sample arrays. Additionally the table lists the ratios of the mean values of wipes to vacuums and minivacs to vacuums. These ratios can be used to derive estimates of sampling efficiencies for the various collection methods. If determined to be reliable and reasonable, these ratios, or estimates derived from them, could be applied to the input parameters in the above Surface Contamination equation.

Table 8-16. Derivation of Normalization Factors

Array	Mean Wipe	Mean MiniVac	Mean Vacuum	Wipe / Vacuum	MiniVac / Vacuum	Comment
Ballroom	419.6	111.4	939.8	0.446	0.119	Minivac onHardwood
Bar	696.0	682.7	1336.8	0.520	0.510	All on Carpet
Basement	70.8	290.5	704.7	0.100	0.412	Very low wipe values
Entry	1,381	1,756	1,858.5	0.748	0.945	Near Plume, Questionable
Hallway	316.24	357.77	746.83	0.424	0.479	Near Plume, Questionable

As noted above in the discussion of the Basement sample array, the wipe values in that array seem anomalously low. Thus we ascribe the Wipe:Vacuum ratio which is derived from the Basement sample array exclusively to samples from the basement floor. The Minivac:Vacuum ratio for the Ballroom sample array is lower than for other sample arrays. The minivacs in the Ballroom sample array were collected on a hard surface, while the other minivacs were recorded as having been collected on carpet. Thus we will ascribe the low ratio noted for the Ballroom sample array only to minivacs collected on hardwood.

Based on the values in Table 8-16 and the preceding paragraph, relative normalization values were derived (Table 8-17). These values can be applied to one of the constituent efficiency values which go to make up sampling efficiency (Table 8-15) to permit BROOM to generate maps using new and presumably improved surface contamination values. These detailed normalization factors take into account fine-grained variations between sample arrays and assign different values for minivacs and wipes depending on surface characteristics and whether they were collected on the main floor or the basement.

Table 8-17. Detailed Normalization Factors.

Collection Method	Surface	Floor	Normalization Factor
Vacuum	All	All	1.00
Minivac	Carpet	All	0.461
Minivac	Hardwood	All	0.119
Wipes	All	Main	0.483
Wipes	All	Basement	0.100
Swabs	All	All	1.852

Table 8-18 lists more generalized normalization factors which may be applicable to the dataset as a whole. The weighted mean column was obtained from Table 8-17 by weighting the normalization factors for a collection method by the number of samples which occupied each subcategory. The median normalization factor takes the median value of the factors for the three sample arrays in Table 8-16, which has the effect of removing the outliers.

Table 8-18. Generalized Normalization Factors.

Collection Method	Weighted Mean	Median
Vacuum	1.00	1.00
Minivac	0.388	0.412
Wipes	0.421	0.446
Swabs	1.852	1.852

8.1.11.5 Applying Detailed Normalization Factors

The detailed normalization factors derived from the sample arrays were applied to the Coronado Club yellow Visolite data set. This was done by inputting factors in Table 8-17 as the collection efficiency values for each sample in the dataset. The normalization factor chosen for a given sample value depended upon the collection method, surface and floor level as indicated in Table 8-17. BROOM calculates surface contamination values at runtime based upon the reported laboratory values and assigned sampling areas and efficiencies. Thus, once the normalization factors had been entered into BROOM, reported surface contamination values reflected the new factors. Mean sample values, standard deviation and coefficient of variation for each sample array before and after normalization are listed in Table 8-19.

A principal goal of the normalization process is to decrease variability between samples collected using different methods. Substantial improvement (i.e. reduction) is obtained from normalization when looking at coefficient of variation (Table 8-19) for the three sample arrays where multiple sample collection methods were employed. Standard deviation is improved for the Ballroom and Bar sample arrays, but increases slightly in the Basement sample array. Preceding analysis of reproducibility of sample measurements within arrays suggests that sampling and measurement errors scale with the mean value. In that case, coefficient of variation should be a better gauge of normalization performance than would simple standard deviation. In either event, the two sample arrays on the main floor achieved much greater decrease in sample value variability by application of the derived normalization values than did the sample array in the basement.

Table 8-19. Effect of Applying Detailed Normalization Factors to Samples.

Sample Array	Mean Surface Contam	Standard Deviation	Coefficient of Variation	Resolvable Means from ANOVA
Ballroom	702.6	637.7	90.7%	4
Ballroom Normalized	907.6	166.8	18.4%	1
Improvement:		*73.8%*	*79.7%*	*Yes*
Bar	977.8	366.5	37.5%	2
Bar Normalized	1,403.1	198.5	14.1%	1
Improvement:		*45.8%*	*64.4%*	*Yes*
Basement	355.3	312.0	87.9%	2
Basement Normalized	680.9	319.1	46.9%	1
Improvement:		*<2.3%>*	*46.6%*	*Yes*

The last column in Table 8-19 summarizes results of analysis of variance (ANOVA) runs on surface contamination values for the three sample arrays before and after normalization. As discussed earlier, ANOVA showed that the mean values for each of the four collection methods in the Ballroom array were distinctly resolvable at $\alpha = 0.05$. The same analysis repeated on the Ballroom array data after normalization shows that the mean for the array cannot be resolved into distinct groups by collection method. Similarly, the two way partition shown by ANOVA for the Bar and Basement sample arrays is lost in the normalized data set at $\alpha = 0.05$ or a 95% confidence level. These results suggest that the derived normalization factors are adequately accounting for variation between values of samples obtained with different collection methods.

The effect of sample normalization on the Ballroom sample array is summarized in Figure 8-14. In these maps and those to follow, the sample sites were mapped as discrete points rather than the larger tiles as represented in earlier maps. Space between the data points are interpolated through inverse distance weighted methods. The maps in Figure 8-14 show that normalized sample values tend more toward the middle of the color range.

The histograms in Figure 8-14 demonstrate that the samples are more normally distributed, with a larger number of samples near the center of the range and fewer extreme outliers. Note that the horizontal axis on the normalized histogram is much expanded over the original.

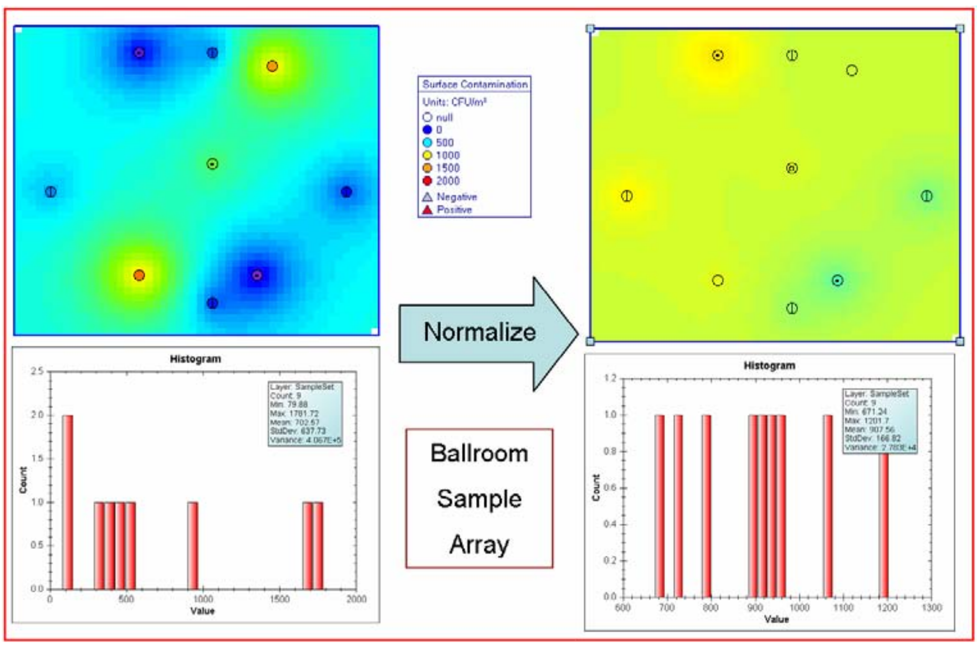

Figure 8-14. Effect of Normalization on Ballroom Sample Array.

The effect of sample normalization on the Bar sample array is summarized in Figure 8-15. The maps show that normalized sample values tend more toward the high end of color range but with reduced dynamic range. The central four vacuum samples were assigned a normalization factor of 1.0, so their value and color does not change. The effect of the normalization on this array is to increase the values of the wipe and minivac samples so that they are more in accordance with the vacuum samples.

The histograms in Figure 8-15 demonstrate that the samples are shifted to higher values. All wipe and minivac samples with values lower than 1,000 were displaced upward. Interestingly, the normalization generated an outlier. The minvac in the NW portion of the map has the highest value in the normalized dataset, whereas it was among the lower values in the original set.

The effect of sample normalization on the Basement sample array is summarized in Figure 8-16. The maps show that normalized sample values tend more toward the high end of color range but with reduced dynamic range. The central four vacuum samples were assigned a normalization factor of 1.0, so their value and color does not change. The effect of the normalization on this array is to increase the values of the wipe samples so that they are more in accordance with the vacuum samples. The minivac samples showed very wide spread in this sample array. When they are scaled to bring their mean into rough equality with the vacuum samples, the variation within the minivac sample set is accentuated. Thus, the two blue and one red sample symbols on the normalized map all correspond to minivac samples.

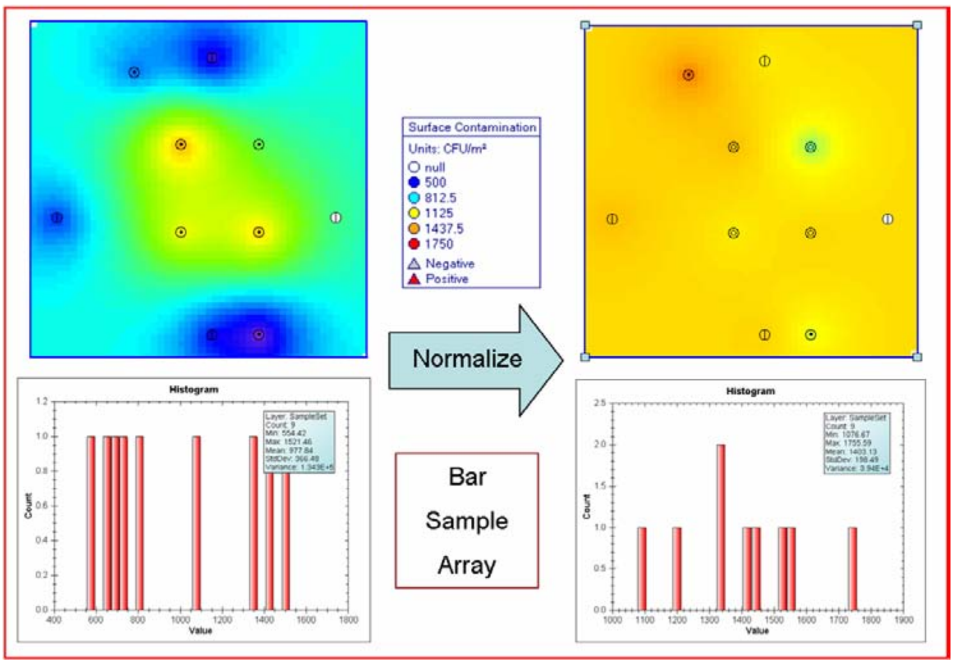

Figure 8-15. Effect of Normalization on Bar Sample Array.

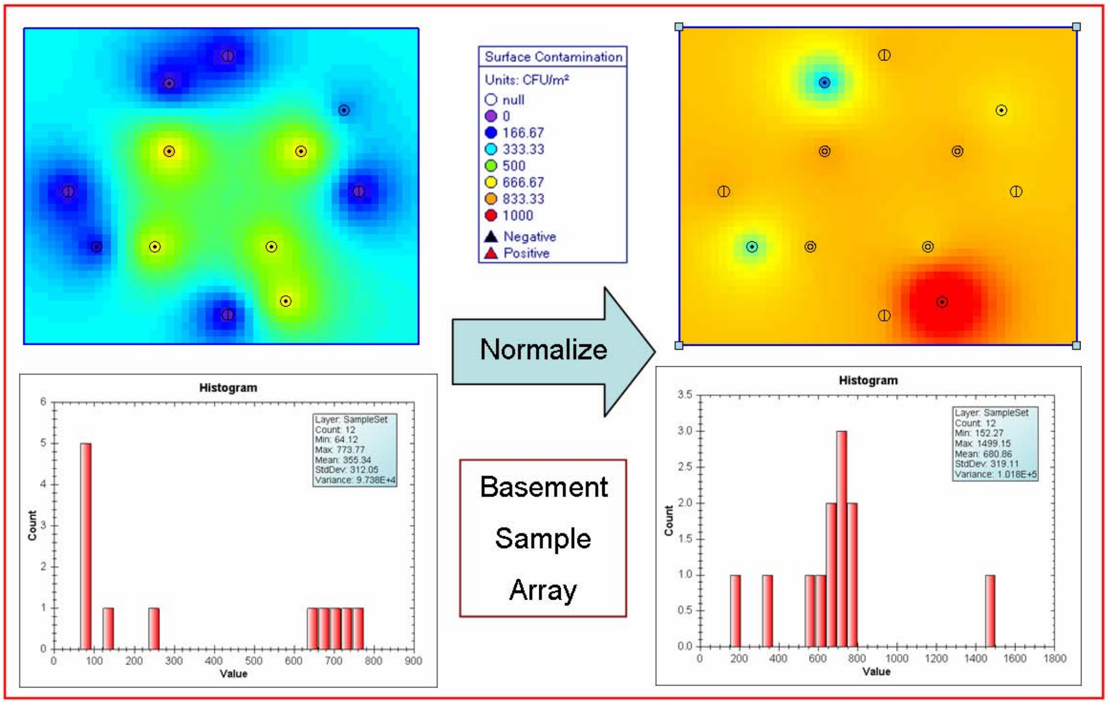

Figure 8-16. Effect of Normalization on Basement Sample Array.

The histograms in Figure 8-16 demonstrate that the samples are shifted to higher values. All wipe samples with values lower than 100 were displaced upward. The two low outliers on the histogram and the single high outlier correspond to the minivac samples discussed above. The maps and histogram for the Basement sample array confirm the interpretations drawn from Table 8-19. In this sample array, applying normalization brings the wipe and vacuum samples into good agreement. However, the already large spread of minivac values is amplified. However, it is notable that after normalization, the minivac values span the vacuum and wipe values, whereas before, the minivac values were consistently below the vacuum values.

We stress that this normalization exercise deals with *relative* adjustment to the BROOM surface contamination values. When the three efficiencies listed in Table 8-15 are known with adequate certainty, the BROOM system computes surface contamination values which have numerical significance. In this instance, we identified vacuum samples as having the best reproducibility of the sample collection methods used. Then we established normalization factors for other sample collection methods relative to vacuum samples. Since we do not know the accuracy of the 85% sampling efficiency figure being applied to vacuum samples, the normalized values presented above remain relative.

8.1.11.6 Applying Generalized Normalization Factors

The generalized normalization factors derived from the sample arrays were also applied to the Coronado Club yellow Visolite data set. This was done by using the "Median" normalization factors in Table 8-18 as the collection efficiency values for each sample in the dataset. The generalized normalization factors chosen for a given sample value do not depended upon the collection method, surface and floor level. Mean sample values, standard deviation and coefficient of variation for each sample array before and after normalization are listed in Table 8-20.

Table 8-20. Effect of Applying Generalized Normalization Factors to Samples.

Sample Array	Mean Surface Contam	Standard Deviation	Coefficient of Variation	Resolvable Means from ANOVA
Ballroom	702.6	637.7	90.7%	4
Normalized	1,160	315.0	27%	1
Improvement:		*50.6%*	*70.2%*	*Yes*
Bar	977.8	366.5	37.5%	2
Normalized	1,482.5	247.6	16.7%	1
Improvement:		*32.5%*	*55.5%*	*Yes*
Basement	355.3	312.0	87.9%	2
Normalized	552.86	443.9	80.3%	2
Improvement:		*<42.0%>*	*8.7%*	*No*

A goal in normalization is to decrease variability between samples collected using different methods. Considerable improvement (i.e. reduction) is obtained from normalization when looking at coefficient of variation (Table 8-20) for two of the three sample arrays where multiple sample collection methods were employed. Standard deviation is improved for the Ballroom and Bar sample arrays, but increases markedly in the Basement sample array. Coefficient of variation improved for both the Ballroom and the Bar sample arrays, but improved only slightly for the Basement array. ANOVA results showed that the means of the samples having different collection methods were successfully merged into a single group mean which for the Ballroom array and the Bar array. However, the mean value of the Basement array could still be resolved into multiple group means since wipe samples are not sufficiently adjusted by the normalization process.

8.1.12 Comparison of Normalization Factors

Detailed normalization factors take into account the surface and floor level that a sample was collected upon (Table 8-17). Generalized collection factors apply to all samples in the facility (Table 8-18). The preceding two sections showed results of applying detailed and generalized normalization factors to the yellow Visolite data set. This section compares the normalization results from the detailed factors and the generalized factors.

Improvements in sample variation within sample arrays due to normalization are listed in Table 8-21. The table lists the three indicators of improvement used in the preceding two sections: standard deviation (“StdDev”), coefficient of variation (“CV”), and analysis of variance (“ANOVA”). The values in the table represent percentage improvement in the measures following normalization. Angle brackets around a value indicate that the indicator did not improve, but worsened by that amount.

Table 8-21. Comparison of Normalization Factors for Sample Arrays.

Sample Array Normalization	Std Dev Improvement	CV Improvement	ANOVA Improvement
Ballroom Detailed	73.8%	79.9%	Yes
Ballroom Generalized	50.6%	70.2%	Yes
Bar Detailed	45.8%	64.4%	Yes
Bar Generalized	32.5%	55.5%	Yes
Basement Detailed	<2.3%>	46.6%	Yes
Basement Generalized	<42%>	8.7%	No

Overall, the detailed factors showed better performance in reducing sample value variability compared with the generalized factors. The detailed normalization factors showed improvement in the majority of measures for each array, whereas the generalized factors showed an unfavorable effect for the Basement sample array.

The detailed factors require much more work to derive and apply than do the generalized factors. It could be argued that the results for the detailed factors are not meaningful since the surface type and floor level for these factors were assigned so as to best reduce sample variation within the sample arrays. The generalized factors, however, are not overly fit to each sample array. Table 8-21 indicates that the generalized factors obtain good improvement in reducing sample variability in the main floor of the Coronado Club.

8.1.13 Geostatistical Nugget Values

A key input in determining spatial correlation is the variance of samples which are separated by zero distance. This value, called the *nugget* in geostatistical terminology, is a measure of the uncertainty in a sample set due to random collection and measurement errors. Typically, the nugget value is estimated from a variogram, which is a plot of variance between sample points as a function of separation distance, by extrapolating the curve to zero separation.

The sample arrays provide an alternative method for estimating nugget values for this data set. The samples within a sample array are very close together compared to other samples in the data set. Table 8-22 shows variance values calculated from sample arrays.

Table 8-22. Variance of Wipe Samples.

Array	Sample Value Set	n	variance
Ballroom Table	Quantity Measured	6	4.34
Ballroom	Quantity Measured	4	44.41
Bar	Quantity Measured	3	16.82
Basement	Quantity Measured	4	0.15
Basement Table	Quantity Measured	8	40.47
Weighted Mean Variance		*25*	*23.22*
Ballroom Table	Surface Contamination	6	600.52
Ballroom	Surface Contamination	4	5,454
Bar	Surface Contamination	3	2,327
Basement	Surface Contamination	4	23.7
Basement Table	Surface Contamination	8	5,601
Weighted Mean Variance		*25*	*3,091*
Ballroom Table	Surf Contam Normalized	6	2,574
Ballroom	Surf Contam Normalized	4	23,380
Bar	Surf Contam Normalized	3	9,977
Basement	Surf Contam Normalized	4	2377
Basement Table	Surf Contam Normalized	8	24,010
Weighted Mean Variance			*13,642*

These variance values show wide variation among the sample arrays. The Ballroom Table and Basement Table shared a similar layout, but one has a low variance and one a high variance. With no objective information which array to weight more than the other, the mean of the array variances is suggested for use as a starting point for variogram nuggets:

- 23.22 when mapping wipe samples using the BROOM Quantity Measured option
- 3,091 when mapping wipe samples using the BROOM Surface Contamination option
- 13,642 when mapping wipe samples using the BROOM Surface Contamination option and the normalization factors in Table 8-17.

8.1.14 Conclusions

Seven closely-spaced arrays of sample locations were laid out for the yellow Visolite test at the Coronado Club. This study examined the sample values in detail for five of those sample arrays. Summary statistics were obtained for each sample array. Reproducibility values were calculated for wipe, minivac and sock vacuum sample collection methods. Within the limits of the small sample set, HEPA vacuums appear to have somewhat better reproducibility than wipe samples and much better reproducibility than minivacs.

Using vacuum samples as a starting point, normalization factors were calculated for wipes and minivacs. Applying these normalization factors substantially reduced the sample value variability within each of the upstairs sample arrays and somewhat reduced the sample value variability within the downstairs array. Generalized normalization factors which do not depend upon sampling surface or floor level were also derived. These factors, approximately 0.4 for both wipes and minivacs, showed good reduction of sample variability in the main floor of the Coronado Club. Mean wipe-sample variance values for each sample array were calculated and tabulated for use in follow-on geostatistical work.

This exercise and the preparation of this report relied heavily on reporting and data export features in BROOM which had to this point been relatively untested. The ability to copy subsets of sample data into spreadsheets and statistical packages functions well and extends the range of tools available to the analyst beyond those included in the BROOM package.

8.2 *Spatial Mapping of Aerosol Deposition*

8.2.1 Introduction

To the extent possible, the Visolite tracers released in these tests are representative of the release and dispersion of a biological contaminant within a building. Samples obtained from these releases allow several aspects of contaminant characterization and contaminant mapping to be evaluated. This portion of the report focuses on the evaluation of the sample data for contaminant mapping. By using two different data sets for each of the tests, the variability of the contaminant maps with respect to the sample configuration can be evaluated. For the pink Visolite release, the two different data sets are due to different sampling strategies as developed by the NIOSH team and by the sample optimization algorithms within the BROOM software. For the yellow Visolite release, the large set of samples are randomly divided into two different sample sets.

Specific goals of this analysis are to

- Test spatial mapping capabilities within BROOM software being developed at Sandia National Laboratories
- Use data collected in a set of tracer tests to evaluate spatial mapping algorithms for use in creating maps of surface deposition.
- Compare estimates of surface deposition as made from two different sampling designs.
- Evaluate the ability of a "data-driven" approach that does not use any flow information to produce accurate estimates of surface contamination in actual facility.

A brief background on the spatial mapping approaches evaluated in this report is presented. For each tracer test, yellow and pink Visolite, the available sample data set, the analyses performed on the data set and the results of those analyses are discussed.

8.2.2 Mapping Approach

Geostatistics is the study of spatially and/or temporally correlated data as well as the application of a set of tools to produce spatial estimates (maps) of spatially correlated properties from a limited set of sample data. The origin and development of geostatistics comes from the mining industry where a precise and unbiased technique was needed to calculate ore reserve estimates from limited borehole data. Geostatistical approaches are now applied in a wide range of areas including mining, petroleum, environmental, meteorological, agricultural and ecological studies.

Several studies in the environmental field have incorporated information on the source location and average transport direction of airborne contaminants using geostatistical approaches to estimate contaminant concentrations within soil. These works have relied on known source locations, such as discharge stacks from smelters, and prevailing wind directions over long periods of time to develop trends that are relatively simple functions of distance and direction (azimuth) from the known source (see Saito and Goovaerts, 2001; Mohammadi et al., 1997). Other work has focused on mapping the spatial and temporal evolution of deposition from atmospheric aerosols over large regions of the earth (e.g., Kyriakidis and Journel, 2001). Environmental applications such as these benefit from the estimation goal being to map the cumulative effects of contamination being deposited over years, or even decades, from a single, continuous, source location.

Little application of geostatistical methods to the estimation of indoor aerosol deposition has been accomplished to date. Work done by NIOSH after the Miami anthrax release used indicator geostatistics to map the probability of a positive test for anthrax conditional to data collected on two different floors of the building. However, the dispersive nature of aerosol transport and deposition make it likely that samples of indoor contamination would exhibit spatial correlation and be amenable to geostatistical analysis. Two unresolved issues regarding the use of geostatistical techniques for mapping indoor aerosol contamination need to be considered:

- The effect of the discretization of the spatial domain into different rooms by walls and doors. Geostatistical algorithms employ a measure of spatial correlation as determined along the straight-line distance between sample points. In indoor settings, this straight-line distance may cross from one room to another where the deposition amounts are very different due to one room having a direct air-flow connection to the source of the contaminant while the other room does not. Samples taken close together, yet on opposite sides of the wall dividing these rooms, will have very different concentrations and will not necessarily fit with the model of smoothly varying concentration employed in the geostatistical algorithms.
- The effect of the air flow within the building on the dispersal of the contaminant may result in complex dispersal patterns. Geostatistical mapping algorithms should be able to reproduce these complex patterns, but the more complex the transport patterns, the more it may be necessary to collect larger numbers of samples to identify these patterns. An advantage of geostatistical algorithms is the capability to incorporate secondary information with the sample data to make improved estimates of the contaminant deposition. One promising source of secondary information is a numerical model of the air flow and aerosol transport within a building at the time of the contaminant release. Multivariate geostatistical algorithms could be employed to combine the discrete sample data with spatially continuous estimates of the concentration as predicted by the transport model to improve the overall estimation. No transport model currently exists for the Coronado Club and these data integration approaches are not considered further in this work.

A brief background on the some of the key geostatistical concepts is presented below. More background on geostatistical theory and algorithms can be found in textbooks by Deutsch and Journel (1998), Goovaerts (1997), Olea (1999) and Wackernagel (1998).

8.2.2.1 Variogram

The semivariogram $\gamma(\mathbf{h})$, or more simply, the variogram, is the basic tool in a geostatistical study and is a measure of the variability of the measured attribute values measured at two locations as a function of the separation distance between those two locations. This separation distance can be calculated across all orientations, in which case it remains a scalar quantity, or it can be calculated in a directionally dependent manner such that it is a vector. The variogram has been used for description of spatial patterns (Western, et al., 1998), as the basis for spatial interpolation (Rouhani, 1996), and for the generation of realizations of spatial processes (stochastic simulation) (McKenna, 1998).

Given a set of data values, z, and the (x,y,z) locations of each value represented by the spatial vector, $\mathbf{u}$, the experimental variogram value, γ, can be calculated as:

$$\gamma(\mathbf{h}) = \frac{1}{2N(\mathbf{h})} \sum_{i=1}^{N(\mathbf{h})} [z(\mathbf{u}_i) - z(\mathbf{u}_i + \mathbf{h})]^2 \qquad (1)$$

where N(**h**) is the number of pairs of data locations a vector **h** apart. This calculation provides the average spatial similarity/dissimilarity of data pairs *z*(**u**) and *z*(**u**+**h**) separated by a vector **h**. The experimental variogram is a set of points calculated using Equation 1, one point for each separation distance, **h**, that defines one-half the average squared difference in values between all data pairs separated by that distance.

The set of points calculated as the experimental semivariogram can be used as the final product when the goal of the study is to identify patterns of spatial variation in the data set. However, most geostatistical studies have a final goal of using the observed spatial variation in the data to make estimates of the data values at unsampled locations. In order to do this, an analytical function must be fit to the experimental semivariogram to provide a variogram measure at all possible distances, not just those at the integer values of **h** calculated in the experimental semivariogram. The chosen analytical function must produce a positive definite covariance matrix, as discussed below, for the kriging equations. This constraint limits the choice of analytical function, or variogram models, to a handful of functions that are guaranteed to produce such a covariance matrix. Three of the most common variogram model functions are the

Spherical,

$$\gamma(\mathrm{h}) = \mathrm{C} \cdot \left[1.5\frac{\mathrm{h}}{\mathrm{a}} - 0.5\left(\frac{\mathrm{h}}{\mathrm{a}}\right)^3 \right] \quad for \quad h < a \qquad (2)$$

$$\gamma(\mathrm{h}) = \mathrm{C} \quad for \quad h \geq a$$

Exponential

$$\gamma(\mathrm{h}) = \mathrm{C} \cdot \left[1 - \mathrm{e}^{-\frac{3\mathrm{h}}{\mathrm{a}}} \right] \qquad (3)$$

and Gaussian

$$\gamma(\mathrm{h}) = \mathrm{C} \cdot \left[1 - \mathrm{e}^{\left(-\frac{(3h)^2}{a^2}\right)} \right] \qquad (4)$$

Each of these functions has two variables: the sill, *C*, and the range, *a*. The sill is the maximum γ value of the variogram model and the range is the separation distance, **h**, at which this sill value is reached. An additional third parameter, the nugget, is defined as the γ value of the model when **h** =0. Due to measurement repeatability issues and/or a minimum sample spacing that is greater than zero, it is not necessary that the variogram model have a γ value of zero when **h** = 0 and the addition of the nugget to the models above makes it possible to capture this behavior. A comparison of the three variogram models is presented in Figure 8-17. Each model has a sill of 1.0 and a range of 100.0. The nugget value is set to zero for all three models. Different combinations of the models defined here can be made to model a complex experimental variogram.

Often the spatial correlation varies with direction, and such a case requires one to compute the variograms in different orientations and to fit anisotropic (direction-dependent) models.

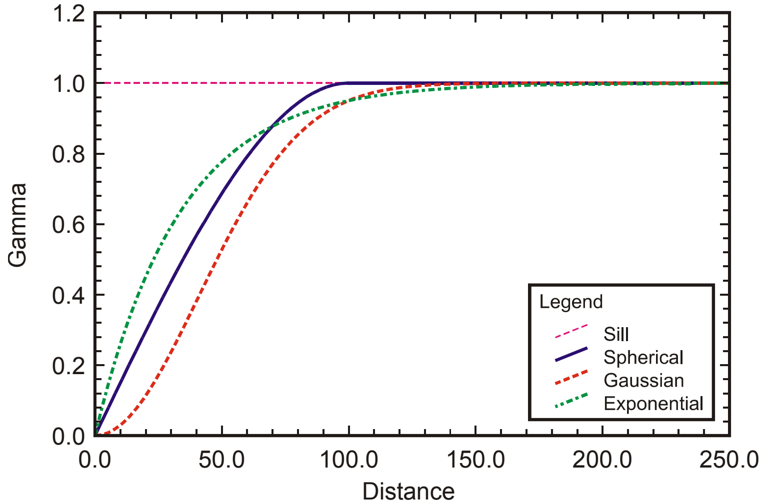

Figure 8-17. Example variogram models all having a sill of 1.0 and a range value of 100.0

The variogram value modeled by the expressions above is, under certain conditions, the complement of the spatial covariance value:

$$\gamma(\mathbf{h}) = C(\mathbf{0}) - C(\mathbf{h}) \tag{5}$$

where C(**0**) is the covariance of the data at **h**=0, which is the variance of the data.

8.2.2.2 Kriging

Kriging, named after D. G. Krige a South African mining engineer whose pioneering work on development of geostatistics is well recognized, is the term for spatial estimation done using a geostatistical algorithm that incorporates spatial covariance information derived from the variogram. Consider the problem of estimating the value of a continuous attribute *z* (e.g. surface contamination) at an unsampled location **u**, where **u** is a vector of spatial coordinates. The information available consists of measurements of *z* at *n* locations $\mathbf{u}_\alpha$, $z(\mathbf{u}_\alpha)$, $\alpha = 1,2, ..., n$. Kriging is a form of generalized least square regression. All univariate kriging estimates are variants of the general linear regression estimate $z^*(\mathbf{u})$ defined as:

$$z^*(\mathbf{u}) - m(u) = \sum_{\alpha_1=1}^{n(\mathbf{u})} \lambda_\alpha(\mathbf{u})[z(\mathbf{u}_{\alpha_1}) - m(\mathbf{u}_{\alpha_1})] \tag{6}$$

where $\lambda_\alpha(\mathbf{u})$ is the weight assigned to the datum $z(\mathbf{u}_\alpha)$ and $m(\mathbf{u})$ is either the stationary mean of the variable, or more generally, a trend component of the spatially varying variable. The observation $z(\mathbf{u}_\alpha)$ can be used directly or replaced by some linear, or even nonlinear, transformation of the measured variable. In practice, only the observations closest to **u** being estimated are retained, that is the $n(\mathbf{u})$ data within a given neighborhood or search window $W(\mathbf{u})$ centered on **u**.

The most common kriging estimate is ordinary kriging (OK), which estimates the unsampled value $z(\mathbf{u})$ as a linear combination of neighboring observations:

$$z^*_{OK}(\mathbf{u}) = \sum_{\alpha_1=1}^{n(\mathbf{u})} \lambda_\alpha^{OK}(\mathbf{u})\, z(\mathbf{u}_{\alpha_1}) \tag{8}$$

OK weights λ_α are determined so as to minimize the error or estimation variance $\sigma^2(\mathbf{u}) = \mathrm{Var}\{Z^*(\mathbf{u})\text{-}Z(\mathbf{u})\}$ under the constraint of unbiasedness of the estimate. These weights are obtained by solving system of linear equations, which is known as the "ordinary kriging system":

$$\begin{cases} \sum_{\beta=1}^{n(\mathbf{u})} \lambda_\beta(\mathbf{u})\, \gamma(\mathbf{u}_\alpha - \mathbf{u}_\beta) - \mu(\mathbf{u}) = \gamma(\mathbf{u}_\alpha - \mathbf{u}) \qquad \alpha = 1,\ldots,n(\mathbf{u}) \\ \sum_{\beta=1}^{n(\mathbf{u})} \lambda_\beta(\mathbf{u}) = 1 \end{cases} \tag{9}$$

The unbiasedness of the OK estimate is ensured by constraining the weights sum to one, which requires the definition of the Lagrange parameter $\mu(\mathbf{u})$. The only information required for a unique solution to this system are the variogram values for different lag distances, and these are readily derived from the chosen positive definite variogram model fit to experimental values.

The estimation variance, or kriging variance, is written as:

$$\sigma^2_{OK}(\boldsymbol{u}) = Cov(0) - \sum_{\alpha=1}^{n(\boldsymbol{u})} \lambda_\alpha Cov(\boldsymbol{u} - \boldsymbol{u}_\alpha) - \mu(\boldsymbol{u})$$

Where $Cov(0)$ is the covariance function evaluated at zero separation distance which is equal to the variance of the data set. The kriging weights, λ_α, are the same as those determined for the solution of the kriging system. The kriging variance provides a measure of the uncertainty in the kriging estimates. The kriging variance is only a function of the data locations and does not directly incorporate the measured values at the data locations. The kriging variance can be thought of as a measure of the data sparsity that is relative to the variogram model fit to the sample data.

It is noted that the kriging algorithm treats the spatial correlation between any two points as being calculated along a straight line. If two sample points are in different rooms and the straight line between them is intersected by a wall that provides a barrier to flow and transport, no consideration of this information is made in the kriging algorithm. Modifications to the kriging algorithm to take this information into account are under development.

8.2.3 Yellow Visolite Test

Two different data sets were collected corresponding to the yellow and pink Visolite releases. Sampling of the yellow Visolite was designed to provide a large number of samples with uniform characteristics across both floors of the Coronado Club facility. These samples could then be used to validate the results of the spatial mapping. Spatial estimation of the surface contamination using the entire yellow data set as well as each of two randomly selected halves of the data set was completed using ordinary kriging.

The yellow Visolite was dispersed in a preliminary test that was designed to provide a large set of samples for use in validating a number of sample collection and mapping goals. Here, this sample set is used to validate approaches to mapping the spatial distribution of Visolite deposited on the floor. Several different types of sampling techniques were used to obtain the yellow Visolite data including wipes, swabs, and large and small vacuum samples. The vast majority of the samples were obtained on the vinyl tiles using wipes and those data are the focus of this validation exercise. A major difference in sampling of the yellow Visolite compared to the pink Visolite is that roughly 240, 12-inch square vinyl tiles were placed throughout the Coronado Club facility prior to releasing the yellow Visolite. A sample was collected from each of these tiles using a wipe. Sampling on these tiles provide a uniform sampling surface at all locations that considerably reduces the variability in sampling efficiency due to sampling on different surfaces and with different sample collection methods.

8.2.3.1 Full Data Set Estimation

The entire wipe data set is used to estimate surface contamination in both the basement and on the main floor. The process of splitting the data set in half and the jackknife procedure for evaluating the estimates is discussed later.

8.2.3.1.1 Basement

The yellow Visolite samples collected in the basement are shown in Figure 8-18. There are 158 total samples in the basement. Similar to those collected on the main floor, these include wipes, swabs and different types of vacuum samples. Only the 131 wipe samples on the vinyl tiles are used in the mapping analysis. The histogram describing the distribution of surface contamination as measured on these wipe samples is shown in Figure 8-19.

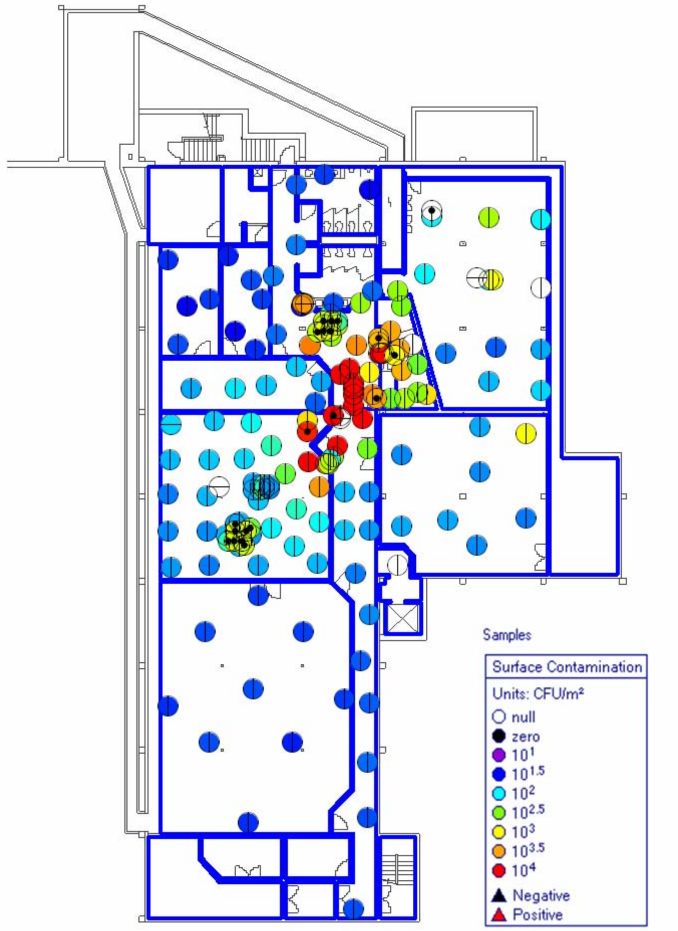

Figure 8-18. Distribution of all surface contamination samples for the yellow Visolite, basement.

The basement samples have a large range in surface contamination values, greater than four orders of magnitude (Figure 8-19), and also show strong positive skew. Therefore, the log10 values of surface contamination are used in the mapping analysis.

Sample W2275 was entered twice into the database. The X,Y coordinates of this sample are (47.3,50.0). The W2275 surface contamination values are109.51 and 106.64 (µg/m^2). In order to complete the mapping exercise, the duplicate W2275 sample with the lower concentration was removed from the data set leaving 130 samples for analysis.

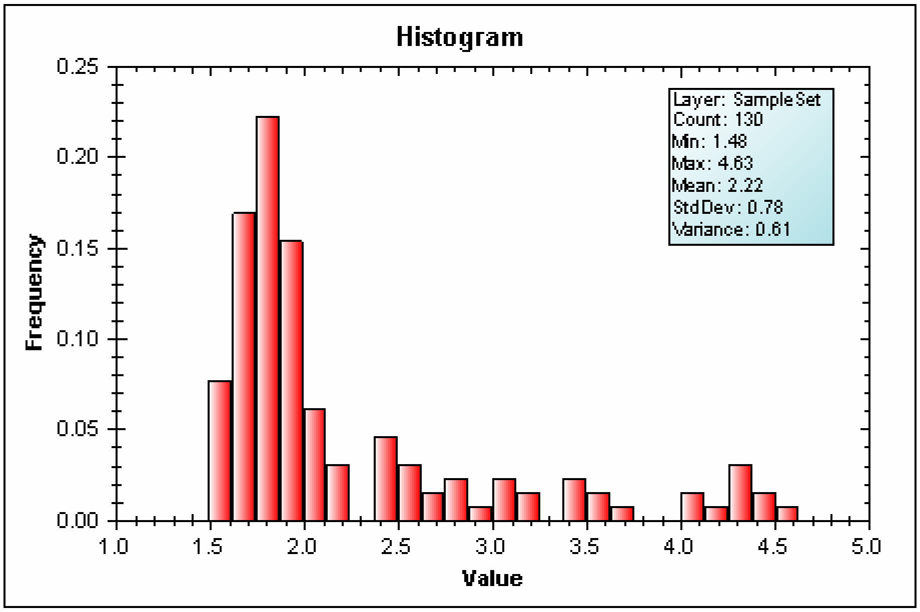

Figure 8-19. Histogram of log10 surface contamination for the yellow Visolite collected with wipe samples, basement.

The 130 samples in the basement were used in the experimental variogram calculation (Equation 1). The lag spacing used was 3.0 meters. The resulting experimental variogram points and the number of pairs used in the calculation of each point are shown in Figure 8-20. These experimental points were fit with an exponential variogram model with a range of 5.5 meters, a nugget of zero and a sill of 0.615. The sill is set to be equal to the variance of the log10 transformed data. The experimental variogram points show a distinct “hole effect” pattern where the experimental points rise above the sill before decreasing again at larger separation distances. This result is due to the higher concentration data found in the hallway near the bottom of the stairs (see Figure 8-18). Samples on either side of this high concentration area are more similar when compared to each other than when compared to samples within the high concentration zone and cause the experimental variogram to reach a peak value at a separation distance of approximately 9 meters. This hole effect is not modeled and the total sill of the model (nugget plus sill) is set to the variance of the data set as shown by the horizontal black line on Figure 8-20.

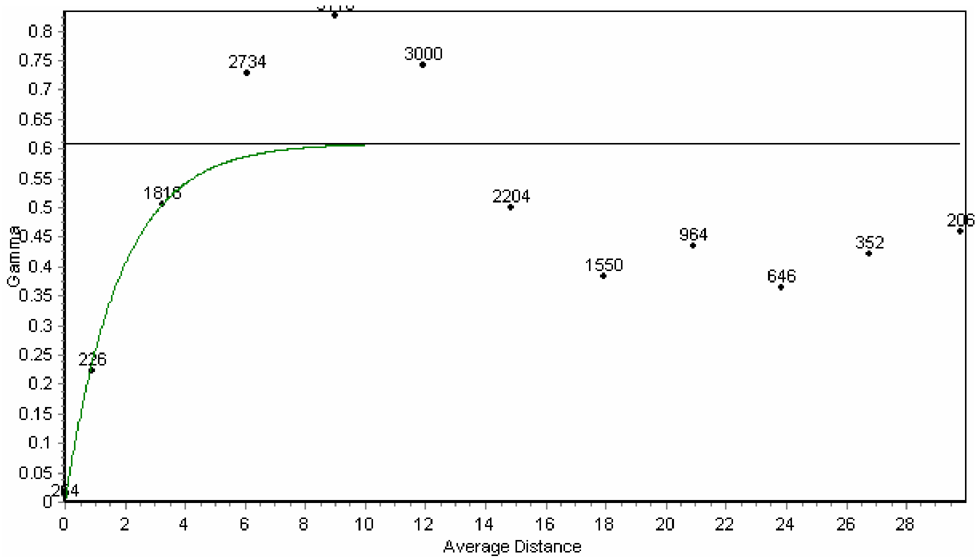

Figure 8-20. Experimental and model variogram for the 130 yellow Visolite wipe samples in the basement. The log10 values of surface contamination are used.

The variogram model and the sample data are used as input to the ordinary kriging process. The surface contamination values are estimated at points arranged on a 0.5 x 0.5 meter square grid. The grid is uniform except in some areas where slight deviations to the grid are made to accommodate the irregular shape of the building. The results of estimating the surface contamination at all locations in the basement are shown in Figure 8-21. These results clearly show the path of the yellow Visolite tracer from the release point in the nearly square conference room on the left side of the basement, out the door in the northeast corner of that room and north along the hallway to the base of the staircase. Some relatively high values of the surface contamination are seen in the northeast and eastern portion of the basement. These estimates indicate that very little tracer was deposited in the room where the release was made and that essentially none of the tracer migrated to the southern end of the basement. The northwestern corner of the basement was also left relatively free of surface contamination.

The kriging variance map (Figure 8-22) shows the relative uncertainty of the estimates across the basement. For the data set used here, the uncertainty is low in the areas of highest surface contamination as the sample coverage is dense in these areas. In the southern and eastern portions of the basement, the kriging variance is higher indicating less confidence in estimates made in those areas.

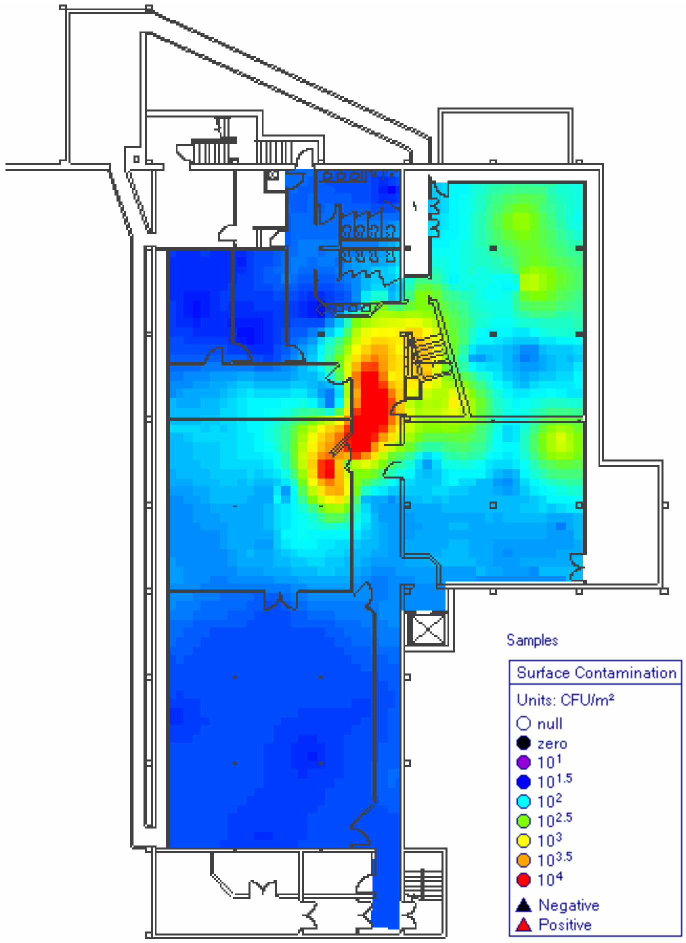

Figure 8-21. Kriged estimates of log10 surface concentration values in the basement using the 130 yellow Visolite wipe samples.

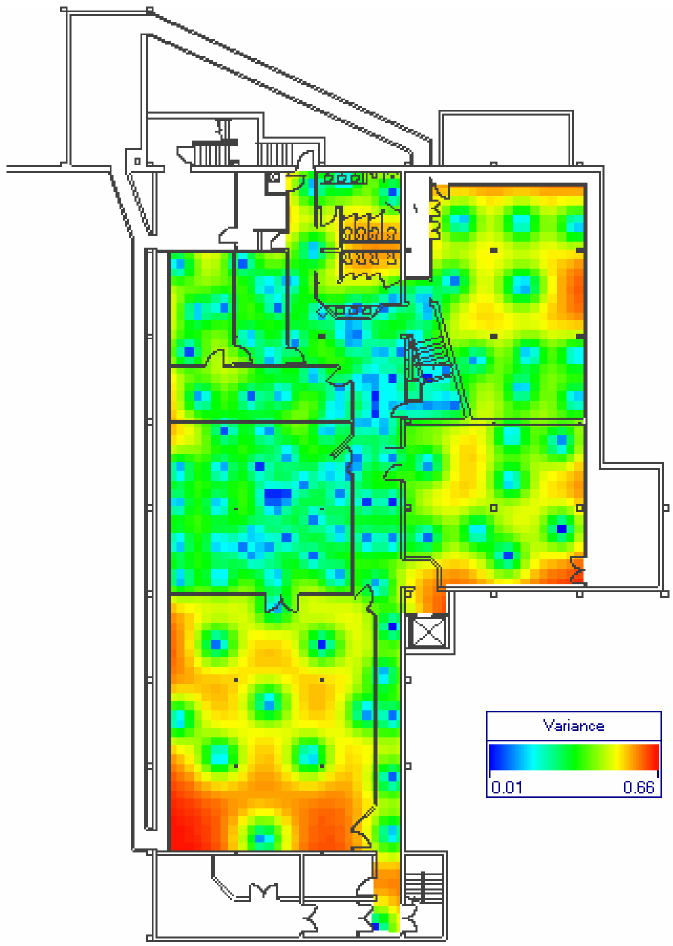

Figure 8-22. Kriging variance for the estimates of surface contamination using the 130 yellow Visolite samples in the basement. The variance values refer to the log10 transforms of the sample data.

8.2.3.1.2 Main Floor

A total of 180 samples were obtained on the main floor. The locations of these samples and the values of the surface contamination in $\mu g/m^2$ are shown in Figure 8-23. Note that the sample design used on the main floor has samples located on a roughly 3 meter square grid with a number of deviations from this grid in the smaller rooms on the east side of the building as well as denser sampling in the area near the top of the stairs. Several clusters of samples were taken to evaluate variability of the deposition over short spatial scales. These were typically four vinyl tiles, one on each edge of a 1-meter square vacuum sample. Additionally several small vacuum samples were taken near these tiles.

The 180 samples shown in Figure 8-23 contain all samples including the continuous air monitors. For evaluation of spatial mapping with ordinary kriging, these additional samples are removed from the data set and only the wipe samples on the vinyl tiles are retained for further analysis. The distribution of the 160 wipe samples on the main floor are shown in a histogram in Figure 8-24. The summary statistics of these data are also shown in Figure 8-24. The data display a positive skew with the majority of the samples being less than 500-600 $\mu g/m^2$ and a few outlier values above 2000 $\mu g/m^2$. The range of the data is not nearly as large as for the data collected in the basement and the analyses done here use the raw measured values without any type of transformation (i.e., log10 transform) used on the basement sample data.

The 160 samples on the main floor were used in the experimental variogram calculation (Equation 1). The lag spacing used was 3.0 meters. The resulting experimental variogram points and the number of pairs used in the calculation of each point are shown in Figure 8-25. These experimental points were fit with an exponential variogram model with a range of 9 meters, a nugget of 30,000 and a sill of 230,000. The units of the nugget and sill values are $(\mu g/m^2)^2$. Similar to the basement data, the experimental variogram points show a distinct "hole effect" pattern. This is due to the higher concentration data found at the top of the stairs (see Figure 8-23). Samples on either side of this high concentration area are more similar when compared to each other than when compared to samples within the high zone and cause the experimental variogram to reach a peak value at a separation distance of 15 meters. This hole-effect is not modeled and the total sill of the model (nugget plus sill) is set to the variance of the data set as shown by the horizontal black line on Figure 8-25.

Variograms were calculated in a number of different directions to detect any preferred orientation in the spatial correlation, but no distinct anisotropy was detected and therefore the omnidirectional variogram shown in Figure 8-25 is used for the kriging of the yellow Visolite data.

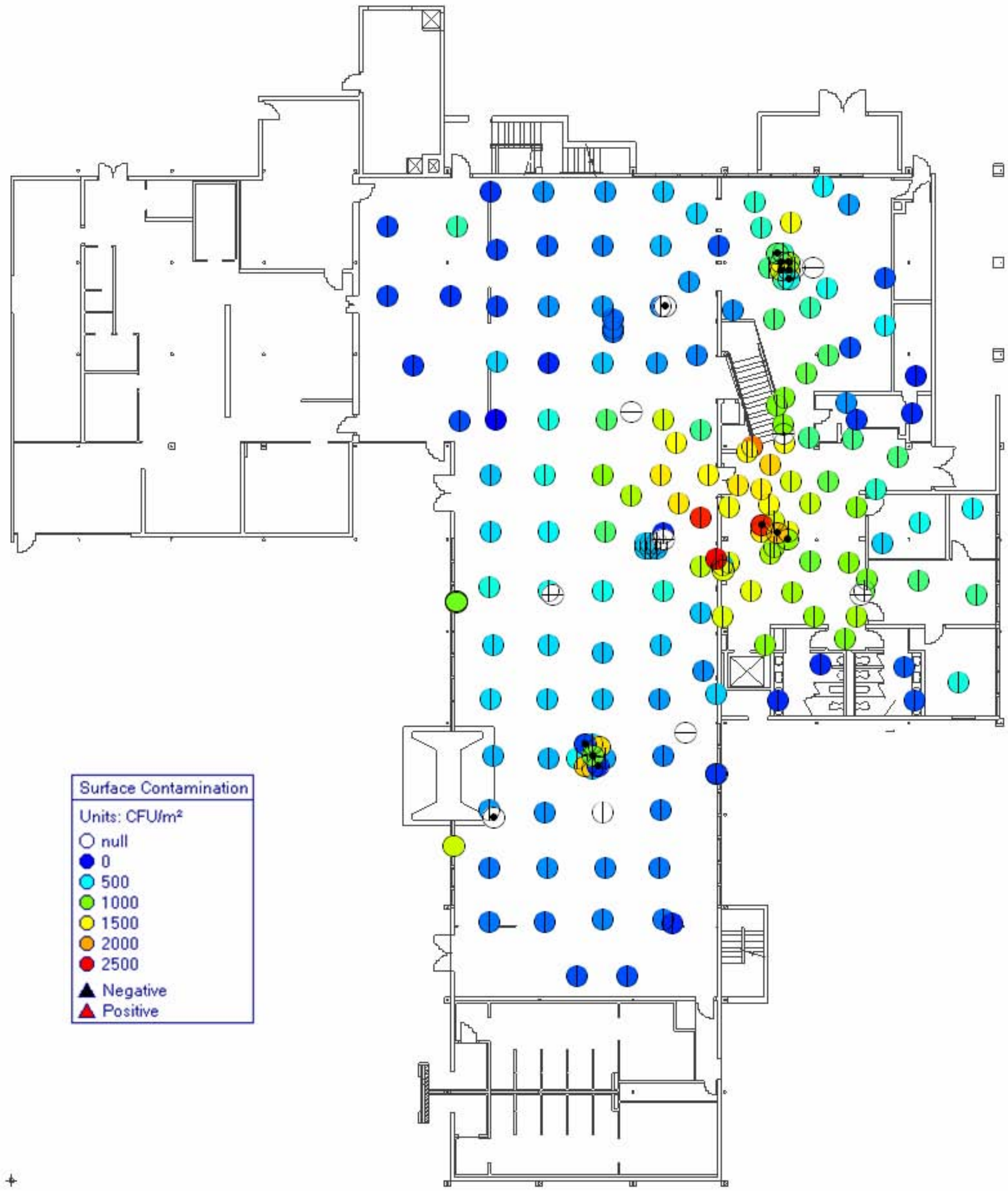

Figure 8-23. Location of all 180 yellow Visolite samples on the main floor

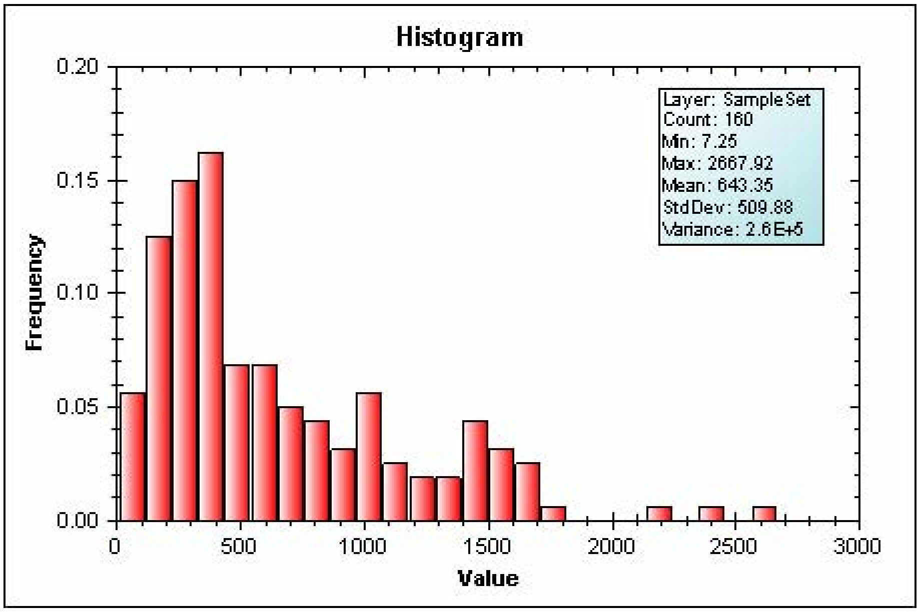

Figure 8-24. Distribution of the 160 wipe samples, main floor.

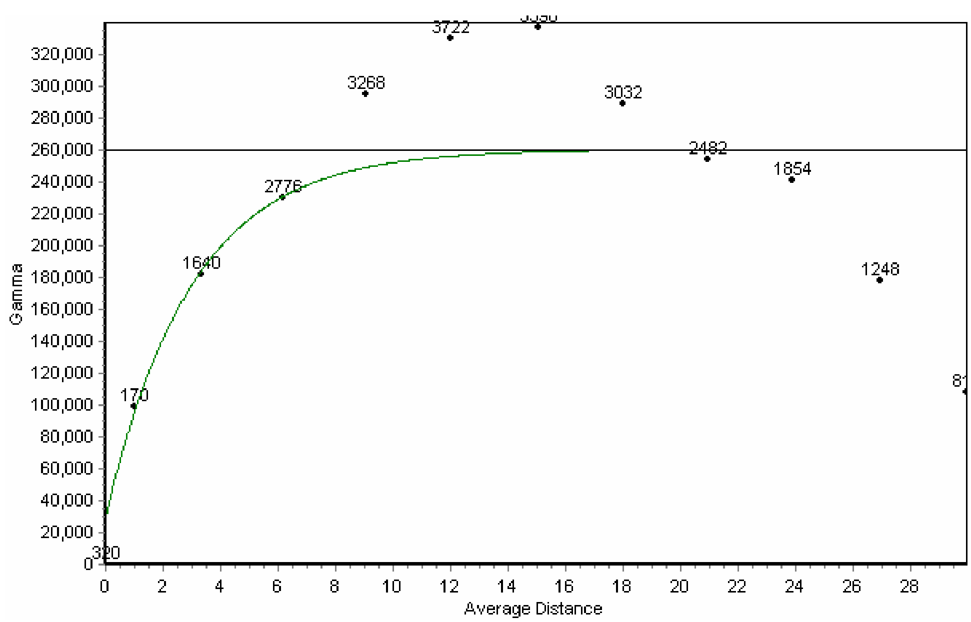

Figure 8-25. Experimental and model variogram for the 160 yellow Visolite wipe samples, main floor.

The kriging estimates of the yellow Visolite surface contamination are shown in Figure 8-26. These estimates were made using the variogram model in Figure 8-25 and all 160 surface contamination samples. The estimated values clearly show the extent of the hotspot at the top of the stairs and dispersal patterns to the north into the bar area and out into the ballroom and towards the western wall and the large fireplace. The highest estimated surface concentration is in the ballroom just to the west of the entry area. Some contamination has made it into the offices on the east side of the building, but the bathrooms are estimated to be relatively free of surface contamination.

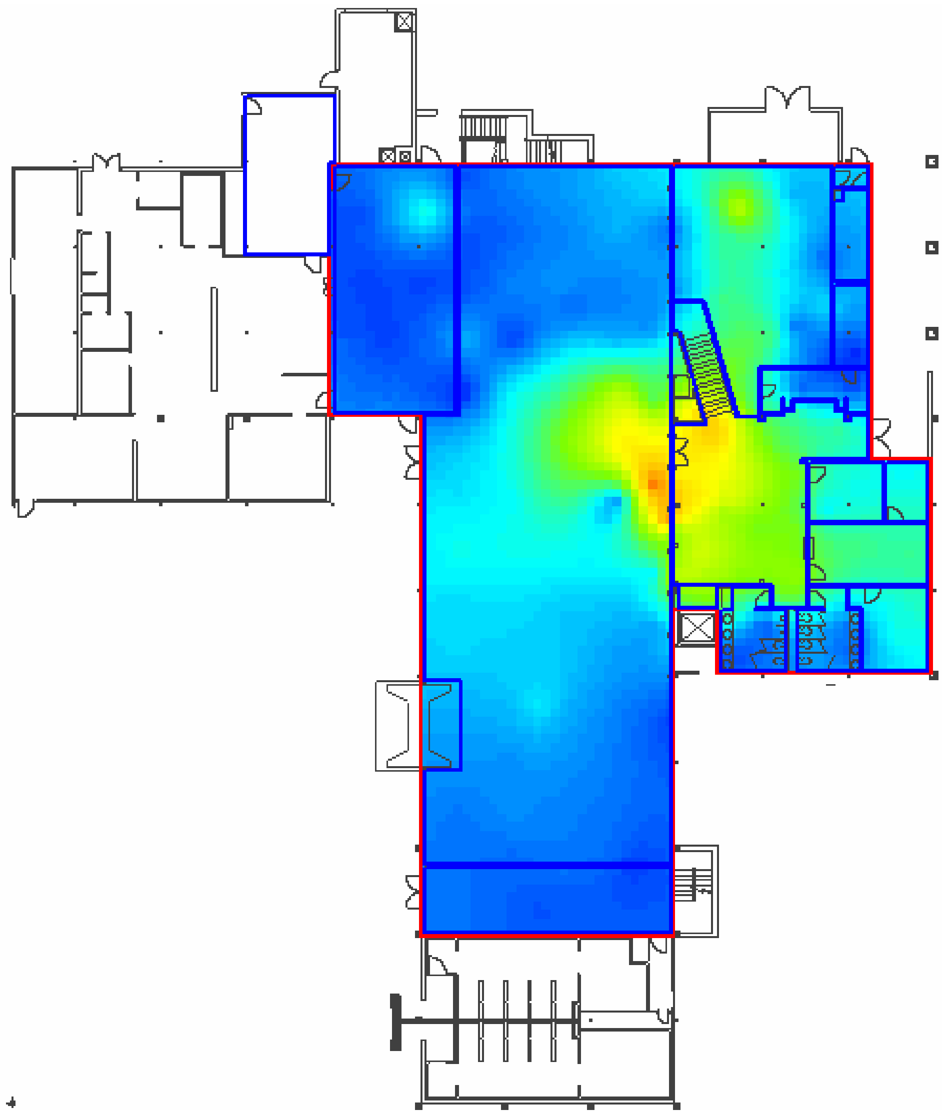

Figure 8-26. Kriging estimates of the yellow Visolite surface contamination, main floor.

Kriging also provides a map of the kriging variance. This resulting map for the main floor of the Coronado Club is shown in Figure 8-27. The gridded nature of the sample locations is evident in the kriging variance map. This map shows that the only areas of very high kriging variance are in the corners of the building where the sampling density is the lowest. This kriging variance map indicates that for the range of spatial correlation of the sample data (9 meters), the nominal 3 meter sampling grid provides estimates with low uncertainty across the main floor.

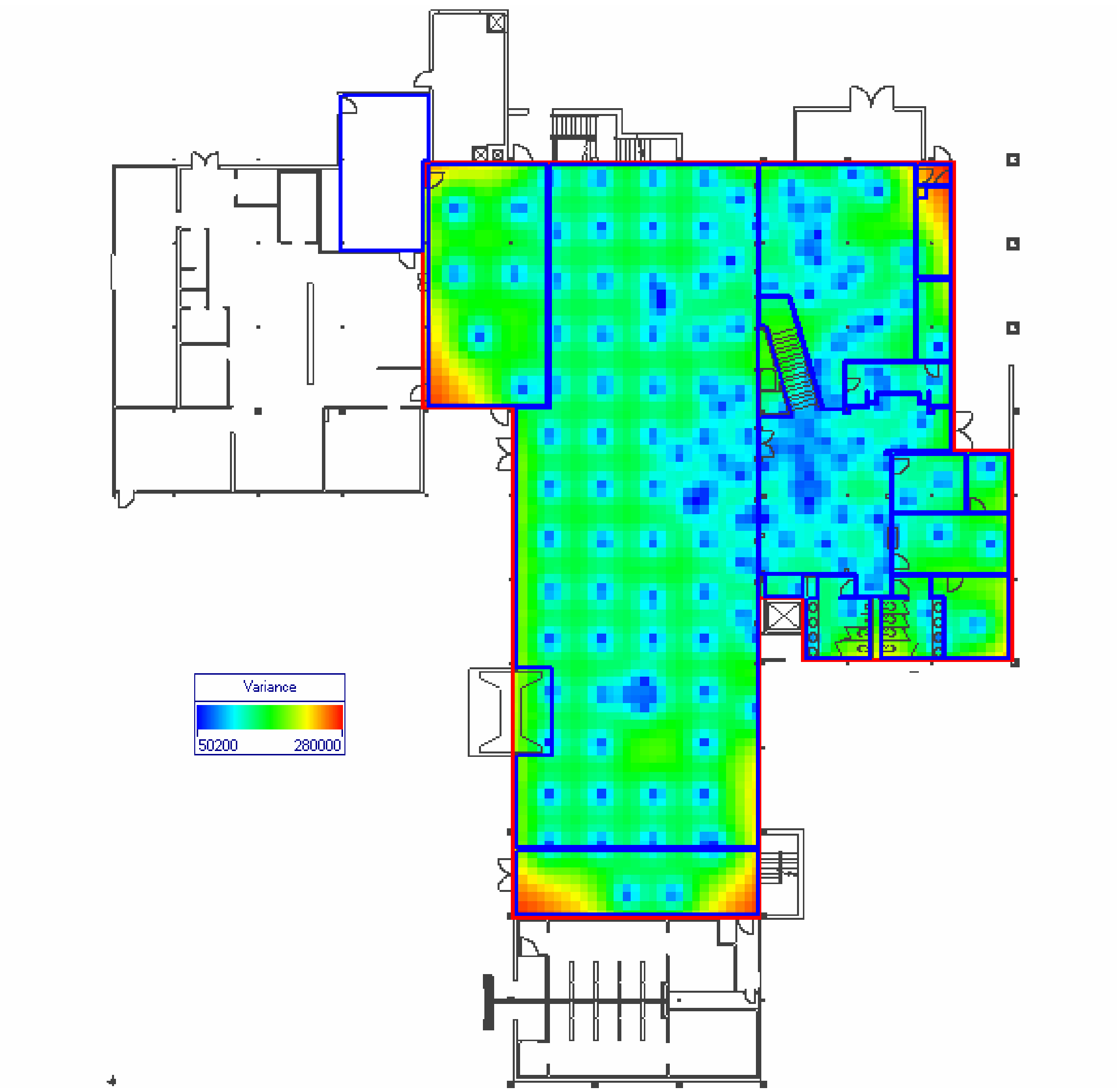

Figure 8-27. Kriging variance for the yellow Visolite estimates, main floor.

8.2.3.2 Summary: Full Data Set Analysis

Spatial analysis of the full set of yellow Visolite wipe samples provides a clear picture of the final distribution of the yellow Visolite within the Coronado Club. The distribution of samples collected within the basement show a strong skew with many low values and just a few high values of surface contamination. This is to be expected given that the samples were distributed over the entire area of the basement, while areas of significant Visolite deposition were limited to just a small fraction of the basement area. On the main floor, the distribution of sample values is much less skewed demonstrating more uniform deposition across the main floor relative to the basement. This sampling distribution is due to both the more omnidirectional air flow patterns on the main floor and the larger and more open rooms on the main floor compared to the basement.

Analysis of the yellow Visolite wipe data demonstrates that the hypothesis of contaminant data exhibiting spatial correlation is correct. The migration and deposition of particulate contaminants through aerosol transport has a dispersive nature and creates deposition patterns with spatial correlation. These patterns result in variograms with well defined hole effect patterns due to areas of relatively higher concentration surrounded by areas of lower concentrations. The variogram calculated on the basement data shows a range of correlation of 5.5 meters while the range of correlation for the main floor data is 9.0 meters. These ranges are consistent with the smaller and more closed rooms in the basement and the larger spaces on the main floor.

The mapped spatial distribution of the deposition fits the conceptual model of transport within the building from the source location, north to the base of the staircase, up the stairs and then out across the main floor. Given the measured levels of spatial correlation in the basement and on the main floor, the sampling design used to collect the characterization samples appears to provide adequate sampling density for both floors as evidenced by the results of the kriging variance calculations.

Estimation of the yellow Visolite deposition using all of the wipe data now serves as the best case situation against which other estimations made with subsets of the total data set can be compared. These analyses are done using a jackknife evaluation procedure.

8.2.3.3 Jackknife Analysis

The yellow Visolite data set is used to quantitatively assess the ability of the spatial mapping algorithms to estimate surface contamination within the Coronado Club. This analysis is accomplished by splitting the yellow Visolite data set into 2 groups. This split is done randomly. Each group of samples is used to independently estimate the surface contamination in the building and then the other group is used to assess the results of this estimation. This approach of holding back some of the samples from the analysis and then using those samples to evaluate the results of the analysis is referred to as “jackknifing”. The results of the mapping using the two groups are shown side-by-side in the figures in this section. However, direct comparison of the two results is not the main goal here, but rather these two sets provide two different, independent checks on the ability of the mapping algorithm to produce accurate estimates of surface contamination at unsampled locations.

8.2.3.3.1 Basement

The locations of all the sample data for the two different sets are shown in Figure 8-28. This figure includes the non-wipe samples as well as the wipe sample locations that are used in this analysis. Figure 8-28 shows that the random split of the complete data set into two groups creates relatively equal sample coverage of the basement by each group. There are 65 samples in the basement within each of the two groups. The distributions of the log10 transformed surface contamination data for the two groups are shown in Figure 8-29. The summary statistics in Figure 8-29 show that the group 1 data have a slightly higher mean and variance, as well as the highest concentration samples compared to the group 2 data.

Both of the experimental variograms show the hole-effect seen in the complete data set. The variogram models fit to the two different groups are shown in Figure 8-30. The Group 1 experimental variogram is fit with an exponential model having a zero nugget value, a sill of 0.66 and a range of 4.5 meters. The group 2 experimental variogram is also fit with an exponential model with a zero value nugget. The sill and range values are 0.58 and 5.5 meters, respectively. These variogram model parameters are similar to those used to fit the complete data set in the previous section.

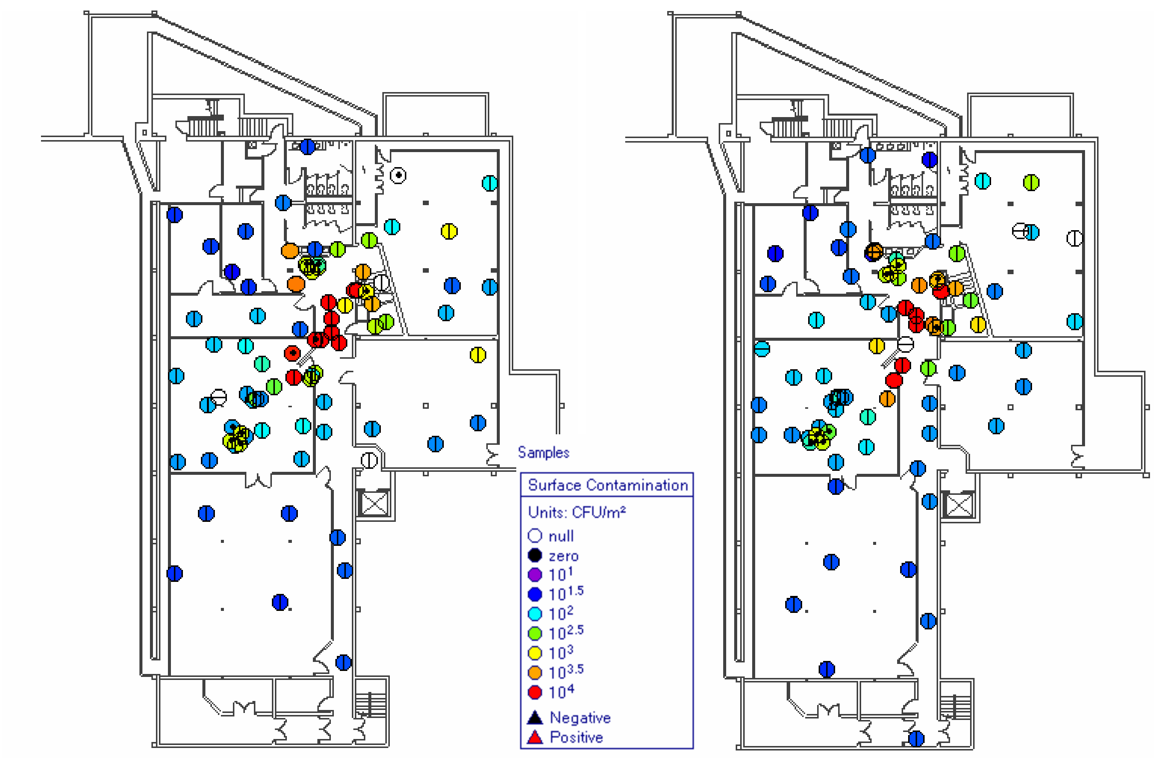

Figure 8-28. Locations of the two sample groups in the basement. Group 1 is on the left and Group 2 is on the right.

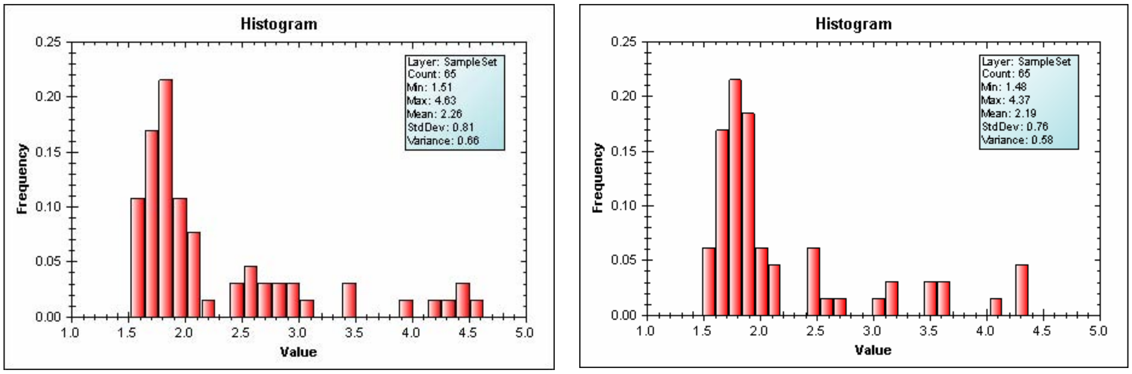

Figure 8-29. Histograms of the log10 yellow Visolite surface contamination for the Group 1 (left) and Group 2 (right), basement.

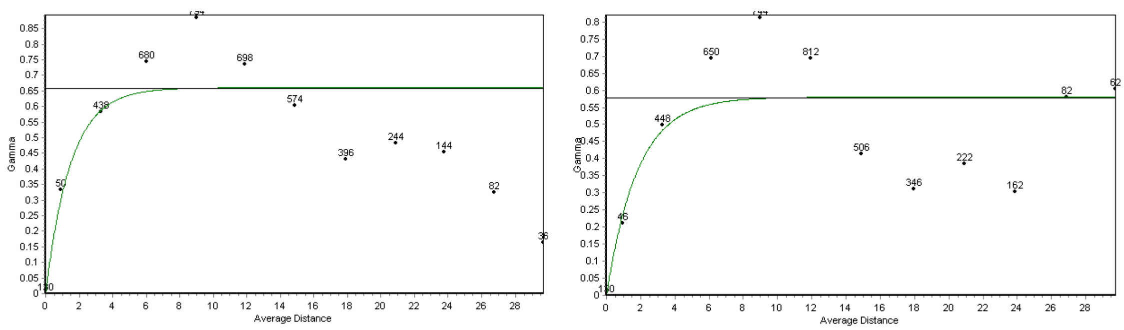

Figure 8-30. Experimental and model variograms for the Group 1 (left) and Group 2 (right) yellow Visolite data in the basement.

The ordinary kriging algorithm was used with each of the data sets and the corresponding variogram models to estimate the surface contamination at all locations on a grid within the basement. The same estimation grid as used with the complete data set, 0.5x0.5 meter spacing, is also used for the estimations made with the two different splits of the data set. The estimated values of the basement surface contamination are shown in Figure 8-31 for group 1, left image, and group 2, right image, respectively. The patterns shown in Figure 8-31 reproduce well the pattern of the surface contamination created with the full data set and shown in Figure 8-21. The path of the contamination from source location to the base of the staircase is evident in both results (Figure 8-31) although due to the lower number of samples, it is not as well defined by either group when compared to using the complete data set to make the estimates. Estimates of extremely little surface contamination in the southern end of the basement are consistent across the two groups and compare well with the estimates made using the complete data set.

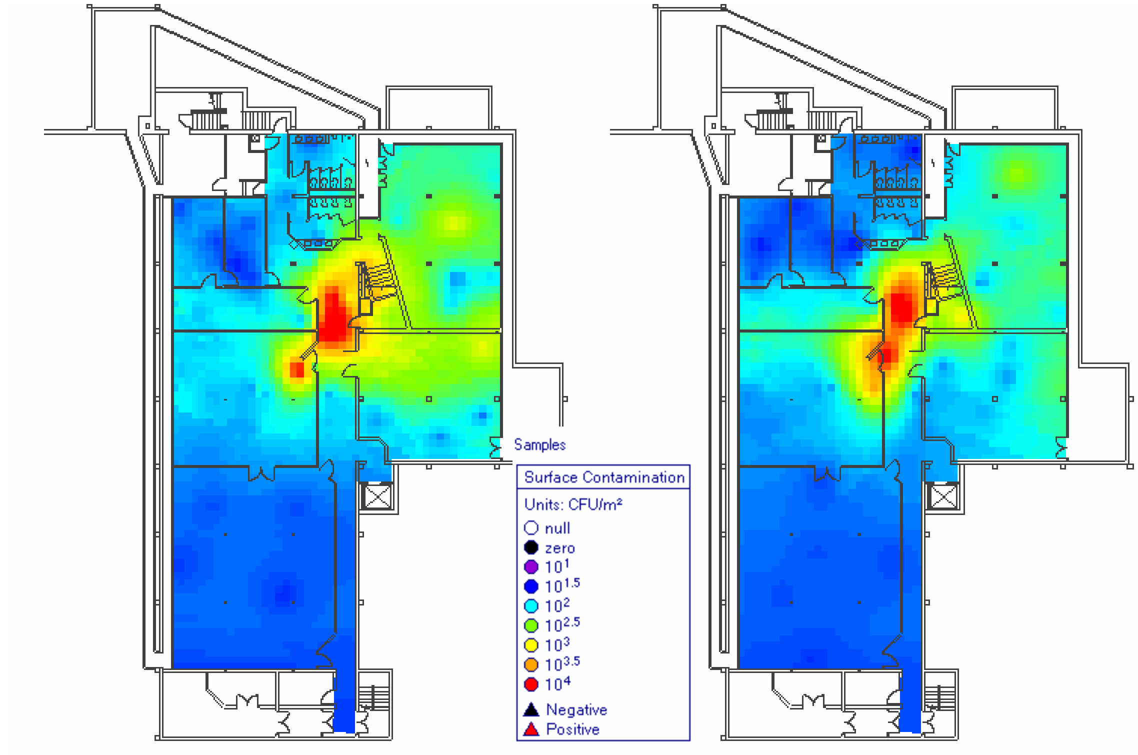

Figure 8-31. Estimated yellow Visolite surface contamination values made with sample Group 1 (left) and sample Group 2 (right), basement.

The kriging variance maps corresponding to the estimates shown in Figure 8-31 are shown in Figure 8-32. Comparison of Figure 8-32 with the kriging variance from the complete data set estimation (Figure 8-22) highlights the decreased data density when only one-half of the complete data set is used. The kriging variance results in Figure 8-32 show many regions of maximum kriging variance indicating that the data density in those regions is not enough data to provide a more precise estimate than what could be obtained by simply using the global mean and variance of the data set as the estimate and the uncertainty about that estimate.

Overall, the results of splitting the data set and estimating the surface contamination in the basement show that while half of the complete data set is enough to define the nature of the spatial correlation and to create estimates that identify the major deposition patterns, these are not enough data to provide high confidence in all estimates. If either data set were collected in a building the resulting kriging variance maps shown in Figure 8-32 could be used to locate additional samples with the specific goal of reducing these areas of high kriging variance.

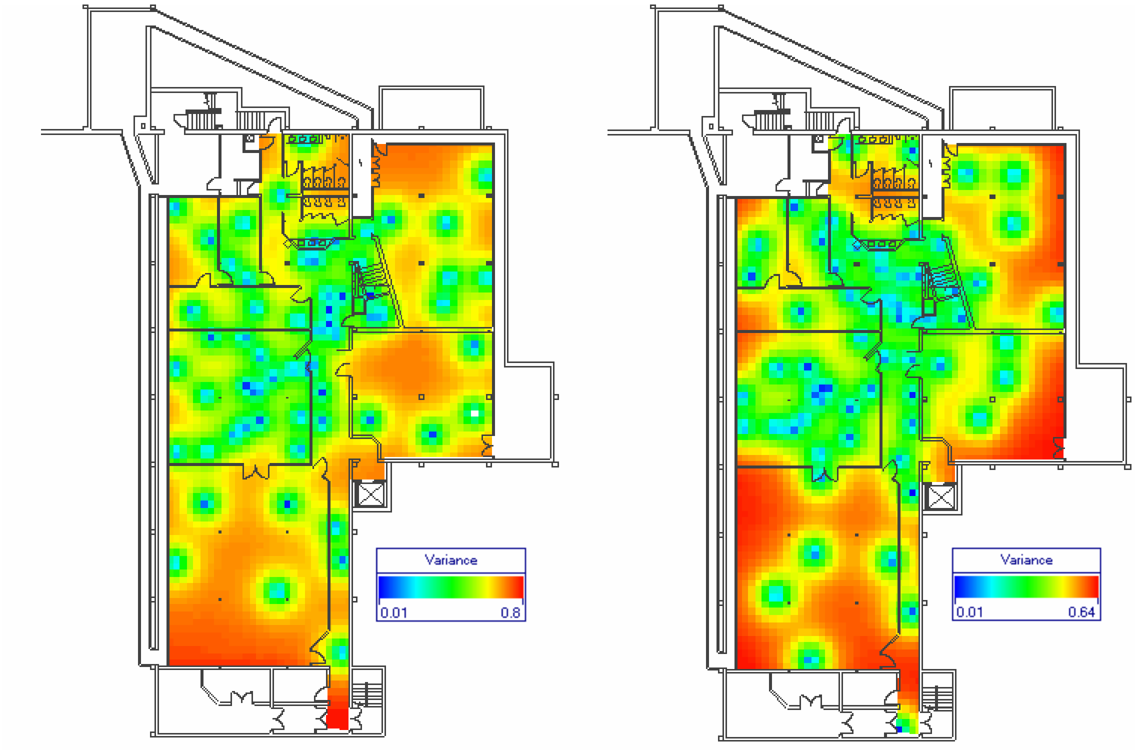

Figure 8-32. Kriging variance maps associated with the estimates shown in Figure 8-31 for Group 1 (left) and Group 2 (right).

Use of only one half of the complete data set at a time to estimate the surface contamination allows the estimates to be checked against the true measured values contained in the other half of the data set. This jackknife analysis was completed for the estimates of the yellow Visolite data in the basement. The results are summarized in Table 8-23 in terms of the errors between the estimated and true values across the 65 locations not used in the estimation, those locations in the other group. Each error is calculated as (*estimated-observed*) so that overestimates are positive errors and vice versa. Additionally, the locations and the magnitudes of the errors are shown in Figure 8-33.

Table 8-23. Summary statistics on estimation errors for the yellow Visolite, basement.

Parameter	Group 1 Estimation Errors	Group 2 Estimation Errors
Mean	0.14	0.07
Std. Dev.	0.40	0.48
Median	0.08	0.09
Minimum	-1.39	-1.16
Maximum	0.93	1.73
Number	65	65

Ideally, the mean error would be zero indicating no preferential bias towards overestimating or underestimating the true observed values. The range of the data (log10 maximum sample value – log10 minimum sample value) for groups 1 and 2 are 3.12 and 2.89, respectively. The mean errors for the group 1 and 2 estimates are 0.14 and 0.07, or just 4 and 2 percent of the respective data ranges. This low amount of bias as calculated across just 65 samples indicates the ability of the ordinary kriging algorithm to produce accurate estimates of the surface contamination from relatively limited sample data.

The spatial distribution of the errors (Figure 8-33) shows that for both groups, the largest errors occur in the areas of the highest surface contamination values between the tracer source location and the base of the staircase. Some of these large errors may be due to the kriging estimates carrying sample values through walls from one room to another where, in fact, that connection may not be physically accurate. Moderately sized errors occur in the rooms on the east side of the basement. The smallest errors occur in the southern end of the basement where the surface contamination values are small. The results in Figure 8-33 show a good mix of positive and negative errors indicating the geostatistical models of surface contamination created here don't have any systematic spatial bias.

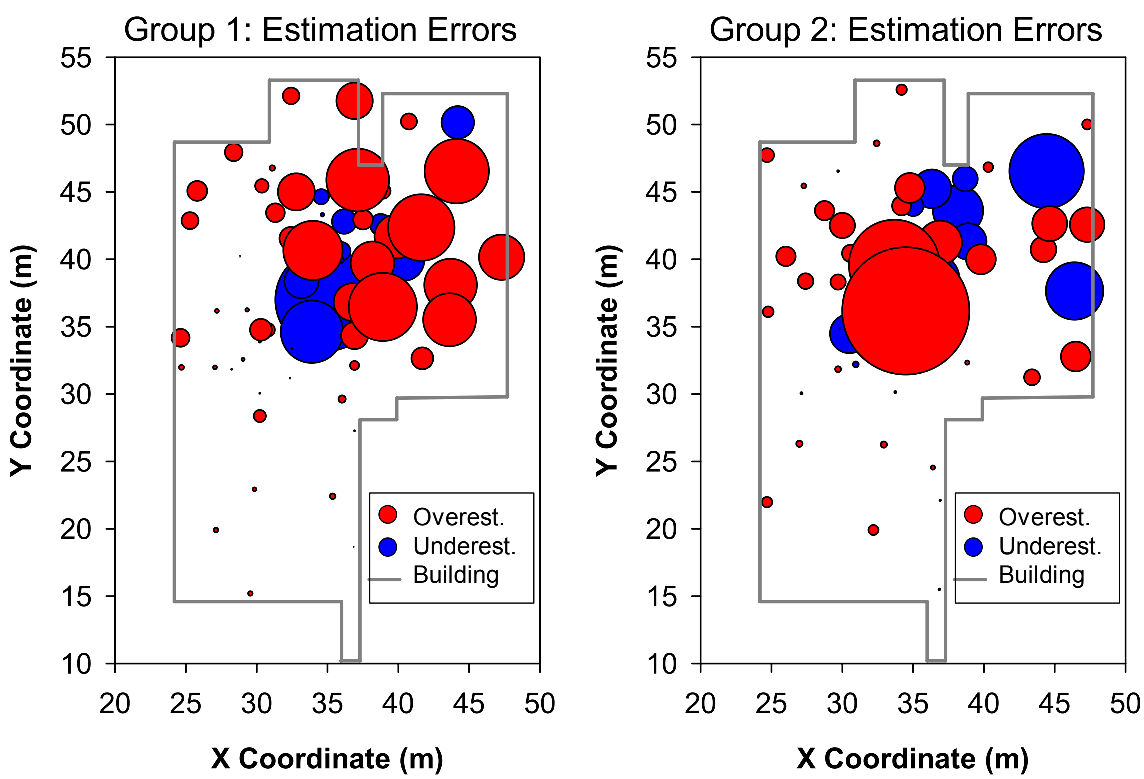

Figure 8-33. Comparison of estimation errors for Group 1 (left) and Group 2 (right) yellow Visolite data sets in the basement. The size of the circles are proportional to the absolute value of the estimation error.

8.2.3.3.2 Main Floor

The same division of the sample set into two groups as done for the basement is also done for the main floor data set. On the main floor, 78 samples are in the group 1 data set and 81 samples are in Group 2. The spatial locations and histograms of these two data sets for the main floor are shown in Figure 8-34 and Figure 8-35. Note that even though the split of the original data into two groups was done randomly, the three samples with the highest surface contamination data, all greater than 2000 $\mu g/m^2$ all ended up in group 2. The lowest values of surface concentration are also in group 2. Note that the X-axes of the two different histograms in Figure 8-35 have different scales.

The variograms for each data set are shown in Figure 8-36. The Group 1 variogram is fit with a spherical model having a 0 nugget, sill of 230,000 and a range of 8.5 meters. The Group 2 variogram was also fit with a spherical model having a zero nugget, a sill of 293,000 and a range of 7.0 meters. The combined data set was fit with an exponential variogram model, while each of the two data sets after the random split are fit with spherical models. In the case of the Group 2 data, this fit is done by ignoring the second point in the experimental variogram that has relatively high variance but few pairs of data to support it (38 pairs compared to 710 pairs in the next point in the variogram – See Figure 8-36). The gamma value of the variogram, the point to point variability, increases less rapidly with the spherical model relative to the exponential model. It appears a few samples that have ended up in Group 2 have a large variability at short spacings between samples. When all data are combined, these few points cause the variogram to be best fit with an exponential model. When the data are split into these two groups, it becomes clearer that the data are best fit with a spherical model with the exception of these few outlier data points.

The results of the kriging estimates made with the two different groups of data are shown in Figure 8-37. These two maps, made with the same color scale, show the striking difference between the data sets with respect to the high values contained in the Group 2 data set that create a large red region near the top of the stairs in the map of estimated values. No values estimated with the Group 1 data set are nearly as high as these estimates. Another noticeable difference between the two maps is the area of surface contamination near 500 $\mu g/m^2$ in the northwest portion of the main floor in the map made with the Group 2 data that does not show up in the map made with the Group 1 data. This difference is due entirely to a single sample (see maps in Figure 8-37) in this area that was assigned to Group 2. Another noticeable difference is that the Group 1 estimates have a region of relatively high surface contamination in the bar area near the northern boundary of the building. This difference appears to be due to a single sample that is in Group 1 and not in Group 2. These differences, mainly attributable to particular samples ending up in one group or the other, do not obscure the fact that, similar to the basement results, the estimations made with either half of the data set are comparable to the estimation made with the complete data set and both of them are capable of capturing the overall character of tracer deposition on the main floor.

The color scales in the kriging variance maps (Figure 8-38) are different between the two images and set to span the minimum and maximum values of the kriging variance in each map. The main differences between the maps are on the edges of the buildings and are caused by single samples being assigned to one group or the other. For example, the offices and the bar area on the east side of the building are not sampled as densely in Group 2 relative to Group 1 and this results in an increase in the kriging variance in these areas for the estimates made with the Group 2 data.

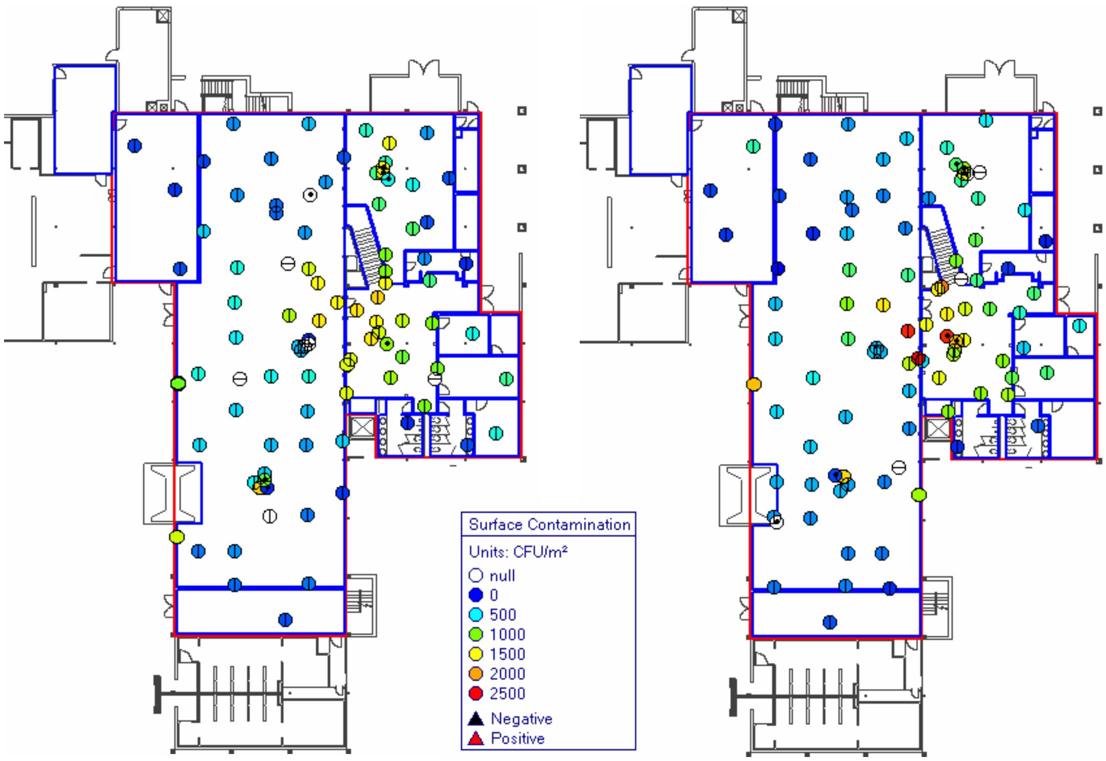

Figure 8-34. Locations of the two sample groups on the main floor. Group 1 is on the left and Group 2 is on the right.

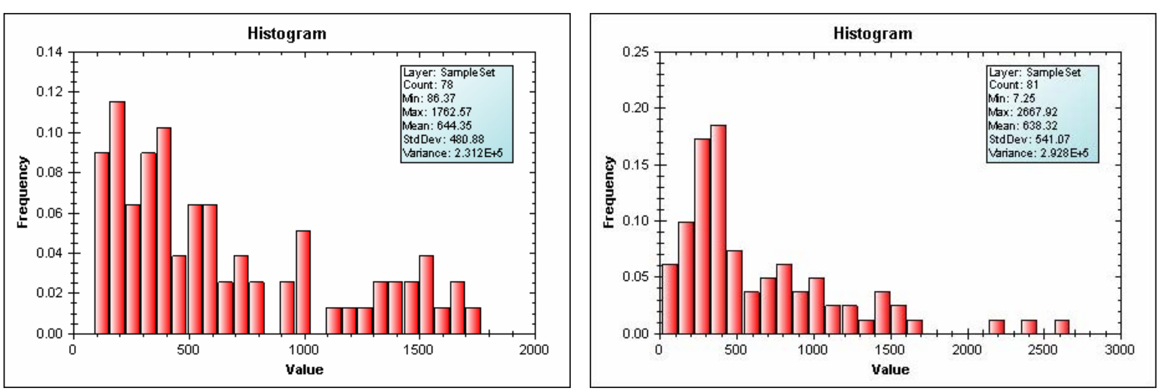

Figure 8-35. Histograms of the yellow Visolite surface contamination for the Group 1 (left) and Group 2 (right), main floor.

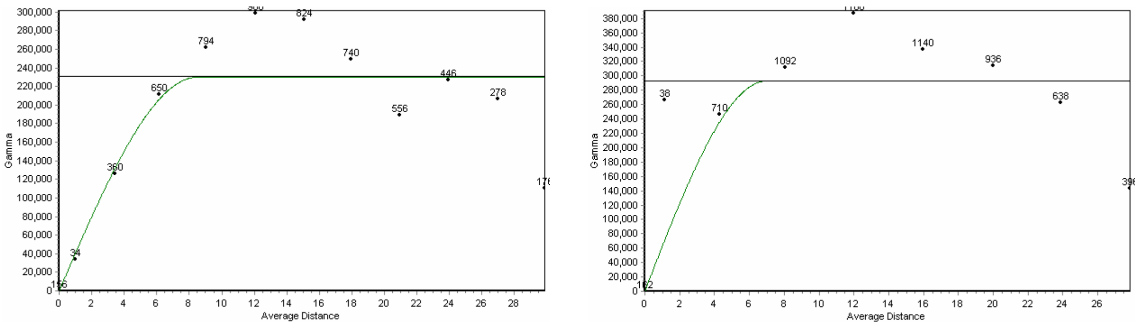

Figure 8-36. Experimental and model variograms for the Group 1 (left) and Group 2 (right) yellow Visolite data, main floor.

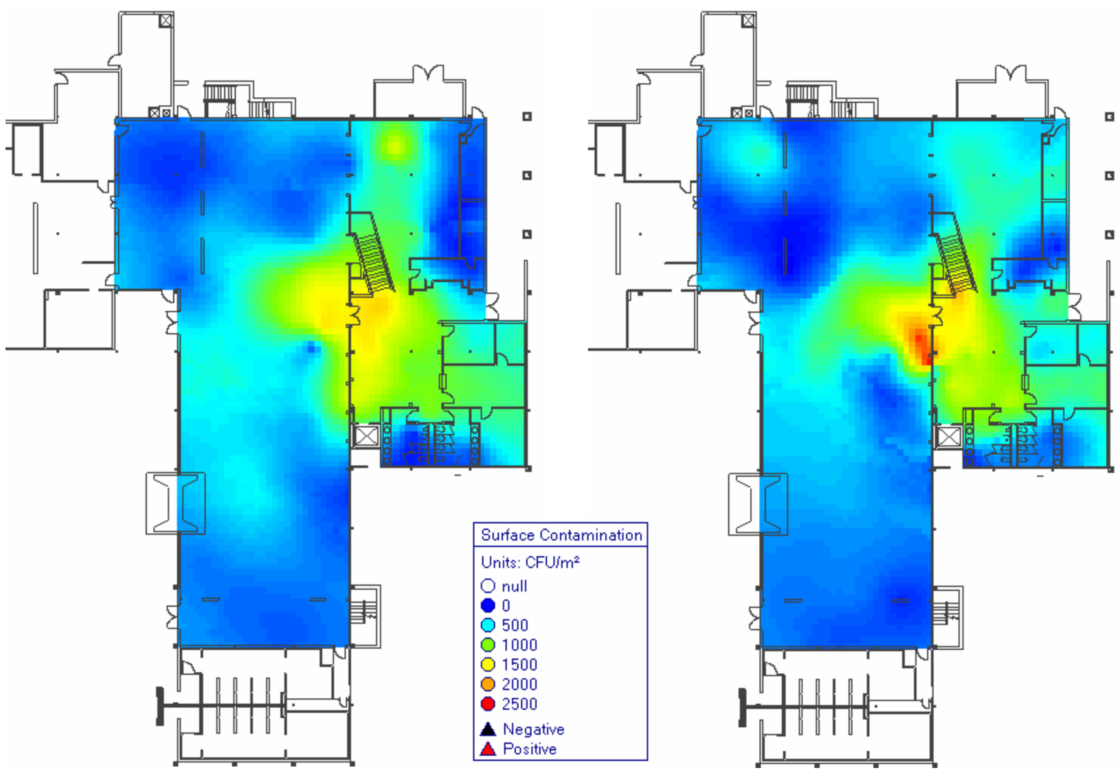

Figure 8-37. Estimated yellow Visolite surface contamination values made with sample Group 1 (left) and sample Group 2 (right), main floor.

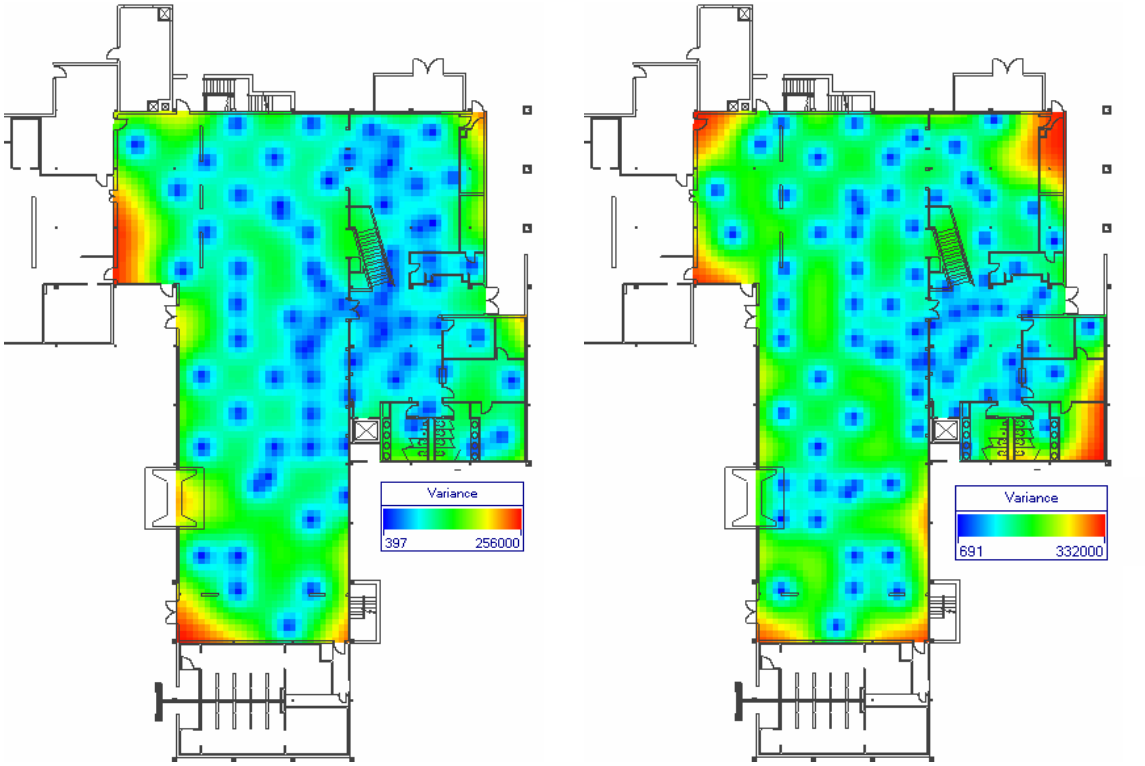

Figure 8-38. Kriging variance maps associated with the estimates shown in Figure 8-37 for Group 1 (left) and Group 2 (right).

Similar to the analysis done for the basement estimations, the main floor estimates are also subjected to a jackknife analysis. The results of the jackknife analysis are summarized in Table 8-24 in terms of the errors between the estimated and true values across the locations (either 78 or 81) not used in the estimation, those locations in the other group. Again, each error is calculated as (*estimated-observed*) so that overestimates are positive errors and vice versa. The locations and the magnitudes of the errors are shown in Figure 8-39.

Table 8-24. Summary statistics on estimation errors for the yellow Visolite, main floor.

Parameter	Group 1 Estimation Errors	Group 2 Estimation Errors
Mean	35.07	-35.55
Std. Dev.	306.07	253.00
Median	47.56	-17.87
Minimum	-1367.92	-866.25
Maximum	931.91	693.64
Number	81	78

The mean error value indicates the amount of bias in the estimates and, similar to the basement estimates, this mean error is calculated relative to the range of the measured values for each group. The ranges of the main floor group 1 and group 2 sample data are 1676.2 and 2660.7, respectively. The corresponding mean errors are 2 and -1 percent of the data ranges for these groups. Again, similar to the basement results, this low amount of bias as calculated across the samples confirms the ability of the ordinary kriging algorithm to produce accurate estimates of the surface contamination from relatively limited sample data.

The spatial distribution of the errors (Figure 8-39) shows that for both groups, the largest errors occur in the areas of the highest surface contamination near top of the stairs in the entry hall. For the group 2 estimates, a relatively large error also occurs in the bar area. Moderately sized errors occur in the bar, offices and kitchen areas of the northern half of the main floor. The smallest errors occur in the southern end of the main floor where the surface contamination values are small. The results in Figure 8-39 show a good mix of positive and negative errors indicating the geostatistical models of surface contamination created here don't have any systematic spatial bias. The images in Figure 8-39 are comparable to each other, but the circle sizes indicating the magnitude of the errors are not necessarily comparable to the circle sizes used for the basement errors in Figure 8-33.

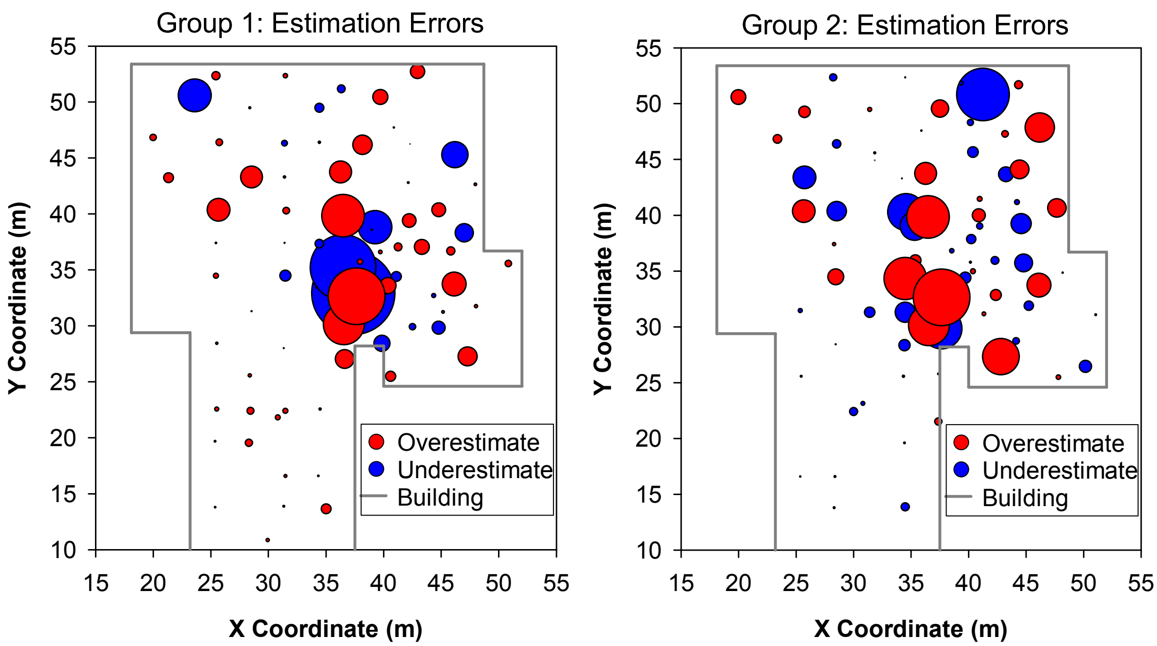

Figure 8-39. Comparison of estimation errors for Group 1 (left) and Group 2 (right) yellow Visolite data sets. The size of the circles are proportional to the absolute value of the estimation error.

8.2.4 Pink Visolite Test

The two different groups of samples for the pink Visolite data were not created by arbitrarily splitting a larger data set, but were, for the most part, collected at locations designed to meet two different sampling goals. These two groups of data were collected in a sequential manner over three consecutive days. The samples collected on the first day (24 in the basement and 20 on the main floor) are common to both data sets. For both sampling approaches, the samples were collected in an adaptive manner where each new set of locations was determined using information gained in the previous round of sampling.

The main goal behind the collection of the pink Visolite sample data was to evaluate experience-based, or judgmental, sampling design against a sampling design optimized to meet specified sampling objectives. The judgmental locations were determined by the NIOSH building characterization team and are known as the “NIOSH” set for the remainder of this report. The actual goals of the team that drove the choice of judgmental sampling locations were not quantified; however, the sampling design appears to have had some focus on identifying the location of the contaminant sources and surrounding areas of high concentration. The resulting sampling design can be considered a judgmental approach with some focus on hot spot detection (Gilbert, 1987, Chapter 10).

The sampling locations determined with the sampling optimization algorithm, referred to as the “Sandia” set for the rest of this report, were determined by using a discrete optimization algorithm to try and achieve four different sampling objectives simultaneously. These four objectives were:

1) Locate samples in areas of “high” surface contamination. In the basement, this meant locating samples as close to possible to estimated surface contamination values of 40,000 $\mu g/m^2$ (log10 = 4.6). On the main floor, high surface contamination was defined as 125,000 $\mu g/m^2$ (log10 = 5.1).
2) Locate samples in areas of high kriging variance. At the time of the initial characterization high variance was defined as 0.30 in the basement and 0.19 on the main floor.
3) Spread samples away from each other
4) Keep all sample locations within the building area.

The values used in objectives 1 and 2 are based on initial analysis of the laboratory data and of the sampling efficiency. Several changes to both the laboratory data determination of mass and the sampling efficiency have occurred since the initial analyses. As an example, sampling efficiency of the swabs was changed from 60 percent to 80 percent after the first day of samples were obtained and analyzed. Therefore the numbers used to define objectives 1 and 2 may not apply to the current state of the data set. The fourth objective sounds obvious, but mathematically there is no constraint on where the samples could be placed unless this objective is added.

Several issues regarding the sample collection make direct comparison of the two sample sets questionable. These issues are the combination of swab, wipe and micro-vacuum samples into the same data set. Some work was done to identify the relative efficiency of each of these sampling techniques through analysis of different sample types located close to one another, but a more quantitative evaluation of the sampling efficiency for each technique is still needed.

The spatial mapping done in this report and as developed within the BROOM software is two-dimensional with the estimated values created for horizontal surfaces, mainly the floor, within the building. The implicit assumption in creating these maps is that the final fate of the Visolite tracer is deposition onto these horizontal surfaces. This assumption is generally correct with the exception of the Visolite tracer that was captured within the ventilation system, for example the material captured within filters, ducts and air diffusers. Contrary to the analysis of the yellow Visolite – where the sample sets were defined to only include wipes on the vinyl tiles placed onto horizontal surfaces, the pink Visolite does include sampling of other surfaces including portions of the ventilation system. No correction for the amount of tracer focused onto a given surface by the ventilation process has been attempted. Additionally, some of these surfaces are in the ceiling of the Coronado Club and are simply translated to a common horizontal plane, the floor, for the two-dimensional analyses done herein.

8.2.4.1 Basement

The basement sample locations for the Sandia and NIOSH data sets are shown in Figure 8-40. Note that 24 of the samples are common to both data sets. A major difference of the pink data sets compared to the yellow Visolite data set is that there are numerous zero values within the pink data. Even though the estimation calculations use the log10 transform of the data, the BROOM software has been developed to represent zero values as zeros in both the raw and the transformed data sets when the log10 transformed values are all greater than zero. This feature is used to here to honor the zero data when working with log10 transformed values.

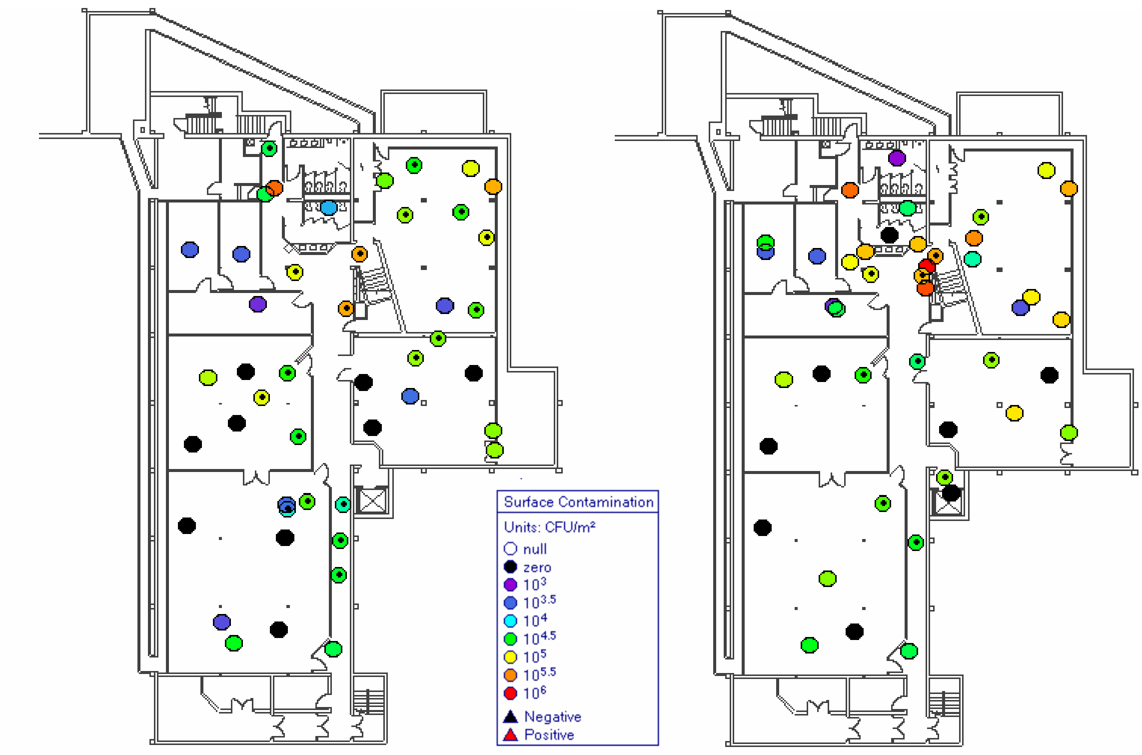

Figure 8-40. Basement pink Visolite sample sets. The left image shows the Sandia and the shared data sets. The right side shows the NIOSH and the shared data sets.

The distribution of the log10 transformed surface contamination values for the Sandia and NIOSH data sets are shown in Figure 8-41. The means, standard deviations and number of samples of the two data sets are very similar, although the highest values are in the NIOSH data set. The Sandia data set has one more zero value than the NIOSH data set.

The variograms calculated and modeled for the two basement data sets are shown in Figure 8-42. The Sandia data set is fit with a spherical model having a zero nugget, a sill of 2.7 and range of 5.3 meters. The NIOSH data set is fit using two nested spherical variogram models. The first model has a zero nugget, range of 1.5 meters and a sill of 2.4. The second model has a range of 19 meters and a second sill of 1.15. The clear hole-effect variograms calculated using the yellow

Visolite data are not seen here in the variograms calculated using the pink Visolite data. This lack of a hole-effect variogram is probably due mainly to relatively few samples being placed in the high concentration areas near the source of the tracer in either the Sandia or the NIOSH tracer as compared to the yellow Visolite data sets.

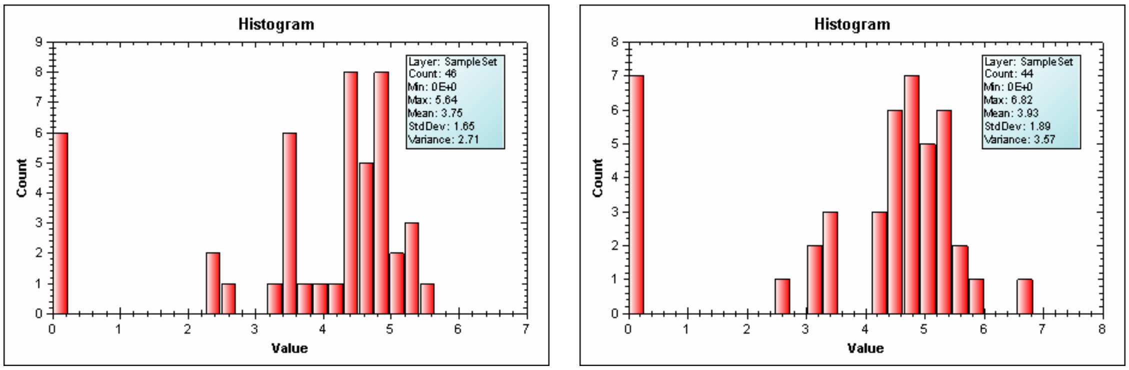

Figure 8-41. Distributions of the log10 transformed Sandia (left) and NIOSH (right) data sets for the pink Visolite. basement.

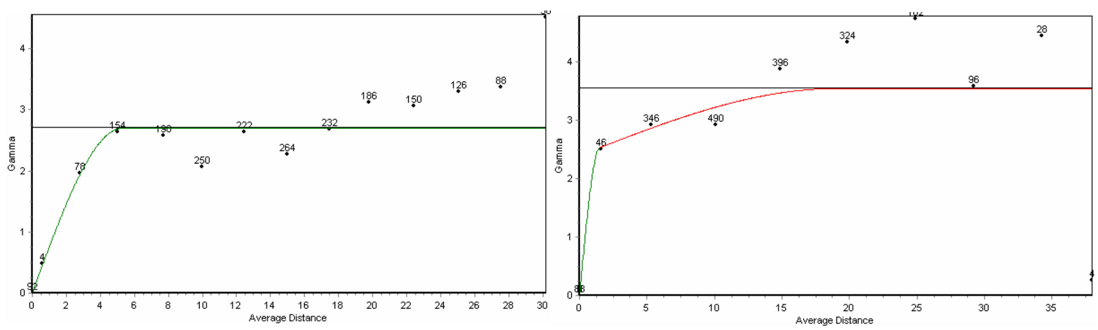

Figure 8-42. Variograms for the log10 transformed Sandia (left) and NIOSH (right) data sets for the pink Visolite, basement.

The sample data and the variogram for each data set are used as input to the ordinary kriging algorithm. The kriging estimates are made on a 0.5x0.5 meter grid. The results of the kriging estimates for both data sets and the corresponding kriging variance maps are shown in Figure 8-43 and Figure 8-44, respectively. The two estimated maps show similar results with the highest estimates occurring in the northern half of the basement and lower estimated values in the southern end. The zero value samples have a strong effect on the estimates made from both data sets. The effect of the variogram model used for the NIOSH data set is evident in the estimation results. The estimations made with the NIOSH data set (right image, Figure 8-43) show that the influence of each sample is limited to a very local area in contrast the estimations made with the Sandia data set in the left image of Figure 8-43. This result is due to the first model fit to the NIOSH data having a short range and a sill that accounts for the majority of the total sill of the variogram.

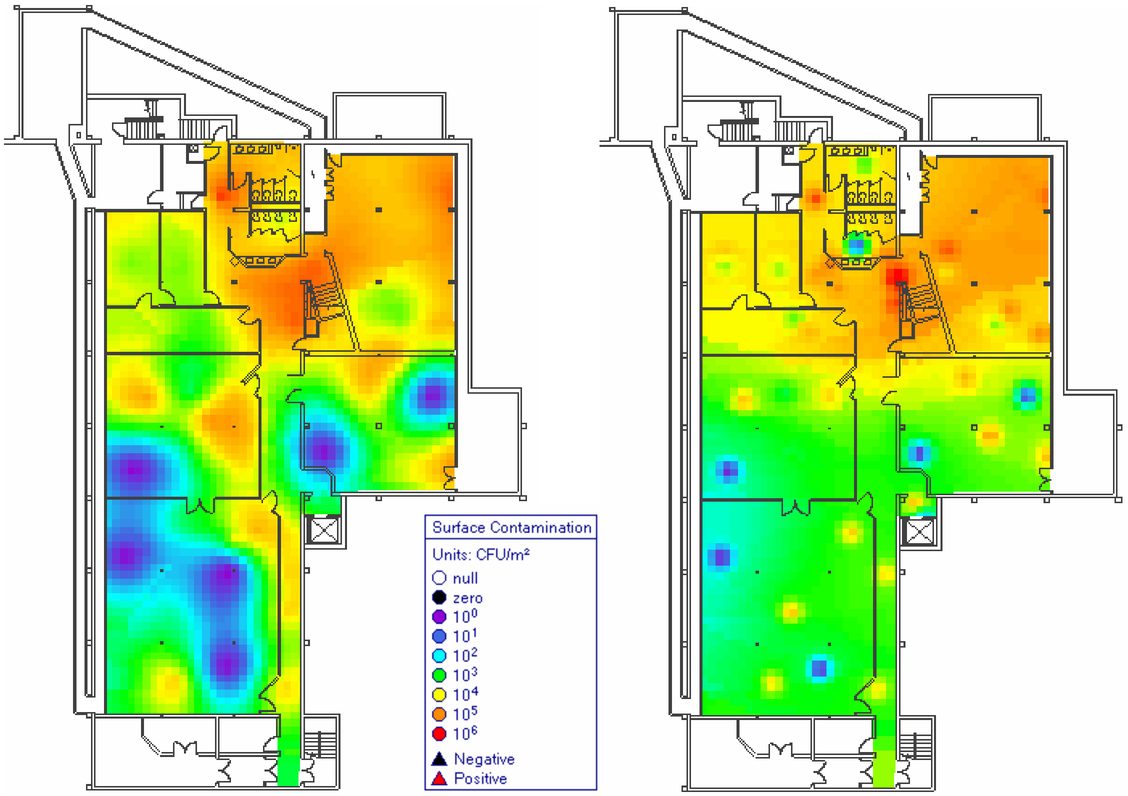

Figure 8-43. Ordinary kriging estimates of the pink Visolite in the basement using the Sandia data set (left) and the NIOSH data set (right)

The maps of kriging variance (Figure 8-44) also highlight the differences in the variogram models fit to the two data sets. The effect of a single sample on the kriging variance is diminished for the NIOSH estimates (right image, Figure 8-44) relative to the effect a single data point has on the estimates made with the Sandia data set (left image, Figure 8-44).

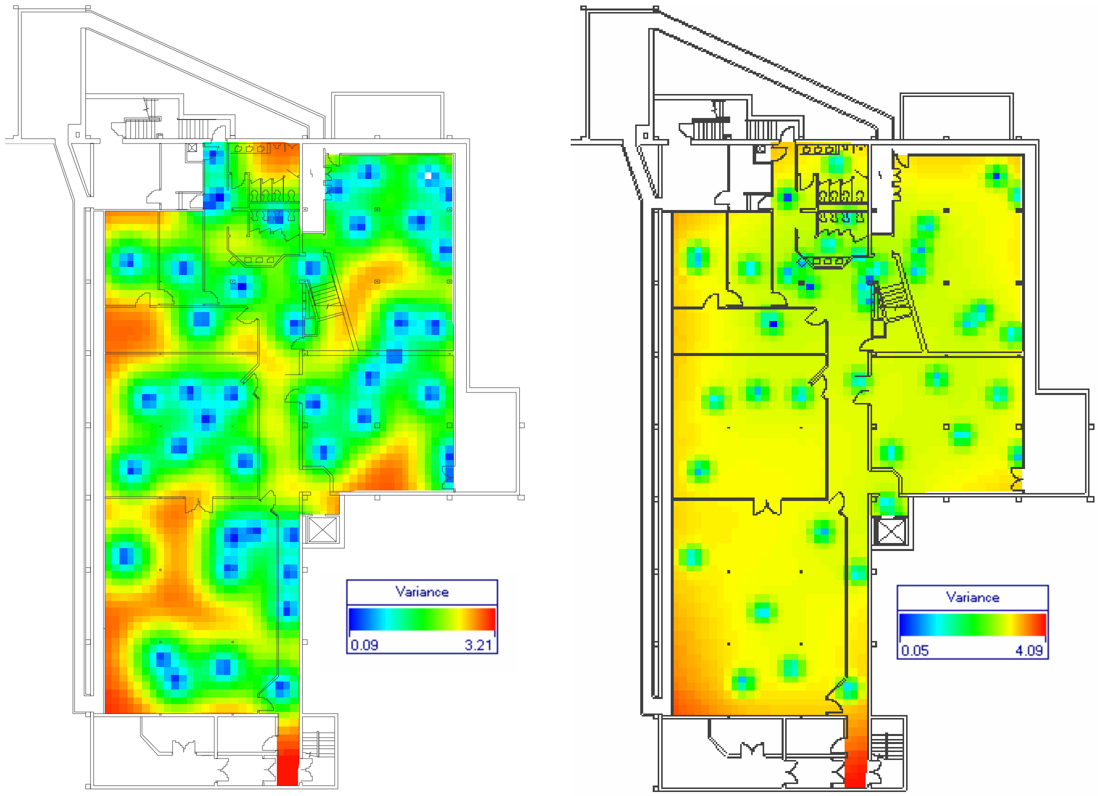

Figure 8-44. Kriging variance of the pink Visolite in the basement using the Sandia data set (left) and the NIOSH data set (right)

The results of the pink Visolite estimation are evaluated using a jackknife procedure similar to that used to evaluate the results of the yellow Visolite estimates. The difference here is that the results of the estimates made with the two different data sets are evaluated using the other data set. The two data sets have 24 samples in common, so the two sets of estimated values are not independent. Another complication of evaluating the results using the other data set is that neither data set was optimized to predict the values at the locations of the other data set. The two sets of estimates are evaluated at essentially randomly chosen locations as defined by the locations of the data obtained in the other data set. The results of the jackknife procedure are shown in Table 8-25 and in Figure 8-45. The number of evaluations are relatively small, 20 and 22 locations, compared to the 65-80 locations used for evaluation of the yellow Visolite data sets.

Table 8-25. Summary statistics on estimation errors for the pink Visolite in the basement.

Parameter	Sandia Data Set	NIOSH Data Set
Mean	-0.36	-0.20
Std. Dev.	1.68	1.03
Median	-0.69	-0.14
Minimum	-3.12	-1.58
Maximum	4.30	3.09
Number	20	22

The amount of bias in each set of estimates is evaluated in the same way as done for the yellow data set evaluation. The range of the sample data is 5.6 for the Sandia data set and 6.8 for the NIOSH data set. The mean estimation errors (Table 8-25) are -6 and -3 percent of the respective data ranges showing a minor amount of bias towards underestimating the true values. The largest positive and negative estimation errors are quite large and are most likely influenced by including the zero value samples directly into the estimation procedure. In both data sets, the next closest value to the zero data are approximately 2.5 indicating that the detection limit for these data may be such that values at the detection limit produce surface contamination values of approximately 315 $\mu g/m^2$ (log10(315) = 2.5).

The locations of the predicted values and the errors of the log10 predictions of surface contamination are shown in Figure 8-45. The largest values of the errors are not necessarily located in the regions of highest surface contamination and again it appears that these may be influenced by the dichotomy of having zero valued samples near those with sample values that are orders of magnitude larger. Another option for these zero data would be to set them to be equal to the non-zero detection limit of the analysis technique.

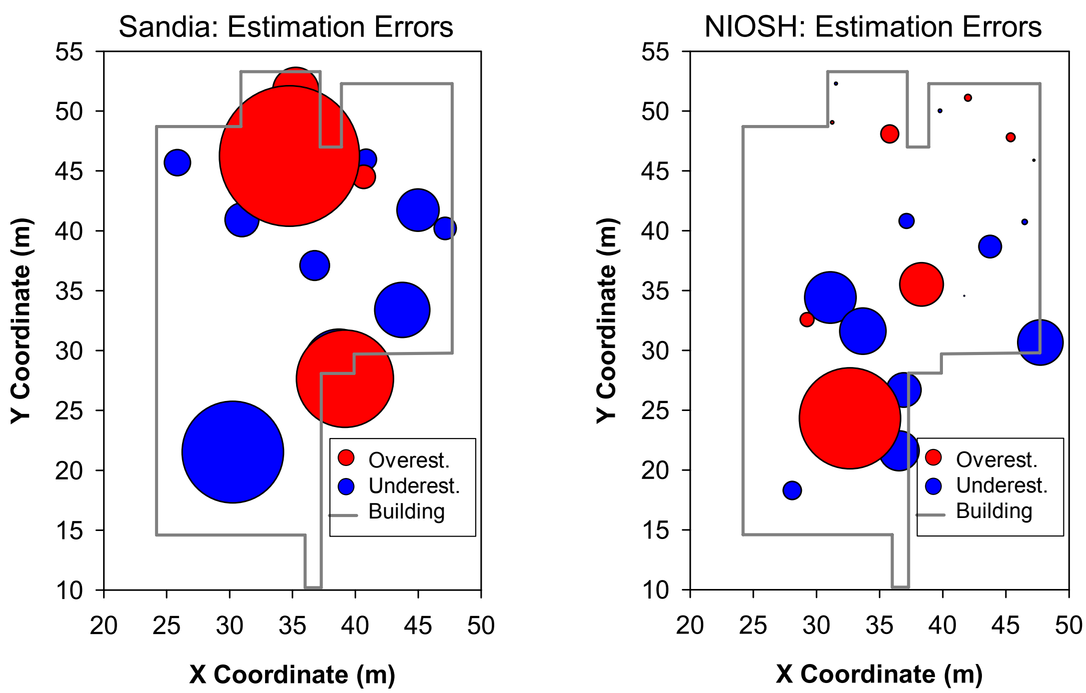

Figure 8-45. Comparison of pink Visolite estimation errors in the basement for the Sandia (left) and NIOSH (right) data sets. The size of the circles are proportional to the absolute value of the estimation error.

8.2.4.2 Main Floor

The locations of the pink Visolite data for the Sandia and NIOSH data sets obtained on the main floor are shown in Figure 8-46. Similar to the basement samples, the two data sets share 20 samples in common. There are a total of 35 samples in the Sandia data set and 43 samples in the NIOSH data set. Similar optimization criteria as used in the basement were used on the main floor to locate the samples in the Sandia data set. The locations of the NIOSH samples were again determined using the judgment of the NIOSH building characterization team.

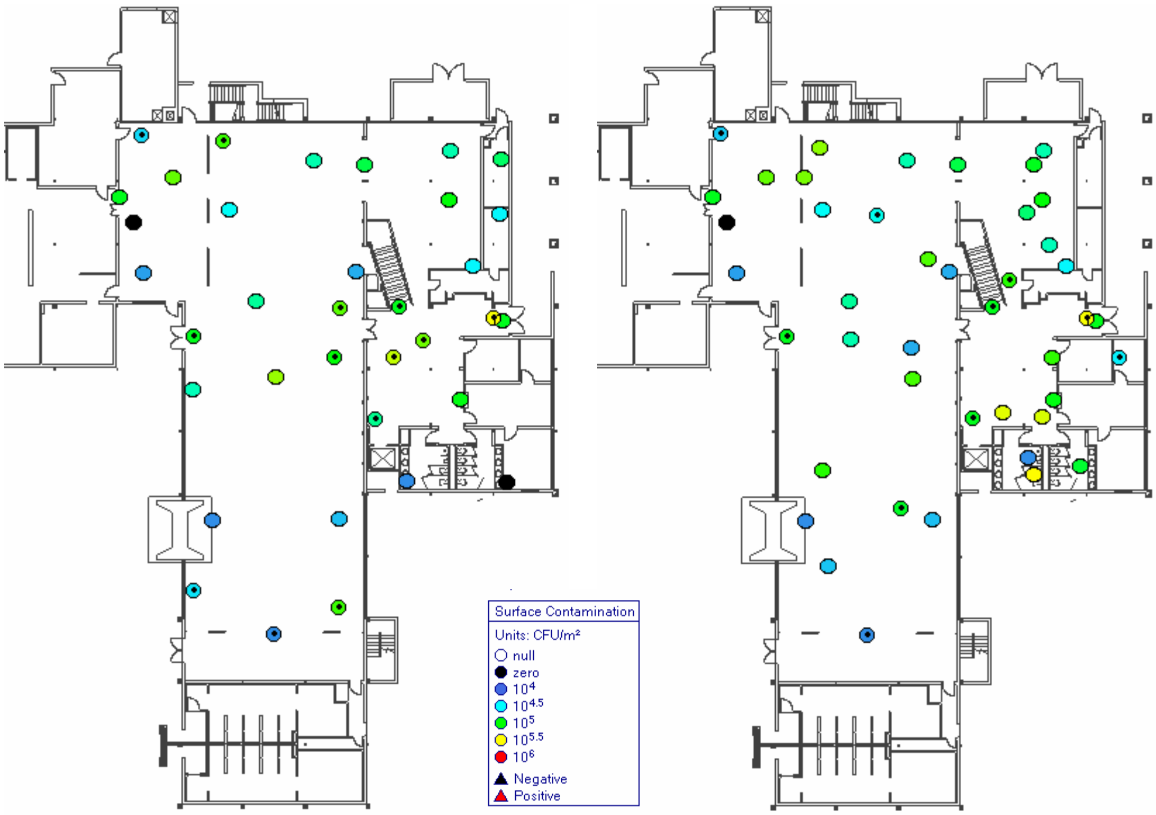

Figure 8-46. Main floor pink Visolite sample sets. The left image shows the Sandia and the shared data sets. The right side shows the NIOSH and the shared data sets.

The distributions of the log10 transformed main floor sample data are shown in Figure 8-47. The means, minimum, maximum and standard deviations of the two data sets are nearly identical. It is interesting to note that compared to the basement data, the means of these distributions are nearly an order of magnitude higher and there are no zero-valued samples on the main floor. Based on the distributions of the basement and main floor samples, it would appear that the majority of the tracer was deposited on the main floor.

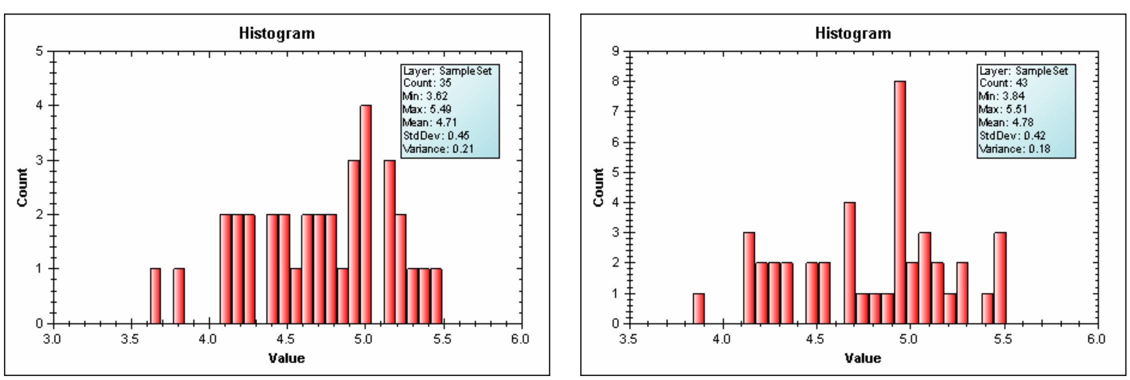

Figure 8-47. Distributions of Log10 transformed pink Visolite data for the Sandia (left) and NIOSH (right) main floor data sets.

The log10 transformed sample data are used to construct and model variograms to define the spatial variability on the main floor. These variograms are shown in Figure 8-48. The Sandia data set was fit with an exponential model with zero nugget and range of 11m and sill of 0.206. The NIOSH data set was also fit with an exponential model having a zero nugget, range of 10.0 meters and sill of 0.18. In both cases, the experimental variogram point at the second lag spacing was ignored in the model fitting due to the low number of pairs of data (2 and 22 for the Sandia and NIOSH data sets respectively) that were used to calculate that point.

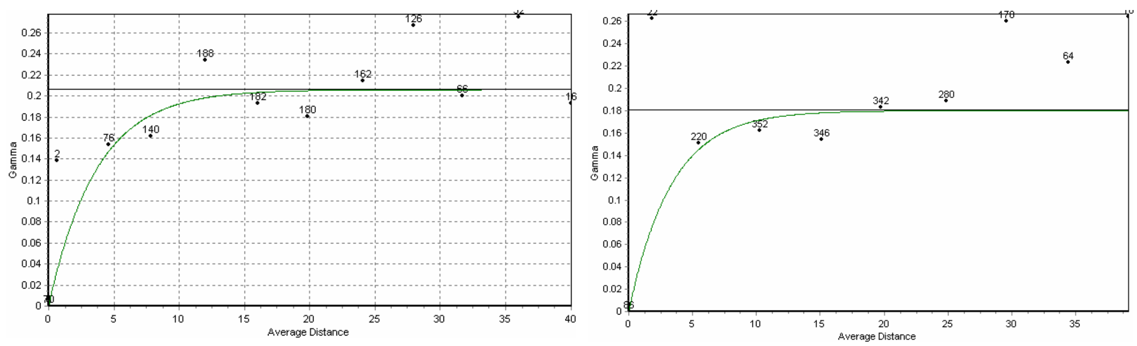

Figure 8-48. Variograms for the pink Visolite datasets (Sandia on the left and NIOSH on the right) for the main floor.

The variogram models and sample data were used with ordinary kriging to estimate the surface contamination across the main floor. The kriging estimates were made on a 0.5x0.5 meter square grid. The results of the kriging estimates based on both data sets are shown in Figure 8-49. The general pattern of high and low surface contamination across the main floor is the same when the Sandia and NIOSH results are compared. There are differences between the estimates of high concentration area near the top of the stairs and in the offices on the east side of the building and in the bar area. These differences appear to be due to single samples being in one data set or the other.

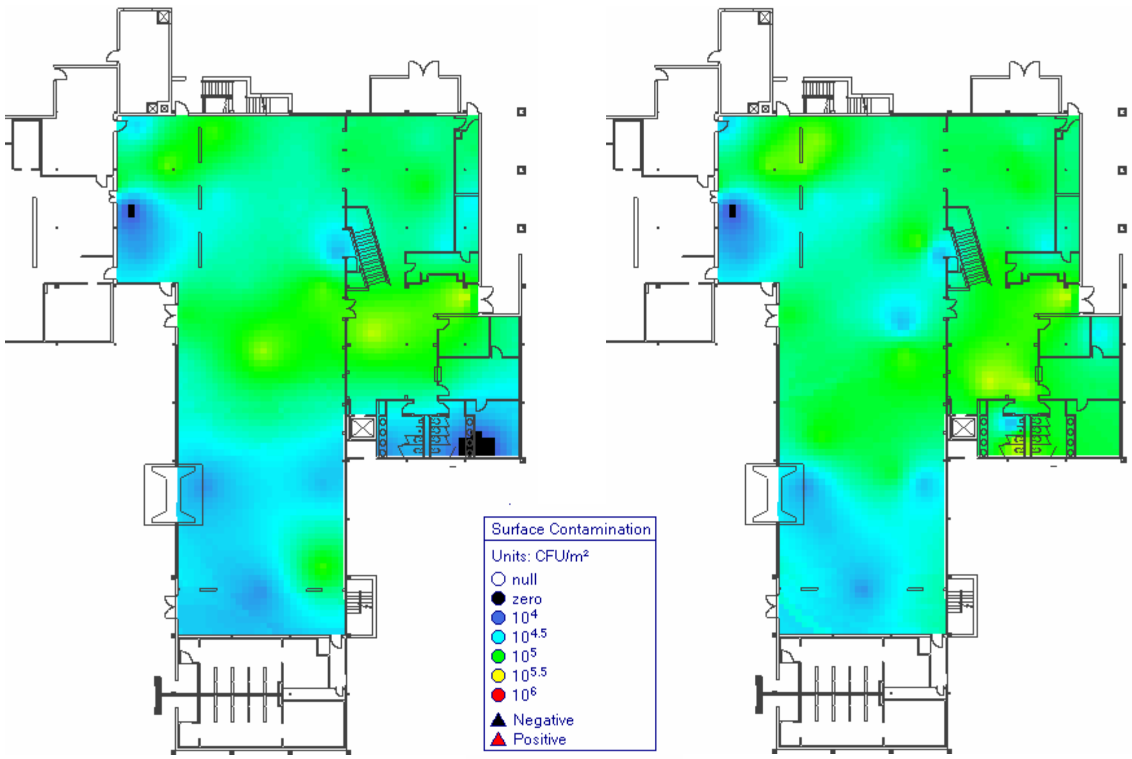

Figure 8-49. Kriging estimates of the pink Visolite surface contamination for the main floor as created with the Sandia (left) and NIOSH (right) data sets

The kriging variance maps in Figure 8-50 also show similar patterns between the two data sets with the individual sample locations producing the obvious low variance locations in the maps. In both maps, the areas of highest kriging variance are in the southern end and eastern edge of the main floor. The NIOSH data set has 8 more samples than the Sandia data set and this higher sample density results in a lower average kriging variance when calculated across the entire main floor.

Similar to all of the previous estimations, the quality of the estimates is evaluated through jackknifing where the data set not used in the estimations provides the control against which the estimates are checked. The estimation errors are summarized in Table 8-26 and the locations and magnitudes of the errors are shown in Figure 8-51. Compared to the estimation of the pink Visolite in the basement, the absolute values of the estimation bias and the magnitudes of the smallest and largest errors are reduced. When compared to the total range of the data, the bias is -10 percent for the Sandia data set and 1 percent for the NIOSH data set. The relative bias for the Sandia estimates is larger than it was for the estimations in the basement and this increase is due mainly to not having any zero-valued samples on the main floor making the range of the sample data smaller than it was for the basement.

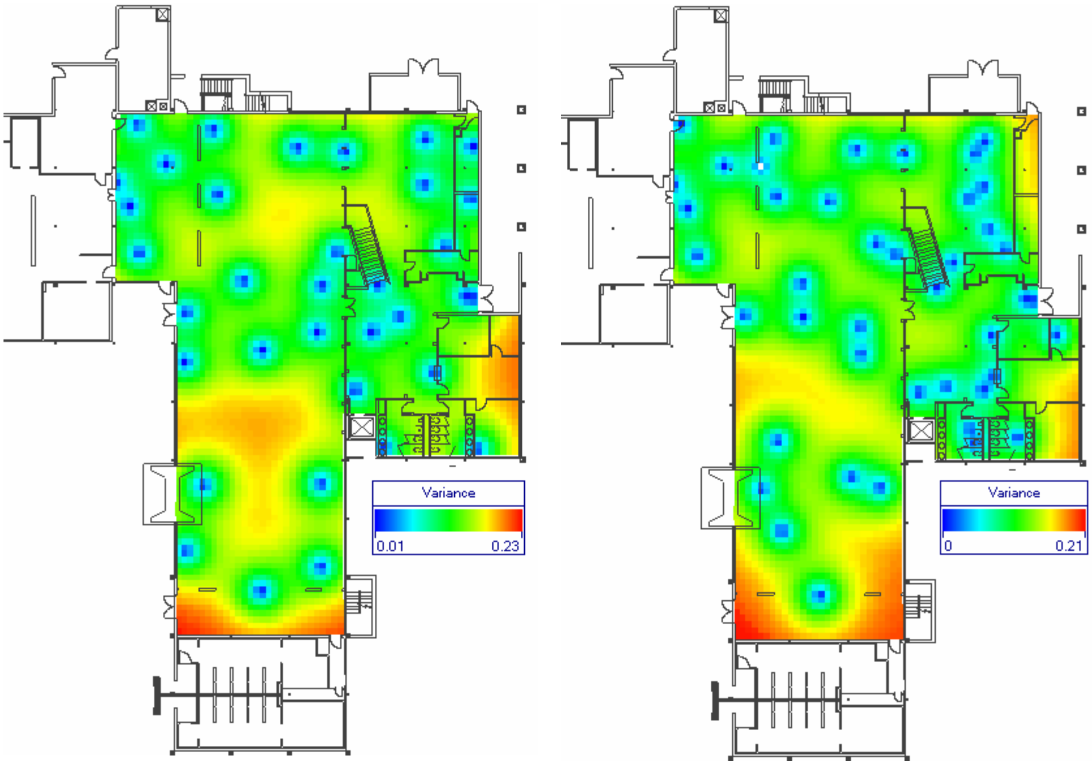

Figure 8-50. Kriging variance of the pink Visolite on the main floot using the Sandia data set (left) and the NIOSH data set (right)

Table 8-26. Summary statistics on estimation errors for the pink Visolite on the main floor.

Parameter	Sandia Data Set	NIOSH Data Set
Mean	-0.19	0.02
Std. Dev.	0.45	0.50
Median	-0.16	0.05
Minimum	-1.21	-0.59
Maximum	0.80	1.30
Number	23	15

The locations of the largest estimation errors for both data sets occur in the small office rooms on the east side of the building (Figure 8-51). The Sandia data set creates large underestimations in this area while the NIOSH data set produces large overestimations in this area. In general, both data sets tend to underestimate the high surface contamination values near the top of the stairs.

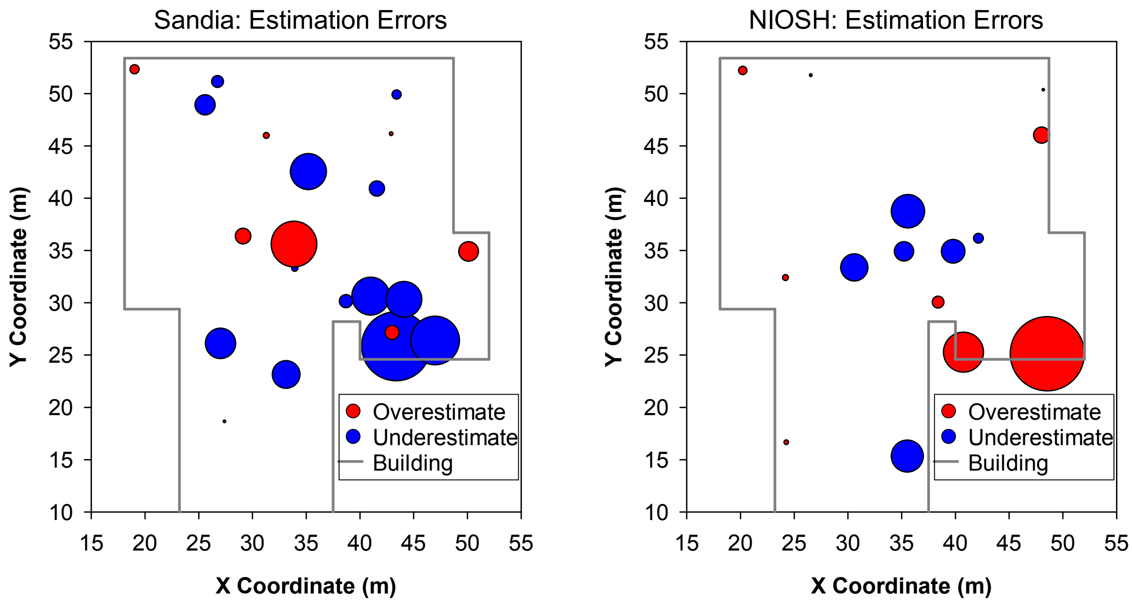

Figure 8-51. Comparison of pink Visolite estimation errors on the main floor for the Sandia (left) and NIOSH (right) data sets. The size of the circles are proportional to the absolute value of the estimation error.

8.2.5 Discussion

The integrated mass of the tracer deposited on the horizontal surfaces within the Coronado Club is calculated from the estimated surface contamination values. These integrated totals are compared to the amount of mass released in the experiment and results show both over and under estimation of the original mass. Potential future technical directions for extending surface contamination mapping are suggested.

8.2.5.1 Mass Balance

As a final check of the estimation procedure, the total amount of estimated surface contamination as integrated across each floor is calculated from the kriging estimates and compared to the amount of mass released in each tracer test. The results of these calculations are shown in Table 8-27. In each box of Table 8-27, the estimated amount for the basement is shown on the top line, the estimated amount for the main floor is shown on the middle line and is underlined and the sum of the values for the two floors is shown on the bottom line. Results are shown in units of ug, g and as a percent of the amount released. A total of 207 grams of yellow Visolite were released and a total of 37 grams of pink Visolite were released.

Table 8-27. Estimated total mass deposited as calculated with each data set.

Tracer Release	Sample Set	Released Mass (g)	Estimated Mass Deposited (μg)	Estimated Mass Deposited (g)	Percent of Release Deposited
Yellow Visiolite	All Data	207	2.669E+05 5.223E+05 7.892E+05	0.27 0.52 0.79	0.13 0.25 0.38
	Group 1	207	2.555E+05 5.489E+05 8.044E+05	0.26 0.55 0.81	0.13 0.27 0.40
	Group 2	207	2.082E+05 5.223E+05 7.305E+05	0.21 0.52 0.73	0.10 0.25 0.35
Pink Visiolite	Sandia	37	1.478E+07 5.813E+07 7.295E+07	14.8 58.1 72.9	40.0 157.0 197.0
	NIOSH	37	1.523E+07 6.584E+07 8.107E+07	15.2 65.8 81.0	41.0 177.8 218.8

The results in Table 8-27 show that across all three data sets, the estimations show that less than 0.5 percent of the yellow Visolite tracer ended up being deposited on the floor. Contrary to the yellow Visolite results, the two estimations for the pink Visolite show that approximately 200 percent of the released tracer is deposited on the floor. For both tracers, the majority of the mass is deposited on the main floor, not in the basement. This result indicates rapid and focused transport of both tracers from the source location down the hallway and up the stairs to the main floor.

The calculations of integrated mass deposited within the Coronado Club are both quite far from the amount of mass released in the tracer tests. The yellow Visolite tracer results may be plausible if the majority of the tracer leaves the building during air exchange with the outside and/or is caught within the ventilation system and does not get deposited on the floor. Other factors that could lead to low estimation of deposited mass may include the fact that large amounts of the tracer were deposited on the floor right at the source location and fully representative samples of this local deposit mass may not have been obtained. Systematic bias in the kriging estimates is ruled out as the estimations done with the two different splits of the yellow data set produce low amounts of bias when evaluated with jackknifing and give results that are consistent with each other as well as being consistent with the estimates made using the entire data set.

No physical process can be responsible for estimates of the deposited pink Visolite mass being nearly twice the amount of mass that was released. The kriging estimates have been checked and do not systematically overestimate the true measured values of the sample data. The relative values of the pink surface contamination appear to be correct as the spatial patterns predicted for both floors agree with what is known about the flow system in the Coronado Club. It is possible that the laboratory estimates of mass and/or the conversion from mass to surface contamination that includes the estimated sampling efficiencies have some positive bias. In particular, the laboratory analyses may be affected by the samples of the pink visolite also containing remnant yellow visolite from the previous test.

8.2.5.2 Future Extensions

The estimations done in this report are for a continuous variable, surface contamination. The same ordinary kriging algorithm used herein can also be applied to discrete variables such as simple "positive/negative" results from analysis of a sample for a suspected bioagent. In this case, the sample values are set to "0" for negative and "1" for positive and the resulting map shows the probability of having a positive sample at any location. This type of mapping is referred to as indicator kriging and is a well studied approach to mapping discretely valued data and this capability is functional within the BROOM software. These types of maps were not produced in this exercise mainly due to the complications in verifying them against the existing samples. The comparison between discretely valued samples and estimates of probability are more complicated than the model evaluations done for the continuous variable samples done in this report.

The spatial estimations created in this report do a remarkable job of estimating the actual surface contamination at unsampled locations. The average estimation error is near zero in all cases and for the estimates done in log10 space, 95 percent of all estimates fall within +/- 1 order of magnitude of the true value. The exception to this result is the estimation of the pink tracer surface contamination in the basement, where inclusion of the zero-value samples creates larger errors. The spatial patterns produced by the kriging estimates are consistent with the known tracer source location and the conceptual model of transport away from that source location. These estimates were made without any knowledge of the flow conditions within the building and can be completed quite rapidly using the BROOM software.

The estimation algorithm does not currently account for walls and other barriers to flow. This leads to problems when a high concentration value is sampled on one side of a wall are used to estimate concentrations nearby locations, but on the other side of the wall where no contamination exists. Techniques for incorporating walls as flow barriers into the spatial estimation are under development and show strong potential to improve the estimates in areas where open and closed rooms complicate the deposition patterns.

The current estimation approach is focused on mapping the deposition of the contaminant onto horizontal surfaces, principally the floor of the building. The estimation algorithms are capable of estimating concentrations in 3-D space and this capability will be added to the BROOM software. The major difficulty with 3-D estimation is determining the degree to which the contaminant adheres to walls and ceilings relative to the amount of deposition on the floor. The ability to estimate concentration in 3-D will facilitate incorporation of air flow models into the contaminant estimations. While the estimation approach demonstrated here is data driven and works without knowledge of the HVAC system, if that HVAC system knowledge is available, then improved estimates of the contamination distribution could be produced.

8.2.6 Conclusions

Two different releases of particulate tracers, yellow and pink, were done in the Coronado Club facility. The source location was the same for each tracer. After the release of each tracer, numerous samples were obtained throughout the facility. A large number of wipe samples taken on square vinyl tiles provide nearly 300 consistent measures of the surface contamination for the yellow Visolite tracer. Estimates of surface contamination were created using the entire data set. The data set was also split in half and each half was used independently to estimate the surface contamination throughout the building . Splitting the data set allows for the estimates created with one-half of the data set to be verified by the other half that was not used in the estimation (jackknifing).

Analysis of the yellow Visolite data shows that the sample data do exhibit spatial correlation. The length of this correlation is shorter in the basement, roughly 5 meters, than it is on the main floor, roughly 8-10 meters, and these results are consistent with the number and size of rooms on each of the floors. Ordinary kriging is used to estimate the two-dimensional surface contamination throughout the building. The results of this estimation are consistent with the conceptual model of air flow within the building showing high levels of surface contamination from the source location, north in the hallway to the stairs and then dispersing in all directions from the top of the stairs across the main floor. The jackknife analysis of the estimations done for the basement and for the main floor show little bias in the estimates and reasonable maximum and minimum values of the estimation error. Some of the locations of the largest errors are generally associated with samples near walls that divide rooms with high concentration from rooms with low concentration and the current estimation algorithm is not capable of handling large shifts in the concentration data as caused by discrete flow and transport barriers such as walls.

The sample locations for the pink Visolite tracer were determined in two different ways. Locations for the “Sandia” data set were determined using a discrete optimization algorithm within the BROOM software to simultaneously meet four different objectives. The “NIOSH” data set locations were determined by the NIOSH building characterization team using experience gained in previous characterization activities. Samples collected on the first day of characterization are common to both sample sets. These common samples make up roughly half of each sample set. Similar to the evaluation of the estimations with the yellow data set, the estimations made with each of the pink data sets are evaluated using the unique samples in the other data set. The pink data sets are complicated by several zero-valued samples occurring in the basement.

Analysis of the pink Visolite samples show levels of spatial correlation similar to that seen in the yellow data – approximately 5 meters in the basement and 8-10 meters on the main floor. Two-dimensional surface contamination is estimated throughout the building with both data sets and then checked against the other data set. The estimates are unbiased but large estimation errors can occur. These large errors are associated with the zero-valued samples and areas near these samples.

In summary, ordinary kriging of surface contamination within a building has been shown to produce unbiased estimates of the sample data. This approach to estimating surface contamination is “data-driven”, provides rapid estimates of the extent and magnitude of the surface contamination, and does not rely on knowledge of the HVAC system within the building to make these estimates. Extensions to this approach to account for walls serving as barriers to air flow, to incorporate HVAC models, if they exist, and to create three-dimensional estimates of surface contamination are being pursued.

8.2.7 References

Deutsch, C.V. and A.G. Journel, 1998, *GSLIB: Geostatistical Software Library and User's Guide*, Oxford University Press, 369 pp.

Gilbert, R.O., 1987, Statistical Methods for Environmental Pollution Monitoring, Van Norstrand Reinhold, New York, 320 pp.

Goovaerts, P., 1997. *Geostatistics for Natural Resources Evaluation*. Oxford Univ. Press, New York., 483 pp.

Kyriakidis, P. and A.G. Journel, 2001, Stochastic Modeling of Atmospheric Pollution: A Spatial Time Series Framework: Part II, Application to Monitoring Monthly Sulphate Deposition over Europe, *Atmospheric Environment*, 25, (13), pp. 2339-2348.

McKenna, S.A., 1998. Geostatistical approach for managing uncertainty in environmental remediation of contaminated soils: case study. *Environmental & Engineering Geosciences*, 4(2), pp. 175-184.

Mohammadi, J., M. Van Meirvenne and P. Goovaerts, 1997, Mapping Cadmium Concentration and the Risk of Exceeding a Local Sanitation Threshold Using Indicator Geostatistics, in GeoENV-1, Geostatistics for Environmental Applications (Soares, Gomez-Hernandez and Froideveaux, editors), Kluwer Academic Publishers, Dordrecht, pp. 327-337.

Olea, R.A., 1999, *Geostatistics for Engineers and Earth Scientists*, Kluwer Academic Publishers, 303 pp.

Rouhani, S., 1996. Geostatistical estimation: kriging. In Rouhani. S., et al., editors, *Geostatistics for environmental and geotechnical applications*, ASTM, West Conshohocken, pp 20-31.

Saito, H. and P. Goovaerts, 2001, Accounting for Source Location and Transport Direction into Geostatistical Prediction of Contaminants, *Environmental Science and Technology*, 35 , pp. 4823-4829.

Wackernagel, H., 1998, *Multivariate Geostatsitics*, 2nd Completely Revised Edition, Springer, Berlin, 291 pp.

Western, A. W., Bloschl, G. and Grayson, R. B., 1998. How well do indicator variograms capture the spatial connectivity of soil moisture? *Hydrological Processes*, 12, pp. 1851-1868.

8.3 *Shortest Path Kriging*

8.3.1 Introduction

Section 8.2 of this report discussed the use of geostatistical analysis of the Coronado Club to generate maps showing estimated Visolite levels throughout the facility. That analysis applied a method known as Kriging to derive estimates of Visolite levels at unsampled locations. Kriging maps of the Coronado Club tests show the extent and magnitude of the Visolite deposition in the building.

Kriging generates these useful maps by estimating values at unsampled locations from known values of nearby samples. The value assigned to an unsampled location depends upon the distances to nearby samples. In wide open areas, these separation distances can be calculated unambiguously. However, the interiors of buildings contain walls, doors and other obstacles which complicate determination of the exact separation distance needed for Kriging.

The problem can illustrated as finding the distance between locations in two adjacent rooms (Figure 8-52). The true shortest path distance must include the distance from the first point to the door of the first room, the distance between the doors of the two rooms and the distance from the door of the second room and the second point. A traditional Kriging estimation involving the two green points in Figure 8-52 would use the length of the red line as the distance used to determine the effect of a measured value at one green dot on an estimate being calculated at another green dot. The true shortest path distance, the length of the blue path, should give a more realistic estimate of the true spatial relationship of the two green points and thus a higher quality estimate.

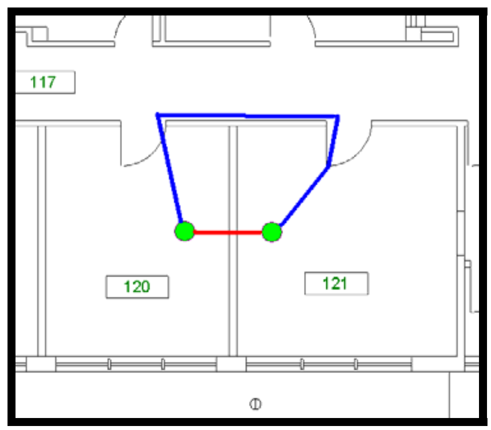

Figure 8-52. Straight-Line (red) and Shortest Path (blue) Distance.

BROOM now provides a mapping option called Shortest Path Kriging which uses a novel image processing, graph-theory based method to calculate these corrected shortest path distances. The shortest path Kriging method was developed using theoretical studies and synthetic contaminant data. The purpose of this paper is to document the use of shortest path Kriging methods in BROOM on the sample data generated from the yellow Visolite release at the Coronado Club. This section simply illustrates the use of an intriguing new technology on this unique data set. The in-depth geostatistical study in Section 8.2 constitutes the definitive analysis of the data set.

8.3.2 Study Area

The shortest path Kriging technique is intended to correct for the effects of walls, doors and other barriers inside buildings. However, much of the Coronado Club facility consists of large, open rooms. The basement is dominated by four large meeting rooms, while the ballroom lounge and serving area take up most of the main floor. Therefore a small area in the basement of the building with many doors and walls was selected for studying the performance of the shortest path Kriging methods (Figure 8-53). In addition to the walls and doors, the study area contains the release point, a wide range of sample values, and areas within the Visolite plume and outside of the plume. The sample area covers parts of three large conference rooms, two small offices, a restroom, a store room, the stairwell and the north part of the basement corridor.

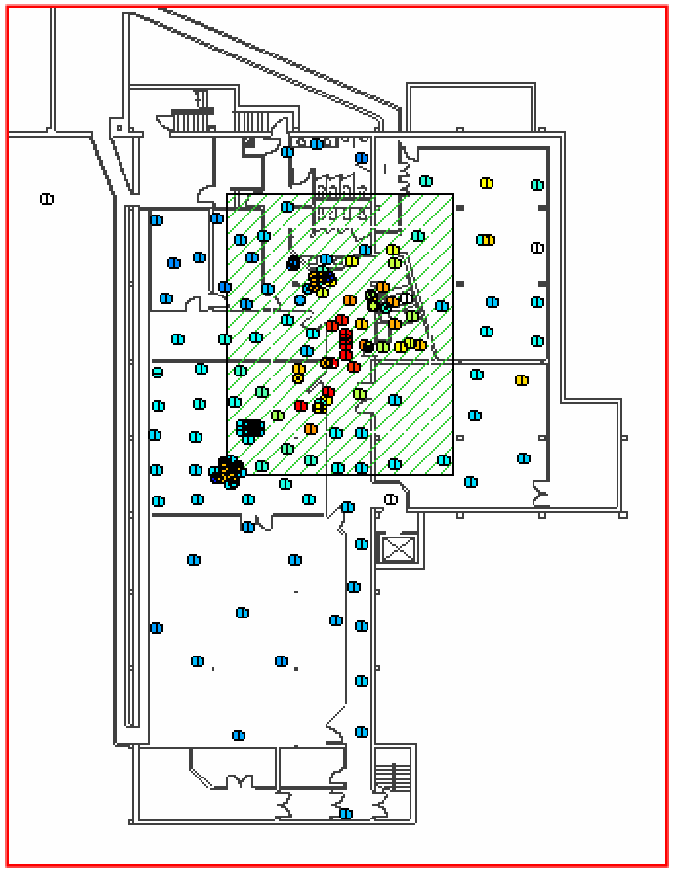

Figure 8-53. Location of Study Area. Area shown in green hatch pattern.

To avoid inconsistencies between sample collection methods, only wipe samples were included in the study. The sample dataset consists of 76 wipes collected on 1ft^2 vinyl floor tiles. Since the areas of all sample tiles were the same, laboratory quantity measured values are used for this study, without any correction for sample surface area or collection efficiency. A log histogram plot of the study data set in Figure 8-54 shows a large number of samples with values less than 10, presumably in the offices and conference rooms away from the release. The sample set also contains some high-value samples, a grouping in the histogram with values of 1,000 or greater represents samples taken within the main release area of the plume.

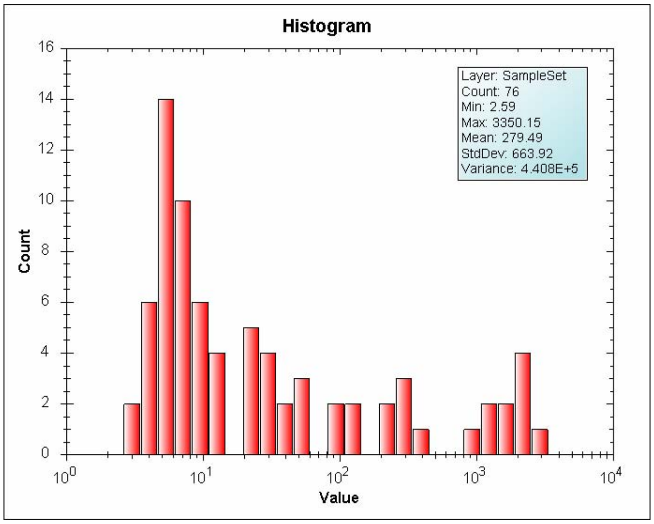

Figure 8-54. Histogram of Study Sample Set.

8.3.3 Variogram

A variogram represents the spatial correlation of a data set. A variogram shows a measure of variability between sample pairs on the vertical axis and separation between sample pairs on the horizontal axis. The variogram for the study data set is shown in Figure 8-55. The purple line in the represents a best-fit line which was visually fit to the sample data shown by the red dots. The analytical form of the purple line is termed the *model variogram.* Its parameters are used in the Kriging procedure to determine the values to assign to locations within the study area for which sample data are not available.

The variogram pictured was derived using the standard method to calculate the distance between sample locations. The parameters of the shortest path variogram and standard variograms used in this study are identical.

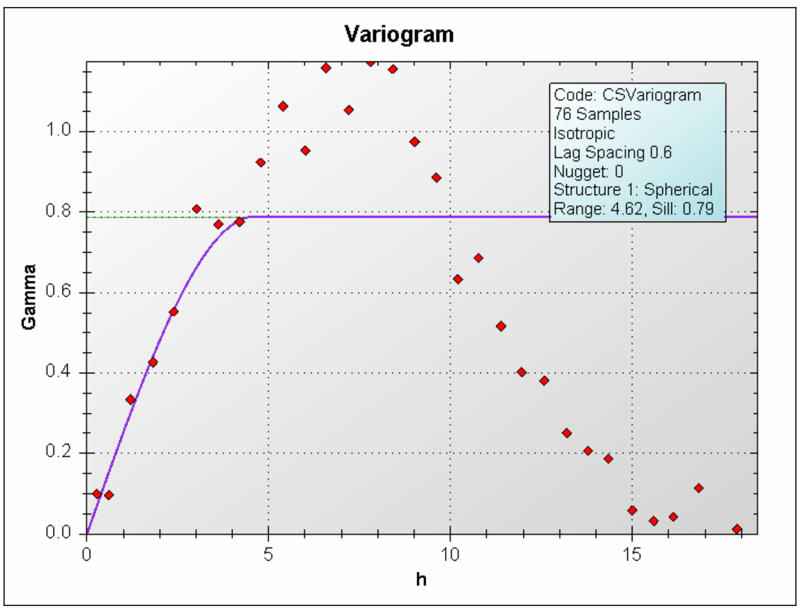

Figure 8-55. Variogram for Study Data Set.

8.3.4 Standard Kriging

The study area was mapped using traditional Kriging methods. The map of the area is shown in Figure 8-56. The general shape of the Visolite plume is clearly delineated by the map. The release into the main corridor, and the subsequent flow of material up the stairwell is reflected in the interpolation of the samples in the basement. For the purposes of this study, the important point to note about Figure 8-56 is how the color gradations representing continuous concentration change continue across solid wall boundaries. Also note that some rooms are shown to have elevated levels of Visolite, even though no samples taken from those rooms show the same elevated levels. For example along the lower right boundary of the map, the yellow color is seen bleeding from the small storage room into the two larger conference rooms and there is no break in concentration across the wall separating the stairwell from the storeroom. However, examining the colors assigned to samples in the conference rooms, none show the elevated levels indicated by the yellow colors; all are blue.

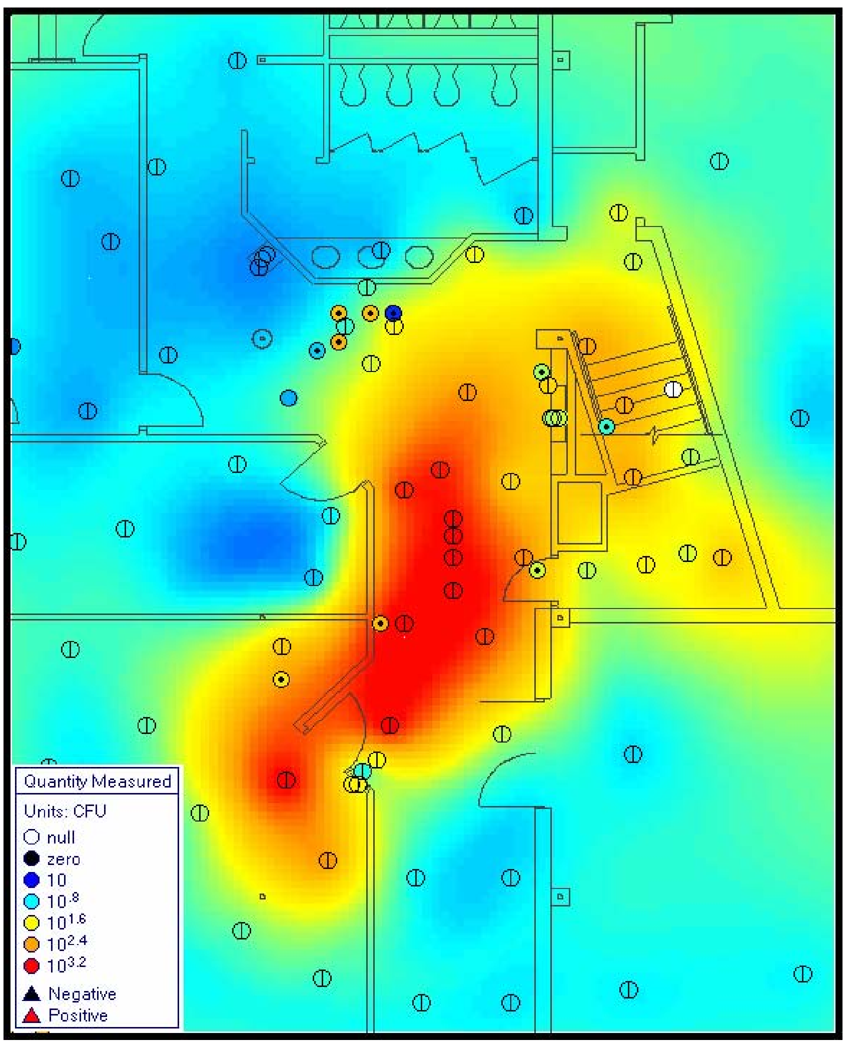

Figure 8-56. Standard Kriging Map of Study Area.

8.3.5 Shortest Path Kriging

The shortest path Kriging map of the study area in Figure 8-57 shows the same general shape and location of the Visolite plume. However, a comparison with the standard Kriging map shows that the concentration gradations as represented by colors do not change gradually across walls. Instead the wall boundaries shown in the overlain CAD linework are well imaged by the Visolite contaminant estimates derived from the shortest path Kriging method. The inconsistent regions noted in the standard Kriging map, such as with the small storage room along the right edge of the map are well resolved in the shortest path map. A number of computational artifacts can be seen on the shortest path Kriging map. The red area just east of the legend block in Figure 8-57 shows some marked striping at 90 and 45 degree orientations. Similarly, many of the concentration color patterns in Figure 8-57 seem to preferentially follow 90 and 45 degree orientation when compared to the smoother patterns seen in Figure 8-56. These artifacts are due to the approach used to calculate the shortest path separation distances.

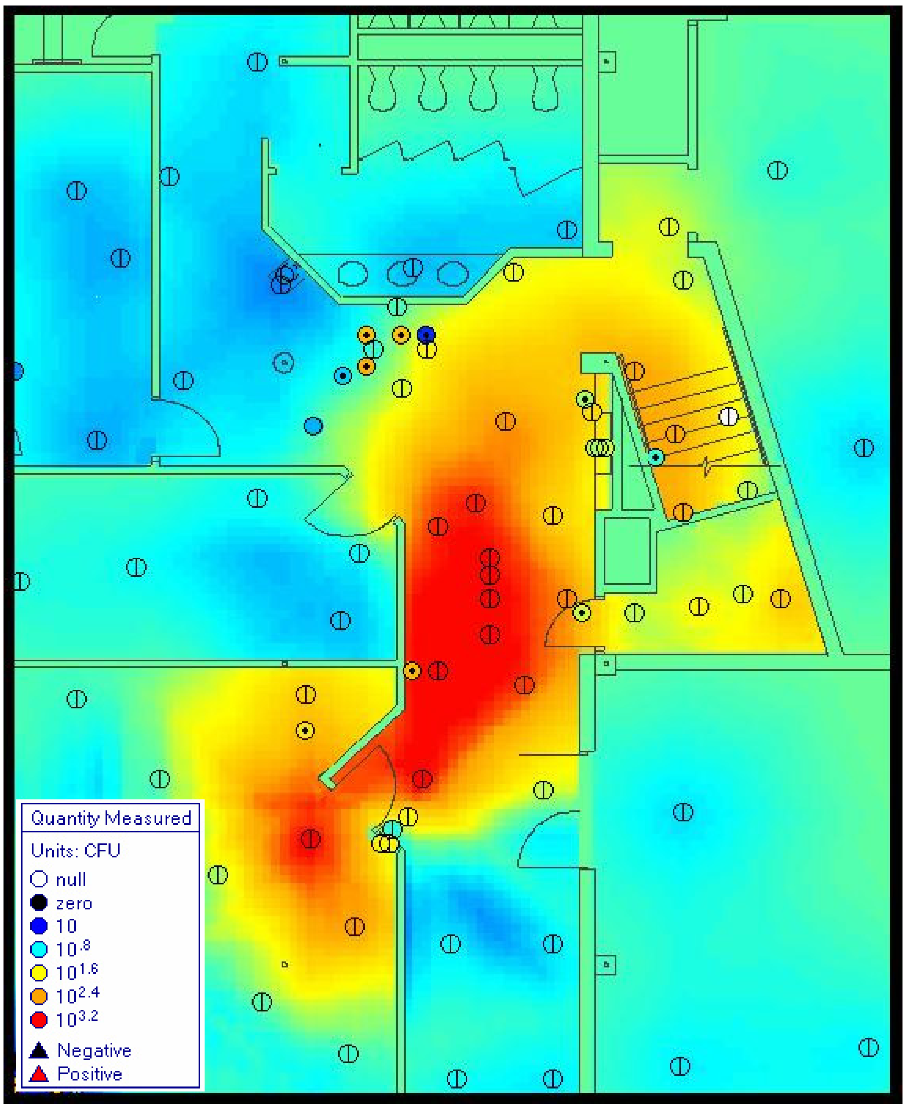

Figure 8-57. Shortest Path Kriging Map of Study Area.

8.3.6 Comparison of Methods

Determining which method gives a better picture of the Visolite deposition in the study area is difficult. The manner in which the shortest path Kriging map honors the walls and doors of the study area is more aesthetically pleasing than the standard Kriging example. However, it is not obvious that the quality of the estimate is superior. Unfortunately, there is no ground truth data set for the Coronado Club with which to compare the two estimation methods.

Since both maps were constructed on identical grid sizes, it is possible to subtract one map from the other and examine the residual surface. The map of the residuals within a sub-region of the estimated area shows where the two maps differ in their estimation of Visolite deposition (Figure 8-58). The residual map shows that most estimation points agree well, with values near zero (green). The major deviation between the maps is along the west wall of the corridor, north of the release point. In this area, the shortest path Kriging process is estimating greater Visolite deposition relative to the standard Kriging process.

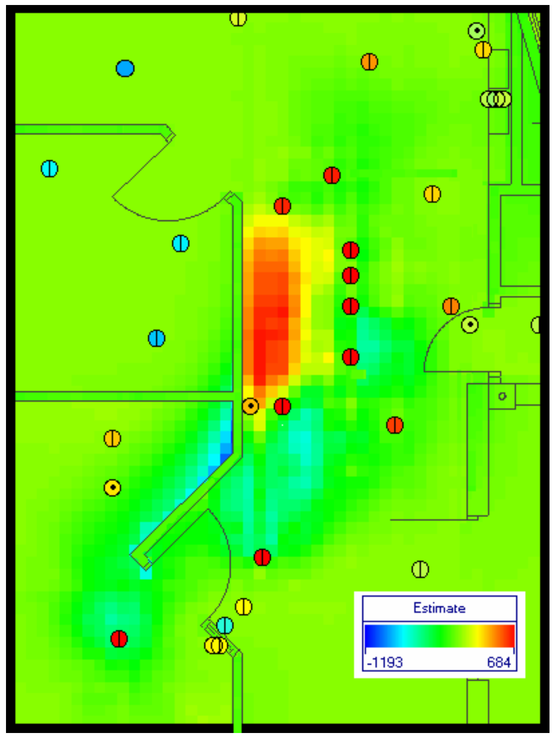

Figure 8-58. Residual Display of Shortest Path vs Standard Maps.

Examination of the two Kriging maps produces a plausible explanation for the different performance of the two processes at this location. The location at which the maps disagree the most is within the plume, but is about 1 m distant from samples. On the standard Kriging map (Figure 8-56), the values of the estimates in the area in question are being influenced by the two low-valued samples located in the office to the west of the corridor. However, in the shortest path case (Figure 8-57), the wall between the corridor and the office is honored, so the values of the estimates for the points just east of the corridor wall are not influenced as much by those two low-valued samples. In the shortest-path case, the closest samples from which to generate estimates are all red-colored high-valued samples, so the estimates are correspondingly higher than for the standard Kriging example.

Low-valued (negative) residuals occur in Figure 8-58 along the wall of the conference room at the southwest portion of the map. These can also be explained by the effects of the wall properly screening the samples in the shortest path case, while the standard Kriging case allows samples which are across the wall to influence the estimation to an extent that is perhaps unwarranted.

Cross validation is a technique to test the accuracy and consistency of a geostatistical model. The process involves removing a sample from the data set and Kriging the data set to obtain the Kriging system's estimate for the value at that missing sample location. This procedure is repeated for every sample in the data set. The result of the process is a pair of values for every sample in the data set. The first entry of the pair is the sample's value. The second entry of the pair is the Kriging system's estimation of that sample's value. The cross validation output is traditionally displayed as an X-Y scatter plot. If the geostatistical model is perfect, all points will line up along the X=Y line. Less scatter from the X=Y line generally means better adherence to the model by the data. Generally, he flatter the line of best fit of the data, the more smoothing of the data has resulted from the estimation process.

The cross validation plot of this study is shown in Figure 8-59. The standard Kriging results are shown in open blue symbols. Shortest path Kriging results are shown in closed red symbols. For reference, the X = Y line is shown with a green dotted line.

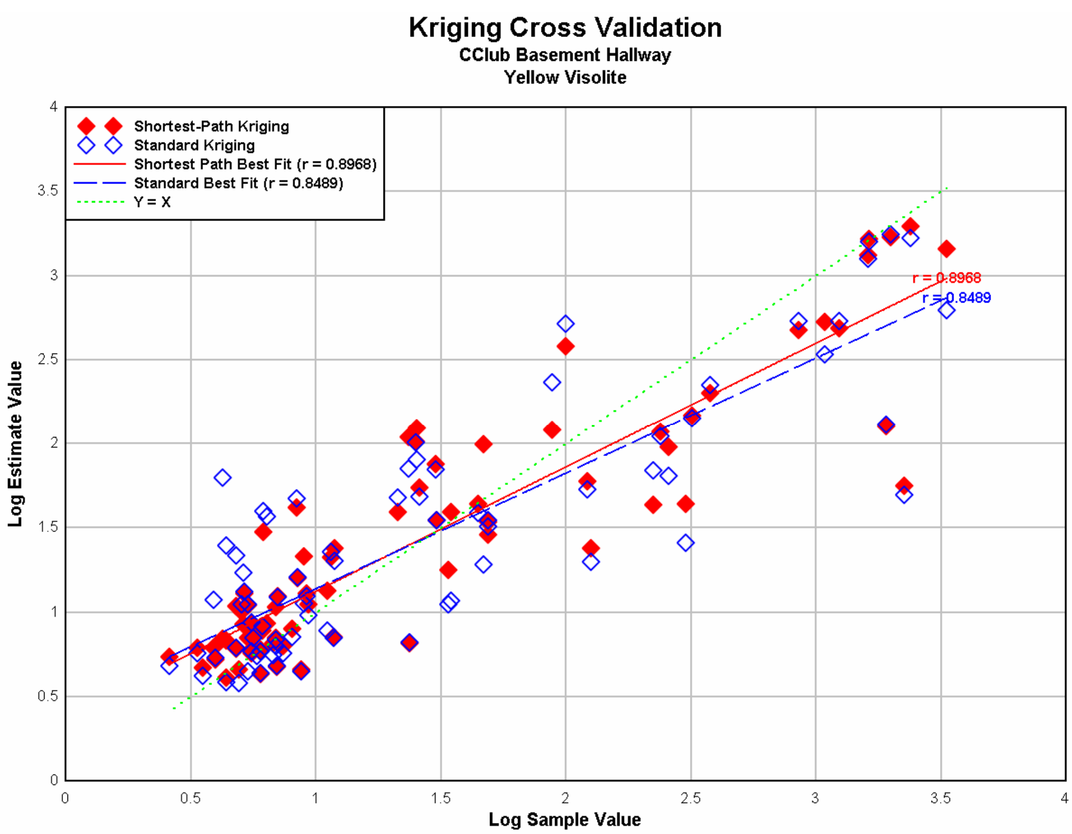

Figure 8-59. Cross Validation Plot for Standard and Shortest Path Methods.

The shortest path solution appears to be better than the standard solution by inspection. In most cases, the solid red dot is closer to the green dotted line than is the corresponding open blue dot. This visual interpretation is supported by the correlation coefficients; the shortest path value or 0.897 is somewhat better than the standard value of 0.849. Also of note is the slightly greater slope of the shortest path best fit line. This suggests that the shortest path method does not produce as smooth an estimation surface as the standard method. As with the correlation coefficient, though, the slope difference between the two methods is quite small.

The errors for each sample location were calculated from the cross-validation data by subtracting the sample value from the estimate value for each of the 76 samples. Table 8-28 shows that the mean of the squared error values is substantially lower for the shortest path method. Similarly, the standard deviation of the errors for the shortest path method is less than that for the standard method.

Table 8-28. Cross-Correlation Statistics.

Kriging Method	Correlation Coefficient	Mean Squared Error	Error Standard Deviation
Shortest Path	0.897	0.156	0.398
Standard	0.849	0.218	0.471

The three measures of model quality listed in Table 8-28 along with the flatter slope of the best fit line as shown in Figure 8-52 all indicate that the shortest path Kriging creates better estimates than the standard Kriging method.

8.3.7 Summary and Conclusions

The Visolite deposition values within a 240m^2 portion of the basement of the Coronado Club were mapped using two different methods. A map of estimated Visolite levels was generated from 76 wipe samples using standard geostatistical methods. A second map was generated from the same samples using a newly developed method called *shortest path Kriging*. Shortest path Kriging uses map distances which reflect the presence of walls and other barriers within buildings rather than the simple straight-line distances used by standard Kriging for estimation purposes. The two methods produced similar looking maps, but the shortest-path map showed concentration discontinuities across walls.

Patterns of residuals between the maps are readily explained by the different methods used to calculate distances between points. Kriging relies on distances to determine relative weighting of a sample's value when generating an estimate. Extreme residual values tend to map to locations where shortest path distance measuring methods changed the set of samples which were closest to the point whose value was being estimated. Cross-validation showed that the shortest path method generates more internally consistent estimates of Visolite deposition.

The initial use of the shortest path Kriging method on this data set demonstrated that the new method does produce usable results. It also showed that in this instance, measurable improvements over standard methods are quite small, perhaps within experimental error. Further work is needed to quantify the possible advantages of the new Kriging approach and to determine its applicability for routine data analysis.

9 Feedback from NIOSH Team

One of Sandia's objectives was to obtain feedback on the BROOM/PDA system from users under real-life conditions. This was obtained via videotaped interviews with the two members of the NIOSH sampling team who used the BROOM tool during the exercise, as well as during the (videotaped) debrief meeting on Friday morning. The tapes and meeting notes were then analyzed for perceived advantages of the system, suggested improvements, and other lessons learned. These are summarized below.

9.1 Major Advantages of system:

- Small size, low weight of PDA.
- Rapid generation of contamination maps to summarize and communicate information. Getting information out in a usable form was important in the Anthrax responses.
- Real-time, electronic record, less error-prone than paper records.
- Ability to click on sample and see collection/location info, rather than paging through many sheets of paper.
- Valuable data management tool.
- Good for a major response, where need for large number of sample takers may mean that many of them are not be experienced industrial hygienists.

9.2 Desired improvements:

Subject	Change(s)	Reason(s)
PDA stylus	Have cord on stylus. Use thicker stylus. Shape back end of stylus so it could be used to push buttons.	Ease of use when wearing several sets of gloves. Small stylus hard to pick up while wearing gloves.
Strap on PDA	Put shoulder strap on PDA.	Free up user's hand for other tasks without having to put PDA on a potentially contaminated surface.
Compass	Fully incorporate compass so map rotates with direction user is pointing it, like a GPS.	In a big building, user can get disoriented very easily.
Batteries	Choose/alter battery compartments so user doesn't have to stick something in a little slot to change batteries.	Fingernails are not available to users wearing several sets of gloves, which makes it hard to open compartments.
Laser	Change z-measurement so it doesn't require flipping the unit over and typing in a number, where everything else is just a button push.	Ease of use. Now took one person reading the value while the other one typed it in.
Sample location dots	Change behavior of red and blue dots. Have blue dot disappear when sample taken and red dot appears. Or be able to show only the samples for that entry. Or have a sample count-down feature, so user knows how many samples they still have to take.	Hard to find "samples to be done" when screen is full of "samples already taken".

Sample types	Include air samples. Record start/stop times, pump numbers, calibration rates, calculate volume and time, then incorporate results into concentration maps/reports.	Routine work is generally for personnel exposure assessments rather than emergency response. Using tool for such work would keep people familiar with system.
Ventilation system information	Incorporate ventilation data in maps and analysis. Be able to label as sample as on a ventilation vent or return.	Ventilation is very important in understanding spread of contaminants and thus to choosing sample locations.
Import/link other data forms	Be able to import photos or sketches, and link to samples.	Help specify/remind user of details of sample location.
Camera	Investigate Bluetooth camera that could send photos remotely, rather than having to remove equipment and download.	Help user record building characteristics and sample locations.
Low-battery warnings	Clarify meaning of low-battery warnings to users and specify procedure to follow. They ignored several until laser locked up, then did soft restarts, changed battery.	After battery warnings, change, and soft restarts, it wasn't clear whether the sample had been entered or not, so it got entered twice.
Volume control button	Warn users during training about volume control button on side of PDA, or find PDA without this feature.	User held PDA in such a way that volume control button was unintentionally toggled, causing screen to appear and users didn't know how to get rid of it.
Buttons across bottom of PDA	Buttons may not be needed. Users always used stylus on screen once they got used to the system.	May be personal preference. These were experienced PDA users.
Network connectivity	Desktop part needs to be able to run in stand-alone mode, rather than assume it will be connected to a network with database.	May not have outside network connection on-site.
Data link to lab	Broom tool should be able to easily transfer sample data to lab, and receive results. In a real event, need to be consistent with chain-of custody protocols for criminal evidence.	Currently need to input sample ID data by hand, which is error-prone and time consuming.
Geo-statistical methods	Figure out how to deal with the fact that air doesn't flow through walls of a building.	If data is not spatially correlated, geo-statistical methods have problems.
Algorithms for choosing sample locations	Alter penalties in algorithm so Broom tool does not suggest sample locations outside of the building.	Doesn't make sense, confuses users.
Algorithms for choosing sample locations	Figure out why Broom tool suggested sample locations very close together in some cases.	Doesn't make sense, confuses users.
HVAC system effects	Make use of information about air flow from HVAC system. Currently have drawings, but not linked to analysis or sample location suggestions.	Such information was heavily used by experts in figuring out contamination source.
Sample types	Improve how different sample types, wipes, swabs, vacuums, are made consistent in analysis.	Sampling efficiency variations of different types of samples have to be accounted for correctly to avoid distortions in analysis.

Sample types	Rectify samples taken on vents or returns with floor samples. Should make use of knowledge that sample was on a vent or return.	Differences in local air-flow environment lead to different amounts of contamination, which can distort analysis.
People patterns	Incorporate information on human behaviors and traffic patterns in choosing sample locations, perhaps by some sort of weighting scheme.	Such information was used by experts in figuring out where to sample.
Training	Supply different amounts of training for PDA users and non-PDA users. Training should also emphasize hands-on, as close to actual use as possible.	Different training needs expressed by two groups of testers. First set were non-PDA users who needed more time. Second set were PDA users who caught on quickly.
Data management	Use different layers in Broom tool to track samples from different teams, or different days.	Useful in a large response, where data management becomes a real issue.
Real time monitors	Be able to include data from real-time monitors on maps, including something on a person moving around in a building.	Would be very valuable to be able to track a person's exposure as they moved around. Or would be a quick route to a contamination map.

9.3 Other Lessons Learned:

- BROOM tool should support expert user, as well as provide expert guidance to non-expert users.
- Want BROOM tool to be dual-use. If it can be used in routine work, people will be have current training and equipment will be maintained in case of an emergency event.
- Sampling team can only go in for ~2 hours per session. But this involves a significant amount of time outside for suiting up, decon, planning and analysis.
- Puffers are not the best way of dispersing powder.
- Hanging toilet paper is an inexpensive way of doing air-flow visualization.
- Taking micro-vac samples is slow. Technology improvements presumably in works.
- Incorporating real-time sound clips probably not useful - respirators garble sounds too much.

10 Summary and Conclusions

In February of 2005, a joint exercise involving SNL and NIOSH was conducted in Albuquerque, NM. The SNL participants included the team developing BROOM, a software product developed to expedite sampling and data management activities applicable to facility restoration following a biological contamination event. The exercise was held at an SNL facility, the Coronado Club, a now-closed social club for Sandia employees located on Kirtland Air Force Base. Sandia's objectives for this exercise included demonstrating the BROOM sample management tool under "real life" conditions by experienced sample collection teams, and developing an extensive surface contamination database following a tracer aerosol release for evaluating statistical algorithms.

BROOM is a sample acquisition, data management, visualization, and analysis tool, designed to speedup and improve the overall efficiency of the restoration process for an indoor facility contaminated by a biological agent. The PDA application utilizes readily available commercial hardware and has unique indoor positioning capabilities. The desktop application works in conjunction with a SQL Server database to store, retrieve, visualize, and analyze the laboratory results of sampling activities. The tool is capable of recommending optimal sampling locations to characterize hotspots or define the extent of contamination.

The expert users saw a number of advantages to using the BROOM tool in sampling:

- Small size, low weight of PDA.
- Rapid generation of contamination maps to summarize and communicate information. Getting information out in a usable form was important in the Anthrax responses.
- Real-time, electronic record, less error-prone than paper records.
- Ability to click on sample and see collection/location info, rather than paging through many sheets of paper.
- Valuable data management tool.
- Good for a major response, where need for large number of sample takers may mean that many of them are not be experienced industrial hygienists.

In particular, although the BROOM tool was originally developed to assist in sampling, they thought that it would be very useful as a data management tool. The users had a number of specific suggestions for improvements, but were enthusiastic about being beta testers.

The exercise, and preparations for it, involved releases of two different particulate tracers in the facility. Yellow and pink fluorescent Visolite powders were used as a simulant for a biowarfare agent. After the release of each tracer, numerous samples were obtained throughout the facility. Wipe samples taken on square vinyl tiles provide nearly 300 consistent measures of the surface contamination for the yellow Visolite tracer. Analysis of the yellow and pink Visolite data shows that the sample data do exhibit spatial correlation. The length of this correlation is shorter in the basement, roughly 5 meters, than it is on the main floor, roughly 8-10 meters. These results are consistent with the number and size of rooms on each of the floors. Ordinary kriging of surface contamination within a building produced unbiased estimates of the sample data. This approach to estimating surface contamination is "data-driven", provides rapid estimates of the extent and magnitude of the surface contamination, and does not rely on knowledge of the HVAC system within the building to make these estimates. Extensions to this approach to account for walls serving as barriers to air flow, to incorporate HVAC models, if they exist, and to create three-dimensional estimates of surface contamination are being pursued.

Distribution

E-copies

5 Dawn Myscofski
U.S. Dept. of Homeland Security
Washington, D.C. 20528

5 Theresa Lustig
U.S. Dept. of Homeland Security
Washington, D.C. 20528

3 Lance Brooks
U.S. Dept. of Homeland Security
Washington, D.C. 20528

1 Beth George
U.S. Dept. of Homeland Security
Washington, D.C. 20528

1 John Vitko
U.S. Dept. of Homeland Security
Washington, D.C. 20528

1 Jeff Stiefel
U.S. Dept. of Homeland Security
Washington, D.C. 20528

1 Caroline Purdy
U.S. Dept. of Homeland Security
Washington, D.C. 20528

1 Mike McLachlin
U.S. Dept. of Homeland Security
Washington, D.C. 20528

1 Julius Chang
U.S. Dept. of Homeland Security
Washington, D.C. 20528

1 Rick Turville
U.S. Dept. of Homeland Security
Washington, D.C. 20528

1 Andrew Avel
USEPA Facilities
26 West Martin Luther King Drive
Mail Code: 163
Cincinnati, OH 45268

1 Jon Herrmann
USEPA Facilities
26 West Martin Luther King Drive
Mail Code: 163
Cincinnati, OH 45268

1 Alan Lindquist
USEPA Facilities
26 West Martin Luther King Drive
Mail Code: 163
Cincinnati, OH 45268

1 Deborah McKean
USEPA Facilities
26 West Martin Luther King Drive
Mail Code: 271
Cincinnati, OH 45268

1 Cindy Sonich-Mullin
USEPA Facilities
26 West Martin Luther King Drive
Mail Code: 163
Cincinnati, OH 45268

1 Oba Vincent
USEPA Facilities
26 West Martin Luther King Drive
Mail Code: 163
Cincinnati, OH 45268

1 Daniel Hawthorne
USEPA REGION 8
999 18th Street
Suite 300
Mail Code: 8OIG
Denver, CO 80202-2466

1 Eric Koglin
USEPA National Homeland Security
Research Center
944 East Harmon Avenue
Las Vegas, NV 89119

1 Dennisses Valdes
USEPA Env. Response Team - West
4220 South Maryland Parkway
Building D, Suite 800
Las Vegas, NV 89119

Distribution (continued)

1 Nancy Adams
USEPA Mailroom
Mail Code: E343-06
Research Triangle Park, NC 27711

1 Paul Lemieux
USEPA Mailroom
Mail Code: E305-01
Research Triangle Park, NC 27711

1 Blair Martin
USEPA Mailroom
Mail Code: E343-04
Research Triangle Park, NC 27711

1 Joseph Wood
USEPA Mailroom
Mail Code: E343-06
Research Triangle Park, NC 27711

1 Peter Jutro
USEPA Headquarters
Ariel Rios Building
1200 Pennsylvania Avenue, N. W.
Mail Code: 8801R
Washington, DC 20460

1 Carlton "Jeff" Kempter
USEPA Headquarters
Ariel Rios Building
1200 Pennsylvania Avenue, N. W.
Mail Code: 7510P
Washington, DC 20460

1 Walter Kovalick
USEPA Headquarters
Ariel Rios Building
1200 Pennsylvania Avenue, N. W.
Mail Code: 5203P
Washington, DC 20460

1 Mark Mjoness
USEPA Headquarters
Ariel Rios Building
1200 Pennsylvania Avenue, N. W.
Mail Code: 5104A
Washington, DC 20460

1 Daniel Powell
USEPA Headquarters
Ariel Rios Building
1200 Pennsylvania Avenue, N. W.
Mail Code: 5203P
Washington, DC 20460

1 Elizabeth Southerland
USEPA Headquarters
Ariel Rios Building
1200 Pennsylvania Avenue, N. W.
Mail Code: 5204G
Washington, DC 20460

1 David Wright
USEPA Headquarters
Ariel Rios Building
1200 Pennsylvania Avenue, N. W.
Mail Code: 2491T
Washington, DC 20460

1 Max Kiefer
NIOSH
4676 Columbia Parkway,
Cincinnati, OH 45226

5 Ken Martinez
NIOSH
4676 Columbia Parkway, MS-R11
Cincinnati, OH 45226

1 Rob McCleery
NIOSH
4676 Columbia Parkway,
Cincinnati, OH 45226-1998

1 Greg Burr
NIOSH
4676 Columbia Parkway,
Cincinnati, OH 45226

1 Brad King
NIOSH
4676 Columbia Parkway,
Cincinnati, OH 45226

1 Chad Dowell
NIOSH
4676 Columbia Parkway,
Cincinnati, OH 45226

Distribution (continued)

1	Donnie Boomer NIOSH 4676 Columbia Parkway, Cincinnati, OH 45226
1	Kevin Dunn NIOSH 4676 Columbia Parkway, Cincinnati, OH 45226
1	James Bennett NIOSH, MS R5 4676 Columbia Parkway Cincinnati, OH 45226
1	Stanley Shulman NIOSH, MS R3 4676 Columbia Parkway Cincinnati, OH 45226
1	Dr. Sushil Sharma US GAO 441 G. St. NW Washington, DC 20548
1	Ellen Raber Lawrence Livermore National Lab P.O. Box 808, Livermore, CA 94551-0808
1	Don MacQueen Lawrence Livermore National Lab P.O. Box 808, Livermore, CA 94551-0808
1	Brent Pulsipher Pacific Northwest National Laboratory PO Box 999, MS-K6-08 Richland, WA 99352

1	MS 0384	Art Ratzel, 1500
1	MS 0701	John Merson, 6110
1	MS 0734	J. Bruce Kelley, 6215
1	MS 0734	Pauline Ho, 6215
5	MS 0734	Mark Tucker, 6215
1	MS 0734	Wayne Einfeld, 6215
1	MS 0734	Gary Brown, 6215
1	MS 0734	Bob Knowlton, 6215
1	MS 0734	Mollye Wilson, 6215
1	MS 0734	Matt Tezak, 6215
1	MS 0734	Ray Boucher, 6215
1	MS 0734	Jonathan Leonard, 6215
1	MS 0734	Caroline Souza, 6215
1	MS 0741	Rush Robinett, 6210
1	MS 0741	Marjorie Tatro, 6200
10	MS 0836	Richard Griffith, 1517
5	MS 0836	James Ramsey, 1517
1	MS 0735	Ray Finley, 6115
1	MS 0735	Sean McKenna, 6115
1	MS 0735	Chad Peyton, 6115
1	MS 0824	Wahid Hermina, 1510
1	MS 0836	Patrick Finley, 1517
1	MS 0836	Brad Melton, 1517
1	MS 0836	John Brockmann, 1517
1	MS 0836	Dan Lucero, 1517
1	MS 0836	Todd Rudolph, 1517
1	MS 1161	Dan Rondeau, 5430
1	MS 1230	Veronica Lopez, 10531
1	MS 9004	Jill Hruby, 8100
1	MS 9004	Pat Falcone, 8110
1	MS 9004	Duane Lindner, 8120
1	MS 9004	Brian Damkroger, 8130
1	MS 9155	Howard Hirano, 8122

Hardcopies

2	MS 0734	Pauline Ho, 6215
2	MS 9018	Central Technical Files, 8944
2	MS 0899	Technical Library, 4536